Characterisation of a cortical neuronal cell model for *SGCE*-mutation positive Myoclonus Dystonia

Thesis submitted for the degree of Doctor of Philosophy

School of Medicine, Cardiff University

2020

Alessandra Sperandeo

Acknowledgements

First and foremost, I'd like to thank my primary supervisor, Kathryn. You deserve to be recognised as one of the most hardworking, dedicated women in science and it has been a privilege to have you as my supervisor; you are a true role model to me. Deep down, I'm even grateful that you signed me up for the half marathon – never again! Meng, thank you for hiring me as a technician all those years ago and for having the belief in me to complete my PhD. I am massively appreciative of all Li Lab members, past and present, for your invaluable help and advice over the past few years. In particular, I would like to thank Claudia for your help with my initial iCRISPR experiments. Zoe, Frankie and Ying, thank you for all of your help with training in whole-cell patch-clamp techniques and advice thereafter; I would have been lost without you all. Marija and Will, thank you for your guidance on all thing's calcium. A special thank you must also go to all of the technical staff and our fantastic lab manager, Emma, for ensuring our days always ran as smoothly as possible. Not least, thank you to everyone who kept lunch times so interesting, there was never a dull day with you guys.

Jess and Vic, thank you for the best holidays I could have wished for, which always seemed to arrive just when I needed them the most. Louise, the endless cups of tea, biscuits and chinwags really got me through the difficult days, and I couldn't have completed this without you. Finally, to my brilliant parents, and my brother, Nick. Thank you for helping me through this journey and always supporting my life decisions. Your unconditional love, encouragement and faith in me always provided the motivation I needed, and for that I'm forever grateful.

Abstract

Dystonia is a hyperkinetic movement disorder caused by co-contraction of antagonistic muscles, resulting in abnormal positions and postures. It is one of the most common and functionally disabling movement disorders, with significant associated lifetime disability. Due to a limited understanding of the underlying pathophysiology of the disorder, there are few therapeutic options available and many patients are resistant to currently available treatments. Myoclonus Dystonia (MD) is caused by mutations to the autosomal dominantly inherited epsilon-sarcoglycan gene (*SGCE*) which encodes the transmembrane ε-sarcoglycan protein. Although *SGCE* is a maternally imprinted gene, mutations are fully penetrant when paternally inherited, making a neuronal cell model of this disorder an ideal platform to further characterise dystonia pathophysiology.

This thesis investigates the impact of loss of expression of the *SGCE* gene upon the development of excitatory cortical neurons *in vitro*. Using the CRISPR/Cas9 gene editing technique, a human embryonic stem cell (hESC) compound heterozygous *SGCE* knockout line (*SGCE*ko) was derived. Differentiation of the *SGCE*ko line towards a cortical glutamatergic neuronal lineage demonstrated no significant differences in neural progenitor cell number and cortical layer markers when compared to their isogenic wild-type control cells.

However, differences between the two lines were observed across multiple functional analyses. These included calcium imaging and whole-cell patch clamp techniques, with higher overall levels of calcium activity, smaller amplitudes, longer rise and shorter fall times in the *SGCE*ko hESC-derived cortical neurons compared to controls using the former technique. A similar pattern of increased excitability was observed in whole-cell patch clamp studies, with *SGCE*ko neurons displaying more frequent and longer trains in response to current step injection, as well as action potentials with shorter half-widths, faster rise times and more rapid rates of repolarisation. Subsequent morphological examination of neurite arborisation also identified differences in neuronal architecture, with *SGCE*ko neurons demonstrating a more extensive and complex dendritic arbor morphology.

Overall, these results suggest that loss of epsilon-sarcoglycan expression in excitatory glutamatergic cortical neurons results in a hyperexcitable and more complex dendritic branching phenotype, which may in part contribute to the observed clinical phenotype. Future work will include replication of these findings in patient-derived induced pluripotent stem cell (iPSC) models, as well as neuronal models of other Mendelian inherited dystonic disorders.

Contents

List of figures

List of tables

List of Abbreviations

aCSF	Artificial Cerebrospinal Fluid
AIS	Axon Initial Segment
AMPA	α-Amino-3-Hydroxy-5-Methyl-4-Isoxazolepropionic Acid
AP	Action Potential
ATP1A3	ATPase alpha 3 subunit gene
BDNF	Brain Derived Neurotrophic Factor
BoNT	Botulinum Toxin
Bp	Base Pair
DBS	Deep Brain Stimulation
CaMKs	Calcium/calmodulin-dependent protein kinases
CBP	CREB-binding protein
cDNA	Complimentary DNA
CNQX	Cyanquixaline
CNS	Central Nervous System
CNVs	Copy Number Variant
CREB	cAMP-response element binding protein
CRISPR	Clustered Regularly Interspaced Short Palindromic Repeats
CSP	Cortical Silent Period
CTIP2	COUP TF1-Interacting Protein 2
CUX1/2	Drosophila Homeobox Cut Gene
D2R	Dopamine-2-Receptor
DAPI	4, 5 Diamidino 2 Phenylindole
DG	Dystroglycan
DGC	Dystrophin-Glycoprotein Complex
DM	Dorsomorphin
DMRs	Differential Methylated Regions
DMRT5	Doublesex and Mab3 Related Transcription Factor 5
DMSO	Dimethyl sulfoxide
DPBS	Dulbecco's Phosphate Buffered Saline
DTI	Diffusion Tensor Imaging
EDTA	Ethylenediaminetetraacetic Acid
EMX2	Empty Spiracles Homeobox 2
ER	Endoplasmic Reticulum

fMRI	Functional magnetic resonance imaging
FOXG1	ForkheadBox G1
FSIs	Fast-Spiking Interneurons
FTD	Frontotemporal Dementia
GAPDH	Glyceraldehyde 3 Phosphate Dehydrogenase
GDNF	Glial Cell Line-Derived Neurotrophic Factor
gRNA	Guide RNA
GW	Gestational Week
hESCs	Human Embryonic Stem Cells
hPSCs	Human Pluripotent Stem Cells
INDELS	Insertions or Deletions
INs	Interneurons
IP$_3$R	Inositol Triphosphate Receptor
IPs	Intermediate Progenitors
iPSCs	Induced Pluripotent Stem Cells
ISI	Inter-spike Interval
KO	Knock-Out
LICI	Long Intracortical Inhibition
LMX1A	LIM Homeobox Transcription Factor 1a
LTD	Long-term Depression
LTP	Long-term Potentiation
MAP2	Microtubule Associated Protein 2
MAPK	Mitogen-activated Kinase
MD	Myoclonus Dystonia
mESCs	Mouse Embryonic Stem Cells
mGluR	Metabotropic Glutamate Receptor
MSNs	Medium Spiny Neurons
MZ	Marginal Zone
nAChR	Nicotinic Acetylcholine Receptor
NCAD	N-Cadherin
NCX	Sodium-Calcium Exchanger
NE	Nuclear Envelope
NEs	Neuroepithelial cells
NESTIN	Neuroectodermal stem cell marker
NEUN	Neuronal Nuclei
NFκB	Nuclear Factor-kappa B
NGS	Next Generation Sequencing

NHEJ	Non-Homologous End Joining
NKX2.1	NK2 Homeobox 1
NMDA	N-Methyl-D-Aspartate
NPCs	Neural Progenitor Cells
NTSD	Non-task-specific Dystonia
OCD	Obsessive Compulsive Disorder
oRGCs	Outer Radial Glial Cells
OTX2	Orthodenticle Homologue 2
PAM	Protospacer Adjacent Motif
PAX6	Paired Box 6
PCR	Polymerase Chain Reaction
PET	Positron Emission Tomography
PFA	Paraformaldehyde
PM	Purmorphamine
PMCA	Plasma Membrane Calcium ATPase
QC	Quality Control
qPCR	Quantitative Polymerase Chain Reaction
RGCs	Radial Glial Cells
RMP	Resting Membrane Potential
RNA-seq	RNA Sequencing
ROIs	Regions of Interest
RyR	Ryanodine Receptor
SATB2	Special AT-Rich Sequence-Binding Protein 2
SERCA	Sarco-/Endoplasmic Reticulum Calcium ATPase
SERT	Serotonin Transporter
SGCE	Epsilon-sarcoglycan gene
SICI	Short Interval Intracortical Inhibition
SNPs	Short Neural Precursor Cells
Svet1	Subventricular Tag 1
SVZ	Subventricular Zone
TBST	Tris Buffered Saline containing 0.1% Tween
TBR1/2	T-Box, Brain 1/2
THAP1	Thanatos-associated Protein Domain-containing apoptosis protein 1
TIF	Tagged Image Format File
TMS	Transcranial Magnetic Stimulation
TRPC	Transient Receptor Potential Type C

TSD	Task-specific Dystonia
TUJ1	Neuron-Specific Class III β-tubulin
VZ	Ventricular Zone
VGCC	Voltage Gated Calcium Channel
WT	Wild-type
wVBM	White Matter Voxel -based Morphometry

1. Introduction

This thesis aims to examine how loss of the epsilon-sarcoglycan (ε-sarcoglycan) protein affects the development, maturation and function of human pluripotent stem cell derived-cortical neurons *in vitro*. In this chapter, I will describe the different forms of dystonia, outlining their clinical features, as well as current models of pathogenesis and treatment. I will go on to discuss the development of distinct anatomical brain regions, and finally the use of pluripotent stem cell models to investigate Myoclonus Dystonia pathophysiology.

1.1. Dystonia Overview

Dystonia is a hyperkinetic movement disorder characterised by involuntary muscle contractions of antagonistic muscle groups leading to twisting, repetitive movements and abnormal postures (Obeso *et al.*, 1983). Hermann Oppenheim first described the disorder in 1991 as *"dystonia musculorum deformas"* (Oppenheim and H., 1911). Remarkably, Oppenheim hypothesised that "hereditary burden likely plays a major role" in the aetiology of the disorder, regardless of the lack of a clear family history, likely providing the first indication of the role of genetics in dystonia (Klein and Fahn, 2013). Since this initial description, we have come to understand that dystonia is highly heterogeneous in clinical phenotype and underlying aetiology (Phukan *et al.*, 2011). It has been estimated that the prevalence of dystonia is between 15 to 30 per 100,000 population, rising to 732 per 100,000 in a random sample of the population over 50 years of age (Epidemiological Study of Dystonia in Europe (ESDE) Collaborative Group, 2000). These numbers are thought to be grossly underestimated due to the general low level of recognition of the clinical features and underdiagnosis of dystonia. This is reflected in the time taken to diagnose dystonia following onset of symptoms, which is estimated to take on average four to six years, even for the most common types of dystonia (Jog *et al.*, 2011; Tiderington *et al.*, 2013; Charles *et al.*, 2014). More genetic testing could potentially aid in diagnosing dystonia at an earlier stage.

Dystonic movements observed in patients are generally patterned, involve consistent muscle groups and can exhibit motor overflow into adjacent muscles. Dystonic movements can be triggered or exacerbated by voluntary movements. Cerebral imaging studies have shown no evidence of structural abnormalities in those with primary dystonia, suggesting that dystonia is a disorder of impaired or disorganised neuronal function (Geyer and Bressman, 2006; Breakefield *et al.*, 2008).

1.1.1. Classification of dystonia

The classification system for different forms of dystonia has been updated on numerous occasions as understanding of the disorder has improved. The current classification system is based upon clinical characteristics (axis I) and aetiology (axis II), summarised in **Table 1.1** (Albanese *et al.*, 2013).

1.1.1.1. Axis I: clinical features

Age at onset is used as a key characteristic in dystonia classification, being sub-divided into five groups: infancy (0-2 years), childhood (3-12 years), adolescence (13-20 years), early adulthood (21-40 years) and late adulthood (>40 years) (Albanese *et al.*, 2013). More severe phenotypes, which are more likely to progress over time and become generalised, are more typically seen in the childhood-onset forms. Those whose symptoms develop after adolescence more typically experience focal dystonia involving the cranio-cervical musculature, with a lower rate of subsequent generalisation (Albanese *et al.*, 2013). However, in spite of the importance of age at onset in being able to classify dystonic disorders, it is often limited by recall and compounded by the delay between symptom onset and diagnosis (Phukan *et al.*, 2011).

The body regions affected by dystonia are also important in classification. *Focal dystonias* are defined when symptoms are localised to a single body region, for example cervical dystonia (neck), blepharospasm (eyes), and hand dystonia (writer's cramp). *Segmental dystonia* refers to involvement of multiple contiguous muscle groups, whereas if multiple non-contiguous muscle groups are affected, it is denoted as *multifocal dystonia*. Unilateral body involvement is termed *hemi-dystonia,* and involvement of the trunk and at least two other body regions, *generalised dystonia.* Dystonia can also be classified as to whether it occurs in isolation, or in combination with other movement disorder(s), such as myoclonus, parkinsonism or spasticity (combined dystonia) (Albanese *et al.*, 2013; Balint and Bhatia, 2014).

Table 1.1 Classification of dystonia (Albanese et al., 2013)

Axis I: Clinical characteristics	
Age at onset	• Infancy: birth to 2 years • Childhood: 3 to 12 years • Adolescence: 13 to 20 years • Early adulthood: 21 to 40 years • Late adulthood: >40 years
Body distribution	• Focal • Segmental • Multifocal • Generalised • Hemidystonia
Temporal pattern	• Disease course: static; progressive. • Variability: persistent; action-specific; diurnal; paroxysmal
Associated features	• Isolated • Combined • Additional neurological/systemic features
Axis II: Aetiology	
Origin	• Inherited: autosomal dominant; autosomal recessive; X-linked recessive; mitochondrial • Acquired: brain injury; cerebrovascular; infection; drug; toxic; neoplastic; psychogenic • Idiopathic: sporadic; familial
Neuropathology	• Neurodegeneration • Structural lesions • Neither

1.1.1.2. Axis II: aetiology

Inherited, acquired and idiopathic dystonias form the principle divisions within the aetiology axis (Albanese *et al.*, 2013). Acquired dystonias are often caused by damage or degeneration of the central nervous system (CNS), for example after brain injury or stroke, or exposure to certain drugs. Inherited dystonias have a defined genetic cause, e.g., primary generalised dystonia (DYT1), whereas idiopathic dystonias have no known clear cause.

1.2. Genetic forms of dystonia

Over the past two decades, significant progress has been made in identifying the causative genes of inherited dystonias. Next generation sequencing (NGS) has been pivotal in this process, allowing higher throughput genetic analysis and genetic comparison of multiple unrelated, but clinically phenomenologically similar cases. In 2012, four dystonia genes were identified by NGS (*CIZ1*, *ANO3*, *GNAL* and *TUBB4A).* At the time of writing, there are 30 genetically defined dystonic disorders, as described in **Table 1.2**. Some of the most extensively studied monogenic dystonias, as evidenced by the quantity of PubMed publications, are described below. These dystonias are reviewed as they are a selection of the most common forms of dystonia and are generally considered to be more treatable than other forms. Myoclonus dystonia (DYT11) is discussed in detail in **Section 1.5.**

Loci for candidate genes have historically been named using the human gene organisation (HUGO) convention, with the prefix identifying the main aspect of the clinical phenotype (i.e., DYT for dystonia), followed by a distinct number for each new loci assigned (e.g. DYT1, DYT2, DYT3, etc.). There are, however, several limitations in using this nomenclature. Inconsistent use and numerous errors have resulted in a perplexing and unclear numbering system. Some DYT labels are associated with multiple genes (e.g. DYT5 – *GCH1, TH* and *SPR*) (Wijemanne and Jankovic, 2015), whereas in other cases, individual genes have been assigned multiple DYT labels (e.g. *SLC2A1* – DYT9 and DYT18). In other cases, incorrect assignment of DYT loci has led to retrospective deletion. This was true for DYT14, which was erroneously numbered, before discovering the gene responsible, *GCH1,* was the same gene responsible for DYT5 (Wider *et al.*, 2008). A new system has been proposed whereby the numbering system will be replaced with the actual gene name, solving several problems highlighted above with the HUGO nomenclature system (Marras *et al.*, 2016).

DYT1: Early-onset generalised dystonia

The first identified and most extensively investigated of the genetic dystonias, DYT1, is caused by a mutation to the *TOR1A* gene that is inherited in an autosomal dominant fashion with a reduced penetrance of approximately 30% (Ozelius *et al.*, 1997). Clinical presentation is typically of an initial focal limb dystonia of onset in childhood or adolescence (5-28 years, mean age at onset 13 years), with subsequent involvement of other body regions, although usually sparing the cranio-cervical region (Bressman *et al.*, 2000). The most common *TOR1A* mutation is a 3-base-pair (bp) in-frame deletion (guanine-adenine-guanine (GAG)), that results in removal of a single glutamate residue from the C-terminus of the encoded TorsinA protein (Ozelius *et al.*, 1997). As a member of the AAA+ superfamily of ATPase proteins, TorsinA functions as a molecular chaperone and has a role in numerous cellular functions, including folding, assembly, and/or trafficking of polytopic proteins to the cell membrane. Wild-type TorsinA is located within the endoplasmic reticulum, whereas its mutant form exhibits enhanced translocation to the nuclear envelope (NE) and is thought to be involved with remodelling of the NE (Goodchild and Dauer, 2004; Naismith *et al.*, 2004). There is also evidence for involvement of wildtype TorsinA in neurite growth (Hewett *et al.*, 2006), synaptic vesicle recycling (Granata *et al.*, 2008), impaired dopamine release, altered tyrosine kinase activity (O'Farrell *et al.*, 2009) and lipid metabolism (Grillet *et al.*, 2016). More recently, using a genome-wide RNAi screen, deficiencies of the eIF2α signalling pathway have also been thought to contribute to DYT1 pathogenesis, with evidence of an attenuated integrated stress response and elevated basal levels of a negative feedback regulator of the eIF2α pathway. The eIF2α pathway could therefore be a potential promising biological target in the diagnosis and treatment of DYT1 dystonia (Rittiner *et al.*, 2016).

DYT6: Adolescent-onset dystonia of mixed type

Thanatos-associated protein domain-containing apoptosis protein 1 (*THAP1*) was the second dystonia gene to be identified and is responsible for causing the DYT6 form of dystonia. DYT6 is inherited in an autosomal dominant fashion with evidence of reduced penetrance (57-60%), independent of sex (Bressman *et al.*, 2009; Ozelius and Bressman, 2011). It is an adolescent-onset dystonia that typically affects the upper limbs initially, before progressing to involve the head or neck, with symptoms often becoming generalised or multifocal at later stages (Bressman *et al.*, 2009). *THAP1* is a transcription factor expressed throughout the brain and thought to be involved in regulating cell proliferation through the pRB/E2F cell cycle target genes (Clouaire *et al.*, 2005; Cayrol *et al.*, 2007). Despite widespread expression of the mutated protein, the disease phenotype is restricted to the central nervous system. Wildtype *THAP1* binds the *TOR1A* promotor, with evidence for repression of *TOR1A* expression upon *THAP1* binding (Gavarini *et al.*, 2010; Kaiser *et al.*, 2010). In addition, there is also evidence for a role of THAP1 in the timing of myelination initiation during CNS maturations (Yellajoshyula *et al.*, 2017).

DYT5a: Progressive DOPA-responsive dystonia with diurnal variation

Approximately 60-80% of autosomal dominant DOPA-responsive dystonia are accounted for by a mutation to the *GCH1* gene, encoding the enzyme GTP cyclohydrolase 1 (Furukawa, 2004). Typically, symptoms first appear during childhood, often with lower limb dystonic posturing as the presenting feature (Nygaard *et al.*, 1990). The dystonic features then usually spread to the upper body, such that by adolescence, symptoms are generalised, and diurnal variation is typically observed (Segawa, Nomura and Nishiyama, 2003). GTP cyclohydrolase 1 is the rate-limiting enzyme in the biosynthesis of tetrahydobiopterin, an essential cofactor for tyrosine hydroxylase, needed to synthesise dopamine. *GCH1* mutations cause a measurable reduction in enzyme activity to <20% of normal levels, resulting in a deficiency of dopamine (Ichinose and Nagatsu, 1997; Hwu *et al.*, 2000). Levodopa, even at low doses, is proficient at improving symptoms sustainably, with 70-100% improvement in clinical symptoms reported.

DYT12: Rapid-onset dystonia parkinsonism

DYT12 is characterised by abrupt (hours to weeks) onset of dystonia followed by the development of parkinsonian features, in response to physical or psychological stressors. It is caused by a mutation to the ATPase alpha 3 subunit gene (*ATP1A3*), which encodes the $\alpha3$ subunit of the Na^+, K^+-ATPase and is responsible for pumping Na^+ out of the cell and K^+ into the cell, both against their concentration gradients (de Carvalho Aguiar *et al.*, 2004; Sweney, Newcomb and Swoboda, 2015). It has been suggested that mutations to *ATP1A3* reduce $\alpha3$ affinity for Na^+ which subsequently affects ion transport and may impair cell viability (Rodacker, Toustrup-Jensen and Vilsen, 2006; Blanco-Arias *et al.*, 2009). This form of dystonia often develops in a rostral-caudal pattern and doesn't tend to progress further (Brashear *et al.*, 2007). Patients do not respond to levodopa or pallidal deep brain stimulation, despite clinical parkinsonism (Deutschländer *et al.*, 2005; Kamm *et al.*, 2008). It is believed cerebellar dysfunction may be central to rapid-onset dystonia parkinsonism, with loss of $\alpha3$ activity in the cerebellum of mice causing dystonia with abnormal Purkinje cell firing (DeAndrade *et al.*, 2011; Ikeda *et al.*, 2013; Fremont *et al.*, 2014a).

Table 1.2 Genetic forms of dystonia

Disorder (MIM number)	Epidemiology	Causative Gene/ Chromosome Locus	Mode of Inheritance	Motor Phenotype	Non-Motor Phenotype	Additional Clinical Characteristics
DYT1 (605204)	Mutation Frequency: 0.17/100,000	GAG deletion of TorsinA; 9q34.11	AD with reduced penetrance (~30%)	Range from mild focal dystonia to more severe generalised form.	Early onset recurrent major depression as an independent expression of the DYT dystonia mutation.	Unknown.
DYT2 (224500)	Unknown	*HPCA;* 1p35.1	Probable AR	Initially affects distal limbs with potential successive generalisation. Slowly progressive but mild overall.	Unknown.	Identified in Sephardic Jewish and Spanish gypsy families.
DYT3 XDP/Lubag's disease (313650)	Worldwide: <1/1,000,000 Philippines: overall 1/322,000; men 1/4000	*TAF-1;* Xq13.1	X-Linked	Focal/segmental dystonia progressing to generalised form. Parkinsonism features in later stages.	Depression, anxiety, social phobia, agoraphobia.	Unknown.
DYT4 Whispering dystonia (602662)	Unknown	*TUBB4;* 19p13.3	AD	Cranio-cervical dystonia with prominent laryngeal dystonia, commonly becoming generalised.	Unknown.	Thin face and body habitus. Alcohol and propranolol can prompt a partial response.
DYT5a Segawa's disease (600225)	0.5/1,000,000	*GCH1;* 14q22.2	AD with reduced penetrance	Lower limb dystonia progressing to generalised form with diurnal fluctuation. Parkinsonism, dystonic tremor.	Depression, anxiety, OCD, eating disorders. Lower intellectual functioning. Difficulties initiating and maintaining sleep.	DOPA-responsive.
DYT5b (605407)	Rare	*TH;* 11p15.5	AR	Encephalopathy apparent in perinatal period. Hypokinesia and rigidity.	High rates of mental retardation.	DOPA-responsive.
DYT5b (612716)	Rare	*SPR;* 2p13.2	AR	Onset in 1st year of life. Diurnal fluctuation, ataxia and myoclonus.	Inattention, irritability, anxiety, hyperactivity, aggression, OCD. Often language delay and learning disability/mental retardation. Sleep disturbance includes hypersomnolence, and difficulties initiating and maintaining sleep.	Cognitive delay, severe neurological dysfunction. Dopamine and serotonin deficiencies in cerebral spinal fluid.
Vesicular Monoamine	Rare	*SLC18A2;* 10q25.3	AR	Hypotonia, parkinsonism, dystonia.	Depression.	Developmental delay. Dopamine agonists improve motor

Transporter 2 (193001)						symptoms, L-DOPA worsens symptoms
Aromatic L-amino acid decarboxylase deficiency (608643)	Rare	*DDC;* 7p12.2-p12.1	AR	Hypotonia, oculogyric crises.	Irritability, emotional lability.	Delayed motor development. Often delayed speech and cognitive development.
Dopamine Transporter Deficiency Syndrome (613135)	Rare	*SLC6A3*; 5q15.33	AR	Infantile dystonia-parkinsonism.	Irritability.	Unknown.
DYT6 (609520)	Unknown	*THAP1*; 8p11.21	AD (approx. 60% penetrance)	Adult-onset torsion dystonia. Prominent cranio-cervical and laryngeal involvement, causing speech difficulties.	Unknown.	More common in women than men.
DYT7 (602124)	Unknown	No gene as yet identified; 18p	Unknown	Focal dystonia, localised to the upper body, typically neck, eyes or hands.	Unknown.	Unknown.
DYT8: Paroxysmal Non-Kinesigenic Dyskinesia (609023)	Rare	*MR-1*; 2q35	AD	Sporadic attacks lasting up to an hour. Dystonia, chorea, ballism, blepharospasm.	Unknown.	Alcohol, coffee, stress and exercise can trigger attacks.
DYT9 (601042)	Rare	*SLC2A1*	AD	Paroxysmal choreoathetosis and spastic paraplegia.	Cognitive impairment.	Seizures, migraine headaches, and ataxia.
DYT10: Paroxysmal Kinesigenic Dyskinesia (614386)	1/150,000	*PRRT2*; 16p11.2	AD (incomplete penetrance)	Attacks involve isolated or mixed dystonia, in combination with chorea, athetosis and ballism.	Depression, ADHD, behavioural disturbance. Mental retardation present in some patients.	Linked to further clinical phenotypes: ICCA, episodic ataxia, hemiplegic migraine.
DYT11 Myoclonus Dystonia (604149)	Rare	*SGCE*; 7q21.3	AD (reduced penetrance due to maternal imprinting)	Onset in first or second decade of life. Myoclonic jerks largely affect proximal muscles. Dystonia, presenting as torticollis or writer's cramp, affects most patients.	Anxiety, especially presenting as social phobia and panic disorder. OCD, GAD, alcohol addiction, depression, personality disorder.	Alcohol responsive.
DYT12: Rapid-onset Dystonia	Rare	*ATP1A3*; 19q13.2	AD with reduced penetrance	Rapid onset in young adulthood of raustro-caudal pattern of dystonia and gait instability.	Psychosis, anxiety, depression, suicidal ideation, mood disorders, substance abuse.	Symptoms are often elicited by a physical or psychological stressor

Parkinsonism (182350)						such as overexertion, heat, fever or trauma.
DYT13 (607671)	Unknown	No gene as yet identified; 1p36.32-p36.13	AD	Idiopathic torsion dystonia typically developing in upper body and cranio-cervical muscles and later progressing to other regions.	Unknown.	Identified in a non-Jewish Italian family, spanning 3 generations.
DYT15 (607488)	Reported in a single 4 generation family	No gene as yet identified; 18p11	Possible AD	Myoclonus dystonia involving trunk, hands upper limbs and axial muscles.	Unknown.	Symptoms are alcohol responsive.
DYT16 (603424)	Reported in two consanguineous Brazilian families and a single German case	*PRKRA*; 2q31.2	AR	Two types: 1) pure generalised dystonia, 2) dystonia-parkinsonism.	Aggression.	Cognitive impairment reported in two cases.
DYT17 (612406)	Reported in a single consanguineous Lebanese family	No gene as yet identified; 20p11.2-q13.12	AR	Primary focal torsion dystonia, initiating with torticollis and later spreading to become generalised or segmental.	Unknown.	Unknown.
DYT18: GLUT1 Deficiency Syndrome 2 (138140)	1 in 90,000	*SLC2A1*; 1p34.2	AD	Childhood onset, exercise-induced dyskinesia, characteristically distal lower limb dystonia. Hunger and exertion can also trigger episodes.	Cognitive impairment, difficulties in verbal learning, attention and frontal lobe functions.	Associated with ataxia, spasticity, epileptic seizures, encephalopathy and haemolytic anaemia.
DYT20: Paroxysmal Non-Kinesigenic Dyskinesia 2 (138140)	Reported in a single 4-generation Canadian family	No gene as yet identified; 2q31	AD	Episodic dystonia symmetrically affecting the hands and feet.	Unknown.	Episodes generally last 2 to 5 minutes. Alcohol, caffeine or excitement not apparent causes.
DYT21 (614588)	Reported in a single large Swedish family	No gene as yet identified; 2q14.3-q21.3	AD (incomplete penetrance)	Pure torsion dystonia. Blepharospasm and torticollis are prevalent. Focal manifestations progressing to generalised symptoms.	Unknown.	Deep brain stimulation of the pallidus effective in some patients.
DYT23 (614860)	Reported in a single German family	*CACNA1B*; 9q34.3	AD	Adult-onset cervical dystonia. Head and limb tremor present.	Panic attacks and hyperventilation syndrome are variable features.	Unknown.
DYT24 (615034)	Reported in a single British family and 3 additional unrelated individuals	*ANO3*; 11p14.3-p14.2	AD	Adult-onset focal dystonia, predominantly involving the neck, laryngeal muscles and	Unknown.	Unknown.

				muscles of the upper limbs. Progresses to the orofacial region.		
DYT25 (615073)	Reported in 28 individuals from 8 families	*GNAL*; 18p11.21	AD	Adult onset focal dystonia, predominantly affecting the neck. Generally progresses to involve face and laryngeal muscles.	Unknown.	Levodopa treatment not beneficial.
DYT26 (616398)	Reported in 2 unrelated families	*KCTD17*; 22q12.3	AD	Onset in the first two decades of life. Presents as myoclonic jerks affecting upper limbs. Progressive, patients later develop dystonia that predominantly affect cranio-cervical regions.	Anxiety, social phobia, depression.	Unknown.
DYT27 (616411)	Reported in 3 unrelated German families	*COL6A3*; 2q37.3	AR	Onset in the first or second decade of life. Segmental, isolated dystonia typically affecting the cranio-cervical region and upper limbs.	Unknown.	Some patients lose the ability to mobilise independently.
DYT28 (617284)	Reported in 31 unrelated individuals worldwide	*KMT2B*; 19q13.12	AD	Progressive dystonia presenting in the first decade of life. Initially affects the lower limbs, later progressing to upper limbs, neck and orofacial region.	Anxiety, ADHD, obsessive compulsive traits, self-harm behaviours.	Elongated face with bulbous nose and abnormal eye movements. Mild/moderate cognitive impairment, with mild intellectual disability and seizures.
DYT29 (617282)	Reported in 7 individuals from 5 unrelated families	*MECR*; 1p35.3	AR	Onset in first decade of life. Optic atrophy and basal ganglia abnormalities.	Unknown.	Cognition unaffected. Changes in bilateral symmetrical basal ganglia signal intensity on magnetic resonance imaging.

Key: AD: Autosomal Dominant, ADHD: Attention Deficit Hyperactivity Disorder, AR: Autosomal Recessive, GAD: Generalised Anxiety Disorder, ICCA: infantile convulsions with choreoathetosis, OCD: Obsessive-Compulsive Disorder.

1.3. Pathophysiology of dystonia

1.3.1. Neurophysiology

1.3.1.1. Loss of inhibition

Dystonia pathophysiology has long been thought to be associated with a loss of inhibition, which is thought to occur at multiple levels within the central nervous system. Focal hand dystonias display loss of reciprocal inhibition of spinal and brainstem reflexes, and blepharospasm shows abnormalities of the blink reflex recovery cycle. There is also evidence of loss of inhibitory activity surrounding excitatory neurons, which may explain the spread of dystonia to neighbouring body parts observed clinically. An overview of motor circuitry within the brain, describing excitatory and inhibitory pathways is shown in …..

Transcranial magnetic stimulation (TMS), a technique that uses electromagnetic induction to stimulate desired areas of the brain in a non-invasive manner, has been used to explore these patterns of inhibition. The brief electromagnetic pulses are generated by an insulated coil which is placed over the scalp, allowing them to pass through the skull and into the brain. By exploiting TMS to investigate the excitability of connections within and among motor areas of the cortex, comprehensive information of the cortical pathophysiology of dystonia has been established. Although variable results are observed both within and between dystonia subtypes, some of the most consistent changes observed include i) loss of short interval intracortical inhibition (SICI), ii) shortened cortical silent period (CSP) and iii) reduced long intracortical inhibition (LICI). Furthermore, increased strength of dystonic contraction has been associated with a shorter cortical silent period (Udupa and Chen, 2019). A reduction in SICI has also been identified in unaffected body parts of dystonia patients, as well as in non-manifesting gene carriers. This suggests that an elevated threshold for triggering inhibition exists in dystonia, which leads to increased excitatory activity. Conversely, a similar phenomenon is observed in the affected body parts of those with functional dystonia, as well as other forms of movement disorders. This therefore potentially indicates a consequence rather than cause of the dystonia (Hallett, 2011).

1.3.1.2. Aberrant neural plasticity

Neural plasticity describes the capability of the brain to reorganise itself by forming new connections in response to both internal and external factors. Excessive synaptic plasticity, potentially relating to hyperexcitability, could be critical to dystonia pathophysiology. Animal models have shown both increased long-term potentiation (LTP) and reduced long-term depression (LTD) in corticospinal projections. DYT1 transgenic mice display an increase in LTP at cortico-striatal synapses, together with loss of LTD and synaptic depotentiation during *in vitro* slice recordings. Over-trained, repetitive movements have been shown to have the capacity to remodel somatosensory cortical maps in animal

models, leading to sensory de-differentiation. This de-differentiation phenomenon is also observed in the somatosensory cortex (S1 and S2), basal ganglia and cerebellum in individuals diagnosed with focal hand dystonia (Perruchoud *et al.*, 2014).

Deep brain stimulation (DBS) is likely to result in symptomatic improvement in individuals with dystonia due to mechanisms involving synaptic plasticity. Although movement disorders such as Parkinson's disease and essential tremor see the benefits of DBS quickly, oftentimes, it takes months to years for patients with dystonia to see any motor improvement. Studies exploiting the paired-associated stimulus technique, alongside DBS stimulation have shown a decrease in LTP-like plasticity, with maximal clinical improvement following the maximal reduction to LTP. This suggests DBS works to normalise the abnormal neuronal plasticity observed in dystonic disorders (Udupa and Chen, 2019).

1.3.1.3.   Disrupted sensory-motor integration

The classic model for cortical connectivity is one of subdivision of the cortex into columns, with neurons in each column maintaining a distinct pattern of connectivity that is maintained by local GABAergic inhibitory connection in adjacent units. There is, however, conflicting evidence as to whether one, or both, of spatial and temporal sensory discrimination represent the primary defect in dystonia. A case-control study focusing on individuals diagnosed with cervical dystonia looked to assess spatial and temporal aspects of cortical inhibition in motor and somatosensory systems of the hand. Only somatosensory spatial inhibition showed significant differences, suggesting that cervical dystonia may be associated with abnormalities in spatial sensory processing. Lateral inhibition, mediated predominantly by GABAergic interneurons, is thought to shape the cortical receptive field. Disturbance to these local inhibitory cortical circuits may potentially underlie these abnormalities in spatial sensory processing (Ganos *et al.*, 2018).

There is recent evidence, however, that other circuit-based changes may also be contributing to abnormal spatial sensory processing. One study used high-frequency repetitive stimulation, a mechanism which has been shown to shorten somatosensory temporal discrimination in healthy individuals potentially due to increased excitation in inhibitory circuits within the somatosensory cortex. They found that in individuals diagnosed with cervical dystonia, when this technique was applied to a body part not affected with dystonia, the opposite was seen with worsening of somatosensory temporal discrimination correlated with reduced measures of inhibition in the somatosensory cortex (Erro *et al.*, 2018). Similar results are observed in unaffected mutation carriers of dystonia causing genes, potentially reflecting an endophenotype, or a pre-disposition towards the generation of dystonia.

1.3.1.4. Role of the cerebellum

The role of the cerebellum in dystonia pathophysiology has become more apparent over recent years. Several animal models of cerebellar dysfunction phenotypically resemble dystonia. In these models, the dystonic features worsen with disruption to the basal ganglia and improve with disruption to the thalamic relay nuclei between the cerebellum and striatum (Kaji, Bhatia and Graybiel, 2018). Furthermore, abnormal-burst firing of the cerebellar Purkinje neurons is observed in electrophysiological studies of rodent dystonia models (Jinnah and Hess, 2018). Rapid-onset Dystonia Parkinsonism (DYT12) is caused by a loss of function mutation in sodium pumps. DYT12 can be pharmacologically induced in mice by partially blocking sodium pumps in the cerebellum with ouabain (Fremont *et al.*, 2014b). Conversely, conditional knock-out of dystonia causing genes in the cerebellum has not recapitulated a dystonic phenotype and clinically, there are few patients with dystonia due to cerebellar legions, and dystonic symptoms can be alleviated through DBS to the basal ganglia.

A disynaptic connection between the cerebellar nuclei and the basal ganglia via the intralaminar thalamic nuclei has been identified through anatomical studies in rodents and primates. The cerebellum has been found to rapidly modulate striatal activity via this disynaptic pathway in murine studies, with high frequency stimulation of the neocortex depressing cortico-striatal responses (LTD), with this changing to enhance synaptic efficiency (LTP) when the stimulation was applied to the cerebellum (Chen *et al.*, 2014).
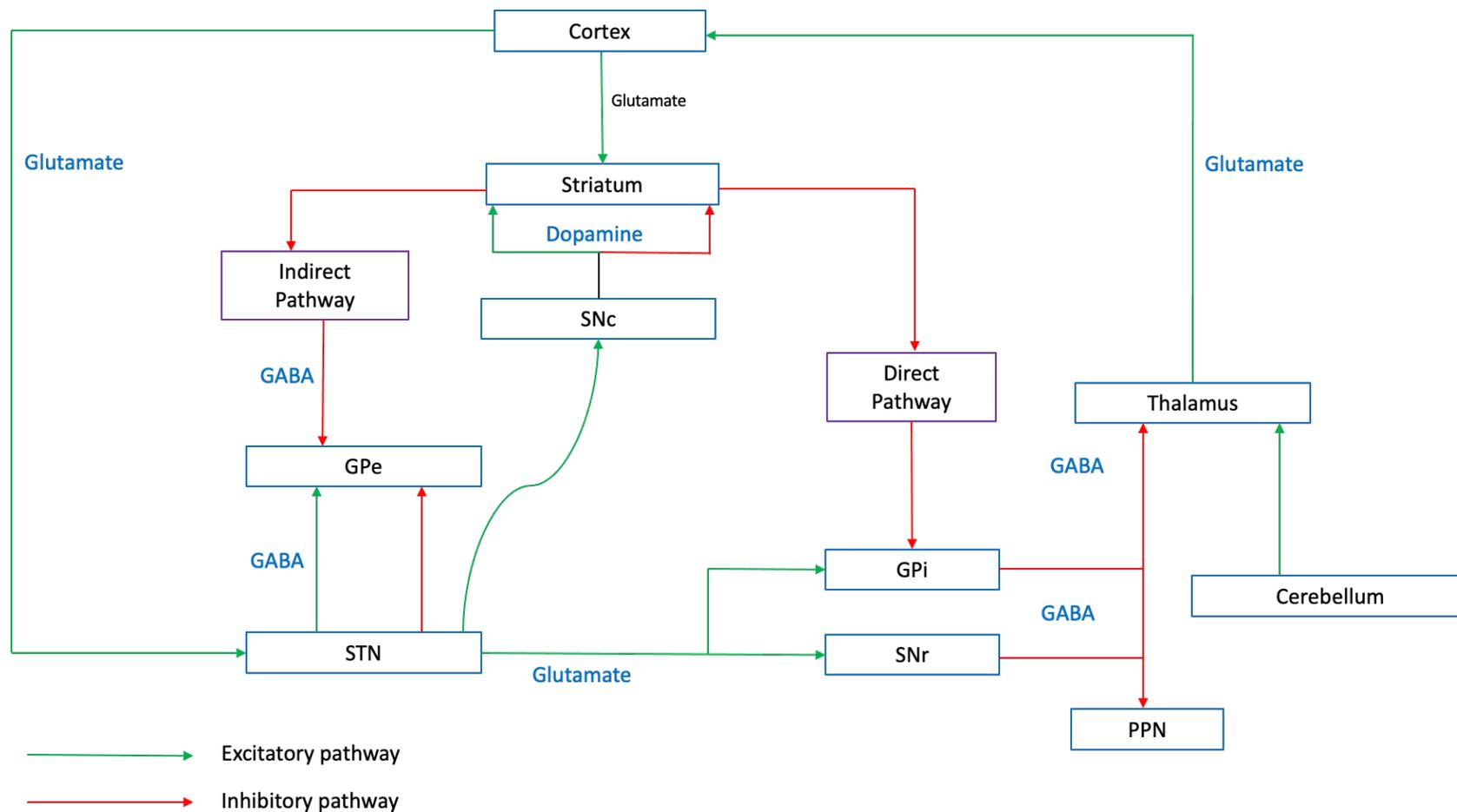
Figure 1.1 Schematic view of the cortico-basal ganglia-thalamus network

An overview of the cortico-basal ganglia-thalamus networkGreen arrows represent excitatory pathways, whereas red arrows represent inhibitory pathways. GPe: Globus Pallidus pars Externa; GPi: Globus Pallidus pars Interna; PPN: Pedunculopontine Nucleus; SNc: Substantia Nigra pars Compacta; SNr: Substantia Nigra pars Reticulata; STN: Subthalamic Nucleus.

1.3.1. Neuroimaging

Over the last decade, a range of structural, functional and molecular imaging techniques have demonstrated changes predominantly in the sensorimotor cortex, basal ganglia and cerebellum in patients with dystonia. In addition, techniques such as positron emission tomography (PET) and functional magnetic resonance imaging (fMRI), have provided insights into the widespread alterations in functional brain activity and structural changes in patients with primary dystonia (Zoons *et al.*, 2011).

Diffusion tensor imaging (DTI) can be used to investigate alterations of brain white matter and fibre tract characteristics *in vivo*. Primary dystonia is widely regarded to be neurodevelopmental circuit disorder, with disruption to cortico-striato-pallido-thalamo-cortical and cerebello-thalamo-cortical pathways. DTI and probabilistic tractography techniques have suggested reduced connectivity of the cerebello-thalamo tracts in individual with inherited forms of dystonia (Argyelan *et al.*, 2009). Additional studies have identified increased activation of the sensorimotor cortex and supplementary motor area, suggesting the abnormalities in cerebellar pathway development are associated with loss of inhibition at the cortical level (Carbon *et al.*, 2010). A reduction of fractional anisotropy, a measure of axonal integrity and coherence, has been identified in patients with primary dystonia suggesting disturbance in cerebello-thalamo-cortical pathways. Some studies have suggested that this loss may provide protection against increased cortical activity driven by changes in the cerebellar-striatal tracts, whereas others suggest that abnormalities in the cerebello-thalamo pathway may increase the risk of developing dystonia (Carbon *et al.*, 2008). Similar findings have also been seen in patients with DYT27 dystonia, with evidence of altered white matter architecture, particularly in parts of the cerebello-thalamo-cortical network such as midbrain, pons, cerebellar peduncles, thalamus, internal capsule and frontal and parietal subcortical regions in comparison to healthy controls (Jochim *et al.*, 2017).

MRI tractography studies have also demonstrated the importance of the pallido-thalamic tracts in dystonia, particularly in the context of Deep Brain Stimulation (DBS), with those with closer placement of the electrodes to these tracts achieving a better clinical outcome (Volkmann *et al.*, 2014; Rozanski *et al.*, 2017). DTI, in combination with white matter voxel-based morphometry (wVBM) has been used to study macro- and micro- structural white matter changes in DYT11 mutation carriers. A comparison between 16 clinically affected DYT-11 mutation carriers and 18 control subjects revealed that there is an increase in white matter volume and fractional anisotropy, along with a decrease in mean diffusivity in the subthalamic area of the brainstem, including the red nucleus, in DYT11 patients compared to controls (van der Meer *et al.*, 2012).

There is growing evidence that the mechanisms underlying task-specific (TSD) and non-task-specific (NTSD) dystonias may differ, with distinct microstructural patterns potentially forming radiological biomarkers. Measurement of grey matter volumetric changes during task-specific dystonias (n= 24; 12 writer's cramp, 12 laryngeal dystonia) compared to focal dystonia (n=21; 11 cervical dystonia, 10 blepharospasm) and healthy controls (n=24) demonstrated alterations in the sensorimotor cortices (primary somatosensory cortex, middle frontal gyrus, superior/inferior temporal gyrus, middle/posterior cingulate cortex, occipital cortex, striatum and cerebellum) in those with TSD and left cerebellum (lobule VIIa) in non-task specific dystonias (Ramdhani *et al.*, 2014; Piccinin *et al.*, 2015). Distinct pathophysiological pathways also appear to underlie dystonia subtypes involving the same body region. A study comparing cases of sporadic laryngeal dystonia (n=60), familial cases (n=24) and healthy controls (n=30) found greater cerebellar involvement in the processing of altered temporal discrimination in those with the familial form of the disorder, whereas the putamen and sensorimotor cortex appeared of greater importance in sporadic cases (Termsarasab *et al.*, 2016).

Task-specific dystonias provide a unique opportunity to investigate both dystonic and non-dystonic states in the same individual. Resting state imaging has demonstrated significantly lower functional connectivity in the cerebellum, thalamus, basal ganglia and frontal cortex in those with writer's cramp compared to healthy controls (n=19 patients, 20 controls) (Bharath *et al.*, 2015). Use of a sequential finger-tapping exercise in the unaffected hand of a similar cohort of patients (n=22 patients, 28 controls), found lower blood oxygen level dependent (BOLD) activity in the anterior right putamen and left globus pallidus, suggesting involvement of the anterior basal ganglia loops in the altered signalling pathways (Zeuner *et al.*, 2015).

Recent studies provide evidence that dystonia is caused by altered communication between the basal ganglia and cerebellar loops (Bologna and Berardelli, 2017). An fMRI study undertaken in patients with cervical dystonia (n=30 patients, 25 controls) involving a visuospatial task demonstrated reduced activation in the posterior cerebellar lobules, premotor, parietal and visual cortices, as well as reduced cerebellar connectivity with the basal ganglia and dorsolateral prefrontal cortex (Filip *et al.*, 2017). Using the same imaging technique, comparison between 16 patients with cervical dystonia and 16 healthy controls, again demonstrated altered motor-related activity in the primary somatosensory cortex, cerebellum, dorsal premotor, posterior parietal and occipital cortices, as well as a correlation between dystonia symptom severity and cerebellar (increased) and somatosensory cortex (decreased) activity (Burciu *et al.*, 2017).

Imaging investigation of genetically homogeneous cohorts has focused on those with torsinA (DYT1) mutations. A study investigating symptomatic and asymptomatic mutation carriers (n=7 manifesting DYT1 cases, 10 asymptomatic DYT1 mutation carriers, 26 healthy controls) using resting state fMRI

identified augmented connectivity in both the dorsal attention network, which comprises functionally connected brain regions including visual motion area, frontal eye fields, superior parietal lobule, intraparietal sulcus, and ventral premotor cortex and the left fronto-parietal network, which includes bilateral precentral gyrus, supplementary motor area, and middle frontal gyrus (areas under the feedback electrode) as well as dorsolateral prefrontal cortex, insula, supramarginal gyrus, and inferior parietal lobule (Premi *et al.*, 2016). Imaging studies of Dyt1 knock-in mice have provided similar findings with increased functional connectivity across the striatum, thalamus and somatosensory cortex, together with reduced functional connectivity in the motor and cerebellar cortices (DeSimone *et al.*, 2016).

PET imaging has tended to focus on dopaminergic neurotransmission, with several studies identifying altered D2/D3 receptor binding and dopaminergic release in several forms of idiopathic dystonia. Reduced striatal dopamine uptake has also been a consistent finding of these studies, observed in isolated idiopathic dystonias (Berger *et al.*, 2007), cervical dystonia (Hierholzer *et al.*, 1994) and genetically determined forms such as DYT1 (*TOR1A*) (Asanuma *et al.*, 2005), DYT6 (*THAP1*) (Carbon *et al.*, 2009) and DYT11 (*SGCE*) (Beukers *et al.*, 2009). Numerous studies have suggested this decrease in striatal dopamine uptake to be the result of reduced striatal D2-like binding (Perlmutter *et al.*, 1997; Asanuma *et al.*, 2005; Carbon *et al.*, 2009; Xu *et al.*, 2010). However, studies using the highly selective dopamine 2 receptor (D2R) radioligand N-methyl-benperidol have suggested that the reduction in striatal dopamine uptake may be caused by a reduction in striatal D3R rather than D2R (Karimi *et al.*, 2011). Additionally, focus on the distribution of dopamine D2-like receptors has shown a potential somatotropic distribution, with variation observed dependent on the body part affected with dystonia (Black *et al.*, 2014).

More recently studies have sought to investigate the role of the serotonergic system in dystonia. A PET study using [123I]FP-CIT SPECT (n=23 CD patients, 14 healthy controls) to assess midbrain serotonin transporter (SERT) binding demonstrated lower extra-striatal binding in those with cervical dystonia and co-morbid psychiatric symptoms, although no correlation was seen between dystonia severity and SERT binding. Comparison of the balance between serotonergic and dopaminergic binding in those with 'jerky' cervical dystonia to those with more static cervical dystonia symptoms, found variation in neurotransmitter balance between these two forms, suggesting that this may, in part, contribute to the variation in symptomatology (Zoons *et al.*, 2017).

1.3.2. Animal models

Animal models of dystonia have provided invaluable tools in identifying key characteristics underlying the pathophysiology of dystonia. They can be categorised into two distinct groups; those that

recapitulate the dystonic phenotype (phenotypic/symptomatic models), and those that introduce mutations in specific genes known to be disease-causing in dystonia (genotypic models). While the genotypic models may better reproduce the molecular and neurophysiological features of dystonia, they may lack the overt motor manifestations more typically associated with dystonia. Using these techniques, a number of potentially important areas have been identified, including basal ganglia connectivity (Gernert *et al.*, 2002; Köhling *et al.*, 2004) and striatal GABAergic (Hamann and Richter, 2002) and dopaminergic (Zhang *et al.*, 2012) neurotransmission. Increasingly, animal model evidence has also suggested a role for the cerebellum with suggestions that the basal ganglia and cerebellum function in an integrated network that is dysfunctional in dystonia (Neychev *et al.*, 2008; Calderon *et al.*, 2011).

The dt^{sz} mutant hamster, one of the few phenotypic models of dystonia, recapitulates a motor phenotype of stress induced dystonia (Löscher *et al.*, 1989; Sander and Richter, 2007). Clinical characteristics of primary paroxysmal dystonia are observed in the dt^{sz} hamster, including co-contraction of opposing muscles and the absence of electroencephalographic changes. Within this model, GABA$_A$R-α1 positive striatal interneurons, along with parvalbumin mRNA levels, are transiently reduced, suggesting a delay in striatal GABAergic interneuron maturation. This could potentially impact neuronal activity and striatal plasticity (Bode *et al.*, 2017). The anti-dystonic effects of tropicamide, an M4 receptor antagonist in this model reveal a potential value for M4 selective anti-cholinergic therapies in dystonia (Hamann *et al.*, 2017).

The Dyt1ΔGAG heterozygous knock-in mouse is the most noteworthy of DYT1 animal models. It exhibits motor deficits, impaired fine motor balance and coordination, abnormal gait and subtle anxiety-like behaviours (Dang *et al.*, 2005). While this model does not show clear dystonic movements, the motor deficits and abnormal gait are thought to represent a dystonia-like phenotype. Studies in this model have shown deficits in striatal dopamine levels and a reduction in striatal D2 dopamine receptor binding (Dang *et al.*, 2012; Song *et al.*, 2012). In addition, significant alteration in synaptic plasticity due to an imbalance in dopamine and acetylcholine levels are observed, comprising loss of long-term depression in parallel with an increase in amplitude of long-term potentiation (Martella *et al.*, 2014). Maltese *et al.*, have furthered this work by demonstrating premature long-term potentiation during a critical developmental window in striatal spiny neurons, together with an increase in mature mushroom spine width and number, heightened α-Amino-3-Hydroxy-5-Methyl-4-Isoxazolepropionic Acid (AMPA) receptor expression and increased brain derived neurotrophic factor (BDNF) levels (Maltese *et al.*, 2018). Specific knock-down of cerebellar torsinA levels is also sufficient to produce dystonia symptoms in mice, with evidence of disrupted cerebellar output, including alterations to the intrinsic activity of cerebellar Purkinje cells and deep cerebellar nuclei (Fremont *et al.*, 2017).

Another well characterised genetic model of dystonia is the paternally inherited *Sgce* knock out (exon 4) mouse model of myoclonus dystonia. Long-term potentiation is not able to be induced at the corticostriatal glutamatergic synapses in this model, however wild-type activity is restored with use of adenosine 2A receptor antagonists (Maltese *et al.*, 2017). Abnormal striatal dopamine-2-receptor function in the context of increased levels of striatal dopamine have also been identified, suggesting that disrupted dopaminergic neurotransmission is likely to play a key role in the pathophysiology of Myoclonus Dystonia (Zhang *et al.*, 2012).

1.3.3. Cell models

Various lineages of neural cells can be generated by differentiating human embryonic stem cells *in vitro*, providing an opportunity to investigate those cell types that are most critically affected in dystonia. Several patient-specific induced pluripotent stem cell lines have been established over recent years, including cells from patients with a *GCH1* mutation (DYT5) (Murakami *et al.*, 2017), *THAP1* mutations (DYT6) (Erogullari *et al.*, 2014) and *SGCE* mutations (DYT11) (Grütz *et al.*, 2017).

Neurons derived from *THAP1* mutation positive iPSCs exhibit higher levels of *THAP1* compared to wildtype controls, suggesting the existence of a feedback loop in the regulation of *THAP1* expression. It has been proposed that the late onset of DYT6 dystonia, or even the reduced penetrance of the disease, could be attributable to this compensatory autoregulation (Erogullari *et al.*, 2014). Mouse embryonic stem cells (mESCs) have also been used to model DYT6 dystonia, with *THAP1* being shown to regulate the survival and proliferation of embryonic stem cells *in vitro*. Loss of *THAP1* has been shown to affect neuronal differentiation of mESCs, with cells showing augmented death, and prolonged expression of *Nanog, Prdm14* and/or *Rex1* (Aguilo *et al.*, 2017). Neural stem cells (NSCs) derived from iPSCs from patients with X-linked dystonia-parkinsonism show decreased expression of the neuronal-specific TAF1 isoform, in comparison to control NSCs, mimicking findings observed in patient post-mortem brain tissue (Makino *et al.*, 2007). This model indicates that defects may occur prior to neurodegeneration, at relatively early stages of development, rather than exclusively at advanced disease stages (Ito *et al.*, 2016). The nuclear factor-kappa B (NFκB) has been strongly implicated in XDP, with fibroblasts and NSCs differentiated from XDP patient iPSCs displaying increased NFκB in response to tumour necrosis factor-α (Vaine *et al.*, 2017).

1.4. Treatment

Overall, therapeutic options for the treatment of dystonia are limited, poorly efficacious, and are often accompanied by side effects. Treatments aim to prevent involuntary movements, amend abnormal postures, lessen discomfort and improve overall function and quality of life. Treatment options can be

divided into three groups: physical, medical and surgical therapies. Medical therapies include oral therapies, botulinum toxin and intrathecal baclofen, whereas surgical therapies are either peripheral or central. Medical therapies are often the primary treatment option, with surgical intervention considered in patients failing to respond or showing a poor response.

1.4.1. Physical therapies

Although botulinum toxin is the primary treatment option in cervical dystonia, not all patients report symptomatic improvement and may therefore also be referred for isolated or combined treatment with physical therapy. Physical therapy programmes can vary from 40 minutes per session every other day for 6 weeks, up to 90 minutes a day for 2 weeks (Tassorelli *et al.*, 2006; Queiroz *et al.*, 2012). While significant motor improvement is not commonly observed with a combinational treatment of physiotherapy and botulinum neurotoxin, it has been found to improve disability, pain and prolong the effects of the botulinum toxin injections (Contarino *et al.*, 2017). A study addressing the long-term effects of physical therapy showed that patients undertaking specialised physical therapy programmes demonstrate large improvements in general health perception and self-perceived improvement, with a lower healthcare cost than regular physiotherapy (van den Dool *et al.*, 2019). Occupational therapy can also be an option for dystonia patients, enabling patients to maintain, regain or improve independence. Cognitive Orientation to daily Occupational Performance Approach (CO-OP) following DBS has been shown to improve performance of personally relevant functional skills (Gimeno *et al.*, 2019).

1.4.2. Medical therapies

Oral Therapies

The most successful oral medications used for the treatment of primary generalised dystonia are anticholinergic drugs. Trihexyphenidyl is the most widely used with a symptomatic response observed in approximately 40-50% of those treated (Burke, Fahn and Marsden, 1986). Levodopa is the mainstay of treatment for those with dopa-responsive dystonia, with patients showing significant and continued improvement of symptoms even with low doses. Benzodiazepines may also be used to provide symptomatic benefit, principally through muscle relaxation. The most commonly used benzodiazepine is clonazepam, with up to 23% of patients with generalised or focal dystonia demonstrating a good clinical response (Hughes, Lees and Marsden, 1991; Chuang, Fahn and Frucht, 2002). Its primary mode of action is to facilitate inhibitory GABAergic transmission by acting upon GABA$_A$ receptors, resulting in the opening of chloride ion channels. Side effects often include sedation and confusion, although the side effects of clonazepam are often milder than those seen for other types of benzodiazepine.

Botulinum Toxin

Botulinum toxin (BoNT) injected locally into dystonic muscles blocks the release of acetylcholine into the neuromuscular junction causing a reduction or elimination of muscle spasms. It generally takes up to 2 weeks to see an effect, however positive effects can last up to 16 weeks, with a mean duration of 13.2-13.5 weeks in patients with cervical dystonia (Sethi, Rodriguez and Olayinka, 2012; Marsh *et al.*, 2014).

Baclofen

For those unresponsive to oral therapy, baclofen, a presynaptic GABA agonist, may be used intrathecally. It is predominantly used in patients with dystonia combined with spasticity of the lower limbs (Motta, Stignani and Antonello, 2008). Data on effectiveness is inconsistent, however, it is thought to be more effective in those with secondary dystonia (Albright and Ferson, 2009; Ghatan *et al.*, 2016; Wendell and Lake, 2018).

1.4.3. Surgical interventions

Selective peripheral denervation

Peripheral denervation, most commonly used to treat cervical dystonia, is a procedure involving the removal of nerves to selected hyperactive muscles. It is occasionally used when patients do not respond to botulinum toxin injections, or for those who develop secondary resistance (Berman, Seeberger and Kumar, 2005). Reports suggest a success rate of between 68-88% (Chen *et al.*, 2000; Munchau *et al.*, 2001; Braun and Richter, 2002; Cohen-Gadol *et al.*, 2003), with no major morbidity associated with the procedure. However, subsequent risks include re-innervation and/or change in the dystonic pattern post-procedure (Bergenheim *et al.*, 2015).

Lesional surgery

Stereotactic lesioning was the surgical intervention of choice in patients with dystonia before the development of deep brain stimulation (DBS) in the mid-1990's, with bilateral thalamic lesions being the most common form. This offered a vast improvement to dystonic symptoms, although was often associated with complications, typically dysarthria. Nonetheless, the recognition of pallidotomies as an effective target in the treatment of dystonia highlighted the importance of this region and resulted in more targeted surgical intervention in the form of DBS, particularly targeting the globus pallidus internus (GPi) (Lozano *et al.*, 1997; Chang *et al.*, 2002; Houeto *et al.*, 2007).

Deep Brain Stimulation

Pallidal DBS is at present the most widely used surgical treatment for dystonia. The first study evaluating the efficacy and safety of bilateral pallidal stimulation was investigated in 22 patients with generalised dystonia. Twelve months post-treatment, the dystonia severity score, disability score, general health and physical functioning were all significantly improved, with only 3 patients displaying reversible adverse effects (Vidailhet *et al.*, 2005). Stimulation of the GPi, the most extensively studied target, provides the greatest benefit amongst those with *DYT1* mutations and improvements are observed for up to a decade post-treatment (Kupsch *et al.*, 2006; FitzGerald *et al.*, 2014; Park *et al.*, 2016).

Different forms of primary and secondary dystonia respond to DBS with varying success. The greatest outcomes are observed in younger patients and those with either shorter disease duration, lower pre-operative severity scores, *DYT1* mutations and those who lack fixed skeletal deformities. Patients with primary dystonia consistently respond to DBS more effectively than those with secondary dystonia (Kupsch *et al.*, 2003; Tagliati *et al.*, 2004; Cif *et al.*, 2010).

Extracranial ultrasound treatment

Extracranial ultrasound allows intracranial focal lesioning, up to 6mm in diameter and with an accuracy of 1mm, without the need for an incision and without damaging surrounding tissues. Recently, lesioning of the ventro-oral nucleus of the thalamus using MRI-guided focused ultrasound has been shown to be effective in a single case of musician's dystonia, with ongoing symptomatic improvement one year post-treatment (Horisawa *et al.*, 2019). Tandem ablation of the ventral intermediate and ventralis oralis posterior nucleus using transcranial magnetic resonance-guided focused ultrasound was successful in a patient with writer's cramp, with immediate clinical improvement, sustained at 6-month follow-up (Meng *et al.*, 2018). Although still experimental, extracranial ultrasound could one day offer a safe, non-invasive alternative to DBS.

1.5. Myoclonus Dystonia

1.5.1. Overview

Myoclonus Dystonia (MD), a rare, combined dystonia, is the specific focus of this thesis. MD is a childhood onset dystonia characterised by rapid, brief jerks (myoclonus) affecting the trunk and upper limbs, in combination with mild to moderate dystonia of the neck and/or hands, with an estimated prevalence of ~2 per million in European populations (Obeso *et al.*, 1983; Quinn, 1996; Asmus and Gasser, 2010). Motor symptoms typically develop within the first decade of life and are usually always

present by 20 years of age. The consumption of alcohol has widely been reported to improve motor symptoms, particularly the myoclonus however, this has led to cases of alcohol abuse secondary to 'self-medication' (Hess and Saunders-Pullman, 2006). Several studies have also identified the presence of co-morbid psychiatric symptomatology amongst MD patients, particularly anxiety, obsessive compulsive disorder (OCD), depression and panic attacks (Foncke *et al.*, 2009; van Tricht *et al.*, 2012; Peall *et al.*, 2013, 2016).

1.5.2. SGCE

In the late 1990s/early 2000s, linkage analysis of several large families revealed MD was associated with a 3.2Mb region on chromosome 7q21 (Nygaard *et al.*, 1999; Klein *et al.*, 2000; Asmus *et al.*, 2001; Vidailhet *et al.*, 2001). Fifteen genes are located within this region and subsequent direct sequencing revealed that affected individuals from 6 unrelated families carried mutations in the *SGCE* gene (Zimprich *et al.*, 2001). Various studies have estimated the frequency of MD cases caused by a mutation or copy number variant of the *SGCE* gene to be between 20-80% (Tezenas du Montcel *et al.*, 2005; Valente *et al.*, 2005; Gerrits *et al.*, 2006; Nardocci *et al.*, 2008; Asmus *et al.*, 2009; Ritz *et al.*, 2011) dependent on the rigor by which diagnostic criteria are applied. Expression of the ε-sarcoglycan protein is highest in the brain, particularly in midbrain monoaminergic neurons, cerebellar Purkinje cells and the olfactory bulb (Xiao, 2003; Chan *et al.*, 2005; Ritz *et al.*, 2011).

1.5.3. Imprinting

Pathogenic *SGCE* mutations are inherited in an autosomal dominant fashion with evidence of reduced penetrance due to maternal imprinting, yet, when paternally inherited, mutations are fully penetrant **(Figure 1.2)**. A characteristic feature of imprinted genes is differential methylated regions (DMRs) which contain methylated cytosines at CpG sites, i.e. sites where a cytosine is followed by a guanine. The promoter region of the *SGCE* gene contains numerous CpG sites, allowing the methylation pattern of CpG dinucleotides to be assessed by methylation specific PCR and bisulphite genomic sequencing (Huang, Bassil and Murphy, 2013). Work in patient peripheral blood leukocytes and iPSC-derived neurons has shown that the maternal allele of the *SGCE* gene is methylated, whereas the paternal allele is unmethylated, leading to the selective silencing of the maternal allele (Grabowski *et al.*, 2003; Grütz *et al.*, 2017). iPSCs from patients with paternally inherited myoclonus dystonia can be differentiated into cortical neurons whereby the imprinting status is maintained. These neurons express brain-specific *SGCE* mRNA and ε-sarcoglycan protein, albeit at lower levels compared to control cells, as anticipated (Grütz *et al.*, 2017).

1.5.1. Epsilon-sarcoglycan protein

ε-sarcoglycan is a member of the sarcoglycan family, a group of single-pass transmembrane glycoproteins that forms a subcomplex of the dystrophin-glycoprotein complex (DGC) (Esapa *et al.*, 2007). The DGC connects the cell's cytoskeleton to the extracellular matrix through the interaction of extracellular matrix proteins with α-dystroglycan, dystrophin, the cytosolic region of β-dystroglycan and cytoskeletal structures (Prins *et al.*, 2009; Allen, Whitehead and Froehner, 2016). In addition to ε-sarcoglycan, there are five other members of the sarcoglycan family: α, β, γ, δ and ζ, all of which share a similar structure. They are predominantly present in striated and smooth muscle and the Schwann cells of peripheral nerves, forming heterotetrameric complexes. These complexes typically consist of a βδ core that is associated with an α/ε and γ/ζ. sarcoglycans. The complex is expressed both embryonically and postnatally, suggesting its importance in the development and maintenance of non-muscular tissue integrity (Ettinger, Feng and Sanes, 1997). Although mutations to sarcoglycans, other than ε-sarcoglycan, are not implicated in dystonia, autosomal recessive mutations in α, β, γ and δ also lead to disruption of the sarcoglycan complex and are responsible for type II Limb Girdle Muscular Dystrophies (Bönnemann *et al.*, 1995; Noguchi *et al.*, 1995; Nigro *et al.*, 1996; Sandonà and Betto, 2009). The precise function of the sarcoglycan complex is unknown, however, a role in stabilisation of the plasma membrane in cardiac and skeletal muscle tissue, both mechanically and non-mechanically, is apparent (McNally, 2013).

Nonsense mutations account for the majority of *SGCE* mutations observed in MD patients, resulting in an elimination of the synthesis of the full-length protein. Missense mutations are also observed, these impairing trafficking of ε-sarcoglycan to the plasma membrane causing the protein to be retained intracellularly, misfolded and broken down by the ubiquitin proteasomal system (Esapa *et al.*, 2007).
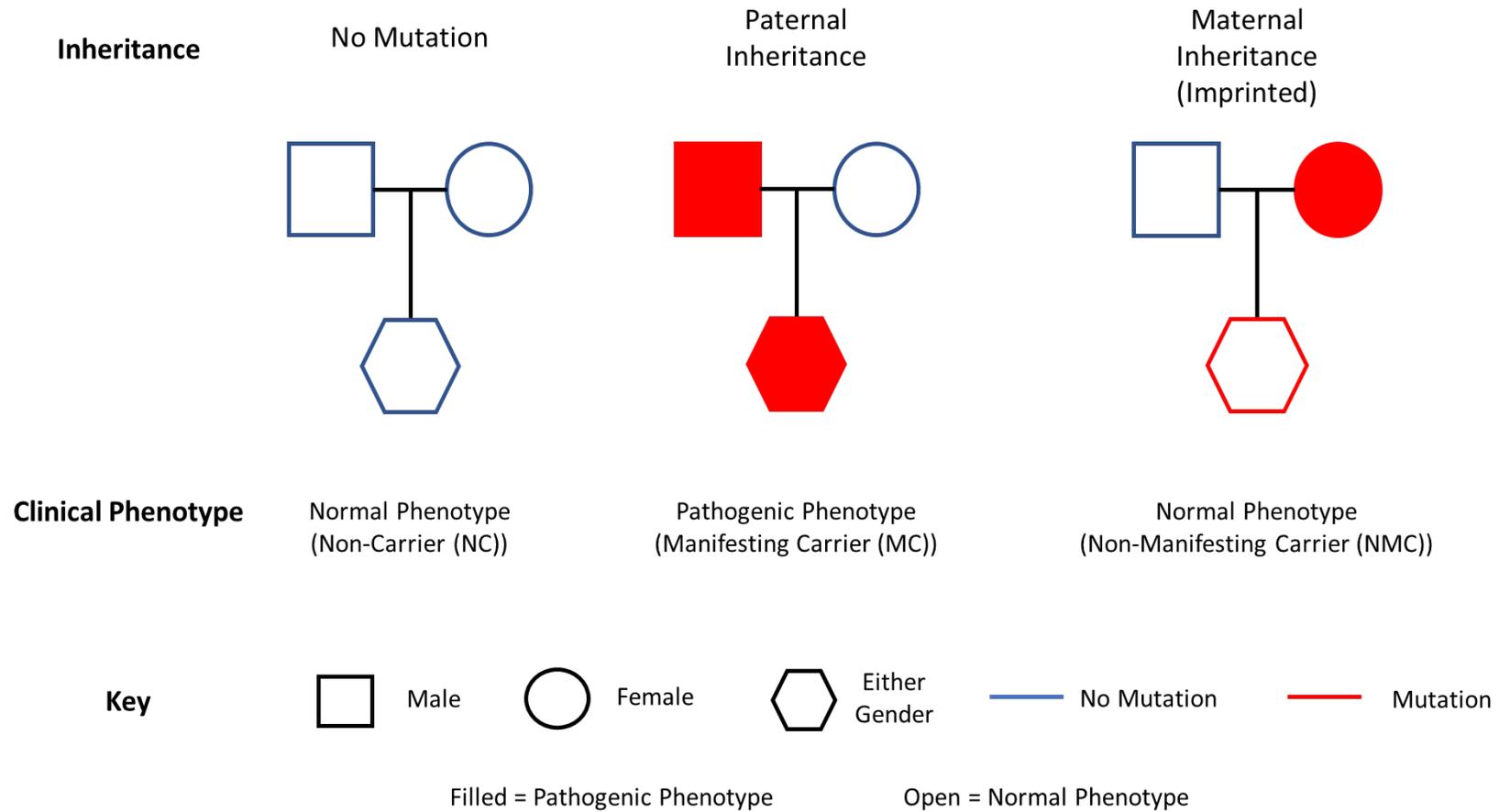
Figure 1.2 Schematic representation of maternal imprinting

Schematic illustrating maternal imprinting. Paternal inheritance of a mutated gene results in a pathogenic phenotype. Maternal inheritance of a mutated gene results in a 'silent state', with offspring acting as carriers of the mutated gene but displaying a normal phenotype.
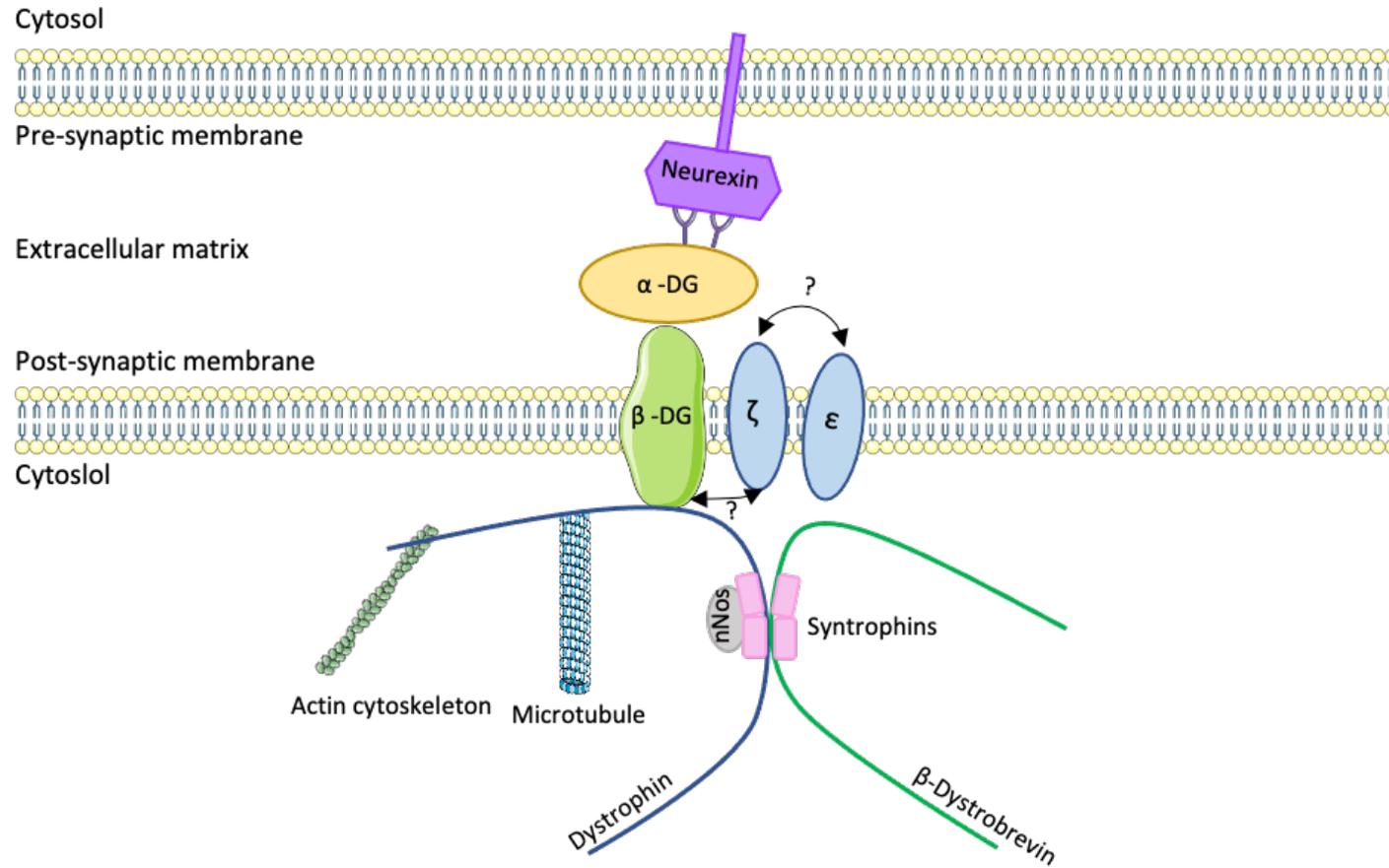
Figure 1.3 Model depicting DGC-like complex in brain.

Diagram of the basic organisation for the core DGC-like complex in CNS neurons. Predicted, but not confirmed protein interactions are depicted by arrows with question marks. Illustration adapted from Waite *et al.,* 2012 and Menozzi *et al.,* 2019. Abbreviations: DG, dystroglycan; nNOS, neuronal-type nitric oxide synthase.

1.6. Cortical Development

The cerebral cortex is a highly complex structure in the mammalian brain, regulating several of its higher order functions, such as attention, memory, thought, language, perception and consciousness (Van Essen, Donahue and Glasser, 2018). The cerebral cortex consists of two major classes of neurons, primarily excitatory pyramidal neurons, which account for more than 80% of cortical neurons, and GABAergic interneurons (INs) forming the remaining 15-20% (Marín and Mü Ller, 2014). Excitatory pyramidal neurons originate from the rostral most region of the neural tube, the embryonic dorsal telencephalon, whereas the medial ganglionic eminence gives rise to approximately 50-60% of GABAergic INs.

1.6.1.1. Corticogenesis

Cortical neurogenesis occurs during a regulated window of development. In humans, the generation of cortical neurons begins at gestational week (GW) 5 and is completed by approximately GW20. Cajal-Retzius cells, located in the marginal zone (MZ) close to the pial surface, are the first neurons to appear in the developing cortex, preceding the generation of cortical plate neurons (layers I to V) (Bystron, Blakemore and Rakic, 2008). They are predominantly generated in the cortical hem and septum and can also originate from neuroepithelial cells in humans. Cajal-Retzius cells are pivotal in cortical lamination, largely due to their secretion of the extracellular matrix glycoprotein, Reelin (Ogawa *et al.*, 1995). Cortical layer neurons of the cortical plate are generated from two main progenitor populations in the dorsal telencephalon; the ventricular zone and the subventricular zone (Tiberi, Vanderhaeghen and van den Ameele, 2012).

There are three types of progenitor cell populations in the developing cortex: neuroepithelial cells (NEs), radial glial cells (RGCs) and intermediate progenitors (IPs). NEs are the first progenitors to arise during development, initially dividing symmetrically and allowing amplification of the initial progenitor pool. They later divide asymmetrically, allowing conversion to radial glial progenitors, which characteristically have long processes that extend from the ventricular wall to the pial surface. RGCs divide both symmetrically and asymmetrically, allowing the maintenance of a pool of progenitors, whilst also permitting the production of cortical neurons. As corticogenesis proceeds, intermediate progenitor (IP) cells are derived from RGCs. IPs divide at non-surface positions within the ventricular zone (VZ) and then migrate away from the apical surface to the subventricular zone (SVZ), an additional proliferative zone above the VZ. They are characterised by their multipolar morphology and expression of the transcription factor TBR2 (Englund *et al.*, 2005). IPs divide symmetrically to give rise to two identical neurons. Another type of progenitor cell important in neurogenesis is the outer radial glial cells (oRGCs), expansion of which is considered to be crucial in expansion of the neocortex. oRGCs are located in the 'outer' SVZ and are derived from apical RGCs by asymmetric division. These cells are highly proliferative, producing either more oRGCs, IPs or

neurons directly (Betizeau *et al.*, 2013). Finally, short neural precursor cells (SNPs) also generate neurons by means of symmetric division. They are similar to RGCs in that they reside in the VZ, however they are transcriptionally distinct and lack basal attachment (Stancik *et al.*, 2010) **(Figure 1.4)**.
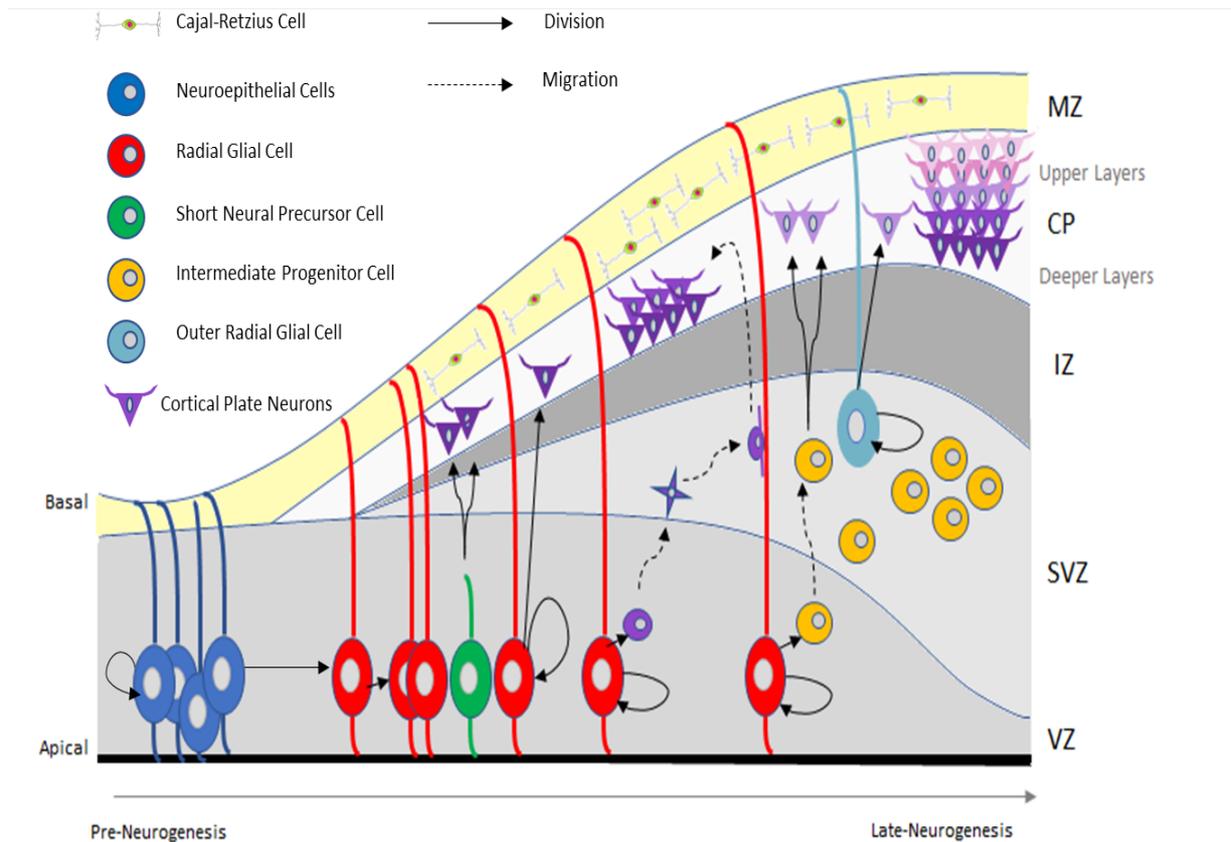
Figure 1.4 Schematic representation of mammalian cortical neurogenesis

The major types of neural progenitor cells with the progeny they yield are specified by different colours. Marginal zone (MZ), cortical plate (CP), intermediate zone (IZ) subventricular zone (SVZ), ventricular zone (VZ). (Adapted from Agirman *et al.,* 2017).

1.6.1.2. Development of cortical layers

Neurons generated from RGCs, oRGCs, SNPs or IPs migrate radially to the cortical plate, with early-born neurons moving via somal translocation and those generated later in corticogenesis migrating via glia-guided locomotion. The cortex is composed of 6 layers assembled in an 'inside-out' manner, whereby the deep layers (VI, then V) are populated by early-born neurons, whereas the late-born neurons migrate past them to the upper layers (IV, then II/III). Upon exit of the cell cycle, post-mitotic neurons are exposed to specific transcription factors that specify their identity (Greig *et al.*, 2013) **(Table 1.3)**. In brief, T-box brain protein 1 (Tbr1) is crucial in the development of layer VI cortico-thalamic projection neurons. Its main mode of action being the repression of FEZ Family Zinc Finger 2 (Fezf2), which subsequently regulates the differentiation of layer V sub-cortical projection neurons (Chen, Schaevitz and McConnell, 2005). Acting downstream of Fezf2, COUP-TF-interaction protein 2 (CTIP2), a marker of layer V neurons, regulates the extension of axons toward subcortical targets (Chen *et al.*, 2008). CTIP2 expression is repressed by the special AT-rich sequence binding protein 2 (SATB2), an essential step in the specification of layer II and III neurons, and determining corticocortical connections in the developing cerebral cortex (Alcamo *et al.*, 2008; Britanova *et al.*, 2008). Layer IV granular neurons, which mostly project locally, also weakly express Satb2 (Alcamo *et al.*, 2008; Britanova *et al.*, 2008) and originate from a population of SVZ progenitors that are positive for Subventricular tag 1 (Svet1). Layer IV neurons express the two homologues of the Drosophila homeobox Cut gene (Cux1/2), which are also present in most of the post-mitotic upper layer neurons (Tarabykin *et al.*, 2001; Nieto *et al.*, 2004).

Table 1.3 Cortical layer markers

Cortical Layer	Marker
Layer VI	TBR1
Layer V	CTIP2, TBR1
Layer IV	Cux1/2, Svet1
Layer II/III	SATB2, Cux1, BRN2

1.7. Disease modelling using hPSCs

1.7.1. Pluripotent stem cells

Human embryonic stem cells (hESCs) are derived from the inner cell mass of an embryo. These cells are capable of self-renewing, and given the appropriate extrinsic signals, can be maintained *in vitro* indefinitely (Thomson, 1998). In 2006, Takahashi et al. developed a technique to induce pluripotency, firstly from mouse fibroblasts (Takahashi and Yamanaka, 2006) and later human cells (Takahashi *et al.*, 2007), bringing about the term 'induced pluripotent stem cells' (iPSCs). Reprogramming of skin-derived fibroblasts was conducted via viral transduction of four key transcription factors: OCT3/4, Sox2, c-Myc and Klf4. Taken together, hESCs and hiPSCs can be termed human pluripotent stem cells (hPSCs). Along with the ability to self-renew, hPSCs have the potential to differentiate into any cell type of the body. In the past, feeder layers of mouse embryonic fibroblasts were essential for the maintenance of pluripotent stem cells, with these secreting numerous unknown factors into the surrounding medium. Nowadays, pluripotent stem cells are maintained on matrices such as Matrigel® and Geltrex™ and in fully defined media (Ludwig *et al.*, 2006). With the correct signals, hPSCs can be directed towards a particular cell fate, allowing us to not only compare developmental pathways and cellular function of healthy and disease cells, but also acquire supplies of specific cells of interest in infinite quantities, a significant advantage over many other model systems.

The use of iPSCs has had a crucial bearing in advancing our knowledge and understanding of neurological disorders, and their underpinning pathophysiology. iPSCs represent a potentially limitless and bankable source of patient-specific cells, with the ability to differentiate into a number of disease-relevant cell types (Takahashi *et al.*, 2007). However, their use is accompanied by a range of limitations, including genetic variability between individuals and their subsequent iPSC lines, potentially limiting interpretation of phenotypic differences (Kilpinen *et al.*, 2017). Thus, in order to generate dependable results, it is imperative that iPSC-based experiments include several clonal lines from different patients. To overcome this problem, gene edited hESCs offer an attractive model to investigate the impact of single gene knock out on neuronal differentiation *in vitro*. This approach allows the investigation of a mutation-specific phenotype in comparison to their isogenic parental line, bypassing the difficulties associated with patient-to-patient genetic variability. The iCas9 hESC line was selected as the parental line to carry out gene editing in order to generate a loss-of-function mutant line. This line offered the advantage of containing a doxycycline-inducible Cas9 protein stably integrated into its genome, was readily available in the lab and was known to differentiate well into cortical excitatory glutamatergic neurons.

1.7.2. CRISPR-based genome editing

The discovery of CRISPR (Clusters of Regularly Interspaced Short Palindromic Repeats)/Cas9 technology has made genome editing faster, cheaper, more accurate and more efficient than previous gene editing techniques. The CRISPR/Cas9 system, a type II CRISPR system, was first identified in bacteria and is used as an immunity mechanism to protect against foreign DNA (Gasiunas *et al.*, 2012; Jinek *et al.*, 2012). In the laboratory, the CRISPR/Cas9 system is comprised of a 20 nucleotide guide sequence, complementary to the target DNA sequence, preceded by a 5'NGG protospacer adjacent motif (PAM) (Jinek *et al.*, 2012). The Cas9 nuclease is directed to the target DNA sequence, initiating the cleavage of DNA and creating a double stranded break. This stimulates cellular DNA repair mechanisms in the form of either Non-Homologous End Joining (NHEJ) or homology-directed repair (HDR), if a donor construct is present. NHEJ is likely to introduce insertions or deletions (INDELS) to either one, or both alleles, with the potential of causing mutations to the protein coding region and loss of function of the protein **(Figure 1.5)**. In 2014, Danwei Huangfu's group developed a system using hESC lines containing a doxycycline-inducible Cas9 that is stably integrated into its genome (iCas9) (González *et al.*, 2014). Upon Cas9 induction, guide RNAs are transfected into cells, leading to a reported 40% efficiency of single gene targeting.

Another relevant use for CRISPR/Cas9 technology is to correct a specific genetic mutation in patient-derived cells. Rescue of any phenotype observed in patient-derived lines would provide an additional layer of evidence to support that the observed phenotype was caused by the gene of interest, rather than epigenetic or off-target effects. The possibility of combining both techniques, i.e., the parallel use of genome engineered hESCs and iPSCs, provides a powerful toolbox to explore the cellular pathophysiology underpinning neurodevelopmental disorders.
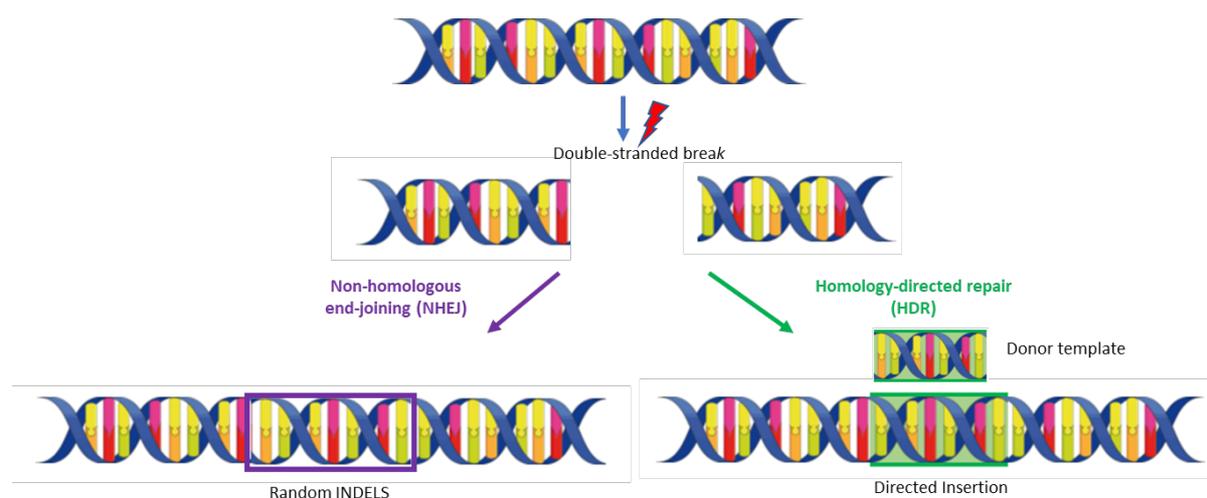
Figure 1.5 Non-homologous end-joining vs Homology-directed repair

Induced double-stranded breaks can be repaired by either non-homologous end joining, or homology directed repair. The former usually leads to gene knockout by causing INDELS in the DNA sequence, whereas the latter can introduce precise gene modification.

1.7.3. Differentiation of hPSCs to neuronal lineages

hPSCs have the ability to differentiate into any cell type in the human body, but possibly their most impressive use over past years has been the modelling of various neuronal subtypes in the investigation of neurodevelopment and disease. The human brain comprises thousands of neuronal subtypes, all of which may differ with regards to neurotransmitter release, electrophysiological properties, cellular morphology and synaptic connections (Nelson, Sugino and Hempel, 2006). Protocols to generate a variety of neuronal subtypes have been established, including midbrain dopaminergic neurons (Jaeger *et al.*, 2011; Kriks *et al.*, 2011; Kirkeby *et al.*, 2012), medium spiny neurons (Arber *et al.*, 2015) and GABAergic interneurons (Cambray *et al.*, 2012; Maroof *et al.*, 2013). However, upon neural induction, the default fate of hPSCs is to one of dorsal forebrain identity. Perhaps consequently, the most widely used and established protocols are those generating forebrain cortical neurons i.e. glutamatergic, excitatory neurons of a cortical fate (Chambers *et al.*, 2009; Shi, Kirwan and Livesey, 2012; Espuny-Camacho *et al.*, 2013).

Many approaches can be used in order to differentiate hPSCs to an enriched population of neurons, including enzymatic dissociation of neural rosettes from embryoid bodies (Zhang *et al.*, 2001), development of organoids (Lancaster *et al.*, 2013) and co-culture of hPSCs with mouse stromal lines (Perrier *et al.*, 2004). Chambers *et al.*, were the first to describe a defined monolayer differentiation method for the conversion of hPSCs to a neuronal fate (Chambers *et al.*, 2009). To achieve neural induction, a 'Dual-Smad inhibition' protocol was developed that used noggin to inhibit BMP and the small molecule SB431542 (ALK4/5/7 inhibitor) to inhibit SMAD2/3 phosphorylation and consequently inhibit the TGFβ/Activin/Nodal pathway. LDN193189 was later found to effectively inhibit the BMP signalling pathway, mimicking the effects of noggin (Boergermann *et al.*, 2010) and generating neurons of a dorsal forebrain identity. As a monolayer, differentiating cells are exposed to specific patterning factors in cell culture medium in a uniform manner, creating a much more synchronous and homogeneous differentiation compared to other methods.

1.7.4. Maturation of PSC-derived neurons

For the most part, studies using PSC-derived neurons often report cell maturity in relation to expression of specific proteins (e.g. MAP2 and NEUN), cortical layer fate (e.g. SATB2 and CTIP2) or the development of synapses (e.g. PSD-95, synaptophysin and GluN1). More recently, studies have centred on advancing protocols to derive more electrophysiologically functional mature neurons. In 2014, Prè *et al.*, investigated the electrophysiological maturation of iPSC-derived neurons over time, showing that although maturation was observed, this was often slow and variable (Prè *et al.*, 2014). Subsequently, several groups have sought to develop protocols that allow for more functionally mature neurons. Bardy *et al.*, investigated the neurophysiological properties of neurons grown in DMEM/F12 and/or neurobasal culture media, observing significant impairments to the generation of action potentials and

synaptic communication. As a result, they optimised inorganic salt and glucose concentrations, along with osmolarity and pH levels in order to create a novel basal medium, BrainPhys™, which more accurately replicated the physiological conditions *in vivo*. Functional maturity of hPSC-derived neurons was shown to be enhanced in this medium, with increased induced and spontaneous activity of neurons, increased synaptic events and reduced input resistance (Bardy *et al.*, 2015).

In 2016, Telezhkin *et al*., developed a further protocol to accelerate neuronal maturation and enhance neurophysiological properties. Their method was based on a standard DMEM/F12 basal medium, with the addition of several small molecules including: DAPT, a γ-secratase inhibitor that blocks notch signalling, PD033291, a CDK4/6 inhibitor, the BDNF receptor agonist LM22A4, the GSK3β inhibitor CHIR99021, Forskolin, an activator of the enzyme adenylyl cyclase, GABA, $CaCl_2$ and ascorbic acid (Telezhkin *et al.*, 2016). After only 21 days from the start of differentiation, spontaneous and induced action potential generation was observed, together with input resistances <800MΩ and relatively hyperpolarised resting membrane potentials. In 2017, Gunhanlar *et al*., described a simple protocol requiring no specialised media that generated high-quality cortical neurons derived from iPSCs with mature electrophysiological properties. Neurons of the human CNS generally have a resting membrane potential of approximately -70mV. Neurons generated using this protocol had resting membrane potentials of −58.2±1.0 mV, with nearly all cells recorded firing evoked action potentials and 59.1% neurons displaying spontaneous action potential firing. Their protocol was based on DMEM/F12 / neurobasal medium, with the addition of the growth factors; BDNF, glial cell derived neurotrophic factor (GDNF), dibutyryl cyclic adenosine monophosphate (dBcAMP) and ascorbic acid (Gunhanlar *et al.*, 2018).

Astrocytes have been shown to encourage neuronal maturation and function *in vitro* by providing trophic support, regulating the extracellular environment and modulating signalling at synapses (Hedegaard, Monzón-Sandoval, *et al.*, 2020). Electrical excitability and the formation and maturation of synapses are influenced by astrocyte-to-neuron signalling (Allen and Eroglu, 2017) and astrocytes also support neurotransmission by regulating concentration changes in extracellular ions and neurotransmitters (Perea and Araque, 2010; Verkhratsky and Nedergaard, 2014). Co-culture of stem-cell derived neurons with astrocytes improves electrophysiological properties of neurons *in vitro*, with neurons displaying a larger capacitance and small input resistance (Rosa *et al.*, 2020). Several studies have shown that the development and maturation of neuron cultures can be improved by pre-conditioning neuron differentiation medium with human or rodent astrocytes. This allows astrocytes to secrete pro-maturation factors, for example thrombospondins, hevin, GDNF, TGFβ and CCL5, into the differentiation medium (Rushton *et al.*, 2013; Pozzi *et al.*, 2017).

Although attempts were made to improve functional maturity of our neurons using the small molecules detailed by Telezhkin *et al*., 2016, in our hands, this approach resulted in a high level of cellular heterogeneity within the cultures, with the appearance of many non-neuronal cells. As a result, the

decision was taken to solely add DAPT and PD033291 for one week in order to synchronise the neuronal cultures. Functional analysis was carried out at later timepoints in order to allow for additional maturation.

1.7.5. Hypoxic conditions

Traditionally, neuronal cultures are maintained at ambient (21%) oxygen levels, providing non-physiological conditions for neuronal maturation and survival. In the mammalian brain, tissue oxygen levels range from 1-5% (Nair, Whalen and Buerk, 1975; Smith, Guilbeau and Reneau, 1977; Wilson *et al.*, 1991; Erecińska and Silver, 2001). In comparison, the stem cell niche requires higher levels of oxygen as it is important for regulating stem cell fate specification. Often, stem cells and differentiating neurons are cultured in the same incubator, therefore failing to recapitulate physiological oxygen levels in the brain. Nevertheless, reduced oxygen levels have been shown to promote survival, proliferation and maturation of neural stem cells (Kaplan *et al.*, 1986; Brewer and Cotman, 1989; Studer *et al.*, 2000; Abbate *et al.*, 2005).

1.7.6. Functional Analysis

1.7.6.1. Calcium Imaging

A large number of functions in the human body are reliant on the generation of versatile intracellular signals that are determined by calcium ions (Berridge *et al.*, 2000), ranging from cardiac cell contraction (Dulhunty, 2006) to regulation of cell proliferation and death (Lu and Means, 1993). The complex morphology of neurons allows calcium ions to reserve their high degree of versatility. For example, in presynaptic terminals, exocytosis of neurotransmitters from synaptic vesicles is triggered by calcium influx, whereas post-synaptically, a temporary rise of calcium levels in dendritic spines is crucial for the induction of activity dependent synaptic plasticity. In neurons, calcium is also vital for the propagation of action potentials. Calcium concentration in resting neurons can vary between 50-100nM, yet during electrical activity, this concentration can rise rapidly to levels ten to 100 times higher (Berridge *et al.*, 2000).

Both calcium influx and efflux are responsible for the maintenance of calcium homeostasis, along with the exchange of calcium with internal stores and binding of free calcium with calcium-binding proteins such as parvalbumin, calbindin-D28k, or calretinin. Calcium influx from the extracellular space occurs via voltage-gated calcium channels (VGCC), ionotropic glutamate receptors (e.g., N-Methyl-D-Aspartate (NMDA) and calcium permeable α-Amino-3-Hydroxy-5-Methyl-4-Isoxazolepropionic Acid (AMPA) receptors), nicotinic acetylcholine receptors (nAChR) and transient receptor potential type C (TRPC) channels. Calcium efflux occurs via the plasma membrane calcium ATPase (PMCA) and the sodium-calcium exchanger (NCX). Inositol triphosphate receptors (IP_3R) and ryanodine receptors

(RyR) allow release of calcium from internal stores, most notably the endoplasmic reticulum (ER) (Berridge, 1998), whereas the sarco-/endoplasmic reticulum calcium ATPase (SERCA) transports calcium ions from the cytosol to the lumen of the ER, maintaining its high internal calcium levels. IP$_3$ can be generated by the activation of metabotropic glutamate receptors (mGluR), which can bind to receptors in the ER and induce calcium release (Niswender and Conn, 2010). Mitochondria are also essential components for maintaining calcium homeostasis as they can act as calcium buffers by taking up calcium via the calcium uniporter and releasing it back slowly to the cytosol through sodium-calcium exchanger (Duchen, 1999). An overview of the components involved in maintaining calcium homeostasis is given in

Figure 1.6.
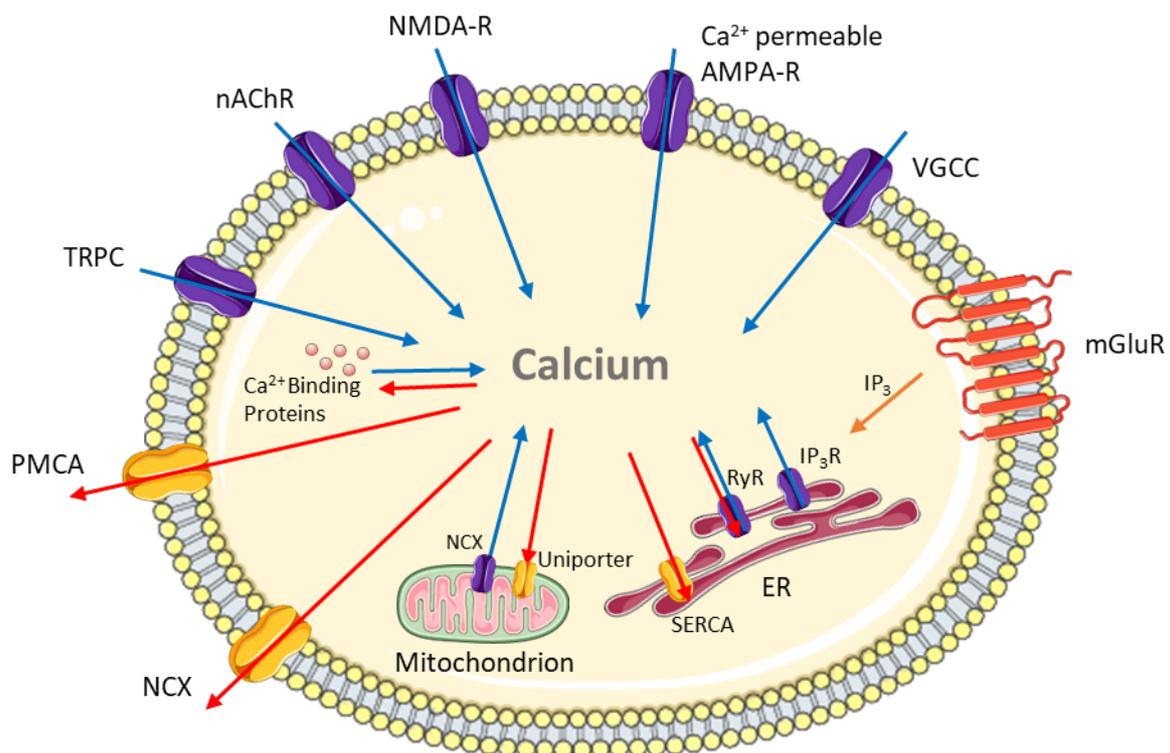
Figure 1.6 Calcium Signalling in Neurons

Schematic depicting the different sources of calcium. Calcium influx occurs via AMPA, NMDA, VGCC, nAChR and TRPC. Calcium efflux occurs via PMCA, NCX and SERCA. Calcium is released by internals stores via IP$_3$R and RyR. Figure adapted from Grienberger et al., 2012.

1.7.6.2. Electrophysiology

Electrophysiology studies allow a direct method to assess neuronal function, detect pathological functional abnormalities and analyse changes in spontaneous and evoked action potentials in response to disease modelling or therapeutics. Whereas calcium imaging allows assessment at the population level, patch clamp electrophysiology techniques allow recordings of neuronal activity at the single cell level. The patch-clamp method can be applied in at least four different configurations; cell-attached, inside-out, outside-out and whole-cell. Each configuration allows currents to be assessed either through single channels or, as in the case of whole-cell clamp, throughout the entire cellular membrane.

In addition, patch clamping can be carried our using either the voltage-clamp or current-clamp technique. During voltage-clamp, the experimenter is in control of the voltage across the cell membrane and resulting currents are recorded, whereas in current-clamp mode, the current is controlled by the experimenter and changes in voltage are recorded. Specific conductances, along with their response to certain drugs or neurotransmitters can be measured in voltage-clamp mode, whereby a puffer pipette can be used to apply drugs focally. In this thesis, current-clamp was used to measure electrophysiological properties of neurons, in part due to the sheer amount of information that could be generated using this technique, but also due to the expertise and knowledge of current-clamp techniques in our lab group and time constraints of the project.

Whole-cell patch clamp experiments have provided important insights into the functional properties of dystonic neurons. Recently, electrophysiological recordings have shown changes in neuronal excitability of the globus pallidus in a dystonia mouse model, whereby pallidal neurons display impairments in firing rate and pattern (Sciamanna *et al.*, 2020). Other electrophysiology studies have reported atypical high-frequency burst firing of cerebellar neurons (Fremont *et al.*, 2014b) and abnormal spiking activity of striatal cholinergic interneurons (Sciamanna *et al.*, 2012).

1.7.6.3. Microelectrode array

Microelectrode arrays (MEAs) are devices that are able to detect neural signals through tens to thousands of microelectrodes. They have been widely used in the neuroscience community to measure neuronal activity both *in vitro* and *in vivo*. They have the ability to be able to record activity from multiple sites of a neuronal culture simultaneously (Hales, Rolston and Potter, 2010). MEA experiments therefore allow the investigation of a whole network, so unlike whole-cell patch clamp which measures changes in potential from a single neurons, MEA technology permits the detection of extracellular changes in potential caused by firing of neurons from a whole population (Negri, Menon and Young-Pearse, 2020). As multiple levels of evidence suggest dystonia to be a network-based disorder, an overview of electrical changes on a network level is a key future area of investigation. This approach is also amenable to pharmacological manipulation and has the potential to be utilised in high throughput drug screening studies.

1.7.6.4. Dendritic arborisation

The correct dendritic architecture of neurons is crucial for appropriate nervous system functioning, with length and morphology of individual neurons grossly affecting their functional properties. Dendrites play vital roles in neuronal plasticity and processing of information, therefore it is imperative that dendrite arborisation is accurately controlled to ensure appropriate functional network activity. Intrinsic and extrinsic signalling, as well as the pattern of electrical activity can impact the development and remodelling of neurites during development, and many neurodevelopmental disorders often display abnormalities in neurite structure and connections (Penzes *et al.*, 2011; Nagy *et al.*, 2017; Caverzasi *et al.*, 2018).

1.7.6.5. Investigation of synaptic transmission

Throughout development, neuronal activity causes changes to both the number and strength of synapses in the brain, with synaptic inputs continuously added, eliminated and refined (Glasgow *et al.*, 2019). Transfer of information in the nervous system relies heavily on the release of neurotransmitters from the presynaptic terminal into the synaptic cleft , which consequently activate postsynaptic neuronal receptors. Downstream signalling processes can be triggered by these receptors and initiate ionic flux through receptor pores, altering the transmembrane electrical potential. This then propagates to the cell body and can evoke an action potential in the postsynaptic neuron (Gerschenfeld, 1973). Synaptic transmission and plasticity can be studied using a variety of approaches, including molecular biology, behaviour, electrophysiology and imaging. These techniques could allow investigation into the presence of various synaptic proteins, for example postsynaptic density protein 95 (PSD95) and synaptophysin, as well as the density of each protein.

1.7.6.6. Gene expression analysis

Gene expression analysis, which can be used to compare the RNA expression levels of multiple genes across multiple timepoints/samples, is a technique that is regularly used to identify the molecular basis of phenotypic differences. This allows more in-depth investigations to be carried out on selected gene expression targets. Valuable insight into the role of differential gene expression in normal and disease processes can be provided by gene expression analysis.

1.7.6.7. Additional assays

Various other assays could also be used to investigate the overall health of neuronal populations. Assays that measure cellular proliferation, cell viability and cytotoxicity can be used to examine the response and health of neurons in culture after treatment with various stimuli. This could give an insight into the number of cellular divisions over time, the metabolic activity and DNA synthesis. Assays the detect and monitor changes in mitochondrial function can also be invaluable. Mitochondria are essential for

calcium uptake and storage, reactive oxygen species generation and detoxification, and synthesis of ATP by oxidative phosphorylation (Brookes *et al.*, 2004). Mitochondrial assays can therefore provide key insight into mitochondrial dysfunction. A variety of fluorescence-based assays can be used to assess disruption of mitochondrial function, including measurements of mitochondrial calcium, superoxide, mitochondrial permeability transition, and membrane potential.

1.8. Aims of project

The aims of this thesis are to investigate how loss of ε-sarcoglycan impacts cortical glutamatergic excitatory neuronal differentiation. To achieve this, the project has five fundamental aims:

1) To generate a homozygous *SGCE* null human embryonic stem cell line (hESC) (Chapter 3)

2) Phenotypic characterisation of the *SGCE*-knockout (*SGCE*ko) hESC line during differentiation towards a cortical glutamatergic excitatory neuronal lineage (Chapter 3)

3) To assess spontaneous calcium activity in *SGCE*ko neuronal populations at distinct stages during cortical glutamatergic neuronal differentiation (Chapter 4)

4) To investigate the electrophysiological properties of *SGCE*ko neurons during cortical differentiation, and their variation at distinct developmental timepoints (Chapter 5)

5) To examine dendritic arborisation during cortical differentiation in *SGCE*ko neuronal cultures (Chapter 6)

Throughout, the results obtained from the hESC *SGCE*ko line will be compared to their isogenic, wild-type parental control line, attempting to ensure that the distinctions derived are due to loss of ε-sarcoglycan function, rather than background genetic variation.

2. Methods and materials

2.1. Cell culture

2.1.1. hPSC culture

All experiments in this study were carried out using:

- the iCas9 cell line (González *et al.*, 2014)
- its iCRISPR engineered compound heterozygous *null* derivative (*SGCE*ko)

Human pluripotent stem cells were maintained in Essential E8 medium (Thermo Fisher) under standard culture conditions (37ºC, 5% CO_2) in Matrigel® (Corning, VWR International) coated 6 well plates. Cell work was carried out under a laminar flow hood (Maxisafe 202, Thermo Scientific) under sterile conditions. Stem cell media was changed every day and cells were passaged every 3-4 days, when 70-80% confluency was reached. In brief, stem cells were washed once with DPBS before a 3-minute incubation at 37ºC with 0.02% EDTA (Sigma). After removal of EDTA, fresh medium was applied and cells were dissociated into small clumps, then seeded into a new plate. Stem cells were routinely split from one well into either 3 or 5 wells i.e. ratio of between 1:3 and 1:5.

2.1.2. Freezing and thawing of hPSCs

Stock of low passage number hPSCs were stored in liquid nitrogen for future experiments. In order to freeze cells, cells were passaged as described above **(2.1.1)**, with an emphasis on maintaining large clusters of cells, centrifuged for 5 minutes at 200g and resuspended in cold Essential 8 medium containing 10% DMSO (Sigma). Cell suspension from one 80% confluent well of a 6-well plate was transferred to a cryovial and relocated to a suitable freezing container to allow for a -1ºC/min cooling rate when placed at -80ºC. The following day, cryovials were transferred to liquid nitrogen storage tanks. A rapid-thaw method was used upon recovery of cells from liquid nitrogen, whereby cryovials were placed in a 37ºC water bath as quickly as possible from storage. The thawed cell suspension was transferred dropwise into pre-warmed medium and centrifuged for 5 minutes at 200g. After centrifugation, the cell pellet was resuspended in an appropriate amount of hESC medium and plated into a single well of a 6-well plate.

2.1.3. Neuronal differentiation of hPSCs

Cells were passaged onto Growth Factor Reduced Matrigel (Corning, VWR) as described in section **2.1.1,** and maintained in Essential 8 medium for up to two days, until 80-90% confluent. Upon reaching a suitable level of confluency, hESC medium was replaced with N2B27 medium (without vitamin A),

the composition of which is listed in **Table 2.1**. The day the media was changed was then designated as day 0 of differentiation.

2.1.3.1.   Cortical glutamatergic neurons

The cortical glutamatergic neuron differentiation protocol used throughout all experiments presented in this thesis is based on previously published versions (Shi, Kirwan and Livesey, 2012; Espuny-Camacho *et al.*, 2013). This procedure is outlined in **Figure 2.1.**

To initiate cortical glutamatergic differentiation, Essential 8 medium was removed, cells were washed once with DPBS and neural induction medium was added to the wells (**Table 2.1**, **Figure 2.1**). The cells were kept in neural induction medium until day 8 and at this point, LDN-193189 (LDN) and SB-431542 (SB) were removed. Cells were re-plated onto fibronectin-coated plates at a ratio of 2:3 on day 7. Fibronectin (Millipore) plates were produced by coating plates with a solution of 15μg/ml fibronectin in DPBS and incubated at 37ºC for at least one hour. For the passage, cells were pre-treated with 10μM ROCK inhibitor (Y-27632, STEMCELL Technologies) one hour prior to passage in order to promote cell survival. Cells were then incubated for 3 minutes in EDTA and manually dissociated using a 2ml serological pipette, keeping large clusters of cells. Cells were resuspended in an appropriate amount of neural induction media and seeded into new plates.

Eight to ten days after the first passage, cells were again split, this time on to Poly-D-Lysine/Laminin-coated plates. Plates were prepared by coating with a 10μg/ml solution of Poly-D-Lysine (Sigma) for a least 30 minutes at room temperature, followed by 3 washes with DPBS. This was followed by an overnight incubation at 37ºC with 10μg/ml Laminin solution (Sigma). For the passage, cells were incubated for up to 10 minutes with StemPro Accutase Cell Dissociation Reagent (Thermo Fisher Scientific), collected and broken up with a more vigorous titration than previous in order to obtain a single cell solution. Cells were plated at a density of 75,000 cells/cm^2 and 125,000 cells/cm^2 for calcium imaging/immunofluorescence and RNA/protein extraction, respectively. At approximately day 20, when cells displayed signs of neuronal morphology, B27 without retinol was replaced with B27 with retinol (Gibco), to promote maturation and neuron survival. Cells were fed every other day throughout the differentiation protocol, unless otherwise stated.

Table 2.1 Composition of media used for monolayer differentiation

Media	Component	Composition	Company
N2B27 *(without vitamin A)*	DMEM-F12 and Neurobasal	2:1	ThermoFisher
	N2	1x	ThermoFisher
	B27 without vitamin A	1x	ThermoFisher
	L-glutamine	2mM	ThermoFisher
	β-mercaptoethanol	0.1mM	ThermoFisher
	Mycozap™ Plus-Cl	1x	ThermoFisher
Neural induction medium	N2B27 without vitamin A	1x	N/A
	SB-431542	10μM	Tocris
	LDN-193189	100nM	Tocris
N2B27 *(with vitamin A)*	DMEM-F12 and Neurobasal	2:1	ThermoFisher
	N2	1x	ThermoFisher
	B27 with vitamin A	1x	ThermoFisher
	L-glutamine	2mM	ThermoFisher
	β-mercaptoethanol	0.1mM	ThermoFisher
	Mycozap™ Plus-Cl	1x	ThermoFisher

Timeline	Day 0	Day 7	Day 16 Day 20
Coating	Growth Factor Reduced Matrigel	Fibronectin	Poly-D-lysine/Laminin
Medium	N2B27 (without vitamin A)		N2B27 (with vitamin A)
Factors	LDN + SB		

Figure 2.1 Monolayer differentiation of hPSCs into cortical pyramidal neurons

The timeline for differentiation of all cell lines is shown in grey, the plate coating used at each stage in blue, the type of media is shown in purple and small molecules shown in pink.

2.2. CRISPR/Cas9 targeting: gRNA design and synthesis

Guide RNAs targeting the first and second exons of *SGCE* were designed using the online CRISPR design tool, developed by the Feng Zhang group from the Massachusetts Institute of Technology (www.crispr.mit.edu). Three gRNAs were designed for each exon to be targeted (**Table 2.2**) and those with the lowest off-target predictive score given by the online tool were selected for CRISPR/Cas9 targeting. All gRNAs selected had an off-target predictive score of 0.

In vitro transcription was used to generate gRNAs. For this process, a 120-nucleotide single-strand DNA oligo was designed, comprising a T7 promoter sequence, a 20 nucleotide-long guide sequence, with an end chimeric guide RNA sequence (tracr-RNA) **(Figure 2.2A)**. A PCR reaction was performed on this single-strand construct using one primer complementary to the T7 region and another complementary to the final 20 nucleotides of the tracr-RNA sequence (**Figure 2.2A, underlined**). The resulting double-stranded DNA amplicon was purified using the MinElute PCR purification kit (Qiagen). The purified product was used as a template for *in vitro* transcription using the MEGAshortscript T7 transcription kit (Thermo Fisher) in order to generate an RNA molecule composed of the guide sequence and tracr-RNA in a 5' to 3' direction. The resulting product was determined by running 2µl of the *in vitro* transcription reaction on a 2% TBE agarose gel (**Figure 2.2C**). The MEGAclear transcription clean up kit (Thermo Fisher) was used to purify the remaining product in order to obtain the gRNAs ready for transfection.

Table 2.2 Guide RNA sequences

Target	gRNA Sequence
Exon 1: CRISPR site 1	AGGATGAGCCCCGCGACCAC
Exon 1: CRISPR site 2	CGCGACCACTGGCACATTCT
Exon 1: CRISPR site 4	CCCCTGTGCTTGGACGGGAC
Exon 2: CRISPR site 1	TCTCCAAGGTACACTCCGAT
Exon 2: CRISPR site 2	AGGTACACTCCGATCGGAAT
Exon 2: CRISPR site 4	CGGAATGTATACCCATCAGC
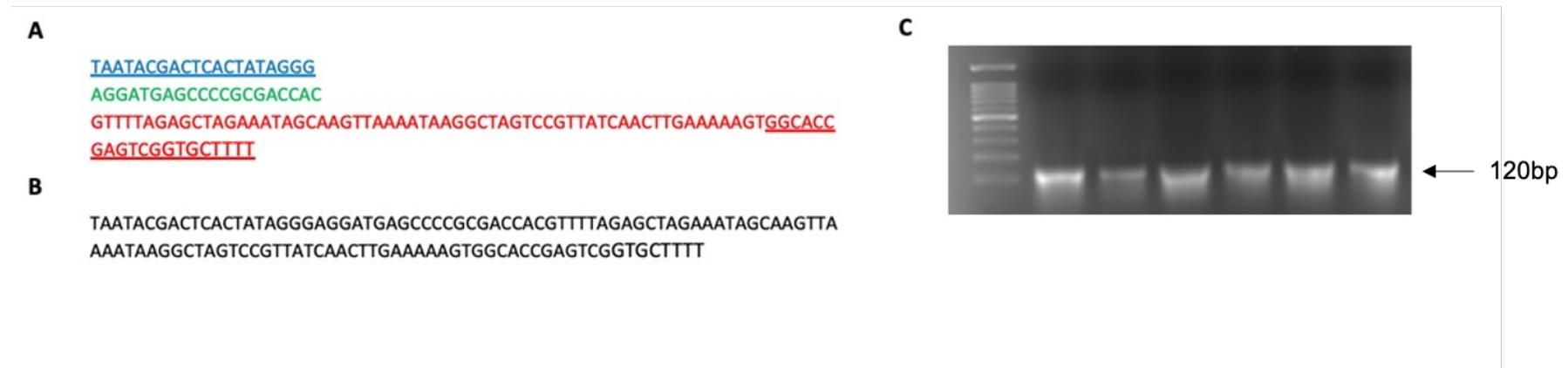
Figure 2.2 Generation of gRNAs

(A) Nucleotide sequence of one of the DNA oligos targeting exon 1 of the *SGCE* gene used as a template for in vitro transcription. The 120-nucleotide sequence included the T7 promotor sequence shown in blue, the guide RNA in green and the tracr-RNA sequence in red. Sequences underlined represent the primers used for PCR amplification of the single stranded DNA oligo. (B) Full DNA oligo sequence. (C) RNA gel showing the in vitro transcription products of the six different guide sequences.

2.3. gRNA transfection of hESCs

RNA transfection was carried out in iCas9 hESCs to deliver gRNAs to produce the *SGCE*-knockout lines (*SGCE*ko). Two micrograms per millilitre (2μg/ml) doxycycline (VWR) was used to induce expression of the Cas9 protein one day before, and during transfection. Lipofectamine® RNAiMAX (Thermo Fisher) was used for gRNA transfection, following manufacturer's instructions. In brief, 1μl of Lipofectamine and gRNAs were diluted separately in Essential 8 medium (250μl each, for one well of a 6-well plate) and then combined and incubated at room temperature for 20 minutes to allow RNA-Lipofectamine complexes to form. Following this, the gRNA-Lipofectamine mix was added dropwise to two wells of iCas9 cells that had been allowed to reach 50% confluency. gRNAs for *SGCE* targeting were added for a final concentration of 20nM. A second transfection was performed 24 hours after the first transfection, in an attempt to improve the efficiency of transfection. An overview of the CRIPSR/Cas9 targeting process is outlined in **Figure 2.3.**

2.4. Establishment of *SGCE* knock-out lines

2.4.1. Expansion of clones

Two days following the second gRNA transfection, the iCas9 cells were dissociated using Gentle Cell Dissociation Reagent (Stem Cell Technologies). Cells were incubated for 10 minutes at 37⁰C, dissociated into small clusters of cells and then passed through a FACS sorting tube to create a single cell suspension. Cells were seeded into 10cm dishes at densities of 500, 1,000 and 2,000 cells/dish. When colonies originating from single cells were large enough, they were mechanically picked, disaggregated and plated into duplicate wells of 96 and 48 well Matrigel coated plates containing Essential 8 medium and RevitaCell. Genomic DNA was extracted from the colonies in the 96 well plates, and then used to check for mutations. Those in the 48 wells plates were expanded, and subsequently frozen down.

2.4.2. Genomic DNA extraction

Cultured cells were washed once with DPBS and incubated with lysis buffer (10mM Tris, pH8.0, 50mM EDTA, 100mM NaCl, 0.5% SDS), supplemented with 0.5mg/ml Proteinase K (all components from Sigma), overnight at 37⁰C. The following day, the cell lysate was transferred to an Eppendorf tube and DNA was precipitated by adding an equal volume of isopropanol, vortexed until the DNA was visible and then centrifuged at 15,000g for 20 minutes at 4⁰C. The DNA pellet was washed with 70% ethanol, air-dried and resuspended in a suitable amount of double distilled H_2O (dd H_2O). A BioSpectrometer® (Eppendorf) was used to measure DNA concentration.

2.4.3. PCR and DNA electrophoresis

SGCE-targeted clones were screened by PCR using the primers defined in **Table 2.3**. The PCR reactions were composed of: ~100ng template genomic DNA, 5µl 10x Standard Taq Reaction Buffer, 0.25µl Taq DNA Polymerase, 1µl primers from a 10µM stock, 1µl dNTPs from a 10mM stock and ddH$_2$O, to make up to a total volume of 50µl. In general, 40 cycles were carried out in a T100 Thermal Cycler (Bio-Rad). Each cycle consisted of a denaturation step (30 seconds at 95ºC), an annealing step (50-55ºC for 1 minute) and an extension step (68ºC for 1 minute). The annealing and extension temperature and time were optimised for each pair of primers (**Table 2.4**). 5µl of the final PCR product was run on a 5% agarose gel.
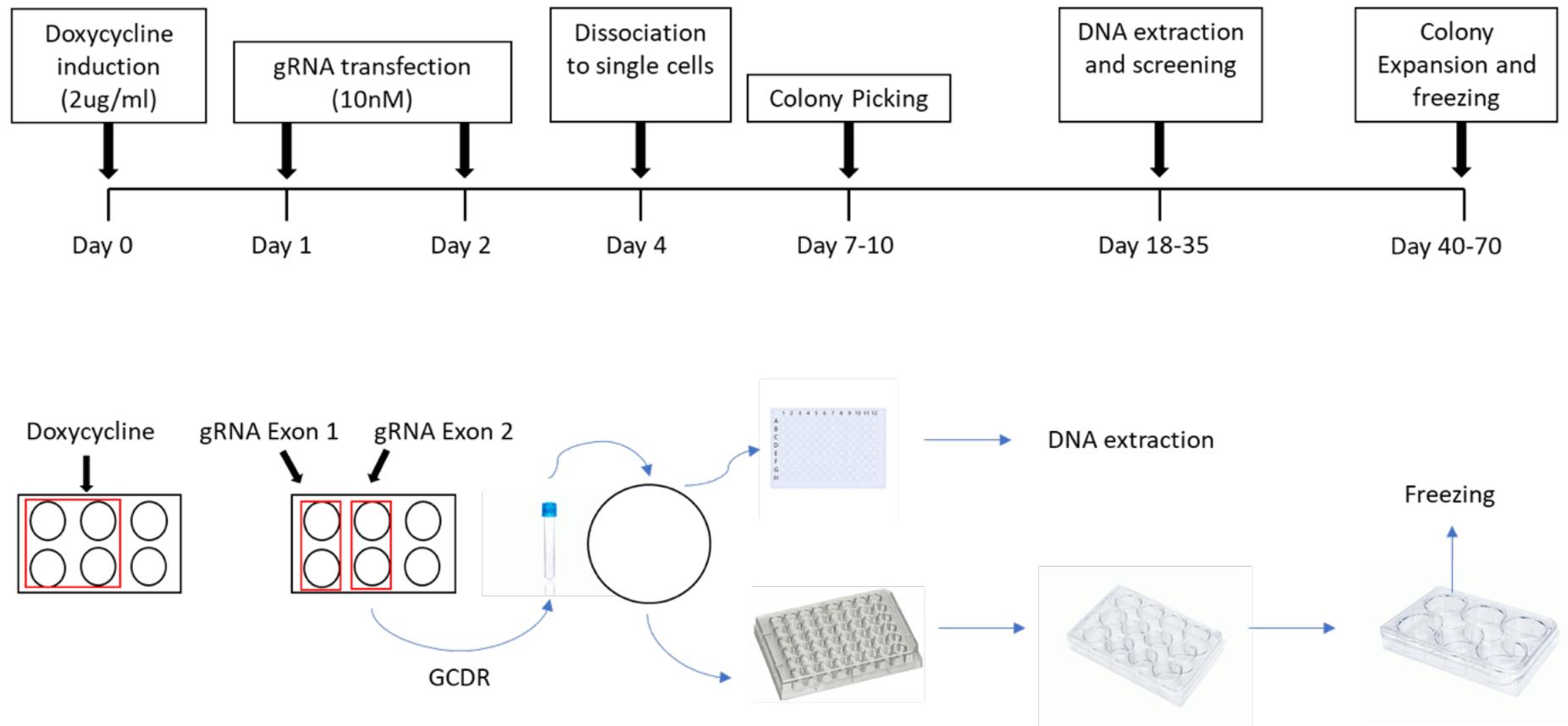
Figure 2.3 Overview of CRISPR/cas9 workflow

hESCs were initially treated with 2mg/ml doxycycline to induce the expression of the Cas9 protein one day before, and during transfection. gRNAs were transfected using Lipofectamine RNAiMAX, with a second transfection 24 hours later. 48 hours after the second transfection, hESCs were dissociated into single cells and seeding into 10cm dishes. When large enough, colonies were mechanically picked and plated into duplicate wells of 96 and 48 well plates. Colonies in 96 well plates were used for DNA extraction and screening for genetic mutations, whereas colonies in 48 well plates were expanded and eventually frozen.

Table 2.3 Primers used for genotyping of *SGCE* locus

Target	Fw Sequence (5'-3')	Rv Sequence (5'-3')	Length
Exon 1 CRISPR site 1/2	CTTGGACGGGACAGGGTC	AGCCTCTCTTTCTGTCCCG	193bp
Exon 1 CRISPR site 4	CAAGCTGGGAGGGAAGAAG	CTTGCTGACAGGTTAGTGGC	191bp
Exon 2 CRISPR site 1/2/4	AGGGCGTATCTCATTATTTGTCT	TCCACCTTACCCAAAACCTG	182bp

Table 2.4 PCR conditions for *SGCE* CRISPR sites

Target	Start Temperature	Denaturation	Annealing	Extension	Cycles	Final Extension	Final Hold
Exon 1 CRISPR site 1/2	95ºC (3 minutes)	95ºC (30 seconds)	53ºC (1 minute)	68ºC (1 minute)	35	68ºC (5 minutes)	4ºC (forever)
Exon 1 CRISPR site 4	95ºC (15 minutes)	95ºC (30 seconds)	55ºC (1 minute)	68ºC (1 minute)	40	68ºC (5 minutes)	4ºC (forever)
Exon 2 CRISPR site 1/2/4	95ºC (15 minutes)	95ºC (30 seconds)	50ºC (1 minute)	68ºC (1 minute)	40	68ºC (5 minutes)	4ºC (forever)

2.4.4. PCR cloning and sequencing analysis

SGCE-targeted hESCs that were identified by PCR to be potential mutants were chosen for single allele sequencing to confirm the presence of insertions, deletions and out-of-frame mutations. The PCR product was initially cloned into the pGEM-T vector (Promega) following manufacturer's instructions. A ligation reaction was set up, comprising of pGEM-T Easy vector (1µl), 2x reaction buffer (5µl), T4 DNA ligase (1µl) and purified PCR product (3µl) and incubated at room temperature for one hour. Two microliters (2µl) of the resulting ligation reaction was used to transform competent cells (NEB® 5-alpha F'Iq Competent E.coli) via a heat-shock mediated transformation. The transformed cells were then plated onto LB-agar plates and incubated at 37ºC overnight. The next day, transformed bacteria were plated onto ampicillin containing LB agar plates and again incubated overnight at 37ºC. On the following day, miniprep reactions were set up from individual ampicillin-resistant colonies.

2.4.4.1. Miniprep

The selected colonies were grown in LB media, constantly agitated at 200rpm overnight at 37ºC. Plasmid DNA was isolated via miniprep the subsequent day, and 1.5ml of bacterial solution transferred to a 2ml Eppendorf tube and centrifuged at 12,000g for one minute. The supernatant was discarded, and the pellet resuspended in 200µl of solution A (25mM Tris HCl, pH8, 10mM EDTA), containing 0.5mg/ml RNAse A. Subsequently, 200µl lysis buffer (200mM NaOH, 1% SDS) was added and incubated at room temperature for no longer than 5 minutes. In order to neutralise the lysis buffer, 240µl solution K (5M potassium acetate, pH5.5) was added, the tubes inverted 5-6 times to gently mix solution, and then incubated at room temperature for 3 minutes. The bacterial solution was centrifuged at 12,000g for two minutes to allow the protein and debris to form a pellet, with the supernatant carefully collected and transferred to a clean 1.5ml Eppendorf tube. Four hundred microliters (400µl) of 100% isopropanol was added to each tube and DNA was precipitated by vortex mixing. Following a one-minute incubation at room temperature, the DNA was pelleted by centrifugation at 14,000g for one minute. The supernatant was immediately removed, and the DNA pellet was washed in 1ml of 70% ethanol. Tubes were again centrifuged at 14,000g for one minute and the supernatant removed. DNA pellets were left to air dry for 10 minutes to remove any trace amounts of ethanol. The DNA was resuspended in 50µl ddH$_2$O.

2.4.4.2. Plasmid digestion

Restriction enzyme digests were carried out with EcoR1 (NEB) to determine the presence of insertions or deletions. Digestions were performed in Buffer 2.1, at 37ºC, for one hour. The resulting digestion product was run on a 2% agarose gel for one hour at 80V.

2.4.4.3. Sanger sequencing

Sequencing was carried out by GATC-biotech using LIGHTRUN tubes to allow monoallelic characterisation of the mutations. Five microliters (5μl) of 100ng/μl purified plasmid DNA was mixed with 5μl T7 forward primer and provided to GATC-biotech in 1.5μl Eppendorf tubes.

2.4.4.4. Genotyping

DNA was extracted from the iCas9 parental cell line, along with any cell lines found to harbour heterozygous or homozygous mutations, and quantified. All cell lines were genotyped using the Psych v1.1 array (MRC Centre for Neuropsychiatric Genetics and Genomics Core Facility). The results were analysed using PennCNV software, with quality control (QC) criteria including exclusion of copy number variants (CNVs) <100,000bp and containing <10 single nucleotide polymorphisms (SNPs). The analysis of data was carried out by the core team, MRC Centre for Neuropsychiatric Genetics and Genomics Core Facility.

2.5. Immunocytochemistry

2.5.1. Immunofluorescence staining

To fix the cultured cells, they were washed once with DPBS, incubated with cold 3.7% PFA for 15 minutes and washed 3 times with DPBS before proceeding with staining. For staining, PBS-T (0.3% Triton-X-100 in PBS) was used to permeabilise cells for 10 minutes, followed by a 30-minute block with 2% BSA and 3% donkey serum (Gentaur) at room temperature. Cells were incubated overnight with primary antibodies in blocking solution at 4ºC. The following day, cells were subjected to three 10-minute washes with PBS-T and then incubated in the dark for 2 hours with AlexaFluor secondary antibodies (ThermoFisher) diluted in PBS-T at room temperature. DAPI (Sigma), diluted 1:3000 in PBS, was used to stain the nuclei, followed by three further washes with PBS. DAKO fluorescent mounting medium was used to mount cells, and the plates were stored at 4ºC until imaging. All primary antibodies used throughout this thesis are documented in **Table 2.5**.

Table 2.5 Antibodies used for immunofluorescence staining

Antigen	Species	Supplier	Product Code	Dilution
CTIP2	Rat	Abcam	AB18465	1:500
FOXG1	Rabbit	Abcam	AB18259	1:250
KI67	Goat	Santa Cruz	SC7846	1:250
GFP	Goat	R&D	AF4240	1:500
MAP2	Mouse	Sigma	M1406	1:500
NESTIN	Mouse	BD Pharmigen	BD611659	1:300
NEUN	Mouse	Millipore	MAB377	1:500
NEUN	Rabbit	Millipore	177487	1:250
OCT3/4	Goat	Santa Cruz	SC8628	1:500
OTX2	Rabbit	Millipore	AB9566	1:300
PAX6	Mouse	DSHB	PAX6	1:1000
TBR1	Rabbit	Abcam	AB31940	1:500
TRA-1-81	Mouse	BD Pharmigen	BD560072	1:100
TUJ1	Mouse	BioLegend	T8660	1:1000

2.5.2. Imaging and picture analysis

A Leica DM6000B inverted microscope was used to image the stained cells, with an average of 10 random fields of view acquired for each staining combination at 20x magnification. Cell Profiler (cellprofiler.org) was used count cells in an automated fashion for DAPI and other nuclear markers. For other measurements, counting was performed manually, using the ImageJ software. Data analysis and representation was performed using Microsoft Excel and GraphPad Prism software. All immunocytochemistry quantifications were collected from three independent experiments, with at least two technical replicates for each marker counted.

2.6. Western blotting

2.6.1. Sample preparation

To isolate protein, cultured cells were collected in ice-cold PBS and then centrifuged at 900g for 5 minutes. The resulting cell pellet was lysed on ice using RIPA buffer (Abcam) supplemented with protease and phosphatase inhibitors (Sigma). Cell lysates were incubated on ice for 30 minutes, vortexing every 5 minutes, and then centrifuged at 15,000g for 5 minutes. The supernatant (120µl) was transferred to a fresh Eppendorf tube and mixed with 4x LDS sample buffer (46µl), and 500mM DTT (18 µl). Samples were incubated at 72ºC for 10 minutes and then stored at -80ºC until use. All centrifugation steps were carried out at 4ºC.

2.6.2. Running samples

Equal amounts of protein for each sample were loaded into a 4-12% Bolt® Bis-Tris gel (ThermoFisher), separated and then transferred to a methanol activated PVDF membrane (0.45µm pore size, Amersham Hybond, GE Healthcare) via electro-blotting. 5% BSA (Sigma) in Tris Buffered Saline containing 0.1%

Tween (TBS-T) was used to block the membrane before incubating with primary antibodies **(Table 2.6)** overnight at 4ºC. The following day, the membrane was washed 3 times in TBS-T and secondary antibodies, conjugated to horse-radish peroxidase (HRP) (Abcam), were applied and incubated for 1 hour at room temperature. The membrane was washed again (3 times) and secondary antibodies were detected following a 3-minute incubation with Luminata Crescendo HRP substrate (Millipore). Chemiluminescent detection was carried out using the iBright CL1000 (ThermoFisher). Images were exported to ImageJ for quantification.

Table 2.6 Antibodies used for western blotting

Antigen	Species	Supplier	Product Code	Dilution
ε-sarcoglycan	Rabbit	Peptide Speciality Laboratories GmbH	Custom	1:1000

2.7. Gene expression analysis

2.7.1. RNA extraction

A phenol/chloroform extraction protocol was used to isolate total RNA from cultured cells in 12-well plates. Cells were first washed once with DPBS, and then lysed in 500µl TRI reagent® (Sigma). Cell lysates were stored at -80ºC until all samples, from multiple time points, were collected. Biological duplicates for each sample were taken for all experiments.

The RNA extraction was performed according to the manufacturer's instructions (Sigma). In brief, the samples were thawed, and 100µl chloroform added to each sample. They were then shaken vigorously and allowed to stand for 15 minutes at room temperature. The samples were centrifuged at 12,000g for 15 minutes to allow separation into a lower red organic phase containing protein, an interphase containing DNA and a colourless upper aqueous phase containing RNA. The aqueous phase was carefully transferred to a new tube, mixed with 250µl isopropanol, and left to stand at room temperature for 10 minutes. The RNA was then precipitated by centrifugation at 12,000g for 10 minutes at 4ºC. The resulting RNA pellet was washed in 75% ethanol and centrifuged again at 7,500g for 5 minutes at 4ºC. The supernatant was discarded, and the RNA pellet was air dried before being resuspended in ddH$_2$O. A BioSpectometer (Eppendorf) was used to measure RNA concentration.

2.7.2. DNase treatment

To remove any DNA contamination in the samples, the RNA was treated with DNase I, RNase-free (ThermoFisher Scientific). For each sample, 1µg of RNA was diluted with nuclease-free water to a final volume of 8µl, to which 1µl 10x reaction buffer with MgCl$_2$ and 1µl DNase I, RNase-free was added. The samples were incubated at 37ºC for 30 minutes. Samples were then incubated at 65ºC for 10 minutes with 1µl 50mM EDTA in order to stop the reaction. Following DNase treatment, the RNA concentration was re-measured.

2.7.3. Reverse transcription

The EvoScript Universal cDNA Master (Roche) was used for reverse transcription. One microgram (1µg) of RNA for each sample was diluted in ddH₂O, up to a volume of 16µl, and combined with 4µl of 5x Reaction Buffer. The samples were briefly centrifuged and placed on ice for 5 minutes to the allow primers to anneal to the RNA. 2µl of 10x Enzyme Mix was then added and the samples placed in a T100 Thermal Cycler (Biorad), and the optimised program was run (42ºC for 15 minutes, 85ºC for 5 minutes, 65ºC for 15 minutes and 4ºC unlimited hold time). The resulting cDNA was diluted 1:10 with ddH₂O and stored at -20ºC.

2.7.4. Quantitative real-time PCR (qPCR)

Quantitative PCR (qPCR) was used to quantify genes of interests. For this, a SYBR MESA green master-mix was used. This contained 10µl MESA green (Eurogentech), 5µM of the forward and reverse primers for the gene of interest (100µM stock; custom-made, Sigma) **(Table 2.7)**, made up to 18µl with ddH₂O for each well of the 96-well plate needed for analysis. The master-mix (18µl) and 2µl of each cDNA sample was pipetted into each well. The reactions were performed in triplicate for each cDNA sample analysed. The Bio-Rad CFX Connect Real-Time System was used to run the qPCR program. This included an initial incubation at 95ºC for 4 minutes, followed by 40 cycles of 94ºC for 30 secs, 60ºC for 15 secs and 72ºC for 30 secs. At the end of the run, a melting curve was produced to check for the specificity of the product. Data was exported to Microsoft Excel for analysis using the ΔΔ-CT method for relative quantification (Livak and Schmittgen, 2001; Pfaffl, 2001). All qPCR data was normalised to 2 reference genes – *GAPDH* and *β-Actin*.

Table 2.7 Primers used for qPCR

Gene	Forward Primer	Reverse Primer
β-ACTIN	TCACCACCACGGCCGAGCG	TCTCCTTCTGCATCCTGTCG
CTIP2	CTCCGAGCTCAGGAAAGTGTC	TCATCTTTACCTGCAATGTTCTCC
EMX2	GCTTCTAAGGCTGGAACACG	CCAGCTTCTGCCTTTTGAAC
FOXG1	TGGCCCATGTCGCCCTTCCT	GCCGACGTGGTGCCGTTGTA
GAPDH	ATGACATCAAGAAGGTGGTG	CATACCAGGAAATGAGCTTG
Nestin	AGCAGGAGAAACAGGGCCTAC	CTCTGGGGTCCTAGGGAATTG
OTX2	TGCCAAAAAGAAGACATCTCCA	AAGCTGGGCTCCAGATAGACAC
PAX6	AACAGACACAGCCCTCACAAACA	CGGGAACTTGAACTGGAACTGAC
SATB2	CAACGCAACTAATAATCATCTCCC	GAGAAAGGGCTGAGAACCCG
TBR1	AGCAGCAAGATCAAAAGTGAGC	ATCCACAGACCCCCTCACTAG
TUJ1	CATGGACAGTGTCCGCTCAG	CAGGCAGTCGCAGTTTTCAC

2.8. Functional phenotypic analysis

The γ-secretase inhibitor, DAPT (10µM, Sigma) and CDK4/6 inhibitor, PD0332991 (2µM, Selleckchem), were used from days 18 to 25 of cortical neuron differentiation to synchronise cell cycles, and advance neural progenitor cells to a post-mitotic stage, allowing them to mature. From day 19 of differentiation, neurons were transferred to an incubator fixed at 2% oxygen and the medium was replaced at least once a week, as required.

2.8.1. Calcium imaging

On the day of recording, the neurons were loaded with the calcium indicator Fluo-4AM (Life Technologies) at a final concentration of 5µM, along with 0.02% Pluronic F-127 (20% in DMSO, Life Technologies) and 0.01% Kolliphor EL (10% in DMSO, Sigma). Neurons were incubated for one hour at 37ºC in the dye mixture. After this time, cells were gently washed twice in DPBS and artificial cerebrospinal fluid (aCSF; **Table 2.8**, sigma), pH 7.4, was applied to cells and returned to the 37ºC incubator for 30 minutes. Prior to recording, aCSF was replaced with fresh recording solution.

An LED system (Rapp OptoElectronic and Lumencor) was used to record calcium activity at 10Hz for 10 minutes, with a final resolution of 1024*1024 pixels. Each time frame was split into 4 approximately equal regions of interest. A standalone MATLAB package, NeuroCa (Jang and Nam, 2015), was used to perform segmentation with the following parameters: the type of image, TIF; the image size, dependent on region of interest; the radius, 2-7 pixels; sensitivity, 0.9 and the frame rate at 10Hz. The segmentation files were retrieved and run in FluoroSNNAP, a MATLAB script for the analysis of calcium activity (Patel *et al.*, 2015). A summary text file was generated from the analysis, displaying values for amplitude ($\Delta F/F_0$), the inter-spike interval (ISI), the number of events and the rise and fall time of the spikes.

2.8.1.1. Quality control of calcium imaging data

All data was subject to rigorous quality control steps. Initially, any cell exhibiting no events was excluded from further analysis. Where data was missing for any parameter, the entire data set for that given cell was excluded. Data for each parameter in each field of view was then plotted alongside each other and any significant outlier was removed. Finally, for each time point, all fields of view were combined for each cell line.

2.9. Electrophysiology

2.9.1. Electrophysiology recording solutions

External solution **(Table 2.8)** was prepared in fresh sterile water and stored at 4ºC for a maximum of one week. Throughout preparation, the solution remained on a magnetic stirrer and following addition and dissolution of all components, 1mM sodium hydroxide was added dropwise to attain a final pH of 7.4. The potassium-gluconate based internal solution (Table 2.8) was stored at -20ºC in 500µl aliquots. Before aliquoting, the pH of the internal solution was adjusted to pH 7.4 using KOH.

Table 2.8 Solution compositions for functional studies

Component	mM	g/L
External Solution (aCSF)		
Sodium chloride	135	7.89
Potassium chloride	5	0.373
Magnesium chloride	1.2	0.244
Calcium chloride (1mM stock)	1.25	1.25ml
D-Glucose	10	1.8
2-[4-(2-hydroxyethyl)-1-piperazinethanesulfonic acid (HEPES)	5	1.192
Internal Solution		
Potassium gluconate	117	27.4
Sodium chloride	10	0.584
HEPES	11	2.62
Na_2-ATP	2	1.1
Na-GTP	2	1.05
Na_2-phosphocreatine	1.2	0.306
Magnesium chloride	2	0.41
Calcium chloride (1mM stock)	1	1.25ml
Ethylene-glycol-tetraacetic acid (EGTA)	11	4.184

2.9.2. Preparation for patch clamp recordings

On the day of the experiment, the internal solution was thawed, filtered through a 0.22μM centrifuge tube filter and stored on ice until required. Recording pipettes (4-8MΩ) were pulled from borosilicate capillary glass (Sutter Instruments, USA) using a programmable mechanical puller (Flaming/Brown Sutter micropipette puller P1000).

2.9.3. Whole-cell patch clamp technique

Neuronal cultures grown on glass coverslips were gradually exposed to external solution to allow them to acclimatise, before being transferred to a recording chamber perfused with aCSF at a flow rate of 2-2.5ml/min. Patch pipettes were filled with internal solution. Cells were visualised using infrared differential interference contrast (DIC) video microscopy through an Olympus BX51 microscope. Whole-cell patch clamp recordings were attained at room temperature (20-22°C) using a Multiclamp 700B amplifier and Digidata 1332 or 1550 analogue to digital converter with pClamp software (all Molecular Devices, USA).

2.9.4. Experimental Paradigms

Upon immediately breaking into the neuron, resting membrane potential was recorded for 10 seconds. In order to establish other neurophysiological features, two whole-cell patch clamp paradigms were performed sequentially on the patched neuron in current clamp mode (holding potential -60mV). In the first paradigm, the patched neuron was injected with current progressing from -60pA to +120pA in 20pA steps (10 steps in total, each lasting 1s). This allowed evaluation of the ability of the neurons to generate an action potential, or train of action potentials. Following current step injection, the neuron was exposed to a current injection drop of 10pA for 1s. From this, the input resistance and membrane time constant (tau) were determined, and also used to determine the capacitance (capacitance=tau/input resistance). In paradigm two, an action potential was evoked by injecting a short 5ms pulse of 200pA current, with the current pulse injection repeated four further times. Action potentials reaching 0mV or above were considered successful. Data were analysed with Clampfit software (Molecular Devices) then exported to and plotted using GraphPad Prism.

2.10.   Dendritic Arborisation

To assess dendritic arborisation, neuronal cultures were transfected with a GFP expression vector using lipofectamine 3000 (Invitrogen, UK) according to manufacturer's instructions. In brief, for each well to be treated, 1μl Lipofectamine 3000 reagent was diluted in 25μl medium (tube A) and 1μg GFP expression vector, along with 1μl P3000 reagent diluted in 25μl medium (tube B). Tube B was then added to tube A and incubated at room temperature for 15 minutes. The DNA-lipid complex was added to the neuronal cultures and left to incubate at 37ºC for six hours, after which they were washed with

medium and cultured for a further 72 hours. Neurons were later fixed with 3.7% paraformaldehyde for 20 minutes, after which they were stained with an anti-GFP antibody as described in section **2.5.1**. Labelled neurons were visualised using a Leica DM6000B inverted microscope. Neurite arbors were assessed using FIJI (ImageJ) software with the semi-automated plugin Simple Neurite Tracer (Longair, Baker and Armstrong, 2011). Soma area was assessed using FIJI (ImageJ) by thresholding the image and selecting the soma body as a region of interest. The 'measure' function was then used to analyse the area of the selected region of interest.

2.11.   Statistical Analysis

All descriptive and comparative statistics presented in this thesis was carried out in either Prism 8 (GraphPad) or RStudio (version 1.1.442). To determine the route of analysis (parametric or non-parametric), normality tests were carried out (Shapiro-Wilk normality test). The statistical tests used for each of the experiments are described in the results of each chapter. Unpaired student's t-tests were carried out to assess statistical differences in means between two independent groups. Two-way ANOVAs were used to assess how two independent variables, in combination, e.g., time and genotype, affect a dependent variable. Unless otherwise stated, all summary plots of data show mean ±SEM. All results presented were the outcome of three independent differentiations.

3. Derivation, validation and characterisation of hESC *SGCE* knockout lines

3.1. Introduction

Myoclonus Dystonia (MD), caused by autosomal dominant mutations of the epsilon-sarcoglycan gene (*SGCE*), is fully penetrant when paternally inherited, making a neuronal cell model of this disorder an ideal platform to further characterise dystonia pathophysiology.

One tool widely used to study neuronal development is induced pluripotent stem cell (iPSC)-derived neurons. Their use has had a crucial bearing in advancing our knowledge and understanding of the pathological processes underpinning neurological disorders. However, their use is accompanied by a range of limitations, including background genetic variability between individuals and the iPSC lines generated from their tissue, potentially limiting interpretation of phenotypic differences. One approach in limiting the impact of background genotype, and therefore providing greater confidence fthat any differences observed are due to changes in expression of specific genes is the use of gene edited human embryonic stem cells (hESCs). These offer an attractive model to investigate the impact of single gene knock out (KO), such as *SGCE*, on neuronal differentiation *in vitro* by comparison with their isogenic control cell line.

The discovery of the CRIPSR/Cas9 gene editing system, and its optimisation for use in mammalian cells, has greatly enhanced our ability to carry out gene editing in human pluripotent stem cells (hPSCs). Conventionally, construction of plasmids or viral vectors that allow co-expression of the Cas9 protein and guide RNAs (gRNAs) into the target cell is required to target genes for genetic modification (Cho *et al.*, 2013; Cong *et al.*, 2013; Jinek *et al.*, 2013; Mali *et al.*, 2013). However, the iCRISPR platform bypasses the use of several cloning steps by using hESCs containing a doxycycline-inducible Cas9 that is stably integrated into their genome. Upon Cas9 induction, gRNAs are transfected into the cells, allowing targeted introduction of insertions or deletions to the gene of interest, with a reported efficiency of up to 40% (González *et al.*, 2014). Due to the ease and high success rates of this method, the iCRISPR platform was selected for the generation of the *SGCE*-knockout hESCs.

The brain-specific isoform of *SGCE* is predominantly expressed in the cerebral cortex, the cerebellum, and the hippocampus (Ritz *et al.*, 2011). Previous studies involving both human and murine brain imaging, and electrophysiological approaches, have demonstrated a key role for the cerebral cortex in dystonia pathogenesis. Measures of long-term potentiation-like synaptic plasticity in cortical circuits, such as the paired associative stimuli response, have been reported to be more responsive in dystonia than in healthy individuals (Weise *et al.*, 2006; Quartarone *et al.*, 2008; Schwingenschuh *et al.*, 2010), suggesting that this excess of neuronal activity may be responsible for some of the excessive involuntary movement observed in dystonia (Ruge *et al.*, 2011). Recent transcriptomic analysis of dystonia-

associated genes revealed functional convergence within specific cell types. Single-nuclear transcriptomic data derived from mouse brain identified the frontal cortex as one of the areas significantly enriched for genes associated with synaptic function. Dysregulation of synaptic signalling in striatal medium spiny neurons, adult nigral dopaminergic neurons and importantly, frontal cortical neurons, is believed to be the likely cause of dystonia pathogenesis, with multiple dystonia-associated genes found to interact and contribute to pathogenesis (N. E. Mencacci *et al.*, 2020). To date, no studies have investigated the effect of loss of ε-sarcoglycan on the generation of excitatory cortical neurons *in vitro*.

Differentiation of hESCs into a cortical fate has been established as a viable method to study cortical development (Johnson *et al.*, 2007; Gaspard *et al.*, 2008; Kim *et al.*, 2011; Shi, Kirwan and Livesey, 2012). Understanding of the key molecular processes and transitions underlying human corticogenesis is key in ensuring that PSCs are differentiating, as anticipated, towards a glutamatergic cortical neuronal fate. An online database providing information relating to changes in RNA expression during hESC-derived cortical differentiation is available at http://cortecon.neuralsci.org/ (van de Leemput *et al.*, 2014).

With neural induction, an increase in several markers of neural specification is observed. This includes an upregulation of *PAX6,* a prosencephalic marker, *FOXG1,* an indicator of telencephalic fate and *EMX1,* a dorsal telencephalon marker. An increase of each of these markers, with highest levels observed at peak NPC production, confirms that correct dorsal, cortical specification has occurred (Manuel *et al.*, 2015). In addition to cortical specification markers, NESTIN is a general marker of NPCs, implicated in radial growth of the axon and is expressed throughout the phase of progenitor cell generation (Lendahl, Zimmerman and McKay, 1990), while KI67 is a marker that signifies cellular proliferation (Miller *et al.*, 2018).

Following the generation of cortical NPCs, neurons fated for distinct cortical layers are produced in a specific order. Deep layer cortical neurons of layer VI are the first to emerge, with these cells expressing the marker *TBR1*. This is followed closely by a rise in expression of CTIP2 positive neurons which are found in layer V of the cortex. Later, upper layer neurons begin to appear, with these identified by the presence of SATB2, a DNA binding protein that controls chromatin organisation and gene expression (Molyneaux *et al.*, 2007; Gaspard *et al.*, 2008; Gaspard and Vanderhaeghen, 2011). The temporal expression of cortical projection markers in outlined in **Figure 3.1** and a summary of cortical differentiation markers can be found in **Table 3.1.**

This chapter will initially focus on the derivation and validation of *SGCE*ko hESCs using the CRISPR/CAS9 gene editing technique, with subsequent characterisation to include estimation of ε-sarcoglycan expression levels and key markers of pluripotency. Given the molecular, tissue and *in vivo* evidence for cortical involvement in the pathogenesis of dystonia **(Chapter 1.3)**, the *SGCE*ko isogenic

control hESCs were differentiated towards an excitatory, glutamatergic cortical neuronal fate. This chapter will also detail the phenotypic characterisation of the *SGCE*ko-hESC-derived cortical neurons, enabling direct comparison of knockout and isogenic wildtype lines, providing greater confidence that the observed phenotypes are related to direct dysfunction of the *SGCE* gene. This characterisation work will include: evaluation of the efficiency of neuronal induction, formation of neural rosettes, and generation of neurons of all cortical layers.

Table 3.1 Cortical differentiation markers

STAGE OF DIFFERENTIATION	ANTIGEN	ROLE IN NEURONAL DEVELOPMENT
NEURAL PROGENITOR MARKERS (D15)	Empty spiracles homeobox 2 **(EMX2)**	Dorsal telencephalon marker.
	Forkhead box protein G1 **(FOXG1)**	Regulates rate of neurogenesis in telencephalon.
	KI67	Expressed in cell cycle during all but G_0 and G_1 phases. Marker of proliferating cells.
	Orthodenticle homeobox 2 **(OTX2)**	Involved in regional patterning of the midbrain and forebrain
	Paired box 6 **(PAX6)**	Regulates regional development and neuronal migration in the cerebral cortex
	N-Cadherin **(NCAD)**	Involved in self-organisation of neurons
	Neuroectodermal stem cell marker **(NESTIN)**	Neural progenitor cell markers. Implicated in radial growth of the axon
CORTICAL NEURONS (D20-60)	COUP-TF-interacting protein 2 **(CTIP2)**	Expressed in post-mitotic layer VI and Va projection neurons.
	Microtubule-associated protein 2 **(MAP2)**	Stabilises neuronal shape by promoting microtubule synthesis and cross-linking with other components of the cytoskeleton.
	Neuronal Nuclei **(NEUN)**	Expression of NEUN corresponds with withdrawal of neuronal cells from the cell cycle and/or the initiation of terminal differentiation. Found in the nucleus of post-mitotic neurons
	Special AT-rich sequence-binding protein 2 **(SATB2)**	DNA binding protein that controls chromatin organisation and gene expression. Post-mitotic determinant for upper-layer cortical neurons.
	T-Box Brain Transcription Factor 1 **(TBR1)**	Expressed in post-mitotic layer VI projection neurons.
	Class III beta-tubulin **(TUJ1)**	Contributes to microtubule stability in neuronal cell bodies and axons. Intermediate neuronal marker.
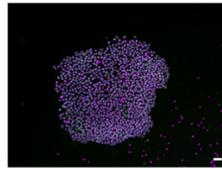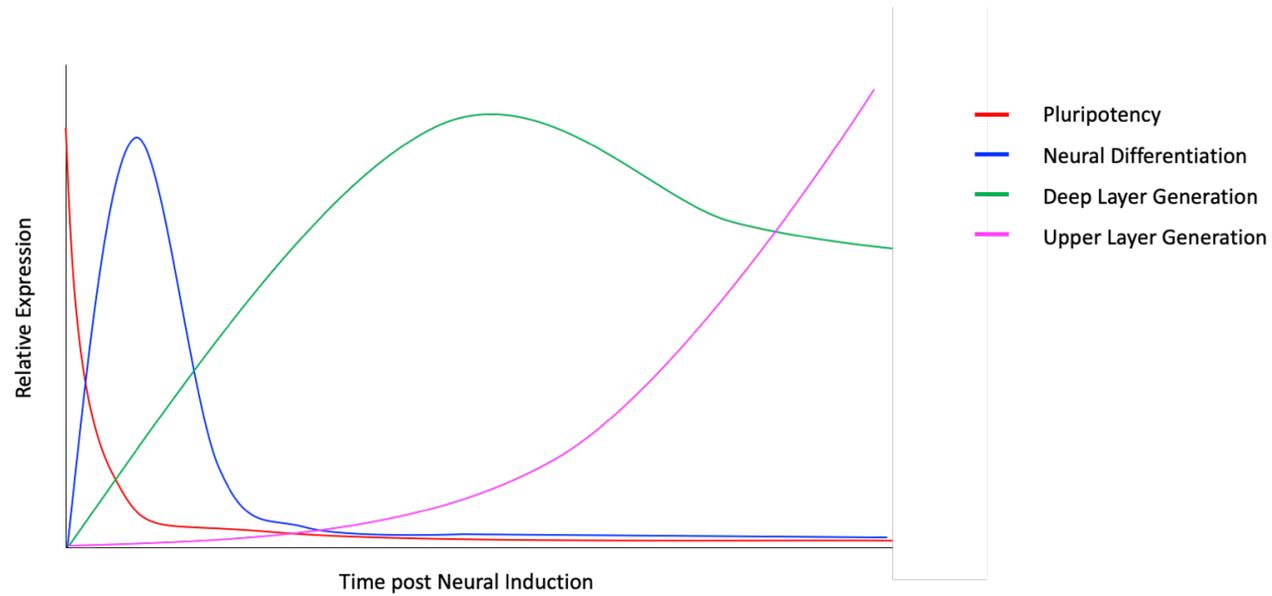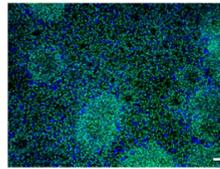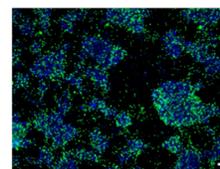
Figure 3.1 Temporal expression of cortical development markers

Schematic describing temporal expression of common markers expressed during different stages of cortical neuronal development; pluripotency (red), neural differentiation (blue), deep layer generation (green), upper layer generation (magenta).

3.2. Results

3.2.1. *SGCE* targeting in iCas9 hESCs

iCas9 cells, a pluripotent hESC cell line that has previously been genetically modified to allow for robust, doxycycline inducible expression of Cas9 nuclease, was used for targeting of the *SGCE* gene (González *et al.*, 2014). This cell line has a normal 46, XX karyotype. For gene targeting, this system requires the induction of Cas9 expression, followed by transfection of gRNA molecules into the cells. Three gRNAs targeting exon one and three targeting exon two of the *SGCE* gene were used to transfect iCas9 hESCs **(Chapter 2.2)**.

The synthesis and transfection of the gRNAs are described in **Chapter 2.2**. Two days after the second transfection, cells were dissociated into single cells and plated onto 10cm dishes, at a density of 500-2,000 cells per dish, and allowed to expand until small colonies emerged. Ninety-six colonies for each exon one and exon two targeted hESCs were manually isolated and expanded as single clones. Genomic DNA was extracted from each of the clones, and subsequently analysed using PCR in order to screen the region of interest in the targeted *SGCE* hESCs. The resulting PCR products were then run on an agarose gel in order to identify bands of differing lengths. This approach led to the identification of multiple insertions and/or deletions (indels) in several of the expanded clones.

Sanger sequencing was then used to confirm the indels revealed by PCR screening and gel electrophoresis, and to establish the precise nucleotide sequences of the targeted locus. A functional compound heterozygous knock-out line was generated by the iCRISPR process; clone #58. Clone 58 had a 12bp and 10bp deletion in one allele and a 5bp deletion in the other **(Figure 3.2)** and was used as the KO line for all of the experiments presented in this thesis. It is denoted as *SGCE*ko. Generation of a compound heterozygous loss of function mutant, rather than a heterozygous mutant that would generally recapitulate an autosomal dominant disorder, was key for this work given the maternal imprinting observed with the *SGCE* gene (Grabowski *et al.*, 2003; Peall *et al.*, 2014). A characteristic feature of imprinted genes is differential methylated regions (DMRs) which contain methylated cytosines at CpG sites, i.e. sites where a cytosine is followed by a guanine. If solely heterozygous lines were generated, the promoter region of the *SGCE* gene, which contains numerous CpG sites, would need to be analysed to assess the methylation pattern of CpG dinucleotides. This could be investigated using methylation specific PCR and bisulphite genomic sequencing (Huang, Bassil and Murphy, 2013). In order for a heterozygous mutant line to be a viable model of Myoclonus Dystonia, the mutation would have to be on the opposing allele to that which is methylated in order to ensure that the resultant cell line is representative of the disease genotype. Although generation of a compound heterozygous loss of function mutant doesn't directly replicate the mutant genotype observed in *SGCE* mutation causative Myoclonus Dystonia, it does provide opportunity to directly observe the loss of *SGCE*

expression, with opportunity for subsequent evaluation of any observed phenotype in patient-derived iPSC models.

The *SGCE*ko line was further evaluated through determination of the level of expression of *SGCE* RNA as well as the ε -sarcoglycan protein. qPCR was used to determine the levels of brain-specific *SGCE* in RNA samples from both hESCs and neuronal cells. A reduction of 82.00% of the brain-specific *SGCE* isoform was observed in *SGCE*ko neurons compared to WT **(Figure 3.3)**. Protein collected from the pluripotent cells and analysed using Western blotting techniques **(Figure 3.3)** demonstrates the absence of a protein band of the size anticipated for the ε -sarcoglycan protein in the *SGCE*ko targeted clone. The lack of a complete reduction of brain-specific *SGCE* alongside a complete reduction in ε -sarcoglycan protein may provide evidence of the presence of a small amount of *SGCE* mRNA, before nonsense mediated decay.

A
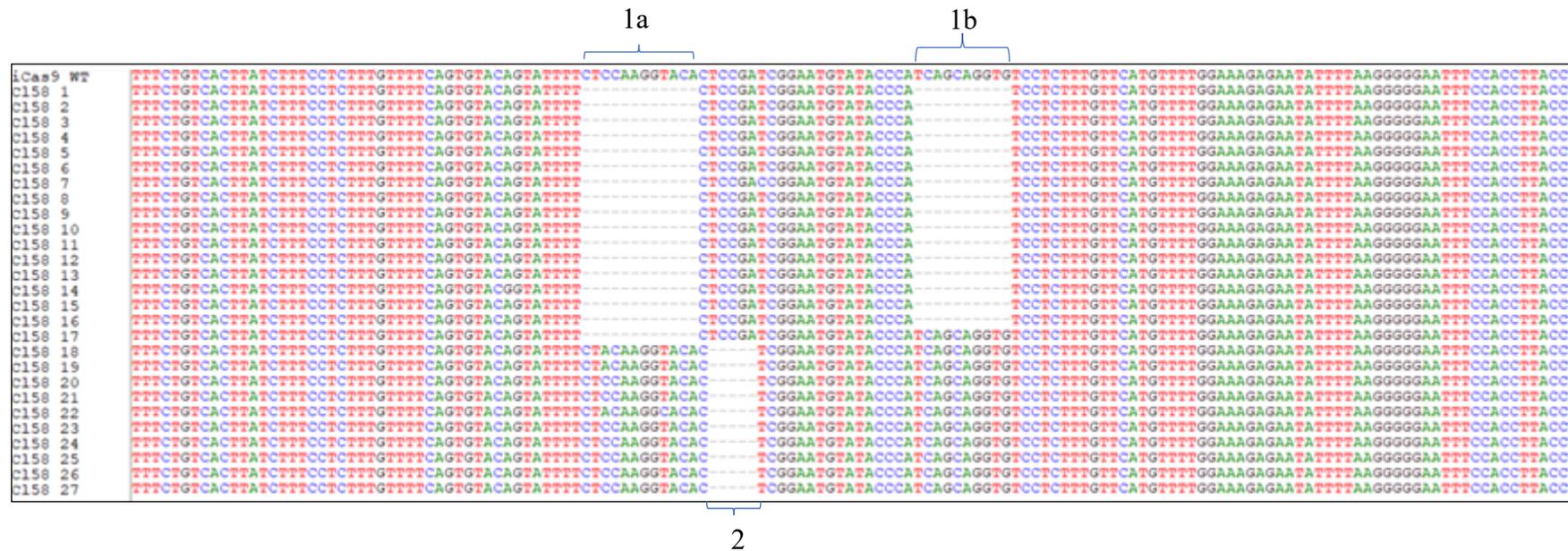
B

Clone 58	Allele	Type of sequence variant	Sequence (insertion/deletion)	Position (relative to transcription start site)		Genotype	Protein coding change	Predicted pathogenicity
	1a	Deletion	CTCCAAGGTACA	123	134	c.127_138del	p.lys43_ser46del	Provean score <-2.5: deleterious
	1b	Deletion	TCAGCAGGTG	157	166	c.270_279del	p.ala54serfs*29	Provean score <-2.5: deleterious
	2	Deletion	TCCGA	136	140	c.138_142del	p.asp47glufs*20	Provean score <-2.5: deleterious

Figure 3.2 Sequencing results of SGCE-targeted hESC

(A) Thirty clonal lines were sent for Sanger sequencing; 3 control iCas9 sequences, 27 clone 58 sequences. (B) Description of the identified deletions and their effect on translation of epsilon-sarcoglycan protein.
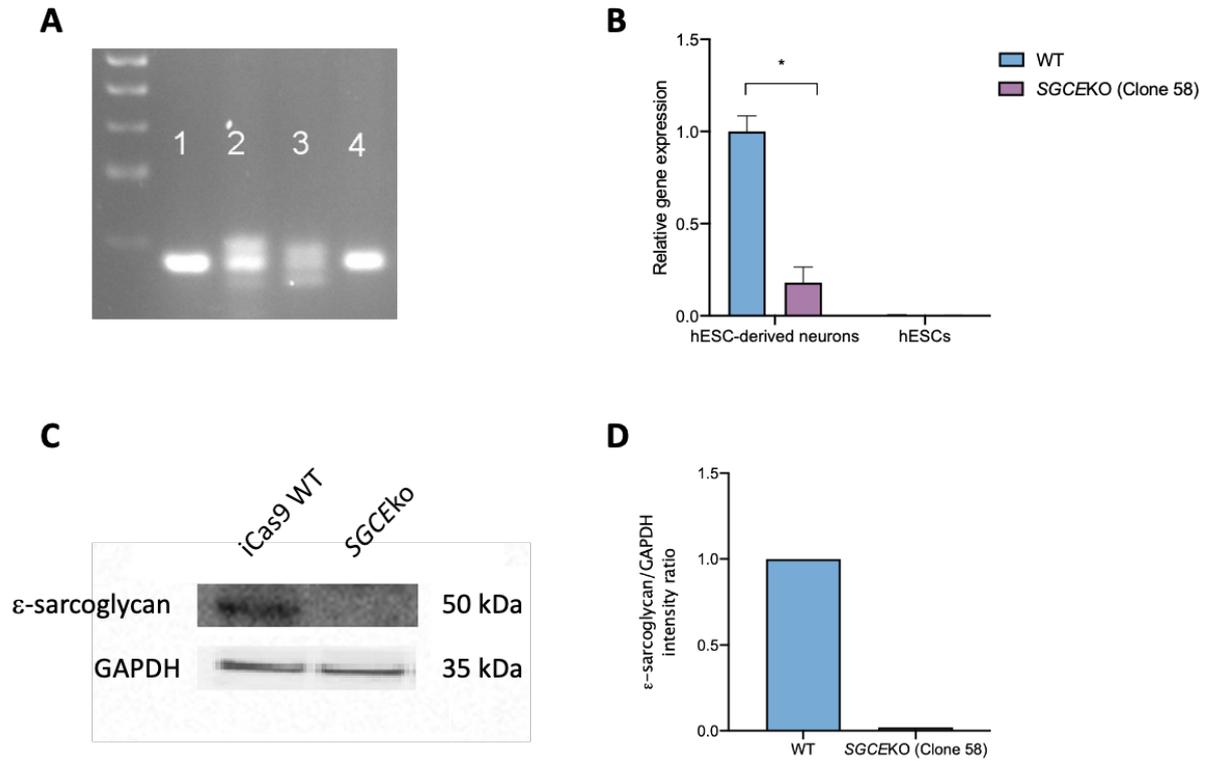
Figure 3.3 Screening of iCRISPR targeted hESCs

(A) Example of a DNA electrophoresis gel showing PCR products of the targeted locus from iCas9 hESCs (lane 1), two targeted clonal lines where indels are present (lanes 2 and 3) and one targeted clone that did not contain any indels (lane 4). (B) Gene expression analysis in *SGCE*ko neurons and WT controls. The level of the brain-specific *SGCE* transcript was determined relative to the expression of the housekeeping gene GAPDH. hESCs from *SGCE*ko and WT lines were used as negative controls and values were normalised to the WT neuronal control. Error bars indicate SEM. Statistics show results of students t-test ; *=p≤0.05 (C) Western blot for *SGCE*ko in control iCas9 and *SGCE*ko (clone 58) lines. (D) Quantification of western blot. Epsilon-sarcoglycan levels were normalised to the housekeeping gene GAPDH and show relative values.

3.2.2. Copy number variant analysis of genetically edited iCas9 lines

DNA was extracted from the iCas9 parental cell line, along with any cell lines found to harbour heterozygous or homozygous mutations, and quantified. All cell lines were genotyped using the Psych v1.1 array (MRC Centre for Neuropsychiatric Genetics and Genomics Core Facility). The results were analysed using PennCNV software, with quality control (QC) criteria including exclusion of copy number variants (CNVs) <100,000bp and those containing <10 single nucleotide polymorphisms (SNPs). All analysis was carried out by the MRC Centre for Neuropsychiatric Genetics and Genomics Core Facility and is summarised in **Table 3.2.** These results demonstrate that the parental line contained two duplications, one of 320,000 base pairs (bp) at chromosomal location 7q11.23, and another of 239,000bp located on the short arm of chromosome eight (8p23.2). Both CNVs were also identified in the compound heterozygous knockout line (Clone 58), with no additional deletions or duplications observed. Due to the larger of the duplications identified in the wild-type genotype being located on the long arm of chromosome 7, the same region as the *SGCE* gene, both loci were mapped to ensure that the duplication didn't also involve the *SGCE* gene **(Figure 3.4)**. This identified a region of 18,304,980bp separating the duplicated region and the *SGCE* gene. Only clone 58, with compound heterozygous deletions in the *SGCE* gene, was used for all subsequent analyses.
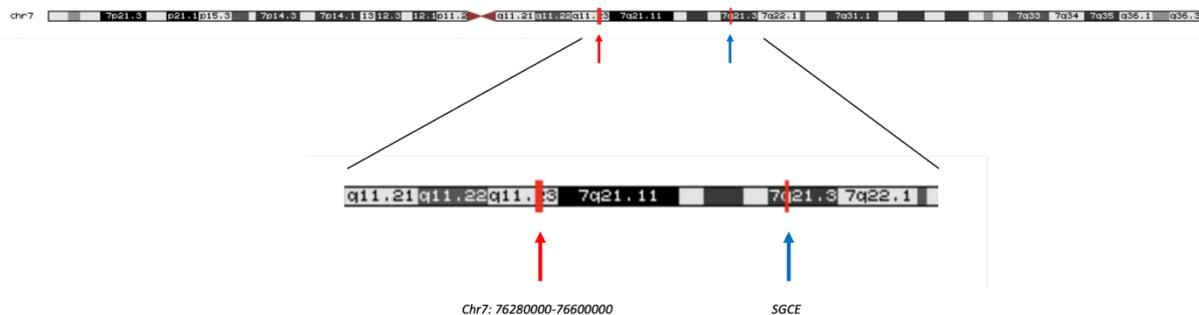
Figure 3.4 Schematic displaying location of duplication found on chromosome 7 following CNV analysis

The location of the 320,000bp duplication (red) and *SGCE* (blue) were mapped out on chromosome 7 in order to demonstrate no overlap in affected regions that may impact ongoing analysis.

Table 3.2 CNV analysis of iCas9 parental line and homozygous and heterozygous lines

Sample Id	CNV Location	Duplication/Deletion	Approximate Position	Length
iCas9 Control	7q11.23	Duplication	Chr7: 76280000-76600000	320,000
iCas9 Control	8p23.2	Duplication	Ch8: 2346000-2585000	239,000
Clone 58	7q11.23	Duplication	Chr7: 76280000-76600000	320,000
Clone 58	8p23.2	Duplication	Ch8: 2346000-2585000	239,000
Clone 35	7q11.23	Duplication	Chr7: 76280000-76600000	320,000
Clone 35	8p23.2	Duplication	Ch8: 2346000-2585000	239,000
Clone 39	7q11.23	Duplication	Chr7: 76280000-76600000	320,000
Clone 39	8p23.2	Duplication	Ch8: 2346000-2585000	239,000
Clone 41	7q11.23	Duplication	Chr7: 76280000-76600000	320,000
Clone 41	8p23.2	Duplication	Ch8: 2346000-2585000	239,000
Clone 43	7q11.23	Duplication	Chr7: 76280000-76600000	320,000
Clone 43	8p23.2	Duplication	Ch8: 2346000-2585000	239,000
Clone 46	7q11.23	Duplication	Chr7: 76280000-76600000	320,000
Clone 46	8p23.2	Duplication	Ch8: 2346000-2585000	239,000
Clone 48	7q11.23	Duplication	Chr7: 76280000-76600000	320,000
Clone 48	8p23.2	Duplication	Ch8: 2346000-2585000	239,000
Clone 69	7q11.23	Duplication	Chr7: 76280000-76600000	320,000
Clone 69	8p23.2	Duplication	Ch8: 2346000-2585000	239,000
Clone 69	19q13.2-q12.31	Deletion	Ch19: 47730000-48100000	370,000
Clone 82	7q11.23	Duplication	Chr7: 76280000-76600000	320,000
Clone 82	8p23.2	Duplication	Ch8: 2346000-2585000	239,000
Clone 75	7q11.23	Duplication	Chr7: 76280000-76600000	320,000
Clone 75	8p23.2	Duplication	Ch8: 2346000-2585000	239,000
Clone 88	7q11.23	Duplication	Chr7: 76280000-76600000	320,000
Clone 88	8p23.2	Duplication	Ch8: 2346000-2585000	239,000
Clone 88	19q13.2-q12.31	Deletion	Ch19: 47730000-48100000	370,000
Clone 93	7q11.23	Duplication	Chr7: 76280000-76600000	320,000
Clone 93	8p23.2	Duplication	Ch8: 2346000-2585000	239,000
Clone 95	7q11.23	Duplication	Chr7: 76280000-76600000	320,000
Clone 95	8p23.2	Duplication	Ch8: 2346000-2585000	239,000
Clone 95	19q13.2-q12.31	Deletion	Ch19: 47730000-48100000	370,000

3.2.3. Immunocytochemistry in *SGCE*ko embryonic stem cells

To verify that the *SGCE*ko hESCs had maintained key pluripotency properties following gene editing, the expression of OCT3/4 and TRA-1-81 was assessed by immunostaining **(Figure 3.5).** OCT3/4, a key regulator of pluripotency, is a transcription factor that plays an essential role in self-renewal, while TRA-1-81 is a surface marker expressed by undifferentiated hESCs. As shown in **Figure 3.5,** *SGCE*ko hESCs maintain high levels of OCT3/4 and TRA-1-81, with these levels being comparable to that of their control parental cell line. Furthermore, no spontaneous differentiation was observed in either cell line, indicating their suitability for disease modelling.
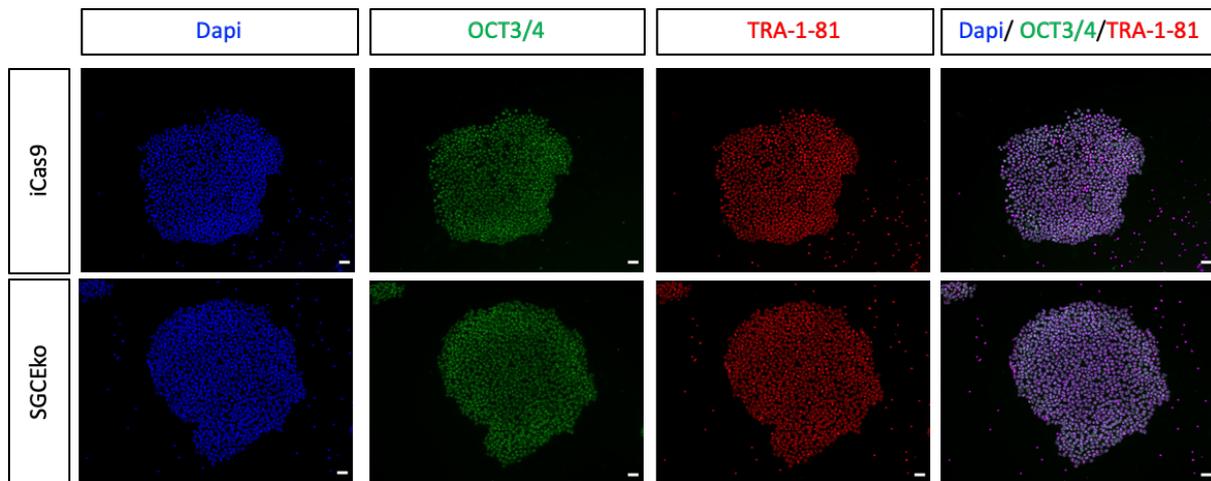
Figure 3.5 Immunocytochemistry in hESCs

Undifferentiated iPSCs stained for the pluripotency markers OCT3/4 (green) and TRA-1-81 (red). All nuclei are counterstained with DAPI (blue) , scale bars = 50μm.

3.2.4. Differentiation of *SGCE*ko hESCs towards an excitatory, cortical glutamatergic neuronal lineage

A dual SMAD inhibition protocol exploiting the small molecules LDN and SB was used to differentiate hESCs towards an excitatory cortical neuronal fate (outlined in **chapter 2.1.3.1).** Region and cell type specific markers, displaying dynamic temporal and spatial expression, can be monitored during neurodevelopment. In order to determine appropriate levels of change during *in vitro* pluripotent stem cell differentiation expression of these markers are typically analysed using immunofluorescence. A summary of these key markers, together with the stage of differentiation at which they are anticipated to be expressed are summarised in **Table 3.1**.

3.2.4.1. Early Cortical Development

3.2.4.1.1. Cortical Neural Progenitor Cells

With the differentiation protocol used in our laboratory (Chapter 2.1.3.1), cell lines are anticipated to differentiate into neural progenitor cells (NPCs), after ~12 days. At this time, the efficiency of NPC production and the positional identity of the differentiated cells was assessed by staining for four key markers, namely NESTIN, PAX6, FOXG1 and KI67. As outlined in **Table 3.1,** NESTIN, is a type VI intermediate filament widely expressed by proliferating cells of the developing central nervous system (Dahlstrand, Lardelli and Lendahl, 1995), while PAX6 and FOXG1 are both transcription factors expressed in dorsal forebrain progenitors and the wider group of forebrain cells, respectively (Greig, Woodworth et al., 2013). Finally, KI67 was used as a marker of the endogenous proliferative capacity of the cells.

As shown in **Figure 3.6 A and B** below, at day (D) 15 of differentiation, the majority of cells from both WT and *SGCE*ko lines stained positive for NESTIN (not quantified), with no significant differences in levels in the levels of expression of PAX6 (WT: 86.24% ±1.665 *vs.* KO: 83.86% ±0.7091, p=0.1914), FOXG1 (WT: 84.37% ±2.461 *vs.* KO: 83.71% ±1.754, p=0.8296), and KI67 (WT: 78.42% ±3.603 *vs.* KO: 78.94% ±2.354, p=0.9004).

A

B
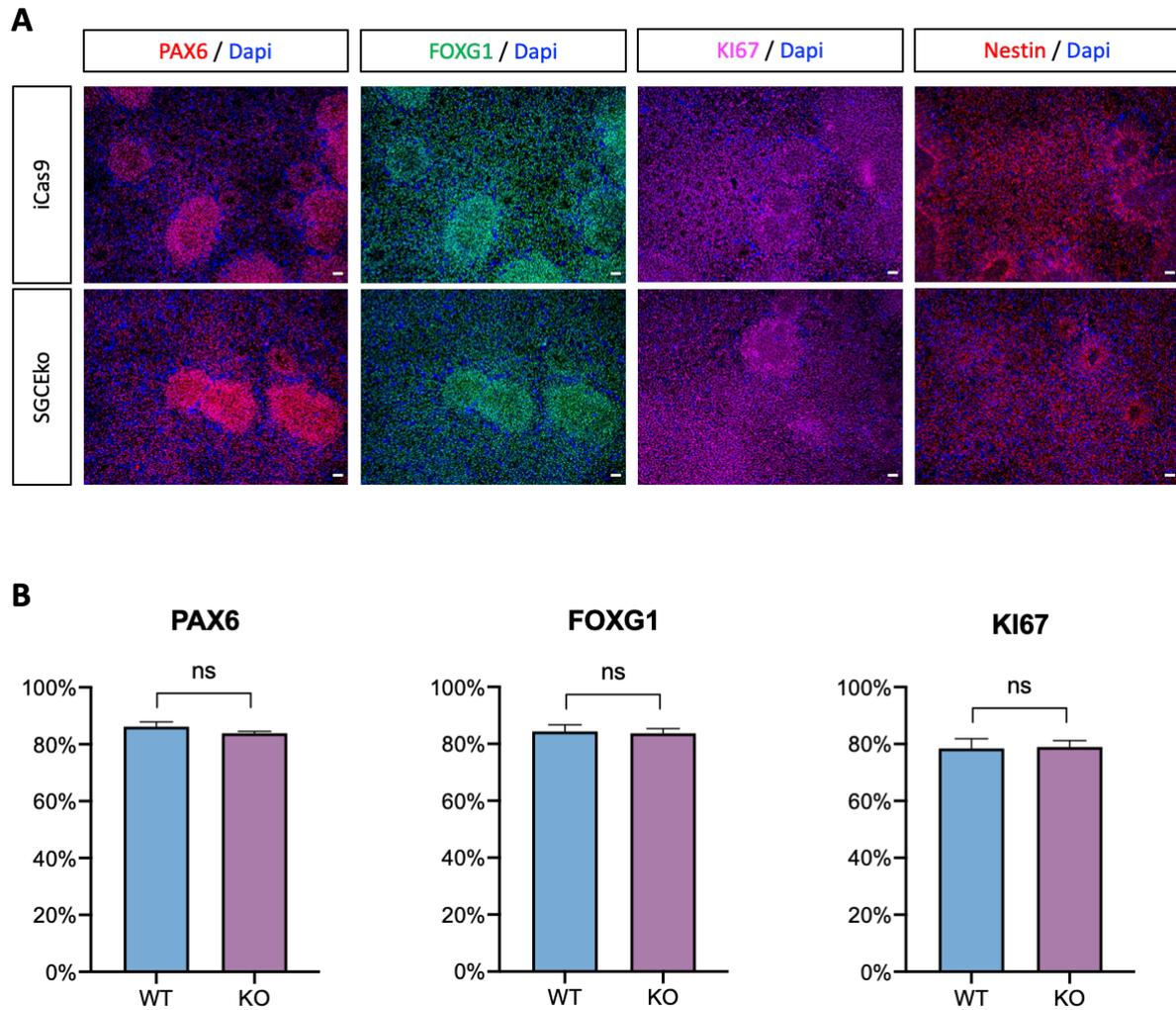
Figure 3.6 Expression of cortical progenitor markers in iCas9 and *SGCE*ko cultures

(A) Immunofluorescence for PAX6 (red), FOXG1 (green), KI67 (magenta) and NESTIN (red) of iCas9 and SGCEko cultures at D15 of differentiation. All nuclei were counterstained with Dapi (blue), scale bars = 50μm. (B) Quantification of the expression of PAX6, FOXG1 and KI67 in D15 iCas9 and *SGCE*ko NPCs. Data represent three independent rounds of cortical differentiation. Error bars represent mean ±SEM. No significant differences were found when quantification data was compared using t-test statistical analysis.

Table 3.3 Two-way ANOVA with post-hoc Tukey's test to analyse differences in NPC protein markers at day 15

NPC markers D15	Mean (%)	SEM	p-value
PAX6			
WT	86.24	1.665	0.1914
KO	83.86	0.7091	
FOXG1			
WT	84.37	2.461	0.8296
KO	83.71	1.754	
KI67			
WT	78.42	3.603	0.9004
KO	78.94	2.354	

In addition to investigating the effect of the loss of ε-sarcoglycan on the protein levels of key excitatory cortical markers, RNA levels were also evaluated to determine whether the differentiation of *SGCE*ko hESCs to cortical projection neurons followed a similar kinetic profile compared to their isogenic control. The expression profiles of these markers were compared to WT D0 levels, enabling calculation of both temporal expression and differential expression profiles **(Figure 3.7)**.

Overall, RNA levels followed a similar dynamic profile to that of the protein levels, with NPC markers PAX6, OTX2 and EMX2 increasing rapidly, peaking at D15 and then decreasing back to basal levels by D40. Interestingly, FOXG1 continued to increase up until D40, before beginning to decrease at D60.

Collectively, these results indicate that both iCas9 and *SGCE*ko cells are able to differentiate and undergo neural induction efficiently, and that no significant phenotypic differences exist between the lines in terms of positional identity or proliferation during these initial stages of differentiation.
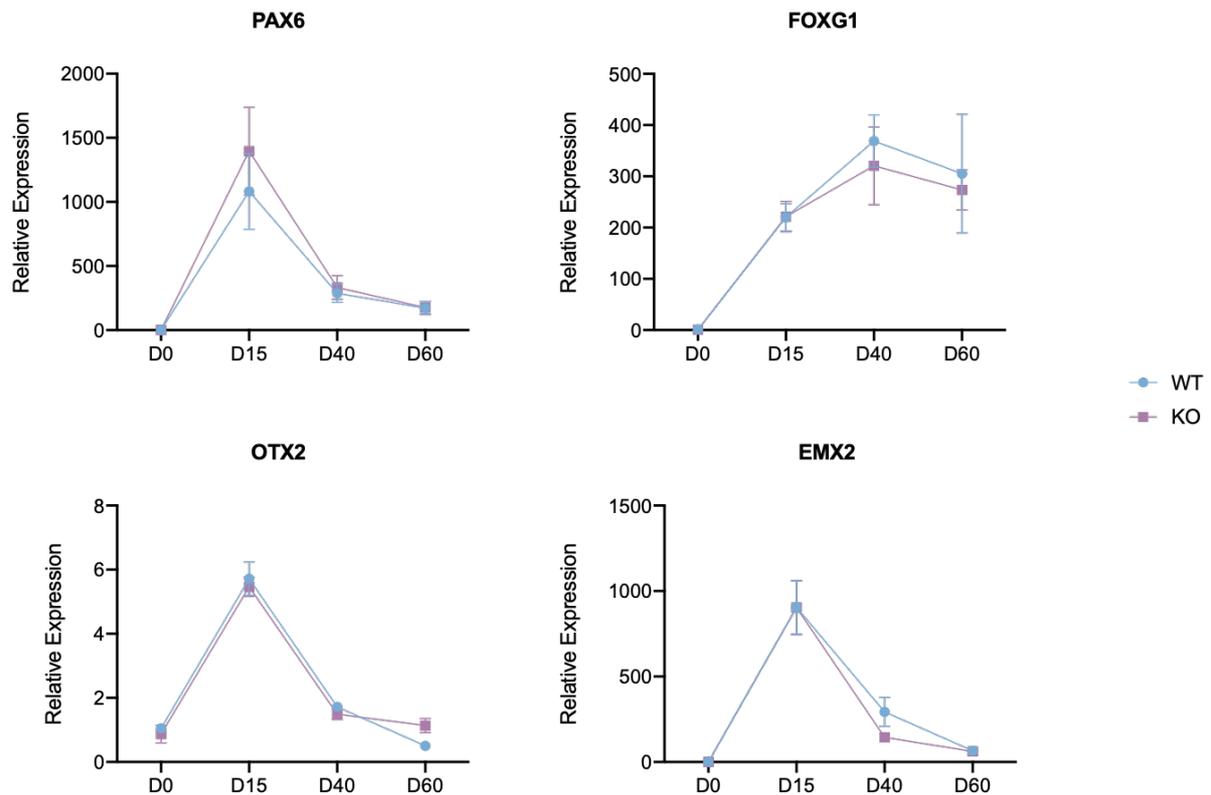
Figure 3.7 Expression of key genes expressed during early cortical development

qPCR data from RNA extracted on days 0, 15, 40 and 60 of differentiation. Key genes expressed during early stages of cortical differentiation were quantified and *SGCE*ko compared relative to control. Data represent three independent rounds of cortical differentiation and show mean ±SEM. Statistics show results of two-way ANOVA with post-hoc Tukey's test.

Table 3.4 Two-way ANOVA with post-hoc Tukey's to analyse differences key markers of early cortical development following qPCR

		Relative Expression	SEM	p-value
EMX2				
D0	WT	1.08	0.14	>0.9999
	KO	0.59	0.08	
D15	WT	771.67	151.20	>0.9999
	KO	793.22	144.90	
D40	WT	352.92	106.18	0.6975
	KO	140.98	4.24	
D60	WT	68.72	5.38	>0.9999
	KO	71.61	10.26	
FOXG1				
D0	WT	1.14	0.20	>0.9999
	KO	0.69	0.11	
D15	WT	220.26	26.87	>0.9999
	KO	221.28	29.58	
D40	WT	369.05	50.78	0.9447
	KO	320.47	76.09	
D60	WT	305.08	115.89	0.9911
	KO	273.60	39.29	
OTX2				
D0	WT	1.05	0.14	0.9843
	KO	0.87	0.27	
D15	WT	5.71	0.53	0.9467
	KO	5.47	0.31	
D40	WT	1.72	0.15	0.9641
	KO	1.49	0.17	
D60	WT	0.50	0.09	0.5663
	KO	1.38	0.22	
PAX6				
D0	WT	1.16	0.2406	>0.9999
	KO	0.86	0.2610	
D15	WT	1126.89	336.30	0.6162
	KO	1396.19	341.71	
D40	WT	286.73	70.21	0.9996
	KO	332.22	92.28	
D60	WT	172.53	51.93	>0.9999
	KO	176.47	48.91	

3.2.4.1.2.   Self-organising ability of cortical progenitors

During differentiation, PSC-derived neural progenitors self-organise into polarised structures named neural rosettes. These structures mimic the formation of the neural tube, with N-CADHERIN (NCAD) localising to the apical surface *in vivo* and marking the centre of the rosette *in vitro* (Elkabetz *et al.*, 2008).

To determine whether loss of ε-sarcoglycan affected the formation and development of neural rosettes, cultures were stained for NCAD at their peak of neural rosette formation **(Figure 3.8)**. Here, the neural progenitors demonstrated the correct radial organisation and circular patterning of NCAD, with the neural rosette identified being comparable in number (WT NCAD+ rosettes/1000 cells: 13.37 ±1.761 *vs.* KO: 17.42 ±0.9178, p=0.0758) and morphology (WT μm: 20.86 ±0.4970 *vs.* KO: 21.79 ±0.7240, p=0.8087) in both WT and *SGCE*ko neural progenitor cell cultures **(Table 3.5)**. These results indicate that the loss of function of the ε-sarcoglycan protein expression does not adversely impact the formation or development of neural rosettes.

Table 3.5 Unpaired t-test to analyse differences in NCAD$^+$ rosette number and morphology

	Mean	*SEM*	*p-value*
NCAD$^+$ Rosettes/1000 cells			
WT	13.37	1.761	0.0758
KO	17.42	0.9178	
Maximum diameter of NCAD$^+$ Rosettes (μm)			
WT	20.86	0.4970	0.8087
KO	21.79	0.7240	
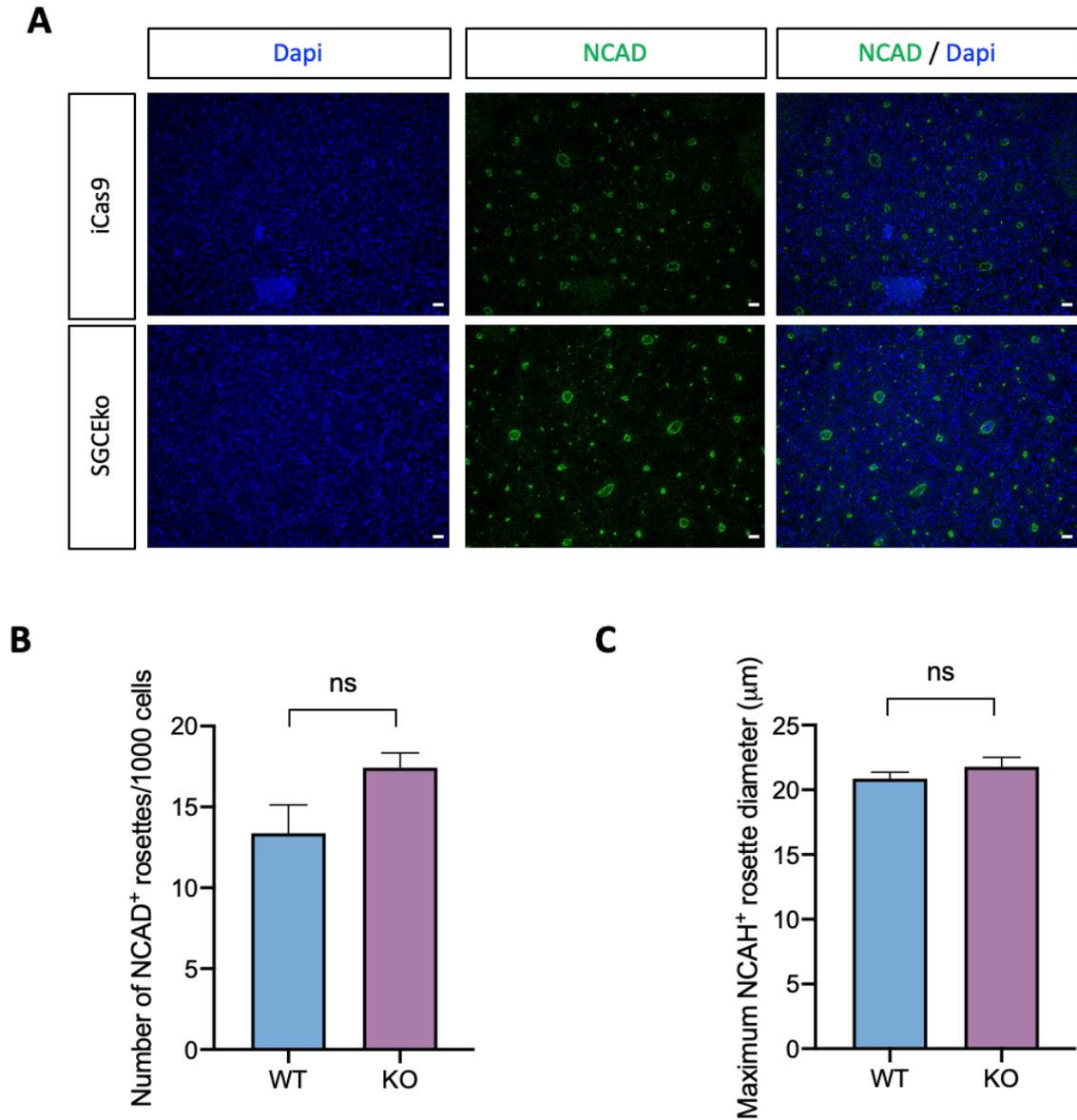
Figure 3.8 Neural rosettes in progenitor cells

(A) Immunostaining for NCAD (green) in iCas9 and *SGCE*ko cultures at D15 of differentiation. All nuclei were counterstained with DAPI (blue), scale bars = 50μm. (B, C) Quantification of NCAD+ rosettes. Quantification performed in ImageJ. Error bars represent mean ±SEM. Data represent three independent rounds of cortical differentiation. No significant differences were found when quantification data was compared using unpaired Student's t-test statistical analysis.

3.2.4.2. Cortical neurons

The development of the cerebral cortex takes place in an 'inside-out' manner. The first projection neurons produced are those of deep layers V and VI, with the remaining 4 layers being produced in successive waves, organising one above the other. Immunocytochemistry analysis showed that by D30 of differentiation, there was a downregulation of the neural progenitor markers PAX6 (WT: 86.24% ±1.665 *vs.* 19.63% ±1.574; KO: 83.86% ±0.709 *vs.* 19.37% ±0.9910) and FOXG1 (WT: 84.37% ±2.461 *vs.* 61.48% ±2.929; KO: 83.71% ±1.754 *vs.* 54.78% ±2.101) **(Figure 3.9A)**.

There was an upregulation of the deep layer cortical identity proteins CTIP2 and TBR1 by the neurons present in the culture **(Figure 3.9B+C)**. The layer VI marker TBR1 increased markedly between D20 and D30, peaking at D40, and the decreasing slightly at D60 in line with the reduced percentage of NEUN$^+$ cells (TBR1 - D20 WT: 2.627% ±0.2780 *vs.* KO: 1.517% ±0.2754, p=0.9996. D30 WT 46.51% ±3.098 *vs.* KO: 49.42% ±3.845 p=0.5634. D40 WT: 50.65% ±2.249 *vs.* KO: 55.16% ±3.075 p=0.3087. D60 WT: 46.44% ±2.988 *vs.* KO: 39.53% ±5.534 p=0.2266). The same was true for the layer V marker CTIP2 (D20 WT: 0.022% ±0.0222 *vs.* 1.134% ±0.2777, p=0.9983. D30 WT: 41.89% ±1.939 *vs.* 44.92% ±1.661, p=0.2414. D40 WT: 51.06% ±2.282 *vs.* 48.52% ±2.197, p=0.4541. D60 WT: 49.27% ±2.388 *vs.* KO: 43.24% ±2.607, p=0.0967), and the neuronal marker, NEUN (D20 WT: D20 6.296% ±1.007 *vs.* KO: 11.29% ±1.102, p=0.6364. D30 WT: 58.83% ±2.949 *vs.* KO: 58.93% ±2.269, p=0.9782. D40 WT: 60.73% ±2.661 *vs.* KO: 64.70% ±2.008, p=0.2547. D60 WT: 51.63% ±1.786 *vs.* KO: 51.26% ±5.344, p=0.2902). All markers were expressed at comparable levels in both the WT and *SGCE*ko lines at each time point analysed. Mean values and simple summary statistics are presented in **Table 3.6.**
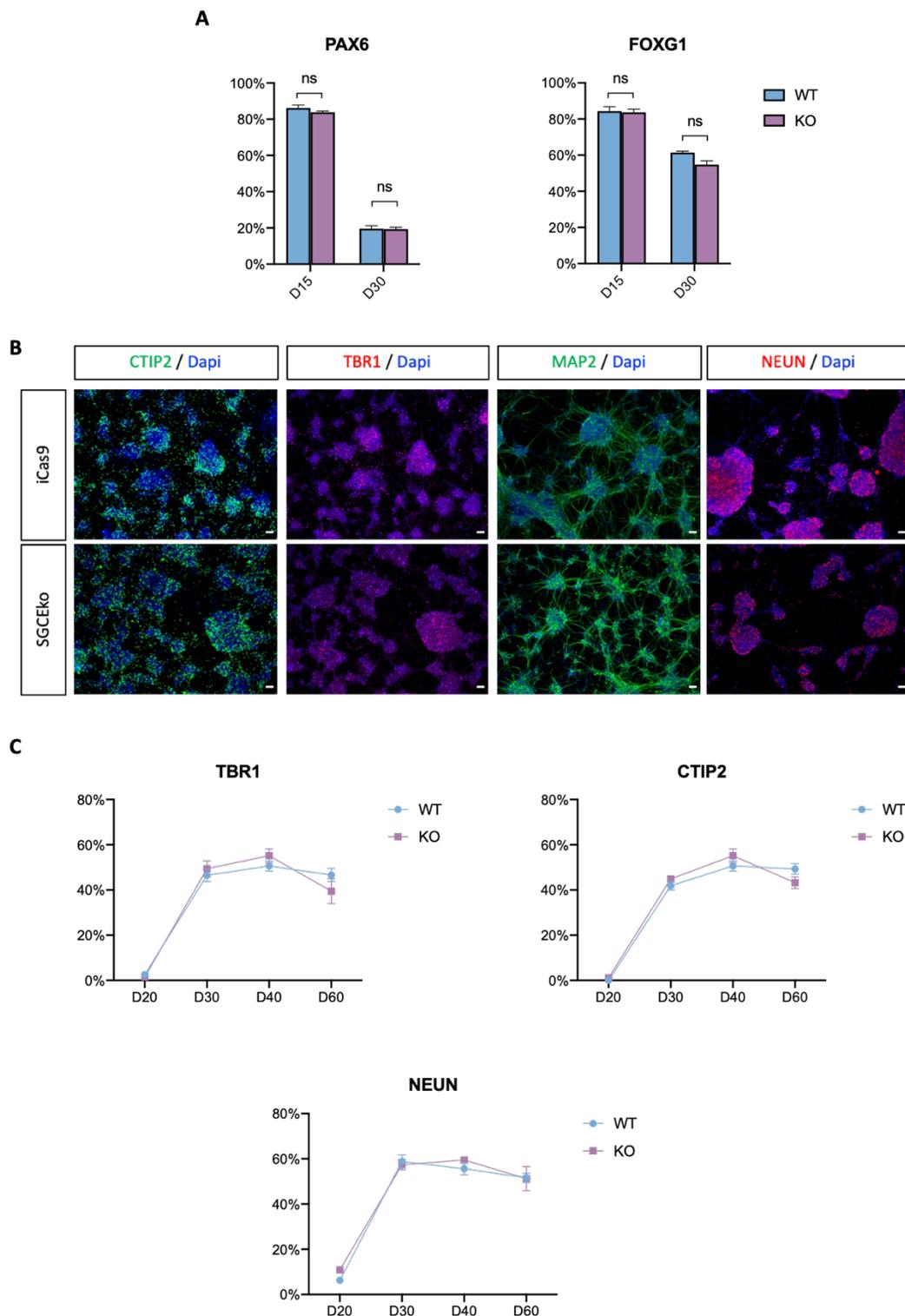
Figure 3.9 Expression of deep layer cortical markers in iCas9 and *SGCE*ko cultures

(A) Quantification of the expression of PAX6 and FOXG1 in D15 *vs.* D30 iCas9 and *SGCE*ko cultures. (B) Immunofluorescence for CTIP2 (green), TBR1 (red), MAP2 (green) and NEUN (red) in iCas9 and *SGCE*ko D30 cultures. All nuclei were counterstained with Dapi (blue), scale bars = 50μm. (C) Quantification of the expression of TBR1, CTIP2 and NEUN in iCas9 and *SGCE*ko cells over the course of the differentiation. Data represent three separate rounds of cortical differentiation. No significant differences were found when quantification data was compared by unpaired Student's t-test (A) or two-way ANOVA with post-hoc Tukey's test (C).

Table 3.6 Two-way ANOVA with post-hoc Tukey's test to analyse differences in neuronal markers

Neuronal Marker	Mean (%)	SEM	p-value
D20			
CTIP2			
WT	0.02222	0.02222	0.8604
KO	1.134	0.2777	
TBR1			
WT	2.627	0.2780	0.9995
KO	1.517	0.2754	
NEUN			
WT	6.296	1.007	0.6987
KO	11.29	1.102	
D30			
PAX6			
WT	19.63	1.574	0.8909
KO	19.37	0.9910	
FOXG1			
WT	61.48	2.929	0.0794
KO	54.78	2.101	
CTIP2			
WT	41.89	1.939	0.1857
KO	44.92	1.661	
TBR1			
WT	46.51	3.098	0.0779
KO	49.42	3.845	
NEUN			
WT	58.83	2.949	0.9826
KO	58.93	2.269	
D40			
CTIP2			
WT	51.06	2.282	0.8403
KO	48.52	2.197	
TBR1			
WT	50.65	2.249	0.9100
KO	55.16	3.075	
NEUN			
WT	60.73	2.661	8332
KO	64.70	2.008	
D60			
CTIP2			
WT	49.27	2.388	0.5681
KO	43.24	2.607	
TBR1			
WT	46.44	2.988	0.5017
KO	39.53	5.534	
NEUN			
WT	51.63	1.786	0.9999
KO	51.26	5.344	

RNA samples were also quantified in order to provide an additional measure of whether the cortical neuronal markers were comparable between *SGCE*ko and WT lines. The expression profiles of these markers were compared to WT D0 levels, again allowing calculation of both temporal expression and differential expression profiles **(Figure 3.10).**

The layer V marker CTIP2 followed the same kinetic profile as the protein levels with relative expression levels increasing to D40 before decreasing slightly at D60. TUJ1, a beta tubulin protein encoded by the *TUBB3* gene and primarily expressed in neurons, followed a similar pattern to CTIP2, with levels peaking at D40 and decreasing thereafter. Although not detected by immunofluorescence, SATB2, a post-mitotic determinant for upper layer cortical neurons, peaked in expression at D60 of differentiation with this comparable between the two lines. Overall, loss of ε-sarcoglycan did not affect the differentiation kinetics of key cortical neuronal differentiation markers when compared to those determined in the isogenic control cell lines.
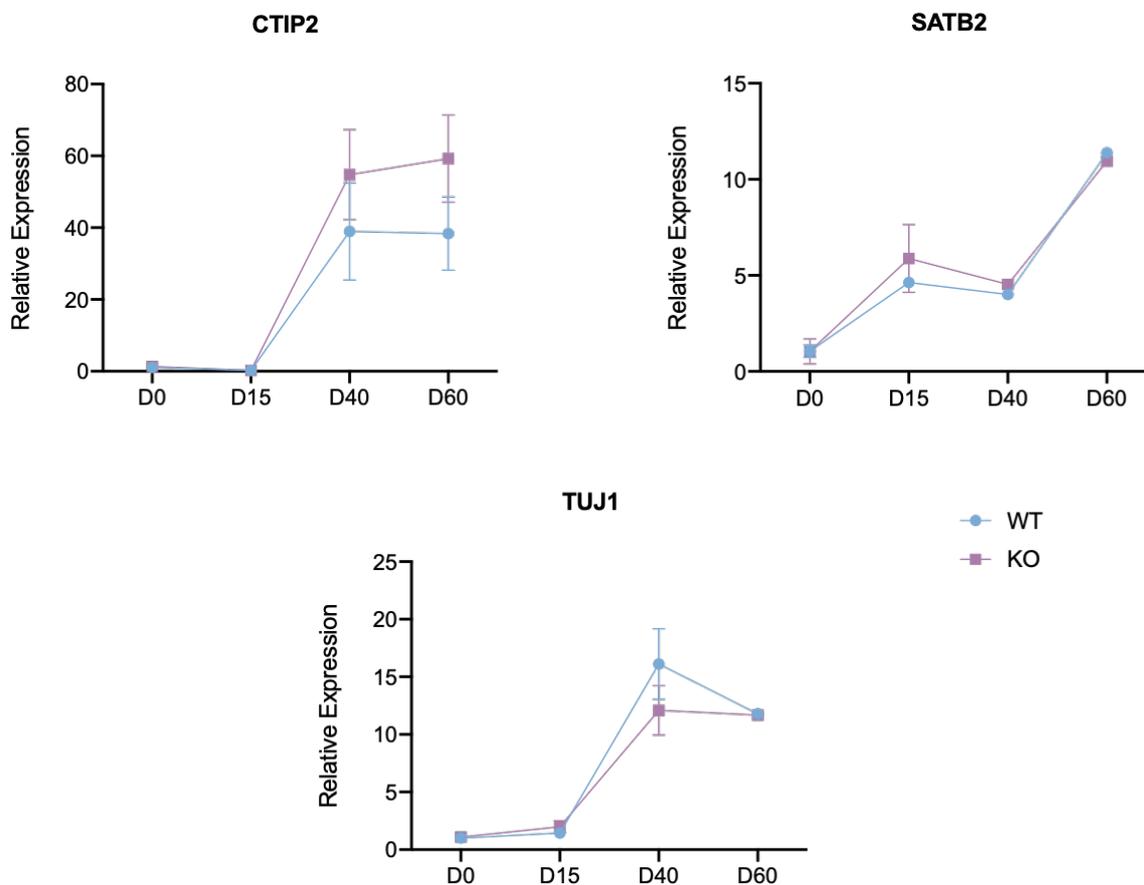
Figure 3.10 Expression of key genes expressed during late cortical development

qPCR data from RNA extracted on days 0, 15, 40 and 60 of differentiation. Key genes expressed throughout differentiation were quantified and *SGCE*ko compared relative to control. Data represent three independent rounds of cortical differentiation and show mean±SEM. Statistics show results of two-way ANOVA with post-hoc Tukey's test.

Table 3.7 Two-way ANOVA followed by Tukey multiple comparison of means to analyse differences in key markers late cortical development following qPCR

		Relative expression	SEM	Difference in means	95% confidence interval	Adjusted p-value	Summary
CTIP2							
D0	_WT_	1.01	0.05	-02725	-36.18 to 35.64	>0.9999	ns
	_KO_	1.28	0.16				
D20	_WT_	0.24	0.03	-0.01125	-35.92 to 35.90	>0.9999	ns
	_KO_	0.25	0.04				
D40	_WT_	38.97	13.54	-15.80	-52.97 to 21.37	0.8788	ns
	_KO_	54.76	12.54				
D60	_WT_	38.37	10.23	-20.89	-59.28 to 17.50	0.6765	ns
	_KO_	59.26	12.14				
SATB2							
D0	_WT_	1.05	0.33	0.01500	-7.021 to 7.051	>0.9999	ns
	_KO_	1.04	0.65				
D20	_WT_	4.63	0.16	-1.255	-8.291 to 5.781	0.9657	ns
	_KO_	5.89	1.77				
D40	_WT_	2.75	1.27	-0.5200	-10.47 to 9.430	>0.9999	ns
	_KO_	3.75	0.78				
D60	_WT_	11.38	0.23	0.4400	-9.510 to 10.39	>0.9999	ns
	_KO_	10.94	0.32				
TUJ1							
D0	_WT_	1.01	0.99	-0.08500	-7.647 to 7.477	>0.9999	ns
	_KO_	0.93	1.24				
D20	_WT_	1.48	1.42	-0.5350	-8.097 to 7.027	>0.9999	ns
	_KO_	1.47	2.50				
D40	_WT_	19.18	13.05	4.020	-3.542 to 11.58	0.4808	ns
	_KO_	9.94	14.25				
D60	_WT_	11.36	12.21	0.1000	-7.462 to 7.662	>0.9999	ns
	_KO_	12.00	11.37				

3.3. Discussion

This chapter initially sets out to describes the derivation of a compound heterozygous *SGCE* knock-out hESC line for the study of *SGCE* function in the development of excitatory cortical projection neurons. To model the loss of ε-sarcoglycan protein in hESCs, the H9-iCas9 line (González *et al.*, 2014) was modified using the iCRISPR technique. Transfection of gRNAs targeted to exons one and two of the *SGCE* gene were used to generate cell lines with loss of *SGCE* expression. A targeting efficiency of approximately 40% was reported in the original publication, however, in our hands, only 13 clones displaying mutations in either one, or both alleles were generated from a total of 192 clones (6.77%) screened. Reasons for this could be the genetic region targeted and/or the efficacy of the guide sequences chosen. Indeed, González et al., did report diversity in the percentage of mutant clones generated dependent on the target gene, varying between 20% and 70% (González *et al.*, 2014). Despite the lower-than-expected targeting efficacy, we were able to generate a compound heterozygous null hESC line, with pathogenic mutations in both alleles of exon 2 of the *SGCE* gene. To ensure the predicted compound heterozygous mutant line generated was not in fact a mixed clone containing homozygous, heterozygous and/or WT cells, approximately 50 independent sequencing runs were performed in total. This confirmed that this line was a true compound heterozygous line with one allele presenting with a 12bp and 10bp deletion, and the other allele a 5bp deletion.

The initial stages of characterisation included ensuring a maintained stem-cell state and pluripotent capacity, with staining for two key markers, OCT3/4 and TRA-1-81. Subsequent genotyping for off-target effects of the gene editing process using the Psych v1.1 array verified that the *SGCE*ko line had not accumulated any additional CNVs as a result of this process. Compound heterozygous loss of function *SGCE* mutations resulted in reduction of brain-specific *SGCE* mRNA, confirmed by qPCR, as well as loss of ε -sarcoglycan protein expression, confirmed by Western blot analysis. Collectively, these provided validation of the *SGCE* compound heterozygous null state of the hESCs, that no off-target effects had been induced by the gene editing process and that the cell line had maintained markers consistent with a pluripotent, stem cell state, indicating that this cell line represented a suitable model from which to investigate the effects of loss of ε -sarcoglycan expression on cortical neuronal development.

In order to explore the impact of loss of ε-sarcoglycan expression on cortical neuronal development, cells were differentiated towards an excitatory cortical pyramidal neuronal fate. The loss of ε-sarcoglycan expression did not appear to impact the rate or efficiency of neuronal induction and the positional identity of differentiating cells was not compromised. This was confirmed by the

identification of neural progenitors expressing dorsal telencephalic markers at comparable levels in both *SGCE*ko and wild-type lines.

Neural rosettes typically appear during the early stages of *in vitro* cortical differentiation and are identified by the polarised radial arrangements of NPCs, with their architecture recapitulating the cellular organisation of the neural tube, both in shape and function, with features such as the presence of interkinetic nuclear kinetics conserved (Lazzari *et al.*, 2006; Elkabetz *et al.*, 2008; Colleoni *et al.*, 2010). Both *SGCE*ko and iCas9 controls formed morphologically similar neural rosettes, suggesting ε-sarcoglycan is not critically involved in the self-organisation of NPCs to identifiable neural rosette structures, suggesting that development of the neural tube in individuals with *SGCE*-mutation positive Myoclonus Dystonia is unlikely to be disrupted, and that any neuronal changes accounting for the clinical phenotype take place at a later stage during neuronal development.

As cortical differentiation of the hESCs proceeds, downregulation of neural progenitor markers is observed, as would be anticipated with the development of cortical neurons. No significant differences were identified between the WT and *SGCE*ko cells in neither their proliferative behaviour or neurogenic rate; TBR1$^+$ and CTIP2$^+$ neurons were generated at comparable rates and efficiency, as were the number of neurons, indicated by the marker NEUN. This suggests that both *SGCE*ko and WT hESCs are able to differentiate to form neurons of deep cortical layers, with no observable differences in their kinetics.

Dystonia is characterised by 'abnormal functioning of a structurally normal-appearing brain' (Tanabe *et al.*, 2009), with conventional MRI unable to detect any gross morphometric brain abnormalities across both Mendelian inherited and 'idiopathic' forms of dystonia. Normal morphometric neuroimaging findings are observed in the majority of dystonia patients and post-mortem studies consistently demonstrate a lack of structural abnormalities (Sharma, 2019). Animal models of dystonia have also demonstrated normal gross neuroanatomy. The *dt*^{sz} hamster, a model bearing close resemblance to generalised paroxysmal dystonia in humans displays a relatively normal brain upon histological examination (Wahnschaffe *et al.*, 1990). Mice that are homozygous for knock-in or knock-out of the *Dyt1* gene do not survive past birth, however, their gross neuroanatomy in normal, with abnormalities instead observed at the level of the nuclear envelope in neurons (Goodchild, Kim and Dauer, 2005). Human diffusion tensor imaging (DTI) studies further support evidence of microstructural differences in individuals diagnosed with dystonia, to date predominantly examined in white matter tracts. Mutant-*DYT1* carriers show reduced fractional anisotropy in the subgyral white matter of the primary sensorimotor cortex (Carbon *et al.*, 2004, 2008), while a more recent study of those with blepharospasm found similar findings in the left anterior lobe of the cerebellum (Yang *et al.*, 2014) and in the left cerebellar white matter of patients diagnosed with cervical dystonia (Blood *et al.*, 2012).

Given the sheer amount of clinical evidence indicating the development of a structurally normal cortex in dystonia patients, it is feasible that there is a basis for functional changes rather than structural changes, with the concept of imbalance between excitatory and inhibitory pathways deserving further investigation.

There are several limitations that should be highlighted in this chapter. Firstly, the pluripotent state of both wildtype and *SGCE*ko hESCs could have been investigated further through the addition of extra pluripotent markers, e.g. NANOG, SOX2, and qPCR of these markers to assess mRNA levels would also have provided a beneficial complementary technique to assess pluripotency. The PluriTest characterisation tool (ThermoFisher) is also a reliable method to verify the pluripotency of stem cell cultures. Stem cells give rise to cells derived from all three embryonic germ layers: mesoderm, endoderm and ectoderm. Demonstrating the ability of the stem cells used in this thesis to differentiate into the different germ layers would provide further evidence for their pluripotent characteristics. Secondly, to further validate the use of the wildtype and *SGCE*ko lines, genomic integrity could have been assessed pre- and post-CRISPR, alongside the genotyping analysis carried out using the Psych v1.1 array, in order to look at copy number variations using BlueFuse multi-software (Illunina). Finally, the differentiation protocol used to generate excitatory cortical neurons in this thesis produced, on average, a culture containing approximately 60% of neurons. This leaves an additional 40% of cells unaccounted for. It would be interesting to identify the remaining cells in our cultures, however, their morphology suggests that they could potentially be glial cells and may be providing an added benefit to the cultures. Glia promote the formation and stabilisation of synaptic contacts by providing a continuous supply of crucial factors to neurons (Shi *et al.*, 2013) and stimulate neuron survival and plasticity (Jones, Cook and Murai, 2012). Glial fibrillary acidic protein (GFAP) is a commonly used astrocytic marker, that could have been used to help identify the presence of astrocytes in our cultures.

The results outlined in this chapter are consistent with human *in vivo* and post-mortem findings, suggesting that the brain-related changes responsible for the development of dystonia are not linked with gross morphological developmental abnormalities, and that further exploration of the microstructural and functional properties of the differentiated neurons is required. As such we move on to determine if loss of expression of the ε-sarcoglycan impacts neuronal function (Chapter 4, Calcium Imaging and Chapter 5, Electrophysiological properties) as well as the microstructural properties of differentiated neurons (Chapter 6, dendritic arborisation) at distinct, successive stages of neuronal development.

4. Investigating spontaneous calcium events in *SGCE*ko hESC derived neurons

4.1. Introduction

Calcium plays an essential role in normal cell physiology and is crucial for the function of excitable cells. Calcium regulates many aspects of neuronal activity, including eliciting neurotransmitter release (Neher and Sakaba, 2008) and the induction of activity-dependent synaptic plasticity (Zucker, 1999), as well as being associated with the control of numerous stages of development, including proliferation, migration, differentiation and survival (Spitzer, 2006; Platel, Dave and Bordey, 2008). Calcium homeostasis is maintained by both influx and efflux of calcium, along with the exchange of calcium with internal stores, and the binding of free calcium with calcium-binding proteins (Schwaller, 2010). As described in chapter 1.7.6, the influx of calcium into cells from the extracellular space is largely controlled by voltage gated calcium channels, NMDA, AMPA and nicotinic acetylcholine receptors, and transient receptor potential type C channels. Efflux of calcium from the cytosol into extracellular space is via the plasma membrane calcium ATPase and the sodium calcium exchanger (Nowycky and Thomas, 2002; Grienberger and Konnerth, 2012). The endoplasmic reticulum (ER) acts as a store for intracellular calcium, with the sarco-/endoplasmic reticulum calcium ATPase transporting calcium ions from the cytosol to the lumen of the ER and inositol triphosphate receptors and ryanodine receptors releasing calcium ions from the ER to the cytosol. Mitochondria are also able to sequester calcium via the calcium uniporter and release it back to the cytosol through the sodium-calcium exchanger (Stutzmann and Mattson, 2011). Concentration of calcium ions in cells can be measured using an optical method known as calcium imaging. Spiking activity in neurons has been inferred from somatic calcium signals. In pre-synaptic terminals, action potentials cause calcium influx in the neuronal cell body which is critical in the translation of electric activity into neurotransmitter release (Neher, 1998). There is growing evidence for atypical calcium homeostasis and signalling in the pathophysiology of dystonia, a summary of which is outlined in the sections below (**4.1.1- 4.1.3**)

4.1.1. Evidence from animal models of dystonia

The tottering mouse model of dystonia harbours a mutation in *Cacna1a*, the gene encoding the pore-forming alpha subunit of the $Ca_v2.1$ calcium channel, causing it to exhibit paroxysmal generalised dystonia with mild ataxic features (Campbell and Hess, 1999). $Ca_v2.1$ channels regulate neurotransmitter release and neuronal firing patterns throughout the brain. An approximately 40% reduction in $Ca_v2.1$ calcium current density has been demonstrated in this model (Wakamori *et al.*, 1998), with this causing an upregulation of $Ca_v1.2$ channels in an attempt to maintain calcium homeostasis (Campbell and Hess, 1999). This compensatory mechanism likely contributes to the

observed dystonic phenotype as use of Ca$_v$1.2 blockers have been shown to reduce the dystonic episodes, and Bay K8644, a Ca$_v$1.2 channel activator, induces dystonic attacks in these mice (Campbell and Hess, 1999). Another mouse model with a dystonic motor phenotype is the *leaner* mouse, which also harbours a mutation in the *Cacna1a* gene. Mice with such mutations present with severe generalised dystonia and ataxia. Diminished Ca$_v$2.1 activity in Purkinje cells from *leaner* mice has been linked with decreased expression of calcium-binding proteins, which in turn reduces the ability of cells to appropriately buffer intracellular calcium (Dove *et al.*, 2000).

The L-Type calcium channel Ca$_v$1.2 has also been implicated in models of dystonia. Wildtype mice display a motor symptom that highly resembles generalised dystonia when administered with L-type calcium channel agonists (Jinnah *et al.*, 2000). In the *tottering* mouse, low-doses of L-type calcium channel agonists induce dystonia whereas antagonists relieve dystonic symptoms. Furthermore, in a hamster model of dystonia that that is not attributed to genetic defects in calcium signalling, Ca$_v$1.2 antagonist have been shown to improve dystonic features (Richter and Löscher, 1996).

The lethargic mouse mutant carries a spontaneous mutation within the auxiliary β4 *Cacnab4* gene, and is associated with minor Ca$_v$2.1 calcium channel aberrations and mild dystonic symptoms (Shirley *et al.*, 2008). There is a suggestion that the level of disruption to calcium signalling directly relates to the severity of dystonia, with the *tottering* mouse model exhibiting more severe symptoms than *lethargic* mouse mutants. Another murine model, *Ip3r1*, in which type 1 inositol 1,4,5-trisphosphate receptors (IP$_3$R1) are conditionally knocked out in the cerebellum and brainstem, consequently disturbing intracellular signalling, also exhibits dystonic movements (Hisatsune *et al.*, 2013). IP$_3$R1s are the brain dominant subtypes of intracellular calcium channels, and are located on the endoplasmic reticulum membrane, the key regulator of intracellular calcium concentration.

Finally, studies in the genetically dystonic rat, an autosomal recessive model of generalised dystonia that harbours an insertional mutation in *Atcay*, show abnormalities in networks associated with calcium homeostasis. Oligonucleotide microarrays and quantitative reserve transcription-PCR have revealed upregulation of calcium-transporting plasma membrane ATPase 4 (PMCA4), with immunocytochemical experiments showing upregulation of PMCA4 in the cerebellar cortex of mutant rats (Xiao, Gong and LeDoux, 2007).

4.1.2. Evidence from other cellular models of dystonia

There have been several other calcium-associated genes that have recently been linked with dystonia. *ANO3,* the gene that encodes anoctamin-3, has recently been linked to a form of adult-onset autosomal dominant cranio-cervical dystonia (DYT23). Although its role is not fully established, anoctamin-3 is suggested to encode calcium-activated chloride channels (Tian, Schreiber and Kunzelmann, 2012).

Further evidence for a role of abnormal calcium homeostasis in dystonia comes from patients with a mutation in *HPCA*, the mutation accountable for DYT2 dystonia. Deficiency in *HPCA* is proposed to directly inhibit voltage-dependant calcium channels or modify membrane potential maintenance mechanisms, leading to abnormal striatal neuron excitability (Charlesworth *et al.*, 2015). Cells expressing *HPCA* mutations display increased calcium influx when depolarised with potassium chloride, mostly driven by N-type voltage gated calcium channels (Helassa *et al.*, 2017). In addition to the indirect effect of the *HPCA* gene on N-type calcium channels, the same channel is also implicated in a myoclonus dystonia syndrome linked with *CACNA1B,* a gene that encodes the a1B subunit of N-type calcium channels. It is important to note, however, that the *CACNA1B* association with myoclonus dystonia syndrome has only been reported in one family and has not been replicated in other cohorts. More recently, it has been implicated in progressive epilepsy-dyskinesia (Gorman *et al.*, 2019).

KCTD17 (DYT26), another recently identified novel disease-causing gene in dystonia, encodes the potassium channel tetramerization domain containing protein 17. Functional studies of fibroblasts isolated from a skin biopsy of a patient harbouring *KCTD17* mutation show that mutant fibroblasts display abnormalities in calcium release from the endoplasmic reticulum (Mencacci *et al.*, 2015).

4.1.3. Dystonia resulting from calcium channel dysfunction in other disorders

Dystonia is often recognised as a phenotypic component in other disorders examples of which include Episodic ataxia type 2 and spinocerebellar ataxia type 6. Both of these disorders have been linked with abnormal $Ca_v2.1$ channel activity, with this change in calcium channel function thought to contribute to the motor phenotypic characteristics of cerebellar ataxia with prominent dystonia (Giffin, Benton and Goadsby, 2002; Spacey *et al.*, 2005; Roubertie *et al.*, 2008; Cuenca-León *et al.*, 2009).

Patients with paroxysmal dyskinesias often present with recurrent episodes of dystonia, with one form of such a disorder caused by mutations to the *KCNMA1* gene. These gene encodes the alpha subunit of the calcium-sensitive potassium channel, otherwise known as the BK channel (Erro and Bhatia, 2019). Mutations to the BK channel have been found to increase calcium sensitivity three- to five-fold (Du *et al.*, 2005), with the increased calcium sensitivity proposed to induce rapid repolarisation, potentially permitting a faster firing rate and consequently increasing neuronal excitability.

4.1.4. Calcium disturbance linking with other proposed pathophysiological mechanisms in dystonia

Impaired dopaminergic metabolism, as a result of atypical calcium homeostasis, has been proposed as a potential pathogenic mechanism in *SGCE*-MD. The dystrophin-associated glycoprotein complex (DGC), whose role is in part to maintain physiological calcium homeostasis (Ozawa *et al.*, 2005), has

been shown to be present in the brain (Waite *et al.*, 2016). Lack of dystrophin in Duchenne muscular dystrophy, leads to augmented activity of calcium channels in neurons and consequently increased levels of intracellular calcium (Burr and Molkentin, 2015). In the brain, dystrophin co-purifies with ε-sarcoglycan, so it is conceivable that dystrophin dysfunction due to loss of e-sarcoglycan in myoclonus dystonia could induce neuronal damage and lead to calcium accumulation. Furthermore, calcium signalling is essential for regulating dopamine 2 receptor (D2R) responses induced by high-dopaminergic states (Brini *et al.*, 2014; Dragicevic *et al.*, 2014). With models of *SGCE*-MD displaying increased striatal dopamine levels and reduced D2R expression (Yokoi *et al.*, 2006; Zhang *et al.*, 2012), it is plausible that aberrant calcium homeostasis could contribute to the pathophysiological mechanisms underpinning *SGCE*-MD.

Although the precise mechanisms linking regulation of calcium homeostasis and dystonia are unclear, there is growing evidence that many forms of dystonia display altered calcium dynamics within neurons, which could play a fundamental role in neuronal excitability, and ultimately underlie dystonia pathophysiology. This chapter will investigate spontaneous calcium activity in mature *SGCE*ko neurons, and compare them to their isogenic iCas9 control line. Both cell lines were differentiated into mature excitatory projection neurons and spontaneous calcium activity analysed at days 60, 80 and 100 during neuronal maturation. This work formed an initial step in determining variation in neuronal excitability between the two distinct cell lines.

4.2. Results

Calcium imaging techniques were used to determine whether there was evidence of disruption to spontaneous cellular calcium transients in the *SGCE*ko neurons compared to the iCas9 control.

As described in chapter 2, the *in vitro* neuronal models were exposed to the calcium indicator, Fluo-4, allowing visualisation of neurons and assessment of calcium transients at a 488nm wavelength filter set. Selected fields of view were captured at 10Hz for 10 minutes. Following image processing, a semi-automated segmentation algorithm was used to select regions of interest (ROIs) in the MATLAB based package NeuroCa. Calcium transients were evaluated only in cell somas, and therefore ROIs were confined to individual cell bodies. Following segmentation of ROIs, the MATLAB package FluoroSNNAP was used to analyse fluorescent traces, and the detection and subsequent analysis of individual calcium events. Analysis involved six distinct calcium transient characteristics, providing an overview of spontaneous calcium activity within the neuronal cells. These included: overall percentage calcium activity, calcium transients, inter-spike interval (ISI), event amplitude, rise-time and fall-time. These features are outlined in more detail in **Figure 4.1**. All p-values presented in this chapter are following Bonferroni correction, unless otherwise stated, and a p-value <0.05 was considered statistically significant throughout.
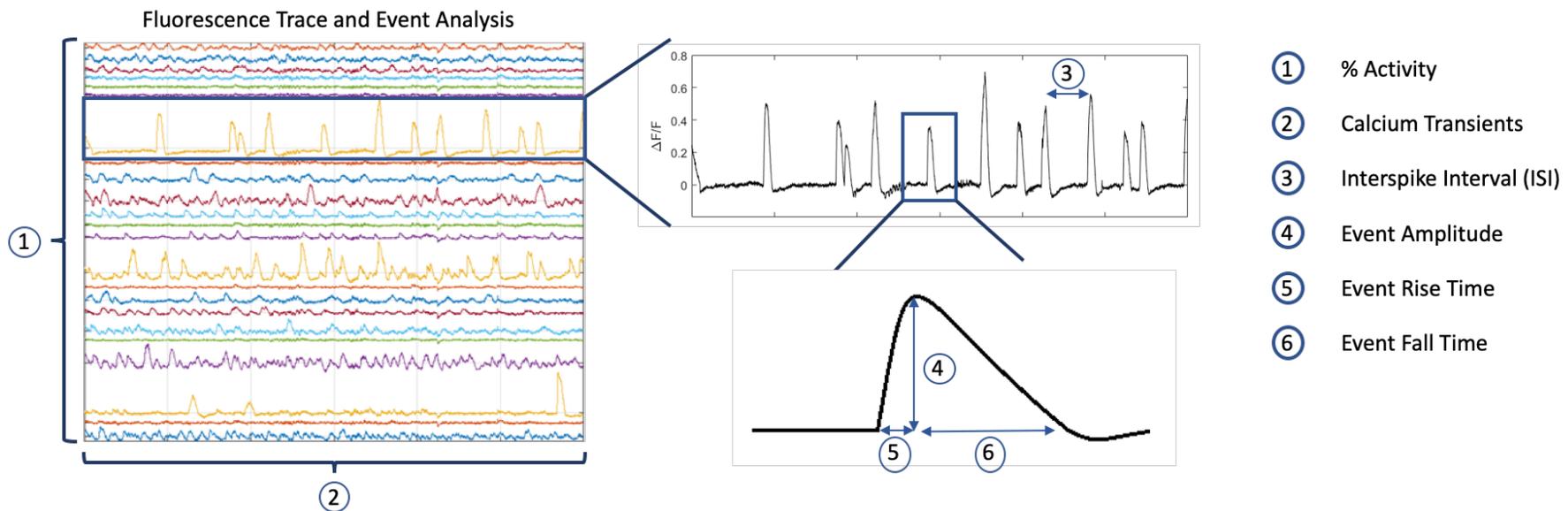
Figure 4.1 Calcium imaging of PSC-derived neurons

Neurons were analysed for spontaneous calcium activity using Fluo-4 dye at D60, D80 and D100 of differentiation. Following exposure of neurons to the dye and accessory agents, neurons were imaged using a fluorescence microscope with a 488 nm excitation filter set. Images were captured at 10Hz for 10 minutes. Individual ROIs were identified using a circular Hough transform-based method through NeuraCa software. FluoroSNNAP was used to analyse single cell fluorescence traces and for the detection and analysis of calcium events. A combination of threshold and template matching was used to select events, with analysis of calcium events limited to the single cell level – no network or cluster analysis was carried out. The six focal characteristics that were chosen for analysis: % activity, calcium transients, inter-spike interval (ISI), event amplitude, rise-time and fall-time.

4.2.1. Calcium Activity

To investigate the effect of loss of ε-sarcoglycan on the spontaneous calcium activity of hESC derived neurons, neurons from three separate differentiations were imaged and analysed at three different time points; day 60 (D60), day 80 (D80) and day 100 (D100). Overall measures of calcium activity were determined using the following parameters: percentage calcium activity, the number of calcium transients and the inter-spike interval.

4.2.1.1. Percentage Calcium Activity

A higher percentage of the neuronally differentiated cells were active in the *SGCE*ko-derived cultures, compared to their WT controls, at each of the time points analysed **(Table 4.1)**. This difference in activity also became more pronounced at successive time points, with a significantly higher level of activity at D80 (77.41% vs. 62.95%, p<0.05), which further increased at D100 (79.73% vs. 56.50%, p <0.001) (**Figure 4.2**, Chi-square test, see **Table 4.2** for statistics).

Table 4.1 Summary of % activity

Day of Differentiation	Cell Line	Mean	SEM
D60	WT	67.34%	28.61
	KO	77.06%	22.24
D80	WT	62.95%	18.96
	KO	77.41%	14.40
D100	WT	56.50%	14.69
	KO	79.73%	6.494

All subsequent analysis was carried out on active neurons only, i.e. those showing one or more calcium transients. Any cells not exhibiting calcium-related activity were excluded from further analysis.
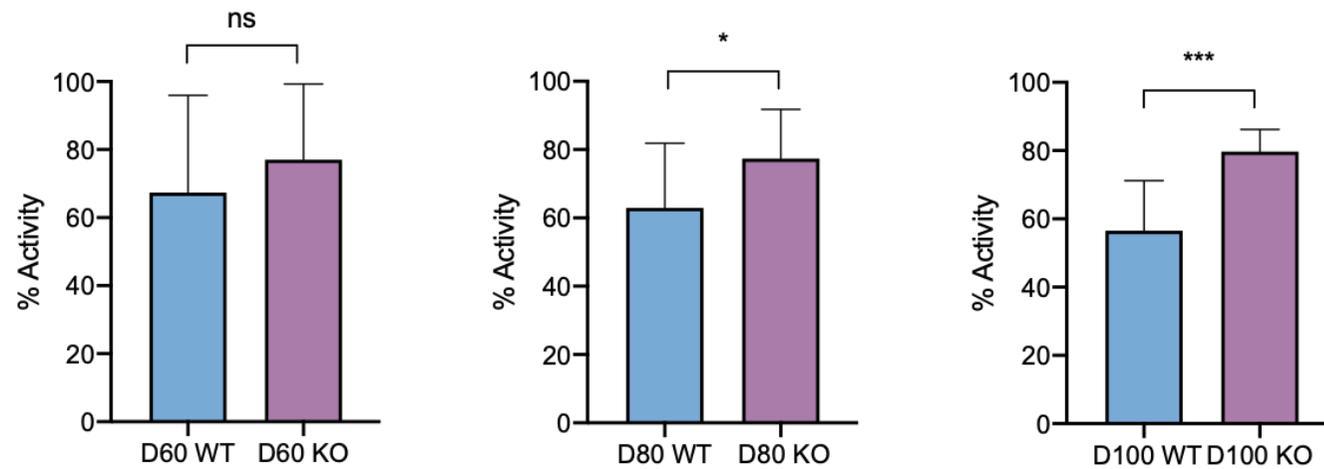
Figure 4.2 SGCEko hESC-derived neurons show more calcium activity compared to WT neurons

*SGCE*ko (KO) and iCas9 (WT) hESCs were differentiated into excitatory glutamatergic neurons. At D60, D80 and D100, coverslips were exposed to Fluo-4 dye and calcium movement was recorded and analysed. Neurons from *SGCE*ko were more excitable in terms of overall calcium activity at all timepoints analysed. Data represent mean±SEM. Statistics show results of Chi-Square Test; *=p≤0.05, **=p≤0.01, ***=p≤0.001, ****p≤0.0001. At each time point, calcium analysis was carried out on 4 fields of view from 4 coverslips for both WT and *SGCE*ko neurons, repeated over 3 differentiations.

Table 4.2 Chi-Square test to analyse calcium % activity differences between WT and SGCEko neurons

	Chi-Square Test			
	Chi-square, df	**z**	**P value**	**Summary**
WT_D60 vs KO_D60	2.480, 1	1.575	0.1153	ns
WT_D80 vs WT_D80	4.667, 1	2.160	0.0308	*
WT_D100 vs WT_D100	13.24, 1	3.638	0.0003	***

4.2.1.2.   Calcium transients

Calcium transients represent the mean number of calcium events in each cell at a given time point. Of the neurons displaying calcium activity, the number of calcium transients were significantly higher in *SGCE*ko neurons at D60 compared to WT neurons (WT: 7.256807 ±4.09 *vs.* KO: 9.068433 ±4.96, p<0.0001). However, this phenomenon was reversed at D80, with calcium transients being significantly higher in WT neurons compared to *SGCE*ko neurons (WT: 9.118314±9.41 *vs.* KO: 6.042365 ±6.02, p<0.0001), with the effect maintained at D100 (WT: 7.820202 ±8.05 *vs.* KO: 6.700935 ±6.07, p=0.0001918) (**Figure 4.3A**, Two-way ANOVA followed by Tukey multiple comparison of means, **Table 4.3**).

4.2.1.3.   Inter-spike Interval (ISI)

The Inter-Spike Interval (ISI) is described as the time interval between two calcium transients (Figure 5.1). During this analysis, statistically significant differences were observed between SGCEko and WT iCas9 neuronal lines at each time point. However, the direction of difference varied; initially at D60 the SGCEko line demonstrated a significantly shorter ISI (WT: 79.20462 ±39.33 *vs.* KO: 53.05208 ±29.32, p<0.0001). However, from D80 onwards this parameter was significantly longer in the SGCEko line compared to controls (WT: 60.19428 ±48.88 *vs.* KO: 101.8463 ±69.50, p<0.0001), with this difference sustained at D100 (WT: 67.37361 ±52.73 *vs.* KO: 93.18544 ±83.36, p<0.0001) (**Figure 4.3B**, Two-way ANOVA followed by Tukey multiple comparison of means, **Table 4.3**).
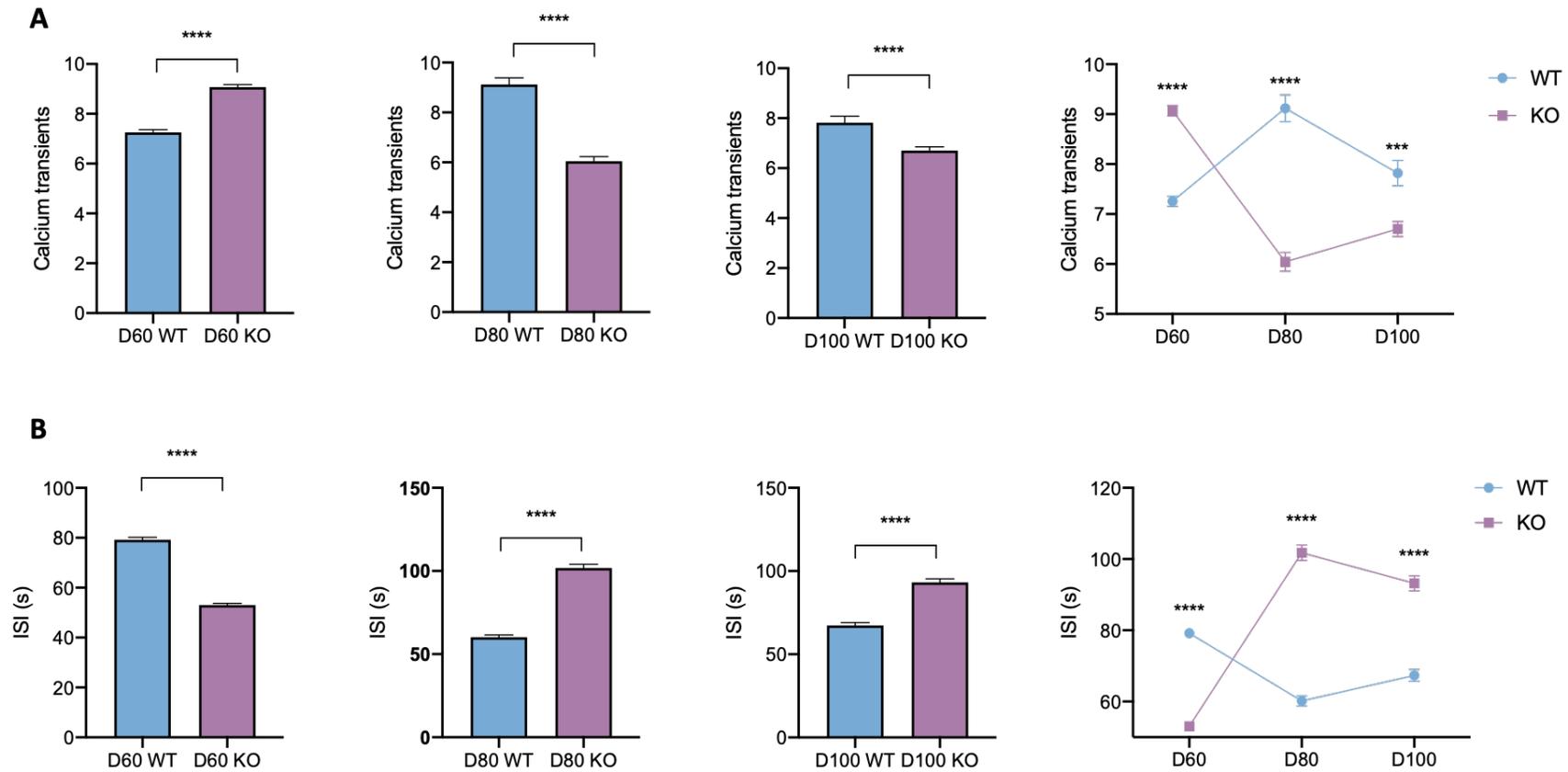
Figure 4.3 Calcium Activity in SGCEko and WT neurons

*SGCE*ko (KO) and iCas9 (WT) hESCs were differentiated into excitatory glutamatergic neurons. At D60, D80 and D100, coverslips were exposed to Fluo-4 dye and calcium movement was recorded and analysed. Neurons from *SGCE*ko displayed more calcium transients (A) and a lower ISI (B) at D60 than their isogenic WT control. By D80, this effect was reversed, with WT neurons exhibiting more calcium transients along with a lower ISI than *SGCE*ko neurons and this affect was maintained at D100. Data represent mean±SEM. Statistics show results of two-way ANOVA with post-hoc Tukey's test; *=p≤0.05, **=p≤0.01, ***=p≤0.001, ****p≤0.0001. At each time point, calcium analysis was carried out on 4 fields of view from 4 coverslips for both WT and *SGCE*ko neurons, repeated over 3 differentiations.

Table 4.3 Two-way ANOVA followed by Tukey multiple comparison of means to analyse calcium transient and ISI differences between WT and SGCEko neurons

	Mean	SEM	Difference in means	95% confidence interval	Adjusted p-value	Summary
D60						
Calcium Transients						
WT	7.256807	4.09	-1.812	-2.40 to -1.22	<0.0001	****
KO	9.068433	4.96				
Inter-spike Interval						
WT	79.20462	39.33	26.153	21.07 to 31.24	< 0.0001	****
KO	53.05208	29.32				
D80						
Calcium Transients						
WT	9.118314	9.41	3.061	2.29 to 3.83	<0.0001	****
KO	6.042365	6.02				
Inter-spike Interval						
WT	60.19428	48.88	-41.652	-48.28 to -35.03	< 0.0001	****
KO	101.8463	69.50				
D100						
Calcium Transients						
WT	7.820202	8.05	1.119	0.39 to 1.85	0.0001918	***
KO	6.700935	6.07				
Inter-spike Interval						
WT	67.37361	52.73	-25.812	-32.12 to 19.50	< 0.0001	****
KO	93.18544	83.36				

4.2.2. Calcium event shape

The shape of individual calcium events is characterised by multiple parameters including amplitude, rise- and fall-times, with differences observed between *SGCE*ko neurons and their isogenic controls for each measure.

4.2.2.1. Amplitude

Calcium transient amplitude, represented as $\Delta F/F_0$, whereby ΔF signifies the variation in calcium intensity at a given timepoint and F_0 indicates baseline fluorescence, was defined as the maximum change in fluorescence over baseline following the onset of a calcium transient. As neurons mature, an increase in the number of functional ion channels expressed on their cell membrane promotes an increase in calcium transient amplitude. Although both cell lines showed an increase in calcium transient amplitude throughout the differentiation, *SGCE*ko neurons demonstrated smaller amplitude transients at each time point, with these effects statistically different at days 60 and 80, (WT $\Delta F/F_0$ D60: 0.03540223 $\pm$0.01051 *vs.* KO: 0.03132009 $\pm$0.006956, p=<0.0001; WT $\Delta F/F_0$ D80: 0.04698541 $\pm$0.01799 *vs.* KO: 0.04441379 $\pm$0.01380, p=0.0013729). Although not statistically different at day 100 (WT $\Delta F/F_0$ D100: 0.04788889 $\pm$0.02587 *vs.* KO: 0.0467352 $\pm$0.01805, p=0.4303247), the overall pattern of lower calcium transient amplitude was maintained (**Figure 4.4A**).

4.2.2.2. Rise Time and Fall Time

Differences in the kinetics, namely the rise- and fall-times, of the calcium transients were also observed. Many different factors impact the kinetics of a calcium transient, including the number and frequency of action potentials, the activation of synaptic sources of calcium entry, and the neuronal buffering capacity. For both parameters the effects reversed between days 60 and 80, with a shorter rise time (WT ms: 1.118756 $\pm$0.3207 *vs.* KO: 0.9888433 $\pm$0.4324, p=<0.0001) and longer fall time (WT ms: 1.140272 $\pm$0.3608 *vs.* KO: 1.228581 $\pm$0.3347, p=<0.0001) at day 60, while at day 80 the SGCEko neurons demonstrated a significantly longer rise time (WT ms: 1.214149 $\pm$0.5118 *vs.* KO: 1.394079 $\pm$0.5118, p=<0.0001) (***Figure 4.4*B**) and shorter fall time (WT ms: 1.187874 $\pm$0.4321 *vs.* KO: 1.053429 $\pm$0.4496, p=<0.0001) compared to their isogenic controls (**Figure 4.4C**). This flux between days 60 and 80 in calcium transient features being mirrored in the changes seen in ISI and calcium transients described above. Maturation of the neuronal lines between days 80 and 100 saw maintenance of the difference in these characteristics, with significantly longer rise time and shorter fall times observed in the KO line compared to control (Rise time WT ms: 1.396707 $\pm$0.5559 *vs.* KO: 1.509003 $\pm$0.6793, p=<0.0001; Fall time WT ms: 1.119296 $\pm$0.4612 *vs.* KO =1.024575 $\pm$0.4084, p=<0.0001).

Overall, there is evidence to suggest that loss of ε-sarcoglycan causes disruption to spontaneous calcium events in hESC-derived cortical neurons, both in terms of overall activity and shape of the calcium events. In general, differentiation of *SGCE*ko hESCs towards an excitatory glutamatergic cortical lineage exposed several significant phenotypic effects in comparison to their isogenic WT control. These included:

- Higher percentage activity
- Lower calcium transients
- Longer inter-spike interval
- Smaller amplitude
- Longer rise time
- Shorter fall time

These effects typically became evident at day 80 and were maintained, if not increased, at day 100, suggesting a sustained phenotypic distinction between the cell lines, with this potentially resulting from the loss of function of the epsilon-sarcoglycan protein.

In addition to the calcium activity recordings taken at baseline, neurons were also treated with the L-type calcium blocker nifedipine, as well as the competitive AMPA antagonist cyanquixaline (CNQX) and selective NMDA antagonist AP5. Each of these pharmacological inhibitors ablated all responses in both WT and *SGCE*ko neurons and were rescued following drug washout. These results suggest that the differentiated neurons both expressed, and had functionally active forms, of the NMDA, AMPA and L-type voltage gated calcium channels.
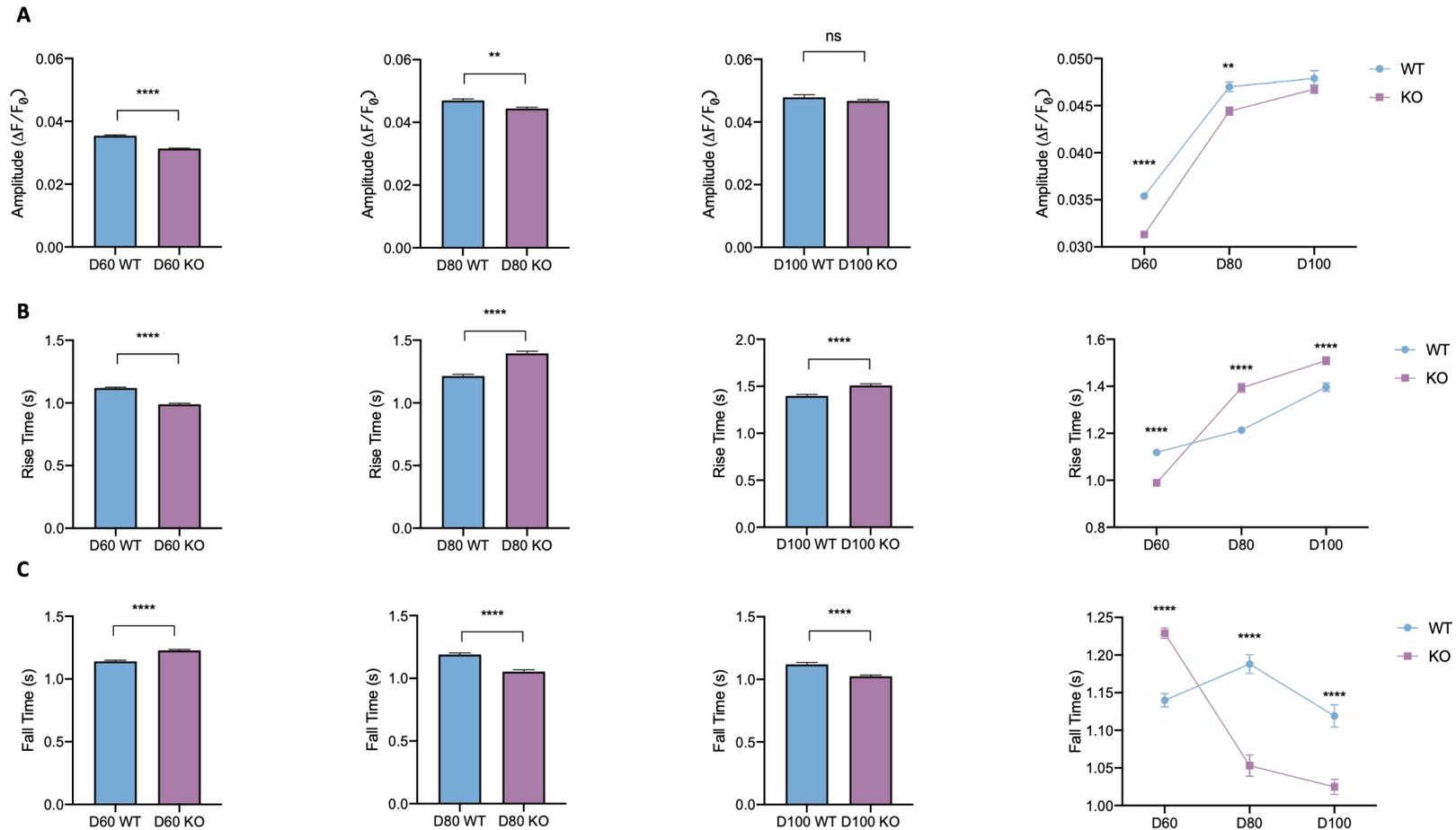
Figure 4.4 Calcium event shape in hESC-derived neurons

*SGCE*ko (KO) and iCas9 (WT) were analysed for calcium event shape. Neurons from *SGCE*ko displayed a lower event amplitude at all timepoints analysed (A). Event rise time was significantly shorter in *SGCE*ko neurons at D60 compared to WT neurons, however, at D80 and D100 event rise time was significantly longer (B). Event fall time was significantly longer in *SGCE*ko neurons than WT at D60, however, at D80 and D100 *SGCE*ko fall time was significantly shorter than in WT neurons. Data represent mean±SEM. Statistics show results of two-way ANOVA with post-hoc Tukey's test; *=p≤0.05, **=p≤0.01, ***=p≤0.001, ****p≤0.0001. At each time point, calcium analysis was carried out on 4 fields of view from 4 coverslips for both WT and *SGCE*ko neurons, repeated over 3 differentiations.

Table 4.4 Two-way ANOVA followed by Tukey multiple comparison of means to analyse calcium event shape differences between WT and *SGCE*ko neurons

	Mean	SEM	Difference in means	95% confidence interval	Adjusted p-value	Summary
_D60_						
Amplitude						
WT	0.03540223	0.01051	0.0004	0.002 to 0.006	<0.0001	****
KO	0.03132009	0.006956				
Rise Time						
WT	1.118756	0.3207	0.130	0.08 to 0.18	<0.0001	****
KO	0.9888433	0.4324				
Fall Time						
WT	1.140272	0.3608	-0.088	-0.13 to -0.05	<0.00010	****
KO	1.228581	0.3347				
_D80_						
Amplitude						
WT	0.04698541	0.01799	0.003	0.0007 to 0.0044	0.0013729	**
KO	0.04441379	0.01380				
Rise Time						
WT	1.214149	0.5118	-0.179	-0.24 to -0.12	<0.0001	****
KO	1.394079	0.5851				
Fall Time						
WT	1.187874	0.4321	0.137	0.09 to 0.18	<0.0001	****
KO	1.053429	0.4496				
_D100_						
Amplitude						
WT	0.04788889	0.02587	0.001	-0.0006 to 0.0029	0.4303247	ns
KO	0.0467352	0.01805				
Rise Time						
WT	1.396707	0.5559	-0.112	-0.17 to 0.05	<0.0001	****
KO	1.509003	0.6793				
Fall Time						
WT	1.119296	0.4612	0.095	0.05 to 0.14	<0.0001	****
KO	1.024575	0.4084				
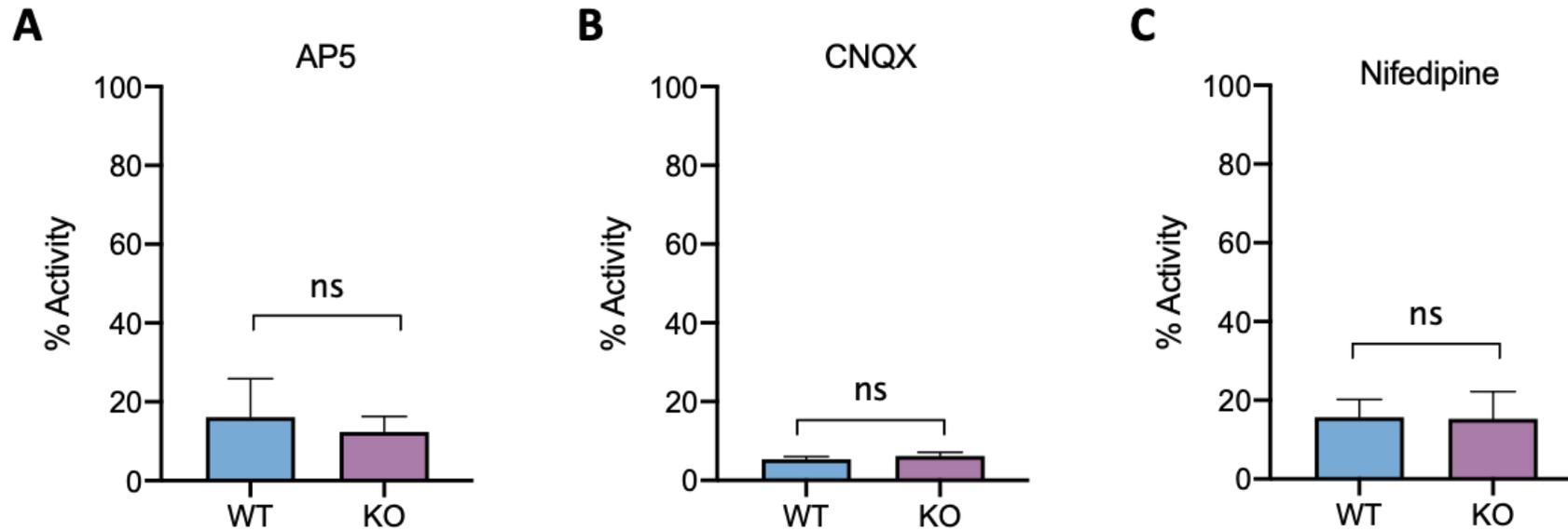
Figure 4.5 Calcium activity in response to pharmacological inhibitors

*SGCE*ko (KO) and iCas9 (WT) hESCs were differentiated into excitatory glutamatergic neurons. At D60, D80 and D100, coverslips were exposed to Fluo-4 dye and calcium movement was recorded and analysed. Calcium activity was decreased in response to the pharmacological inhibitors AP5 (A), CNQX (B) and nifedipine (C) at all time points (day 80 data shown as a representation). Data represent mean±SEM. Statistics show results of unpaired Student's T-Test. At each time point, calcium analysis was carried out on 4 fields of view from 4 coverslips for both WT and *SGCE*ko neurons, repeated over 3 differentiations.

4.2.3. Discussion

This chapter demonstrates the ability to differentiate *SGCE*ko stem cells towards an excitatory cortical glutamatergic neuronal lineage capable of displaying neuronal activity in the form of calcium transients. The results have highlighted several functional phenotypes relating to calcium activity, possibly attributable to the loss of function of the epsilon-sarcoglycan protein in hESCs. Calcium activity in *SGCE*ko neurons and their isogenic control was assessed from D60 of differentiation and then again at 20 days intervals until D100. Overall, *SGCE*ko neurons continuously displayed a higher percentage of calcium activity across the culture, yet within these active cells, lower numbers of calcium transients were generally observed, which was reflected in longer inter-spike intervals. In addition, changes to calcium event shape were also observed in the form of a diminished amplitude, longer rise time and shorter fall time compared to WT cells. For each of the parameters measured, with the exception of calcium transient amplitude, there was a transition in phenotype from D60 to D80, followed by maintenance or increasing of this phenotype distinction between D80 and D100. The consistency of this variation suggests further exploration is needed as to whether this represents a critical time point in the maturation of *SGCE*ko excitatory cortical neurons.

Throughout the differentiation process, a higher percentage of neurons in *SGCE*ko cultures were active compared to WT neurons. At D60, as well as this increased percentage of neuronal activity in the *SGCE*ko line, the number of calcium transients was significantly higher and ISI time significantly shorter. We hypothesise that although active neurons demonstrated more calcium transients at this early time point, with a lower inter-spike interval, these events may represent functionally less mature activity. Calcium transients in *SGCE*ko neurons also had a lower amplitude, faster rise time and slower fall time than WT neurons. It is possible that these early-stage neurons are producing a higher firing rate of action potentials with immature properties, which may have a subsequent impact in influencing the circuit-based neuronal dysfunctional observed in dystonia. Day 80 appeared to be a critical stage in the maturation of *SGCE*ko cortical neurons. Although the percentage of active neurons remained higher in *SGCE*ko cultures, the number of calcium transients decreased to a lower level than that observed in WT neurons, with the ISI being significantly longer. This distinction persisted at D100, suggesting that this divergence in characteristics may be maintained in onward maturation, suggesting that the loss of ε-sarcoglycan function impacts the end excitability levels observed in cortical neurons.

Calcium transient amplitude was consistently lower in *SGCE*ko neurons throughout the differentiation. A smaller calcium transient amplitude suggests a more immature neuronal state, attributed to fewer functioning ion channels in the cell surface membrane. It may also be caused by lower extra- or intra-cellular calcium levels, or aberrant release of calcium from internal stores (Murphy *et al.*, 1992). Few studies have examined calcium transient amplitude in the context of dystonia models to date. However,

one such study involving primary striatal neuronal cultures from heterozygous knock-in mice, recapitulating the genetic mutation of DYT1 dystonia patients, showed that mutant neurons displayed larger calcium transient amplitudes, while all other parameters of calcium dynamics remained unaltered (Iwabuchi *et al.*, 2013). While these results differ from the results outlined in this chapter, several factors may account for these differences, including; i) examination of an inhibitory neuronal lineage rather than the excitatory model investigated in this study, ii) while we investigated spontaneous calcium transients, the DYT1 murine study measured calcium transients following depolarisation with a single electrical stimulus, and iii) our measurements were restricted to the neuronal somas, while the DYT1 study involved measurement of calcium activity in the neuronal dendrites.

From D80, *SGCE*ko neurons displayed a longer rise time, but faster fall time, than their wildtype counterpart. The rise time represents the influx of calcium into the cytoplasm, whereas the fall time represents the removal of calcium into extracellular space. The rise time is typically dependent upon the number and activity of the NMDA, AMPA, nicotinic acetylcholine receptors, and transient receptor potential type C channels, suggesting that fewer of these receptors may be present in the absence of ε-sarcoglycan, or that those present may have a reduced functional capacity. In contrast, calcium transient fall time is determined by the plasma membrane calcium ATPase and the sodium calcium exchanger. A faster fall time in the *SGCE*ko neurons could be due to higher levels of expression and/or activity of these membrane channels. The ablation of the calcium responses when treated with both NMDA and AMPA antagonists in this study, suggests that these receptors are both present and functioning within our model, and that the distinctions in calcium activity observed between *SGCE*ko and control cell lines may be driven by synaptic activity.

 Calcium stores in the endoplasmic reticulum could also have an effect on overall calcium activity and transient shape. ER is the largest store of intracellular calcium in neurons and expresses a large number of calcium channels and transporters. This organelle consequently acts as a key contributor to calcium homeostasis. Alteration to calcium levels within the ER, potentially caused by disruption to channels gating its entry or exit, could provide an additional explanation to the changes observed. An interesting way to assess this could be to treat neurons with thapsigarin, a non-competitive inhibitor of the sarco-endoplasmic reticulum calcium ATPase (SERCA) in order to empty the intracellular calcium stores (Huang and Putney, 1998). This would induce an elevation of calcium in the cytosol and allow the analysis of amplitude of thapsigarin-induced calcium elevation, as well as the kinetics of the calcium rise. *KCTD17* mutations associated with myoclonus dystonia syndrome (DYT26) display significantly reduced and delayed cytosolic calcium signal upon stimulation with ATP, indicating a smaller calcium pool within the ER (Mencacci *et al.*, 2015). A similar phenomenon has been demonstrated in fibroblasts carrying a pathogenic mutation in another dystonia causing gene, *ANO3* (Charlesworth *et al.*, 2012), potentially indicating that altered ER calcium signalling represents a converging pathogenic mechanism in dystonia. Further support for a role for the ER in *SGCE*-mutation positive Myoclonus Dystonia

comes from previous *in vitro* studies, demonstrating that in the presence of missense *SGCE* mutations the mutant ε-sarcoglycan protein is retained in the ER and retrotranslocated to the proteasome via the ubiquitin system (Esapa *et al.*, 2007).

Calcium signalling also plays a vital role in regulating the formation and plasticity of dendritic branching and growth, an important aspect of neuronal differentiation. The number of synaptic connections that a given neuron can form is determined by the relative development and branching of its dendritic tree. Calcium signals appear to impact neuronal morphology in terms of growth and branching of dendrites and the formation of dendritic spines (Konur and Ghosh, 2005) . Rodent and amphibian models have shown that increases in intracellular calcium levels following activation of NMDA receptors promotes an increase in dendritic branching, with pharmacological blockade of synaptic activity *in vitro* and *in vivo* leading to deficits in dendritic growth (McAllister, Katz and Lo, 1996; Rajan and Cline, 1998; Redmond, Kashani and Ghosh, 2002). Calcium/calmodulin-dependent protein kinases (CaMKs) have also been implicated in dendritic growth in cortical neurons, with pharmacological blockade of CaMKs shown to inhibit calcium-induced dendritic growth (Redmond, Kashani and Ghosh, 2002). Given the consistent variation across multiple calcium signalling parameters between the *SGCE*ko and control cell lines, it represents a plausible onward hypothesis that this may also impact dendritic characteristics in these neuronal cell lines. Potential areas of variation including distinctions in axonal length, and variation in dendritic branching pattern.

While dysregulation of calcium appears to be a common phenotype across different forms of dystonia, the underlying mechanism as to how mutations may cause abnormal activity is less well understood. With the presence of the dystrophin-associated glycoprotein complex (DGC) confirmed in the brain (Waite *et al.*, 2016), the notion that myoclonus dystonia caused by *SGCE* mutations is related to DGC dysfunction has gained increased traction. The absence of dystrophin results in the increased activity of calcium channels in neurons (Haws and Lansman, 1991) and as ε-sarcoglycan co-purifies with dystrophin, the loss of ε-sarcoglycan may result in dystrophin dysfunction and lead to calcium accumulation (Menozzi *et al.*, 2019). Ultra-deep amplicon sequencing has demonstrated that the major brain-specific *SGCE* isoform, that includes exon 11b, is differentially expressed in the human brain, predominantly in the cerebellum, hippocampus and cerebral cortex (Ritz *et al.*, 2011), providing further rationale for examining calcium signalling patterns in *SGCE*ko cortically differentiated neurons.

The results described in this chapter provide some initial insight into the role of ε-sarcoglycan in the calcium dynamics of neurons, although further investigation is needed to clarify the underlying mechanisms for these changes. However, two key factors require further consideration: i) cellular calcium transient kinetics may not necessarily reflect underlying spontaneous neuronal activity, and ii) spontaneous calcium activity regulates many processes during neuronal development, including axonal outgrowth, dendritic patterning and synaptic receptor maturation. In order to gain greater understanding

of the role of ε-sarcoglycan in influencing each of these components, Chapter 5 goes on to undertake a more detailed electrophysiological characterisation, including determination of action potential properties (Chen *et al.*, 2013), using patch-clamp techniques, and Chapter 6 a comparative analysis of the patterns of dendritic arborisation between the SGCEko and isogenic control hESC lines

5. Electrophysiological characterisation of *SGCE*ko hESC derived neurons

5.1. Introduction

Increasing evidence indicates that dystonia can be viewed as a network-based disorder, involving various brain regions including the basal ganglia-cerebello-thalamo-cortical circuits. Normal movement is controlled by neuronal activity stimulating wanted movement while also inhibiting unwanted movement, with this balance between excitatory and inhibitory pathways being fundamental. Electrophysiological studies in humans have suggested that there may be a loss of inhibition at multiple levels within the nervous system, including the spinal cord, brain stem and cortex, resulting in neuronal hyperexcitability and an excess of movement. Previous studies, however, imply that there are additional factors contributing to dystonia pathophysiology. Several have demonstrated hyperexcitability of the corticospinal system with increased motor evoked potentials being evident during voluntary targeted muscle contraction. Long-term potentiation (LTP) is an increase in synaptic response following potentiating impulses of electrical stimuli that sustains this activity at a level above baseline for a prolonged period (e.g. hours). LTP-like plasticity has been shown to be exaggerated in patients with dystonia, as well as evidence of an inability of depotentiation of LTP-like plasticity, which may also add to the failure to erase or amend unwanted motor activation patterns after they have been determined. In addition, two markers of GABAergic inhibition in the motor cortex, the cortical silent period and short-interval intracortical inhibition, are reduced in individuals with dystonia, indicating a perhaps crucial change to inhibitory motor cortical control (Chen *et al.*, 1997; Filipović *et al.*, 1997). Collectively, this evidence suggests that the functional phenotype of stem cell models of dystonic disorders is also likely to be key in gaining greater insights into the underlying pathophysiology.

5.1.1. Whole-cell Patch Clamp

Patch clamp techniques allow the analysis of electrical properties and functional connectivity of individual neurons. In brief, in order to patch a cell, the patch pipette is held under a very light positive pressure whilst approaching the cell of interest. The patch pipette is then brought very slowly towards the cell body until the tip touches the cell and a small dimple is observed on the cell membrane. At this point, positive pressure is released in order to create a GΩ seal. Once the seal is formed, fast and slow capacitance is corrected for and the hold potential set to -60mV. To break into the cell, short suction pulses are applied in order to break the cell membrane and provide access to the intracellular space. Analysis can then be carried out in either voltage-clamp or current-clamp mode **(Figure 5.1)**. Electrophysiology recordings in the form of whole-cell patch clamping involves direct contact of a neuron and a micropipette. When the membrane of the neuron is broken, the solution within the micropipette and the intracellular solution becomes one, enabling detection of intracellular changes in

ion concentrations. This also allows membrane potential fluctuations, that take place upon generation of an action potential, to be monitored. Although calcium imaging allowed us to assess neuronal activity on a population level, it is limited by its indirect nature of measurement. Fluctuations in calcium activity can result from various cell stimuli, not just depolarisation, including extracellular signalling molecules and intracellular messengers (Bagur and Hajnóczky, 2017). In addition, calcium imaging does not allow for the determination of the intrinsic physiology or evoked action potential properties of a single neuron.

5.1.2. Action potential

An action potential can be characterised by the rapid rise and successive fall in voltage across the cell membrane. During the resting state, voltage-gated sodium and potassium channels are closed and the resting membrane potential typically remains at approximately -70mV. In order to maintain this negative resting potential, the sodium-potassium pump actively removes sodium from the cell, whilst pumping potassium back in. In response to a stimulus, voltage-gated sodium channels open, allowing a large influx of sodium ions, causing the membrane potential to rise. In an 'all or nothing' fashion, if the threshold is reached, an action potential will be generated. Following depolarisation, rapid sodium channel inactivation as well as voltage-gated potassium channel activation allowing potassium ion efflux, causes repolarisation causing the membrane potential to fall towards the resting potential. A hyperpolarisation phase follows, with repolarisation overshooting the resting membrane potentiation. This causes the action potential to enter the 'refractory period', whereby sodium channels enter a state during which they cannot reopen, regardless of membrane potential. Slowly, sodium channels come out of their inactivated state and the membrane potential rises to reach resting state, allowing further action potentials to be generated **Figure 5.2**.

There have been few *in vitro* electrophysiological studies of dystonia, however one such rat model of *DYT12* dystonia demonstrated that Purkinje cells show erratic burst firing as a result of sodium pump dysfunction. The aberrant firing returns to normal upon restoration of sodium pump activity (Fremont *et al.*, 2014a). To date, there have been no *in vitro* electrophysiology studies of stem cell derived neurons recapitulating dystonic mutations. We have sought to investigate the intrinsic excitatory properties of cortical neurons to assess whether this provides an additional potential explanation for the hyperexcitability observed in dystonia. This chapter aims to investigate electrophysiology properties of *SGCE*ko neurons using whole-cell patch clamp recordings.
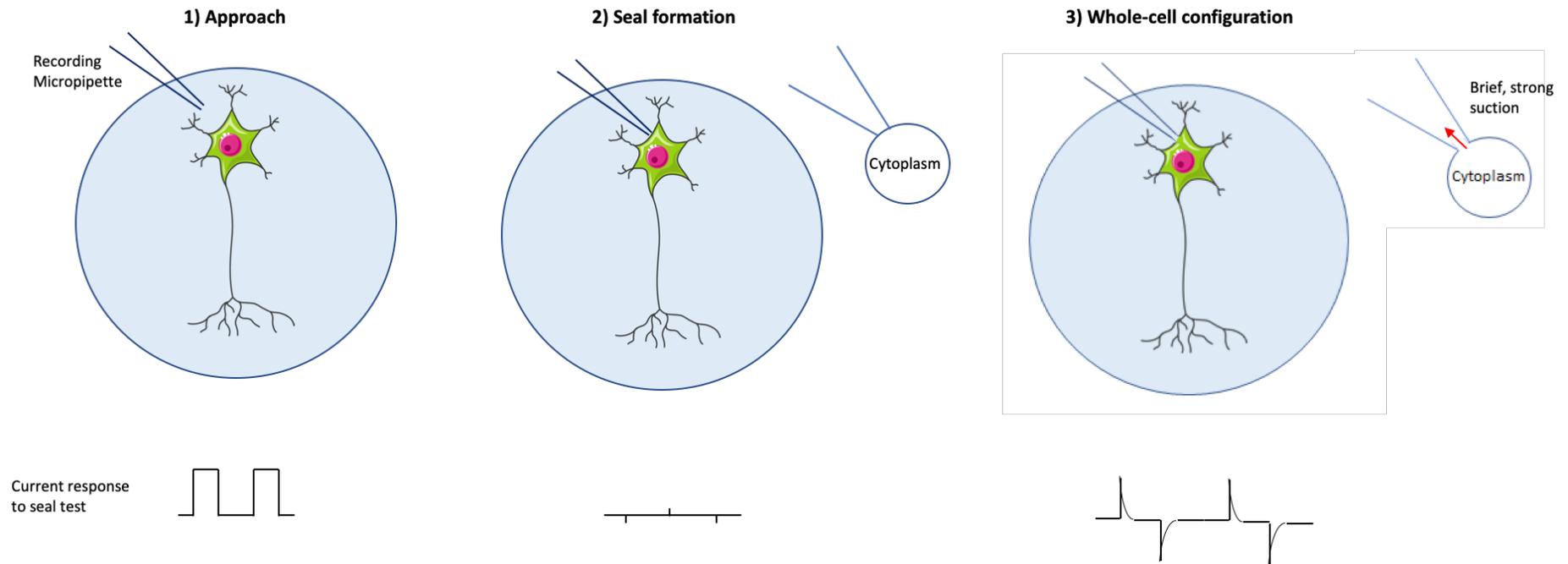
Figure 5.1 Whole-cell patch clamp procedure

Upon approach to the cell of interest, the recording micropipette is kept under a light positive pressure. The oscilloscope shows a square current in response to the seal test. As the micropipette approaches the cell, the amplitude of the square current should decrease, then upon forming a GΩ the current response will flatten, with a few transients remaining. Fast and slow capacitance should be corrected for at this point. To break the cell membrane allowing access to the intracellular space, brief suction is applied. When the cell membrane is broken, the current response to the seal test should show an exponential decay.
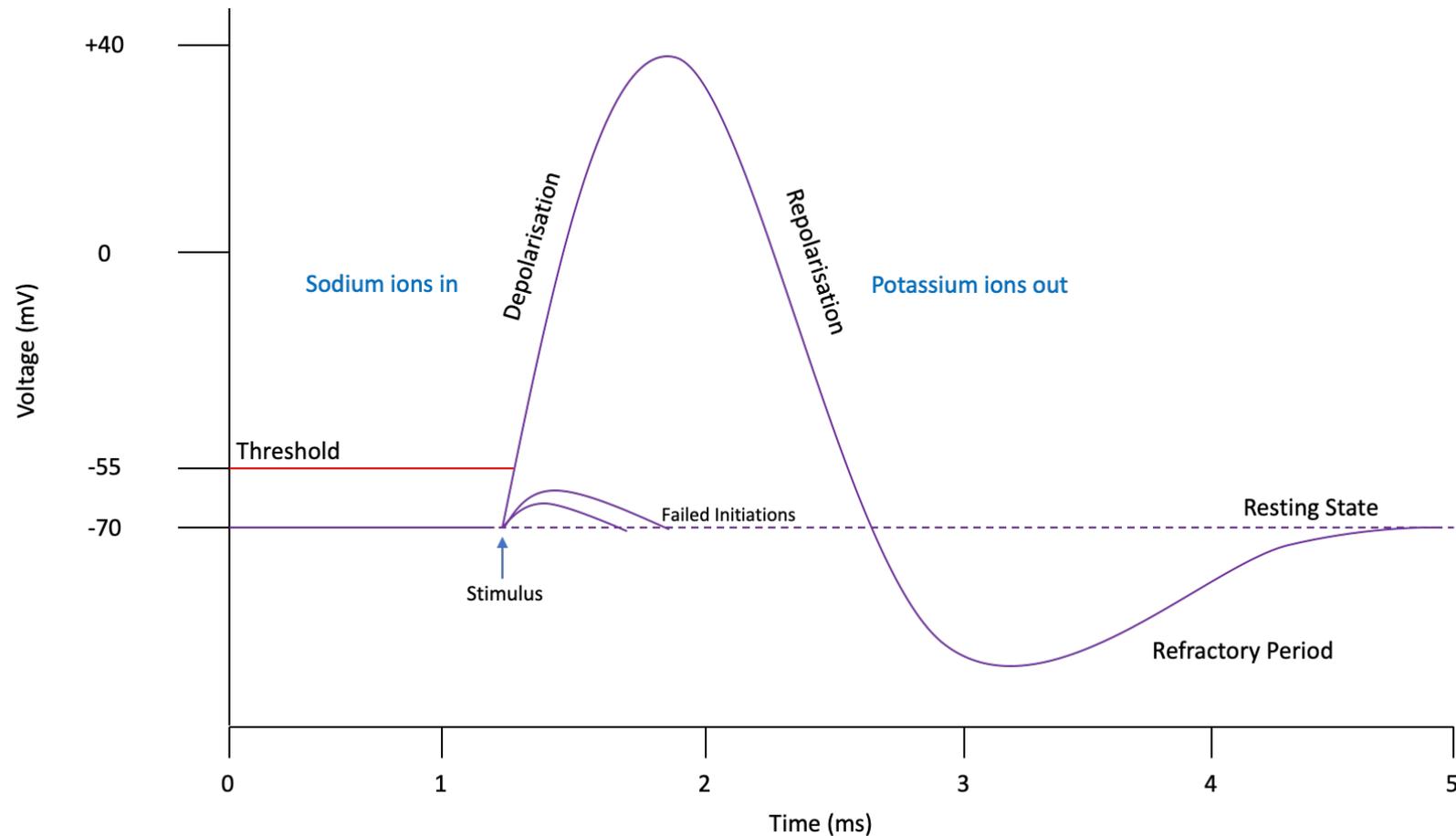
Figure 5.2 Action potential schematic

Neurons have a resting membrane potential of approximately -70mV. In response to a stimulus, voltage-gated sodium channels open, allowing the rapid influx of sodium ions into the cell and causing depolarisation of the cell membrane. If this reaches the threshold, an action potential is generated. Following depolarisation, voltage-gated sodium channels are inactivated and voltage-gated potassium open, allowing the efflux of potassium ions and a repolarisation of the cell membrane towards the resting membrane potential. Due to a repolarisation overshoot, a hyperpolarisation phase follows, generating a refractory period whereby voltage-gated sodium channels cannot open. As these slowly come out of their inactivated state, the membrane potential rises back towards its resting state.

5.2. Results

In order to investigate the electrophysiological properties of *SGCE*ko neurons, at day 16 of cortical differentiation excitatory glutamatergic neural precursor cells were plated at low density onto coverslips. Neurons were cultured in standard N2B27+RA medium from day 18, with the mitotic inhibitors DAPT and PD033291 added to the cultures for 7 days from day 20. Neuronal cultures were transferred to an incubator maintained at 37°C with 5% CO_2 and 2% O_2 on day 19 and were cultured in these conditions until the end of the experiments. Whole-cell patch clamp recordings were performed at day 60 and 80 of differentiation. **Figure 5.3** shows representative images of patched neurons.

5.2.1. Basic membrane properties

5.2.1.1. Resting membrane potential

The resting membrane potential (RMP) provides an indication of the relative maturity of developing neurons. As neurons mature, the RMP should become more polarised due to increased expression of neuronal membrane channels and transmembrane transporters as the cells mature towards more differentiated neurons. Significant differences between WT and KO lines were noted at both day 60 and day 80 of differentiation (D60 WT: -14.45mV ±1.29 *vs.* KO: -21.43mV ±1.34; p=0.005; D80 WT: -13.44mV ±1.48 *vs.* KO: -20.07mV ±1.58; p=0065). However, these values became slightly less, rather than more, polarised at day 80 with this effect greater in the KO lines (WT: -14.45mV to -13.44mV; KO: : -21.43mV to -20.07mV), however, the KO cell line maintained a greater degree of polarisation in comparison to the WT line, and therefore a tendency towards greater electrophysiological maturity (**Figure 5.4A**, for statistics see *Table 5.1*).

5.2.1.2. Input resistance

Input resistance depicts the voltage change recorded in a neuron when injected with a known low current-step. This measurement indicates the extent to which membrane channels are open, with a high input resistance signifying fewer or closed ion channels, while low input resistance implies more, or open channels. The WT line displayed a lower input resistance at D60, although this difference did not reach significance (D60 WT: 1.662 GΩ ±0.122 *vs.* KO: 1.830 ±0.137; p=0.7607). With neuronal maturation there is an expectation that input resistance will decrease, owing to the increased expression of functional membrane channels. This was observed in both cell lines but to a greater degree in the KO lines (1.830GΩ to 1.401GΩ) compared to controls (1.662GΩ to 1.300GΩ). At day 80 these reductions in resistance resulted in near equal values (1.300GΩ ±0.09 (WT) vs. 1.401GΩ ±0.13 (KO)), with no statistically significant difference between the two lines (p=0.9350) **(Figure 5.4B; Table 5.1)**.

5.2.1.3. Membrane time constant

Membrane time constant (also known as tau or t) describes the time for the membrane potential to decay to 37% below baseline following a small current injection. In a similar way to input resistance, tau is expected to decrease as neurons mature due to an increase in expression of functional channels and transporters in the cell membrane. In this study, as with input resistance, both WT and SGCEko cultures showed a reduction in tau from day 60 to day 80 **(Table 5.1)**. Analysis at the individual timepoints found the SGCEko neurons to have a longer membrane time constant than WT neurons at D60, with this difference almost reaching significance (p=0.0628), with SGCEko displaying a tau of 69.06ms ±7.63, compared to 35.87ms ±3.52 in the WT neurons **(Figure 5.4C)**. By D80 the SGCEko cells continued to have a higher average membrane time constant compared to their WT counterparts, but this was again not significant (41.253ms ±4.165 vs. 30.494ms ±2.372 respectively; p=0.1736) **(Table 5.1).**

5.2.1.4. Capacitance

Cell capacitance is a common measure of cell surface area; the larger the cell, the more lipid membrane that is present and the larger the cell's capacitance (Khorkova and Golowasch, 2007; Pineda *et al.*, 2008; Royeck *et al.*, 2008). The cell capacitance in both lines decreased between the two time points, with this difference statistically significant at D80 (D60, p=0.4873; D80, p=0.0494). The capacitance was larger in the KO line throughout remaining relatively consistent at both timepoints, whereas the capacitance of WT neurons decreased from D60 to D80 (29.270pF ±1.189 to 29.711pF ±1.357, compared to 25.373pF ±1.912 to 24.061pF ±1.128 respectively). These results indicate that the cell surface membrane in the KO lines was greater, with this difference increasing with increased neuronal maturity **(Table 5.1**; **Figure 5.4D).**
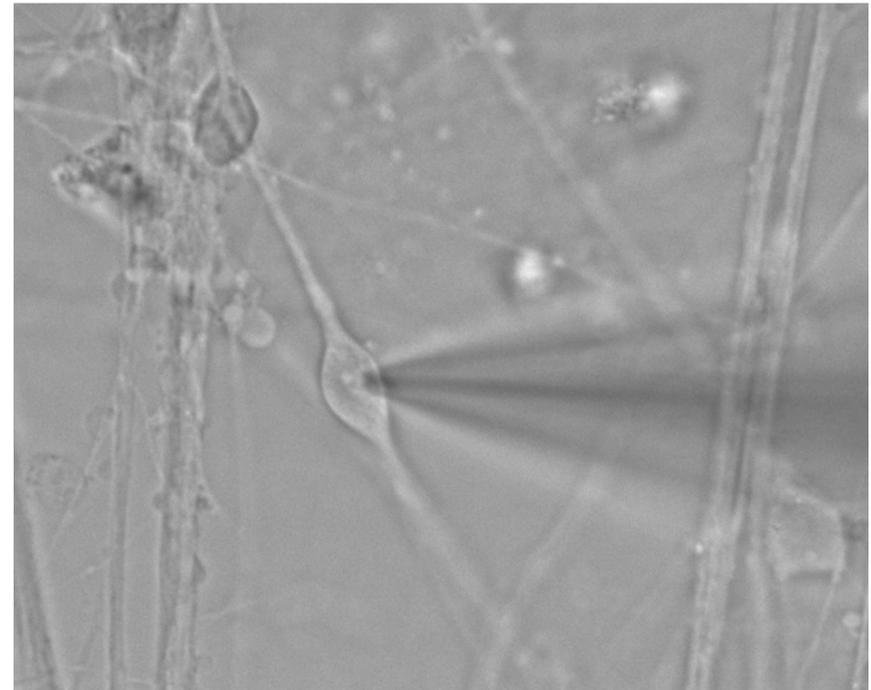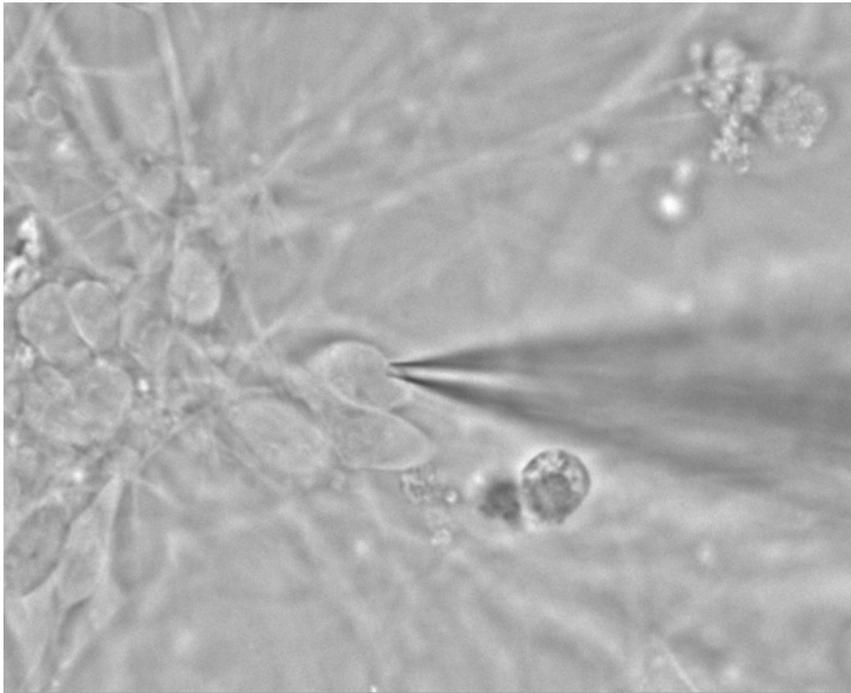
Figure 5.3 Representative images of patched hESC derived cortical neurons

Images were taken using a Q-Imaging Rolera Bolt camera mounted to an Olympus BX51 WI microscope, using an Olympus 10x water immersion objective, with light provided by a CoolLED pE-2 LED system.

Table 5.1 Summary of statistics for intrinsic electrophysiological properties in WT and *SGCE*ko neurons

	Mean	SEM	Difference in means	95% Confidence interval	Adjusted P-Value	Summary
D60						
Resting Membrane Potential (mV)						
WT	-14.45053	1.291085	6.978	1.626 to 12.33	0.005	**
KO	-21.42893	1.340250				
Input Resistance (GΩ)						
WT	1.662196	0.1216448	-0.1678	-0.6124 to 0.2768	0.7607	ns
KO	1.829971	0.1366128				
Membrane Time Constant (ms)						
WT	39.97475	3.529106	-13.20	-26.84 to 0.4425	0.0618	ns
KO	53.17501	4.388255				
Capacitance (pF)						
WT	25.37249	1.912013	-2.937	-8.305 to 2.430	0.4873	ns
KO	29.26977	1.189149				
D80						
Resting Membrane Potential (mV)						
WT	-13.44242	1.482742	6.631	1.420 to 11.84	0.0065	**
KO	-24.82580	1.584234				
Input Resistance (GΩ)						
WT	1.300143	0.08929492	-0.1008	-0.5446 to 0.3430	0.9350	ns
KO	1.400907	0.1295519				
Membrane Time Constant (ms)						
WT	30.49357	2.371986	-10.76	-24.38 to 2.859	0.1736	ns
KO	41.25347	4.164532				
Capacitance (pF)						
WT	24.06108	1.128448	-5.326	-10.64 to -0.009805	0.0494	*
KO	29.71055	1.357397				
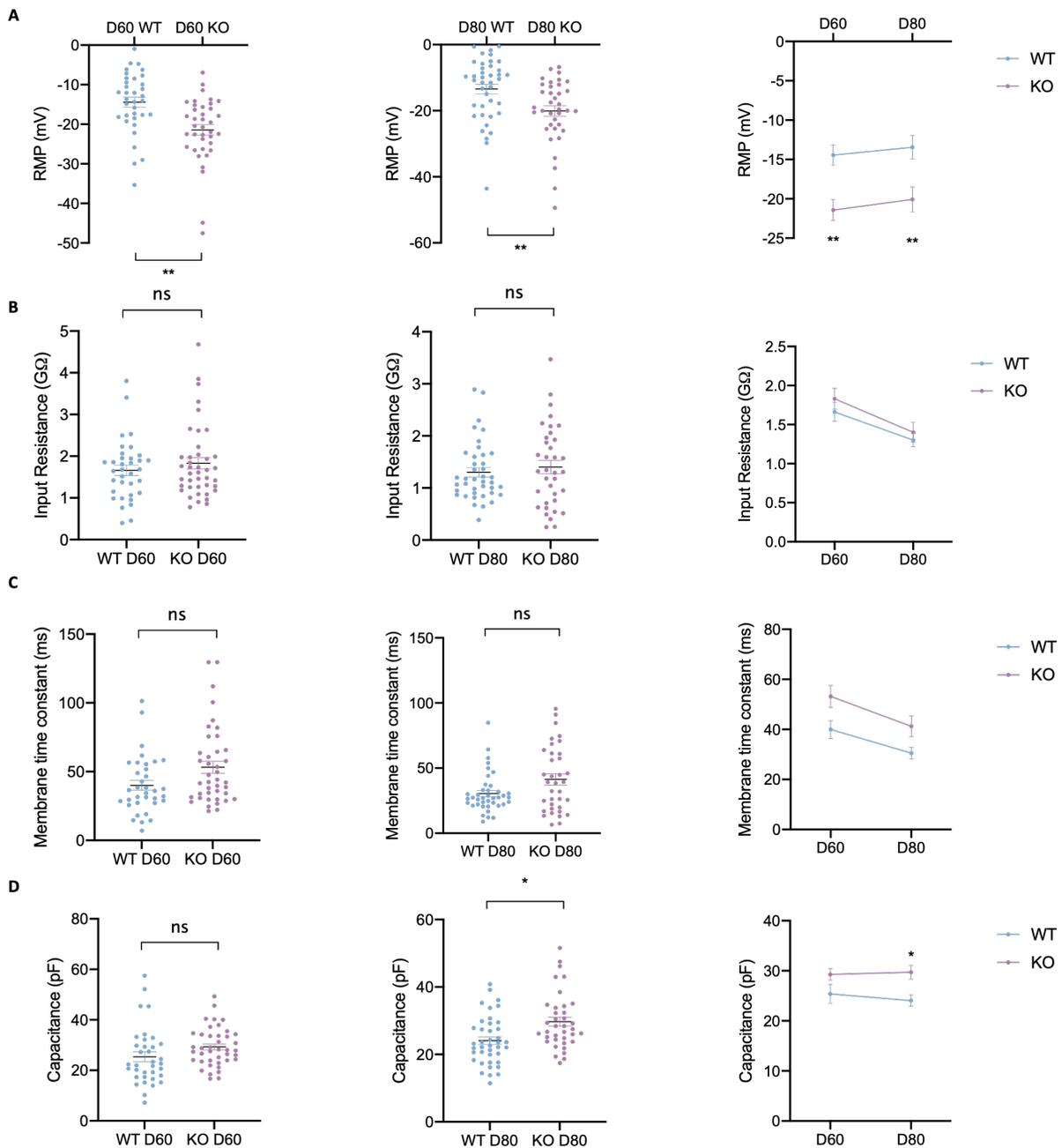
Figure 5.4 Intrinsic electrophysiological properties of WT and *SGCE*ko neurons

hESC derived neurons were patched at day 60 and 80 of cortical glutamatergic differentiation to assess changes in intrinsic electrophysiological properties as cells mature (A: Resting membrane potential (RMP), B: Input resistance, C: Membrane time constant, D: Capacitance) . Each point in scatter plots represents a single patched neuron, with mean ±SEM also displayed. Statistics show results of two-way ANOVA with post-hoc Tukey's test; *=p≤0.05, **=p≤0.01, ***=p≤0.001, ****p≤0.0001. Data represent three independent rounds of cortical differentiation.

5.2.2. Induced action potentials

The capability of neurons to produce action potentials when injected with increasing current steps relates to their baseline membrane properties outlined in sections **5.1.2**. In this study, cells were recorded in current clamp mode and injected with current steps of 20pA between -60pA and +120pA. It's possible to classify the induced action potentials, making use of this as a marker of neuronal excitability and maturity at successive timepoints. Induced action potentials can be categorised into five groups **(Figure 5.5)**:

1) No action potential (AP) generated
2) An attempted, but failed action potential
3) A single action potential
4) An attempt at generating a series of action potentials (attempted train)
5) A series of action potentials (train)

For these recordings, all cells were held at -60mV. At day 60, 77.14% of WT neurons (27/35) were classified as being active, including single action potentials (51.43%; 18/35), attempted trains (8.57%; 3/35) and trains (17.14%; 6/35). At the same timepoint, *SGCE*ko cells demonstrated a higher level of excitability with 95.12% of neurons (39/41) classed as active, 31.71% firing single action potentials (13/41), 12.19% attempting to fire a train of APs (5/41) and 51.22% firing trains of APs (21/41). Both cell lines displayed an increase in the percentage of active cells from D60 to D80 (WT: 77.14% (27/35) to 80.00% (32/40); KO 95.12% (39/41) to 100.00% (37/37)), however, *SGCE*ko cultures continued to display a trend of increased excitability compared to controls at D80. At D80, 2.5% of WT cells (1/40) failed to display any signs of an action potential, and 17.5% of WT cells analysed (7/40) showed only attempted action potentials. 37.5% of WT cells (15/40) displayed single action potentials, with 10.00% cells (4/40) attempting to fire a train and 32.50% (13/40) firing a train of APs. In contrast, all of the *SGCE*ko neurons analysed (37/37) at D80 were active in some capacity, with a greater number moving towards more active characteristics such as action potential trains, 70.27% (26/37) compared to day 60 (51.22% (21/41)). **(Figure 5.6A, Table 5.2)**.

An additional means of assessing the intrinsic excitability of neurons is to calculate the frequency of evoked action potentials with current step injection. At day 60, WT neurons fired a median of a single action potential compared to two action potentials under the same conditions in *SGCE*ko neuronal cultures. By day 80, the median number of action potentials fired by WT neurons remained as one, but increased to three in *SGCE*ko neurons, with 32.43% of the neurons analysed firing 5 or more action potentials in a row **(Figure 5.6B, C, D)**.
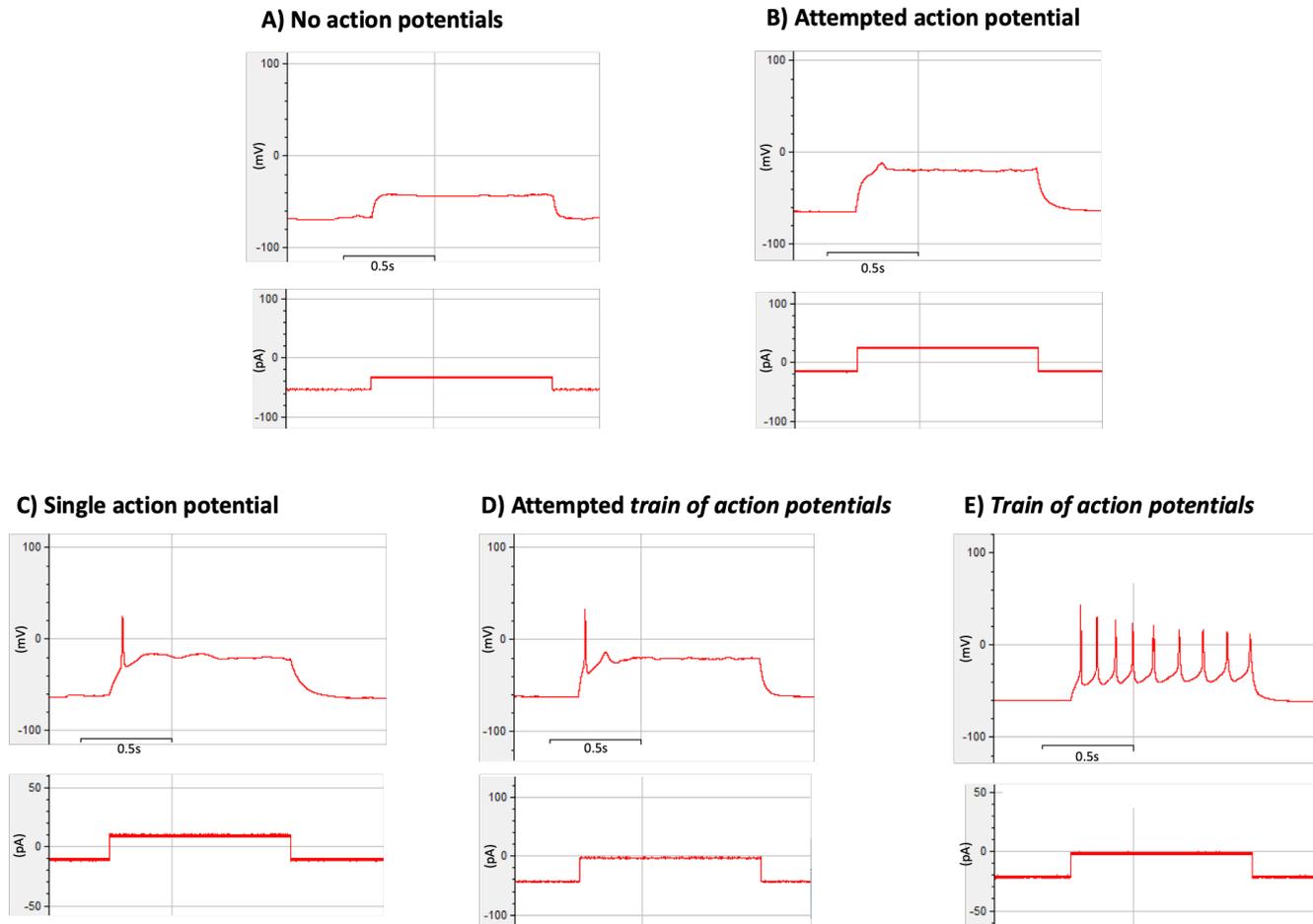
Figure 5.5 Categories of neuronal activity observed upon current step injection

Representative traces for each of the five categories of responses to current step injection. A) No action potential generated. B) An attempt, but failure, to generate a full action potential response (passive response). C) Generation of a single action potential. D) An attempt, but failure, to generate a second action potential (attempted train). E) The generation of two or more action potentials in response to a single current step injection.
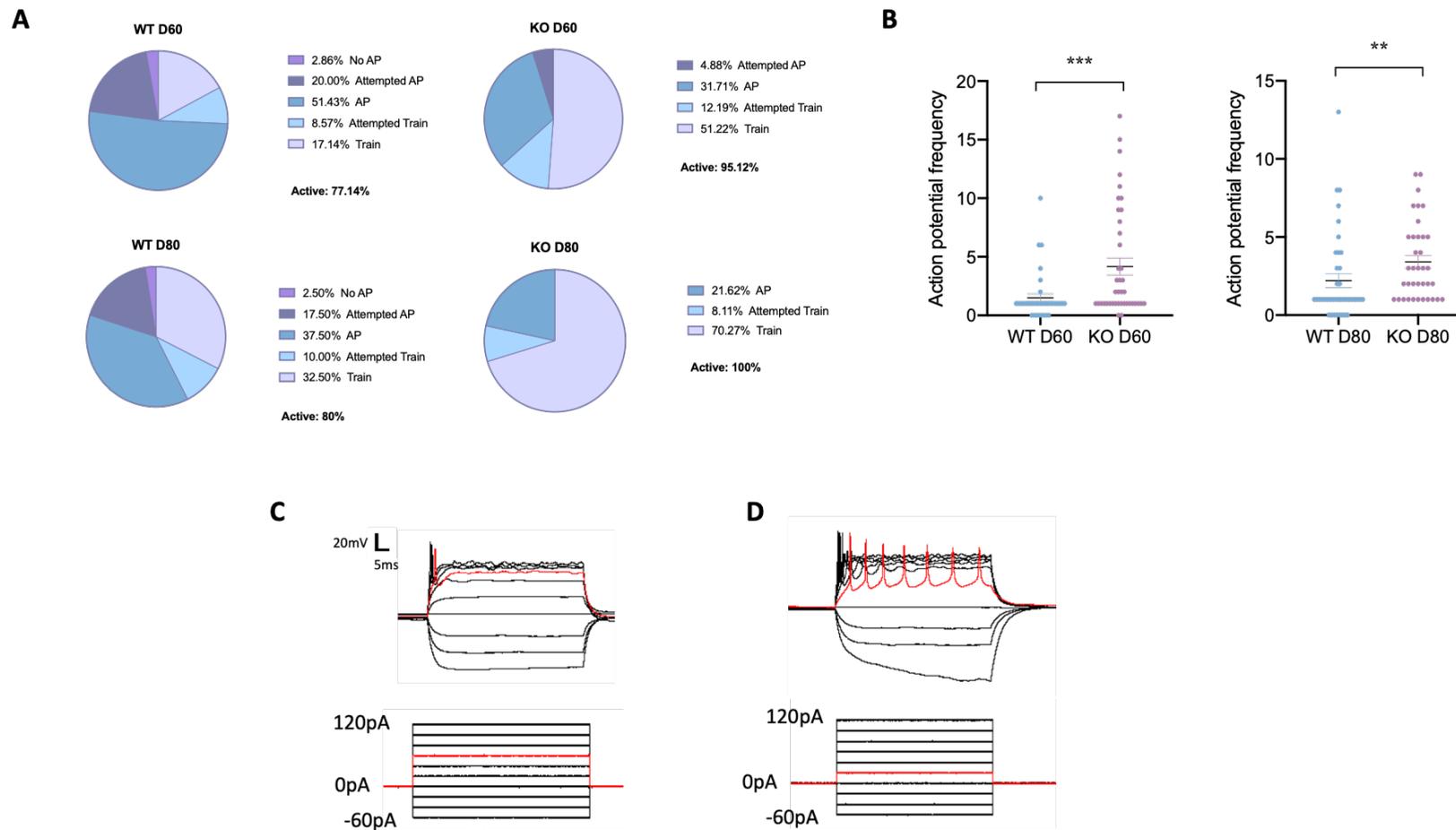
Figure 5.6 Neuronal activity observed in WT and *SGCE*ko neurons in response to current step injection

A) Pie charts displaying the proportion of neurons that displayed either no action potential, an attempted AP, a single, full AP, and attempted train of APs or a train of APs, from a holding potential of -60mV. B) Quantification of the maximum number of action potentials fired in response to any single step of current injection. Representative trace of evoked activity from current injection steps in C) WT neurons and D) *SGCE*ko neurons. Data represent three independent rounds of cortical differentiation

Table 5.2 Summary of types of induced action potential fired

	No AP	Attempted AP	Single Ap	Attempted Train	Train	Overall % Active Cells
D60						
WT	2.86%	20.00%	51.43%	8.57%	17.14%	77.14%
KO	-	4.88%	31.71%	12.19%	51.22%	95.12%
D80						
WT	2.50%	17.50%	37.50%	10.00%	32.50%	80.00%
KO	-	-	21.62%	8.11%	70.27%	100%
% Increase						
WT	-0.36%	-2.50%	-13.93%	+1.43%	+15.36%	+2.86%
KO	0%	-4.88%	-10.09%	+4.08%	+19.05%	+4.88%

5.2.3. Action potential spike properties

Evoked single action potential events were analysed from each patched neuron at D60 and D80 in order to assess five key action potential properties: action potential threshold, amplitude, half-width, maximum rise time and maximum decay time. These properties are illustrated in **Figure 5.7**. Throughout neuronal development, the shape of an action potential changes to reflect the maturity of the cell. When neurons are immature, they produce action potentials with smaller amplitudes and longer half-widths. As they mature, their amplitude becomes larger, and the shape of the action potential appears narrower, in line with a faster rise and decay time and a shorter half-width. This difference can be attributed to an increase in functional voltage-gated sodium and potassium channels expressed on the cell membrane throughout development.

5.2.3.1. Action potential threshold

As a neuron matures, the threshold for action potential initiation will become more polarised in line with the polarisation of the RMP. This relationship however is not always linear and can depend on the neuronal lineage. In this study, the action potential threshold became more polarised between days 60 and 80 in both cell lines, although to a greater extent in the WT line (WT: -17.85mV ±0.8267 to -19.43mV ±0.8240; *SGCE*ko: -22.40mV ±1.233 to -22.51mV ±0.9728; **Figure 5.8A)**. A statistically significant difference was observed between the two lines at day 60 (p=0.0102), with these values becoming more similar by day 80 (p=0.1403) (**Table 5.3**).

5.2.3.2. Action potential amplitude

As neurons mature, it is expected that action potential amplitude will be become larger due to an increase in the number of functional cell membrane ion channels. Here, both cell lines showed an increase in action potential amplitude from day 60 to day 80, with the rate of increase being approximately equal in both cell lines (55.40mV ±2.886 to 59.69mV ±1.986, compared to 52.45mV ±2.428 to 56.40mV ±1.833 in the KO and WT lines respectively). Although not statistically significant (D60 p=0.8179; D80 p=0.7593), *SGCE*ko neurons maintained a higher action potential amplitude at both time points (**Figure 5.8B**; **Table 5.3**).

5.2.3.3. Action potential half-width

The action potential half width is measured as the voltage midway between the threshold and peak amplitude and describes the duration of the action potential at this point. This measure provides an important insight into the maturity of the cells, with the half-width typically seen to decrease over time, a change that accompanies physiological maturation. The action potential half-width observed in both neuronal lines shortened between day 60 (WT: 3.432ms ±0.1789; KO: 2.767ms ±0.1362) and day 80

(WT: 3.168ms ±0.1648; KO: 2.485ms ±0.0852), with this difference being statistically different at both time points measured (D60: p=0.0085; D80: p=0.0046) (**Table 5.3; Figure 5.8C**).

5.2.3.4. Action potential maximum rise slope

The action potential rise slope defines the speed at which an action potential reaches its maximum amplitude from threshold. This is directly linked to the expression of functional voltage gated ion channels, in particularly voltage gated sodium ion channels, that are predominantly responsible for the rising phase on an action potential. As might be anticipated, both cell lines demonstrated a faster rise time at day 80 (WT: 59.22mV/ms ±3.908; KO: 70.53mV/ms ±5.533) compared to day 60 (WT: 46.37mV/ms ±6.305; KO: 65.76mV/ms ±6.664), indicating recruitment of a greater number of functioning voltage-gated sodium channels at the successive time points (**Table 5.3; Figure 5.8D**). The *SGCE*ko neurons displayed faster rise times than their isogenic WT controls at both timepoints, although statistical significance was not reached (D60: p=0.0915; D80: p=0.5045).

5.2.3.5. Action potential maximum decay slope

The maximum decay time describes the maximum velocity of the downward phase of an action potential and is largely determined by the expression of voltage gated potassium ion channels in the membrane. As with the maximum rise slope, the maximum decay slope in both cell lines increased in velocity between days 60 and 80, with the decay slope being significantly faster in the *SGCE*ko line compared to WT at D60 (D60 WT: -18.63mV/ms ±1.891 *vs.* KO: -27.98mV/ms ±2.606. D80 WT: -22.46mV/ms ±1.811 *vs* -28.59mV/ms ±1.581) (**Table 5.3**; **Figure 5.8E**).

5.2.4. Summary

Analysis of intrinsic electrophysiological properties of neurons lacking ε-sarcoglycan protein, and their wildtype counterpart revealed that *SGCE*ko neurons displayed a significantly lower resting membrane potential in comparison to WT neurons, which was accompanied by a higher cell capacitance, representative of a larger cell surface area. Input resistance was comparable between WT and KO neurons at both timepoints, and although the membrane time constant was higher in the *SGCE*ko line at both time points, statistical significance was not reached.

When injected with increasing current steps in order to attempt to evoke single or trains of action potentials, *SGCE*ko neuronal cultures not only produced a higher percentage of active neurons, but also a higher percentage of neurons firing a series of action potentials, a characteristic associated with more mature/functional neurons.

The key findings from more detailed examination of AP properties is that loss of function of the ε-sarcoglycan in the cell surface membrane of neurons results in a shorter AP half width, faster maximum

rate of rise of the AP upstroke, and more rapid maximum rate of AP repolarisation (maximum rate of decay), as well as a lower threshold for action potential initiation. These distinctions were generally consistent across both time points, with the exception of maximum rise stroke. Action potential amplitude remained unaffected by the loss of ε-sarcoglycan protein. Overall, these data suggest that the *SGCE*ko line has a higher level of intrinsic neuronal excitability which may be contributing to the pathogenesis observed in Myoclonus Dystonia.
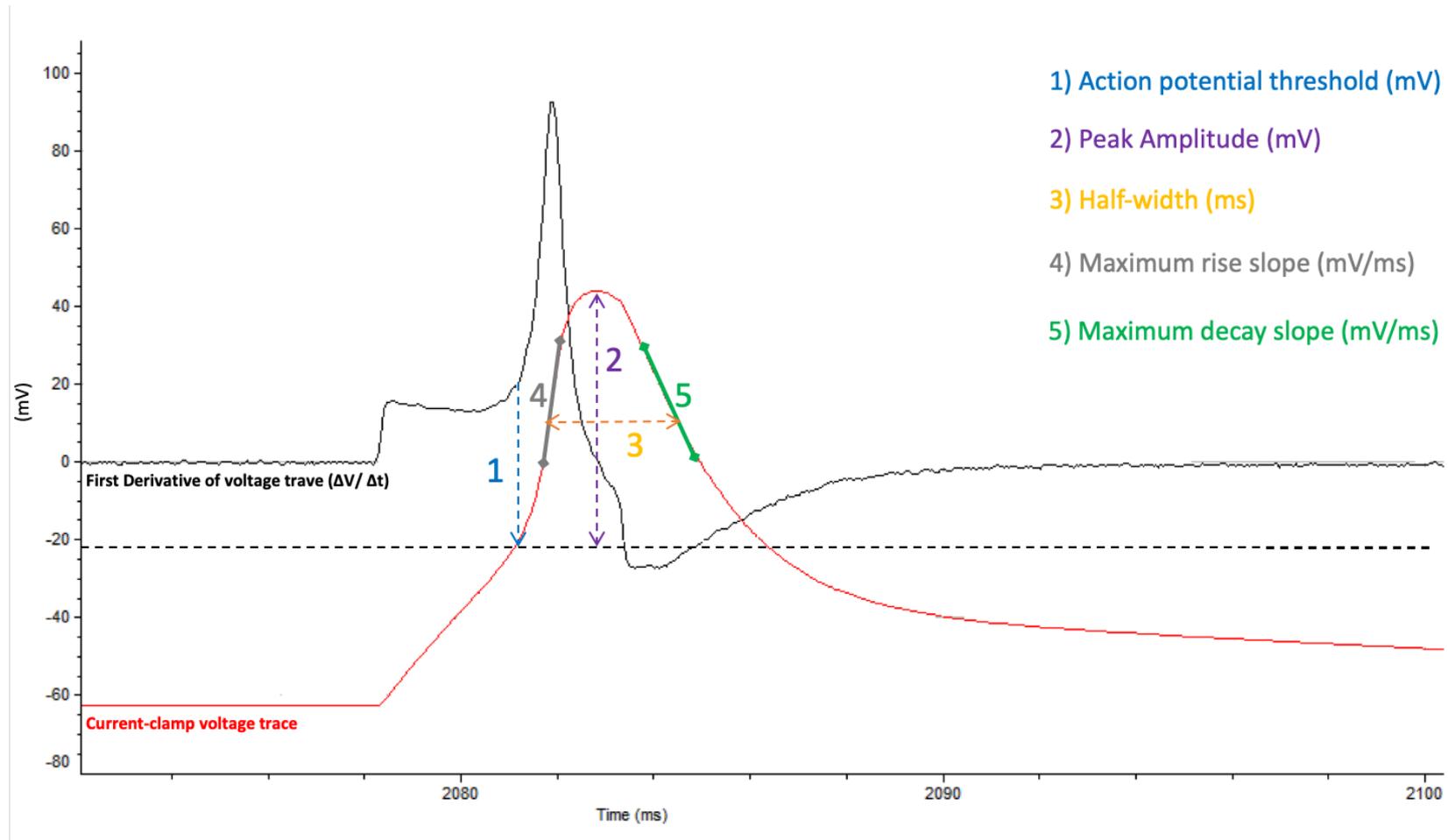
Figure 5.7 Illustration of an evoked action potential

Respresentative example of an evoked action potential depicting: 1) action potential threshold; 2) peak amplitude (mV); 3) action potential half-width (ms); 4) maximum rise slope (mV/ms); 5) maximum decay slope (mV/ms). Action potential threshold was determined by the first derivative method, whereby action potential threshold corresponded to the point of major upward deflection of the derivative trace.

Table 5.3 Summary of statistics for comparison of WT and *SGCE*ko neuron action potential properties

	Mean	SEM	Difference in means	95% Confidence interval	Adjusted p-Value	Summary
D60						
Action Potential Threshold (mV)						
WT	-17.85423	0.826732	4.545	0.8118 to 8.278	0.0102	*
KO	-22.39918	1.232856				
Action Potential Amplitude (mV)						
WT	52.45427	2.427507	-2.942	-11.69 to 5.809	0.8179	ns
KO	55.39661	2.886271				
Action Potential Half-Width (ms)						
WT	3.431786	0.178902	0.6661	0.1290 to 1.203	0.0085	**
KO	2.765676	0.136189				
Action Potential Max Rise Slope (mV/ms)						
WT	46.37418	6.304711	-19.38	-40.82 to 2.053	0.0915	ns
KO	65.75756	6.663874				
Action Potential Max Decay Slope (mV/ms)						
WT	-18.62545	1.891476	9.353	1.638 to 17.07	0.0106	*
KO	-27.97866	2.605989				
D80						
Action Potential Threshold (mV)						
WT	-19.43244	0.8239689	3.076	-0.6312 to 6.783	0.1403	ns
KO	-22.50853	0.9727570				
Action Potential Amplitude (mV)						
WT	56.40188	1.832618	-3.283	-11.97 to 5.407	0.7593	ns
KO	59.68526	1.985944				
Action Potential Half-Width (ms)						
WT	3.167941	0.1648344	0.6829	0.1629 to 1.203	0.0046	**
KO	2.485000	0.08529831				
Action Potential Max Rise Slope (mV/ms)						
WT	59.22245	3.907563	-11.31	-32.39 to 9.779	0.5045	ns
KO	70.52883	5.533481				
Action Potential Max Decay Slope (mV/ms)						
WT	-22.46035	1.810766	6.128	-1.461 to 13.72	0.1580	ns
KO	-28.58874	1.581802				
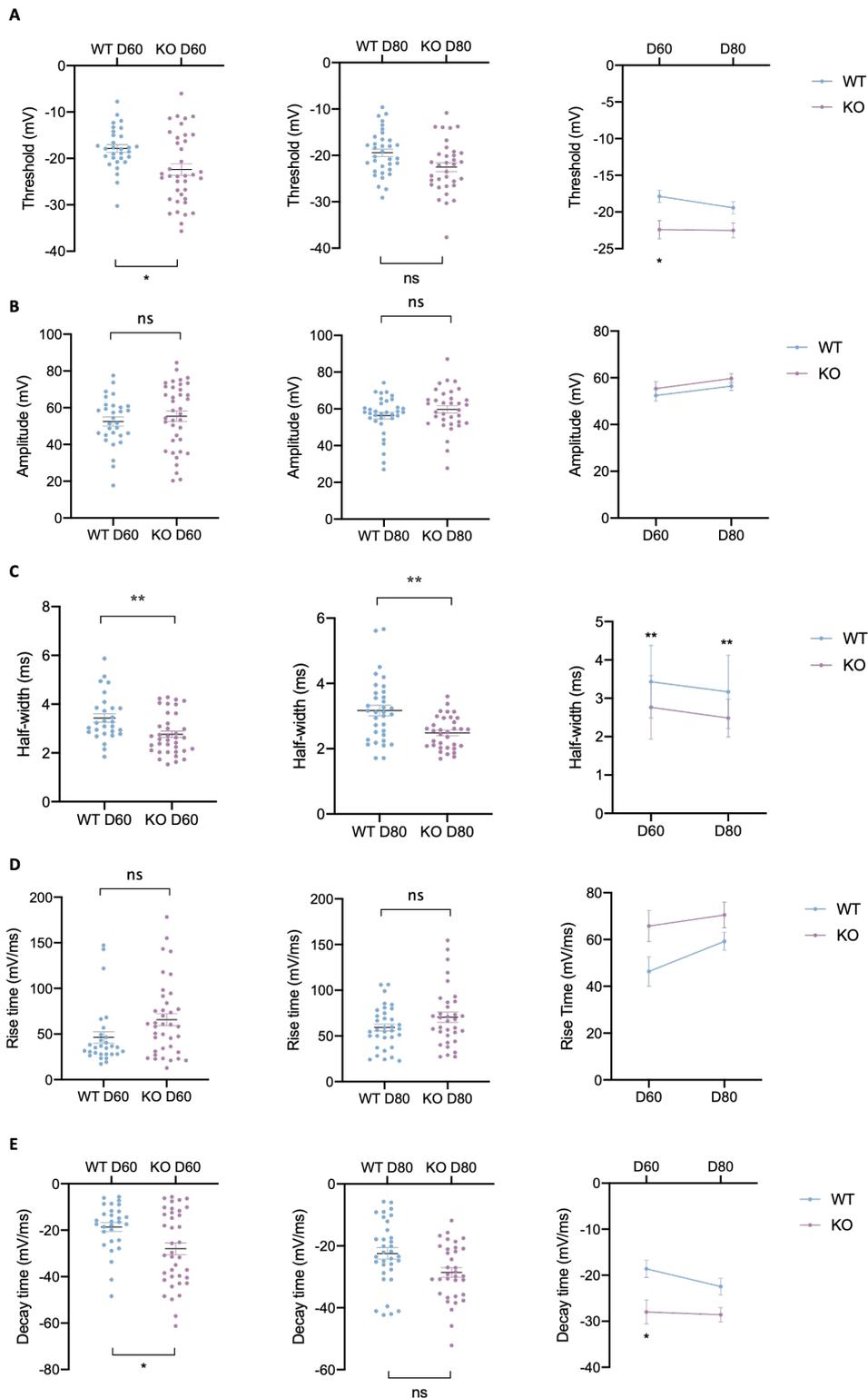
Figure 5.8 Evoked action potential properties in WT and *SGCE*ko neurons

Current evoked action potential properties of patched neurons held at -60mV, including A) action potential threshold, B) action potential amplitude, C) action potential half-width, D) action potential rise time and E) action potential decay time. Each point in scatter plots represents a single patched neuron, with mean ±SEM also displayed. Statistics show results of two-way ANOVA with post-hoc Tukey's test; *=p≤0.05, **=p≤0.01, ***=p≤0.001, ****p≤0.0001. Data represent three independent rounds of cortical differentiation

5.3. Discussion

This chapter has provided further understanding of the neurophysiological properties of WT and *SGCE*ko neurons by using single-cell patch-clamp techniques leading to the identification of several functional phenotypes. Cells with loss of ε-sarcoglycan activity display an overall increase in excitability compared to their wildtype counterparts further supported by the action potential spike properties of shorter half-width, faster maximum rise time and a more rapid decay. *SGCE*ko neurons also displayed a higher capacitance indicating a larger cell surface membrane. In addition, both WT and *SGCE*ko neurons show an increase in the number of open and/or functional membrane channels over the course of differentiation, as suggested by a decrease in input resistance and membrane time constant. Interestingly a single-cell RNAseq study of iPSC-derived neurons also found a strong correlation between action potentials, synaptic activity, dendritic complexity and gene expression (Bardy *et al.*, 2016), suggesting that those neurons with the most mature action potential properties also have the highest expression levels of voltage-gated sodium and potassium channels.

5.3.1. Voltage-gated Potassium Channels

The emergence of significantly faster decay times in *SGCE*ko neurons, in conjunction with a higher percentage of neurons firing action potential trains upon current step injection compared with WT controls, suggests that *SGCE*ko neurons are able to repolarise at a much faster rate, enabling them to fire more action potentials in a shorter period of time. The decay phase of an action potential is largely the consequence of voltage-gated potassium channels opening and allowing a large efflux of potassium ions, resulting in membrane repolarisation. Several distinct subtypes of voltage gated potassium channels (Kv), thought to influence AP width, are present to varying proportions in differing cell types. The Kv7 potassium channels have recently been shown to be upregulated during striatal neuron development and promote maturation of human iPSC-derived neurons (Telezhkin *et al.*, 2018), while Kv3 currents are responsible for the manifestation of narrow spikes observed in fast-spiking GABAergic interneurons (Boddum *et al.*, 2017). Furthermore, an increase in the size of voltage gated potassium currents and the expression of specific subtypes of Kv1 and Kv3 channels has been shown to increase over time in developing human pluripotent stem cell derived neurons (van de Leemput *et al.*, 2014).

An array of cellular physiological processes during normal brain function are critically affected by the role of potassium channels. Potassium channels are able to regulate cellular excitability in multiple ways, including the control of resting membrane potential, regulation of membrane resistance, control of the repolarisation rate of action potentials and control of the extent of spike frequency adaptation (Storm, 1990; Jan and Jan, 2012; Kole and Stuart, 2012). Recent exome sequencing studies in epilepsy patients have identified pathogenic potassium channel variants exhibiting a gain-of-function (GOF)

phenotype, raising the possibility that enhanced potassium channel activity could lead to hyperexcitability. Here epilepsy patients with pathogenic Kv1.2 variants leading to GOF channel activity display a large increase in the Kv1.2 current, with this proposed to quieten interneuron activity, leading to disinhibition and network excitability in parallel with increasing the activity of pyramidal neurons (Niday and Tzingounis, 2018).

Activation of the large calcium- and voltage-activated potassium channel known as the Big K (BK) channel leads to a fast afterhyperpolarisation phase that lasts 10-20ms. In pyramidal neurons, calcium influx during the repolarisation phase of the action potential drives this activation. This rapid afterhyperpolarisation shortens the action potential width, causing briefer action potentials and promoting quicker recovery of sodium channels from inactivation. Therefore higher firing frequency can in part be associated with BK channel activation (Niday and Tzingounis, 2018). In 2005, a family with coexistent generalised epilepsy and paroxysmal dyskinesia carrying a variant in the *KCNMA1* gene, encoding the BK channel that led to a gain of function, was described (Du *et al.*, 2005). The mutant BK channel showed an increase in open-channel probability due to increased calcium sensitivity, inducing rapid repolarisation of action potentials and consequently allowing neurons to fire at a faster rate.

5.3.2. Cell Membrane Properties

*SGCE*ko neurons displayed a consistently higher cell capacitance than WT neurons. Cell capacitance is directly linked to cell surface area, with a larger capacitance signifying a larger cell, and therefore more lipid membrane. An increase in cell surface membrane could potentially permit an increase in expression of functional ion channels. With the significantly faster action potential decay time observed in *SGCE*ko neurons, it is plausible that an increase in cell surface membrane may result in a higher number of voltage-gated potassium channels. Future work of interest would be to explore whether these changes were due to: i) a higher number of potassium channels expressed at the cell surface membrane, ii) a higher number of functionally active channels, or iii) a combination of both points (i) and (ii). An initial approach to determining these factors would be quantitative PCR and western blot experiments, providing a degree of quantification of the RNA and protein levels of potassium channels in *SGCE*ko cultures compared to their isogenic controls. Another important avenue to explore would be potential explanations for the observed higher capacitance levels in the *SGCE*ko lines, with a potential explanation being an increase in dendritic arborisation.

A limitation of this study was the relative immaturity of the excitatory glutamatergic neurons produced using this protocol, particularly relating to the high resting membrane potential observed in both WT and *SGCE*ko neurons. Although we have attempted to improve functional maturity by maintaining neuronal cultures in hypoxic conditions (Studer *et al.*, 2000; Bilican *et al.*, 2014; Ramirez *et al.*, 2018),

other approaches could also be considered. A number of studies have described differentiation protocols that aim to improve the physiological maturation of stem cell derived neurons (Bardy *et al.*, 2015; Telezhkin *et al.*, 2016). However, the requirement for multiple small molecule supplements or non-standard medium can often be an obstacle in generating a homogeneous population of a specific neuronal subtype. An alternative method is to use pre-conditioned astrocyte differentiation medium. The use of astrocytes either in co-culture with neurons or as pre-conditioned neuronal medium has been shown to enhance the maturity of neurons, particularly in relation to improvements in functional synapse formation (Johnson *et al.*, 2007; Tang *et al.*, 2013; Kemp *et al.*, 2016; Fang *et al.*, 2019).

One method that was attempted to improve functional maturity of the neurons in this study, not described in this thesis, was based on work carried out by Telezhkin *et al.*, 2016. In order to accelerate neuronal maturation and enhance neurophysiological properties, several small molecules including the mitotic inhibitors DAPT and PD033291, the BDNF receptor agonist LM22A4, the GSK3β inhibitor CHIR99021, Forskolin, an activator of the enzyme adenylyl cyclase, GABA, $CaCl_2$ and ascorbic acid were added to standard N2B27 differentiation media. Telezhkin *et al.*, observed spontaneous and induced action potential generation after only 21 days of differentiation, as well as input resistances <0.8GΩ and relatively hyperpolarised membrane potentials. In our hands, this approached resulted in a higher level of cellular heterogeneity within the cultures, with the appearance of many non-neuronal cells. The non-neuronal cells in the cultures eventually forced the neuronal cells to clump together, and in many circumstances, detach from the underlying coverslips. Consequently, after several attempts, the decision was taken to remain with the original protocol, solely adding the mitotic inhibitors DAPT and PD033291 for one week in order to synchronise the neuronal cultures. Electrophysiology recordings were then taken at later timepoints in order to allow for additional maturation.

Further electrophysiology experiments will be needed to support the findings from current-clamp whole cell patch clamp studies. This could involve performing voltage-clamp whole cell patch clamp experiments, whereby the membrane voltage in a given cell is controlled and the transmembrane current required to maintain that voltage is measured. This would also allow the application of various drugs, e.g., GABA and glutamate via the puff technique, in order to determine the cells response. The strength of the response could give an insight into the number of available GABA/glutamate receptors on a given neuron.

In summary, the findings presented in this chapter suggest that loss of cell membrane expression of the epsilon-sarcoglycan protein results in a more hyperexcitable functional phenotype when these cells are differentiated towards a cortical neuronal lineage. These findings, together with the increased capacitance observed in the *SGCE*ko cell lines suggest an earlier increase in potassium permeability and ion channel expression.

6. Neuron morphology in *SGCE*ko neurons

6.1. Introduction

The functional properties of individual neurons are influenced by neurite length and morphology, with abnormalities to neurite structure and connections being the primary cause of many neurodevelopmental disorders (Penzes *et al.*, 2011; Nagy *et al.*, 2017; Caverzasi *et al.*, 2018). Dendrites are the principal components for receiving and processing information from other cells, with appropriate dendrite morphology essential for correct nervous system functioning. Several factors impact the development and remodelling of neurites, including intrinsic and extrinsic signalling factors, as well as the pattern of electrophysiological activity.

The processing of neuronal information is influenced by the structure and arborisation of dendrites. Voltage-gated sodium channels located at the axonal cell surface membrane allow the propagation of action potentials along the length of the axon to presynaptic terminals, stimulating vesicular release of neurotransmitters at the presynaptic terminals. Many aspects of neuronal function are influenced by the structure and interaction of their associated dendrites, with these including: i) proportion of excitatory and inhibitory synapses, ii) receptors and channels located in the cell surface membrane, iii) locally acting signalling molecules.

Dendrite extension, addition, elongation, retraction and pruning are all key phases in the establishment of dendritic arbor **(Figure 6.1)**, with each stage influenced by synaptic activity (Cline, 2001; Jan and Jan, 2010; Emoto, 2012). Correct dendritic architecture is regulated by a number of distinct molecules; secreted molecules, cell surface receptors, cell adhesion molecules, postsynaptic density proteins, signalling molecules, regulators of the actin cytoskeleton, molecules that control Golgi trafficking, calcium signalling proteins, and transcription factors **(Table 6.1)** (Arikkath, 2012). Development of the brain during embryogenesis was previously believed to be independent of its electrical activity, however, more recent work suggests that this too plays a major role in early development of the nervous system, with calcium elevation and neurotransmitter receptors also contributing to dendritic stability (Wong and Ghosh, 2002).
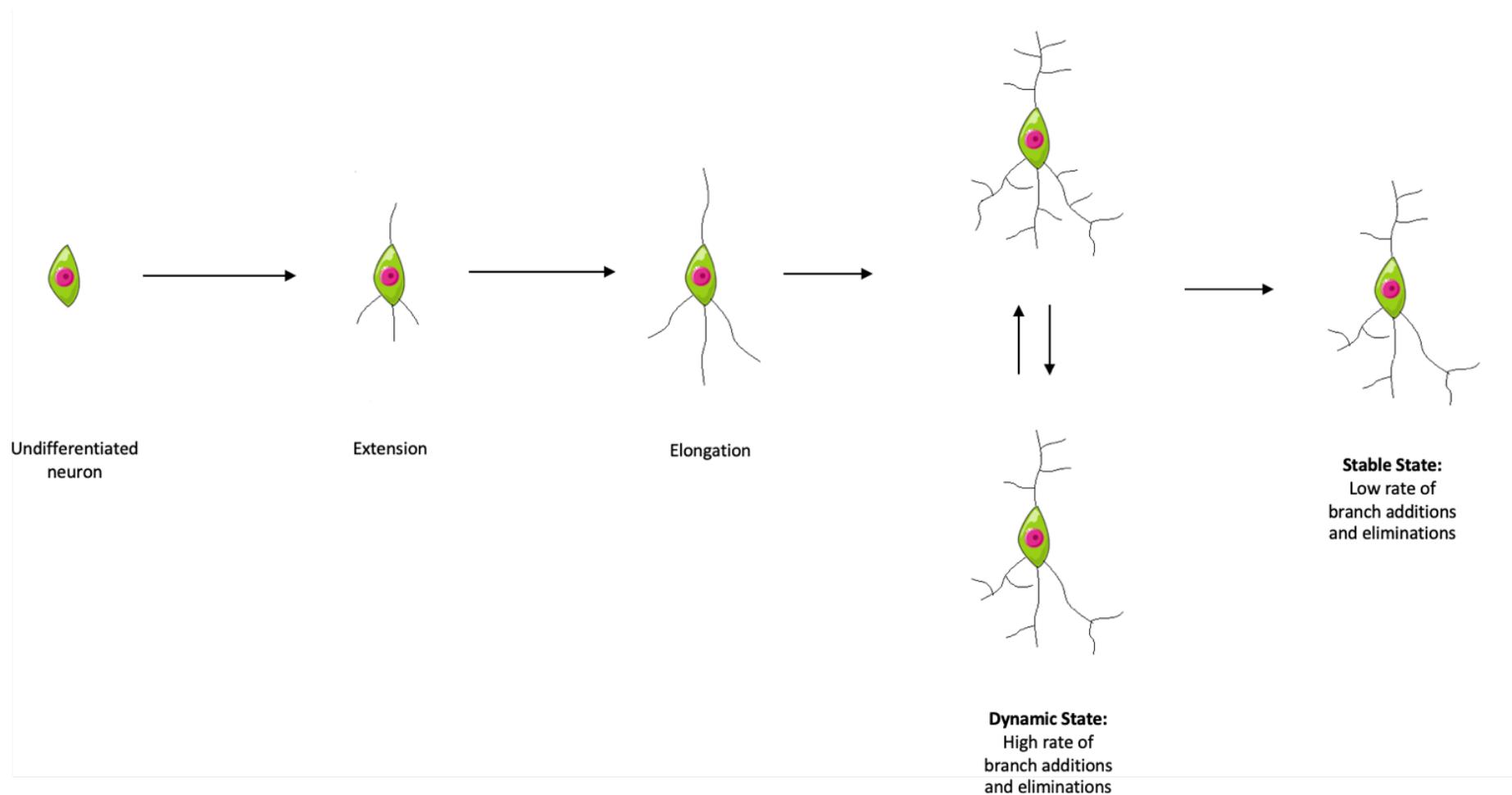
Figure 6.1 Development of dendritic arborisation

Schematic of normal dendritic arbor development involving stages of extension, elongation, addition and retraction.

Table 6.1 Molecules implicated in dendrite arborisation

Class	Examples of molecules
Transcriptional Regulators	NFκB
	CREB
	Cux1/2
	Neurogenin2
	CREST
Centrosome Signalling	CamkIIb
Secreted Factors	BDNF
	Reelin
	Wnts
Secretory Pathway Components	Sar1
	CLIMP63
	Cul7Fbxw8
Synaptic Scaffolding Proteins and their Regulators	PSD95
	Cypin
	Densin-180
	Erbin
Cytoskeletal Regulators	Rac/Rho/Cdc42
Signalling Molecules	CRMP
	CRP1
	NDR kinases
	Stk25
	Cdk5 and related proteins
Cell Adhesion Molecules	Cadherin-catenin complex
Cell Surface Receptors	Eph/Eph receptors
	Semaphorins/Plexin/Neuropilin
	Wnt/Frizzled/Deshevelled
	Notch/Delta/Jagged

6.1.1. Dendritic development in cortical excitatory neurons

The extent and pattern of dendritic growth can demonstrate wide variability both between cell types and brain regions. Evidence to date suggests that basal dendritic morphology varies between cortical layers, for instance, layer III basal dendrites have been shown to be longer than those observed in infragranular layers (Petanjek *et al.*, 2011).

There are four essential stages to dendritic growth: i) extension, whereby axons and dendrites emerge, ii) dendrites extend, branch and increase the volume they occupy, iii) dendrites begin to interact with incoming axons, forming synaptic junctions, iv) dendrite growth terminates and is stabilised, with regressive changes often observed. Soma size, total dendritic length and branching points of layer V pyramidal neurons increase rapidly from 26 to 38 gestational weeks, highlighting the third trimester as a key period during neuronal development. In the prefrontal cortex, basal dendrites of pyramidal

neurons demonstrate steady growth from 17 weeks of gestation up to one year of age, with growth reduced thereafter. Peak synaptic density is observed in mid-childhood in humans (defined as around five years of age) (Huttenlocher and Dabholkar, 1997; Liu *et al.*, 2012), with pruning of synapses extending into the third decade of life (Petanjek *et al.*, 2011).

During neurodevelopment, dendritic tree morphology is very plastic, with high rates of branch additions and retractions, whereas the mature dendritic arbor is a lot more stable, with little branch turnover observed (Williams and Truman, 2004). Arborisation is controlled both temporally and spatially by extrinsic and intrinsic molecular mechanisms to ensure appropriate generation and maintenance of dendritic architecture. In the developing cortex, these signals include, but are not limited to Semaphorin 3A, controlling apical dendrite orientation (Polleux, Morrow and Ghosh, 2000); neurotrophins such as BDNF and NT3, which regulate layer-specific dendritic growth (McAllister, Katz and Lo, 1996, 1997); Notch1, which limits growth of dendrites (Šestan, Artavanis-Tsakonas and Rakic, 1999; Redmond *et al.*, 2000; Redmond and Ghosh, 2001); the protein Slit-1, which enhances dendritic growth and branching in the developing cortex (Whitford *et al.*, 2002) and; classical cadherins, along with their signalling partner β-catenins, which together are involved in the stabilisation of dendrites and spines **(Table 6.1)** (Togashi *et al.*, 2002; Yu and Malenka, 2003; Abe *et al.*, 2004).

6.1.2. Disorders exhibiting excitatory cortical neuron arborisation abnormalities

Some neurodevelopmental disorders, such as autism and Rett syndrome, show deficient cortical dendritic branching. The morphological maturation of pyramidal neurons in layer III of the prefrontal cortex is protracted during prenatal development and childhood in those diagnosed with attention-deficit/hyperactivity disorder and autism spectrum disorder. Data from individuals diagnosed with autism, and animal models of autistic disorders, indicate a reduction in size and number of dendrites, together with abnormal dendritic morphology. They also show an increase in dendritic spine density, yet these spines display an immature morphology (Martínez-Cerdeño, 2017). Post-mortem studies of layer III and V cortical pyramidal neurons from individuals diagnosed with Rett syndrome display reduced dendritic arborisation (Armstrong *et al.*, 1995), while patient's with Williams syndrome, a unique neurodevelopmental disorder characterised by growth delays, intellectual disability and distinctive facial features, see layer-specific changes to dendrite morphology of the basal dendrites extending from cortical pyramidal neurons (Hrvoj-Mihic *et al.*, 2017). Some neuropsychiatric disorders also exhibit atypical development of cortical dendritic branches and spines. For example, in Schizophrenia, there is a reduction of spine density of layer III pyramidal neurons of the neocortex (Glantz and Lewis, 2000), while post-mortem studies show reduced complexity of basal dendrites in layer III and layer V pyramidal neurons of the prefrontal cortex (Kalus *et al.*, 2000; Broadbelt, Byne and Jones, 2002; Konopaske *et al.*, 2014).

6.1.3. Evidence for disrupted axonal and dendritic architecture in dystonia

<u>DYT1</u>

Models of a number of distinct genetic forms of dystonia have suggested that axonal and dendritic structural abnormalities may contribute to dystonia pathogenesis. DYT1 (ΔGAG deletion of *TorsinA*), resulting in a childhood-onset generalised dystonia is the best characterised form, with disruption identified in several distinct neuronal subtypes. Murine knock out models have shown a reduction in the length of large primary dendrites and a decrease in the number of spines on the distal dendrites of cerebellar Purkinje cells (Zhang *et al.*, 2011), while knock in models demonstrate thinner dendrites and fewer, less complex dendritic spines (Song *et al.*, 2014). Subtle microstructural changes to striatal medium spiny neurons are also observed in a DYT1 knock-in mouse model, with fewer and thinner dendrites, together with loss of dendritic spines. Cell body changes have also been observed with the somata of striatal choline acetyltransferase-positive interneurons being larger in the DYT1 knock-in model, compared to controls (Song *et al.*, 2013).

<u>DYT6</u>

RNA-Seq studies in mice harbouring *Thap1* mutations, the gene responsible for DYT6 dystonia, identified neurite development as an enriched pathway across brain regions. Signalling by the Rho family of GTPases, a pathway critical in neuritogenesis and axonal pathfinding (Hall and Lalli, 2010), was the highest pathway detected in the striatum following analysis. In addition, striatal medium spiny neurons cultured from *Thap1*$^{+/-}$ mice overall demonstrate shorter processes compared to wildtype controls (Zakirova *et al.*, 2018).

<u>DYT5</u>

In a knock-in mouse model of Dopa-responsive dystonia (DYT5), subtle morphological differences in the dendritic arborisation of striatal cholinergic interneurons were found in the middle and caudal tiers of the striatum. In these areas, dendritic length was significantly reduced and there were significantly fewer dendritic intersections, collectively suggesting a reduction in the complexity of the dendritic arbor (Yalcin-Cakmakli *et al.*, 2018).

<u>DYT12</u>

A pharmacological mouse model of rapid-onset dystonia-parkinsonism revealed dendritic spine loss in striatal medium spiny neurons, accompanied by loss of cholinergic and GABAergic interneurons in the striatum (Rauschenberger *et al.*, 2020). Immunohistochemical analysis of post-mortem sections from those diagnosed with rapid-onset dystonia-parkinsonism in life also found a reduction in dendritic arborisation of cerebellar Purkinje cells (Oblak *et al.*, 2014).

This chapter seeks to build on the distinct functional and electrophysiological characteristics of *SGCE*ko and WT neurons, with this work aiming to investigate whether loss of function of the ε-sarcoglycan protein may also influence the growth and morphology of neurons during cortical development.

6.2. Results

Morphological structures of excitatory glutamatergic cortical neurons were assessed at days 40, 60, 80 and 100. At day 16 of differentiation, cells were dissociated into single cells and plated at low density (100,000 cells/well) on 24 well culture plates. Seventy-two hours prior to fixing, cells were transfected with 500ng pmaxGFP per well using Lipofectamine 3000 Reagent, producing a transfection efficiency of approximately 10%. This was ideal in order to identify and characterise individual neurons without interference from neighbouring neurons. At days 40, 60, 80 and 100, cells were fixed with 3.7% paraformaldehyde for 20 minutes at room temperature, before staining with an anti-GFP antibody. Labelled neurons were visualised using a DMI60000B inverted microscope and the morphology of GFP expressing cells quantified using FIJI (ImageJ) software with the semi-automated plug-in 'Simple Neurite Tracer'. Soma area was assessed using FIJI (ImageJ) by thresholding the image and selecting the soma body as a region of interest. The 'measure' function was then used to analyse the area of the selected region of interest (See chapter **2.10**). A primary branch was described as a branch emanating from the cell soma, a secondary, one which branches from a primary branch, and a tertiary branch, one which branches from a secondary branch **(Figure 6.2)**.
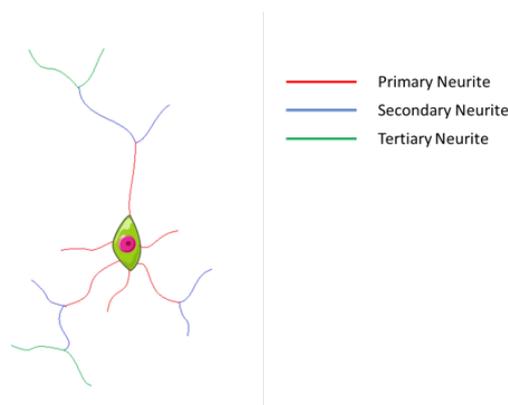
Figure 6.2 Dendritic order

Example of neuron tracing with primary branches (emanating from the soma) depicted in red, secondary branches (branching from a primary) in blue and tertiary branches (branching from a secondary) in green.

6.2.1. Total neurite length

Total neurite length was calculated by summing the length of each individual neurite. Total neurite length was then averaged across all neurons from each group at all time points. At day 40, there was no statistical difference in total neurite length between WT and *SGCE*ko cultures (WT: 937.0μm ±142 vs. KO: 658.2μm ±66.16, p=0.1231). From day 60 onwards, SGCEko neurons displayed significantly longer neurites than that of their isogenic WT controls, with this distinction maintained until day 100 (D60 - WT: 682.6μm ±56.82 vs. KO: 1606μm ±134.4, p<0.0001; D80 - WT: 787μm ±57.44 vs. KO: 1299μm ±113.4, p=0.0003; D100 - WT: 670.4μm ±44.30 vs. KO: 1068μm ±89.87, p<0.0001) **(Figure 6.3,Table 6.2)**. *SGCE*ko neurons showed a dramatic increase in neurite length from day 40 to day 60, with initial evidence of retraction at day 80, whereas WT neurons appear to be more dynamic, with their longest length observed at day 40 **(Table 6.2)**.
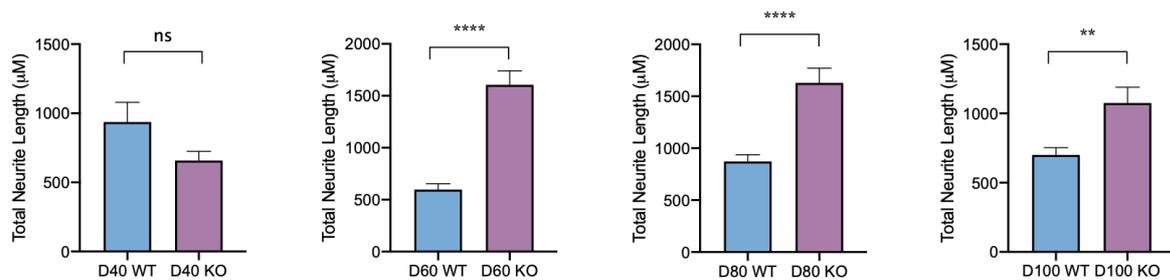
Figure 6.3 Total neurite length

*SGCE*ko (KO) and iCas9 (WT) hESCs were differentiated into excitatory glutamatergic neurons. At D40, D60, D80 and D100, neuron morphology was analysed. Neurons from *SGCE*ko had significantly longer neurites from D60. Data represent three independent rounds of cortical differentiation. Error bars represent mean ±SEM. Statistics show results of Mann-Whitney tests; *=p≤0.05, **=p≤0.01, ***=p≤0.001, ****p≤0.0001.

Table 6.2 Mann-Whitney test to analyse total neurite length differences between WT and *SGCE*ko neurons

Total Neurite Length (*μm*)	Mean	SEM	p-value	Summary
D40				
WT	937.0	142.0	0.3704	ns
KO	658.2	66.16		
D60				
WT	682.6	56.82	<0.0001	****
KO	1606	134.4		
D80				
WT	787.0	57.44	<0.0001	****
KO	1299	113.4		
D100				
WT	670.4	44.30	0.0028	**
KO	1068	89.87		

6.2.2. Branch length

6.2.2.1. Primary branch length

 To determine whether the difference in total neurite length was driven by the length of primary neurites or the growth of subsequent branches, each branch type was analysed in turn. At day 40, in a similar manner to total neurite length, primary branch length of *SGCE*ko neurons was shorter than WT, although the difference was not significant (WT: 638.8μm ±106.7 *vs.* KO: 495.4μm ±72.92, p>0.9999). From day 60 onwards, this observation was reversed, with significantly longer primary neurons observed in *SGCE*ko cultures compared to WT (WT: 536.4μm ±54.05 *vs.* KO: 1007μm ±129.1, p=0.0009). At day 80, although no longer significantly different, the trend of longer primary neurites remained in *SGCE*ko cultures (WT:661.4μm ±63.87 *vs.* KO: 853.9μm ±102.5, p=0.2972). From day 100, the primary branch length began to shorten in both lines to a point whereby the difference between WT and *SGCE*ko was negligible (WT: 588.9μm ±49.75 *vs.* KO: 687.1μm ±50.78, p=0.1294) **(Figure 6.4A, Table 6.3)**. This suggests that the difference observed in total neurite length is attributed to branching neurites rather than primary neurites.

6.2.2.2. Secondary branch length

As with primary branch length, although not significant, the length of *SGCE*ko secondary branches at d40 was shorter than WT (WT: 396.7μm ±93.37 *vs.* KO: 240.1μm ±51.36, p=0.1266). From day 60, *SGCE*ko neurons displayed significantly longer secondary neurites compared to WT, with this trend continuing throughout the differentiation (D60 - WT: 185.0μm ±41.98 *vs.* KO: 695.2μm ±128.3, p=0.0027; D80 - WT: 225.7μm ±38.44 *vs.* KO: 452.1μm ±65.67, p=0.0095; D100 - WT: 112.1μm ±26.11 *vs.* KO: 331.0μm ±67.51, p=0.0072) **(Figure 6.4B, Table 6.3)**.

6.2.2.3. Tertiary branch length

Unlike secondary branches, differences in tertiary branching did not become apparent until day 100 of differentiation. At day 40, only one of the neurons analysed from each cell line displayed any tertiary branching, and therefore was not statistically analysed. At days 60 and 80, the length of tertiary branches in both cell lines was comparable, with no statistical differences observed (D60 - WT: 257.0μm ±93.54 *vs.* KO: 188.1μm ±69.85, p>0.9999; D80 - WT: 171.0μm ±44.87 *vs.* KO: 151.9μm ±77.53, p=0.6905) **(Figure 6.4C, Table 6.3)**. At day 100, none of the WT neurons analysed exhibited any tertiary branching, compared to 31.25% of *SGCE*ko neurons. These results indicate that until day 100 of differentiation, secondary neurites, rather than tertiary neurites are primarily responsible for the difference observed in total neurite length.
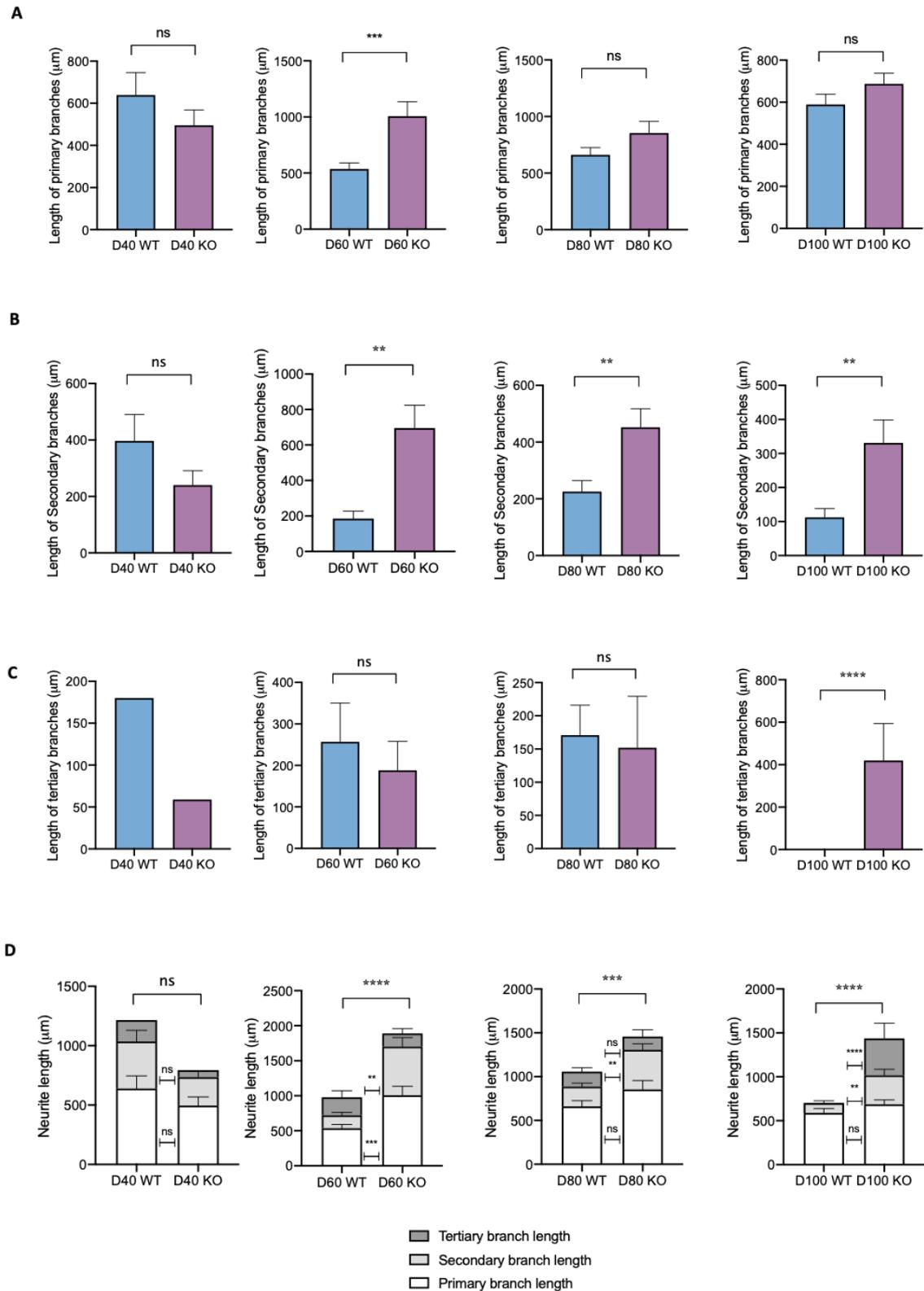
Figure 6.4 Branch length

*SGCE*ko (KO) and iCas9 (WT) were analysed for primary (A), secondary (B) and tertiary (C) neurite length. Total neurite length was divided into primary path length (white), secondary branch length (light grey) and tertiary branch length (dark grey) (D). Data represent three independent rounds of cortical differentiation. Error bars represent mean ±SEM. Statistics show results of Mann-Whitney tests; *=p≤0.05, **=p≤0.01, ***=p≤0.001, ****p≤0.0001.

Table 6.3 Mann-Whitney test to analyse primary, secondary and tertiary neurite length differences between WT and *SGCE*ko neurons

	Mean (*μm*)	SEM	p-value	Summary
Primary Neurite Length				
D40				
WT	638.8	106.7	0.2890	ns
KO	495.4	72.92		
D60				
WT	410.4	36.13	<0.0001	****
KO	1007.0	129.1		
D80				
WT	735.9	76.46	0.2972	ns
KO	1078.0	139.9		
D100				
WT	641.8	54.55	0.1294	ns
KO	649.0	66.68		
Secondary Neurite Length				
D40				
WT	396.7	93.37	0.1266	ns
KO	240.1	51.36		
D60				
WT	185.0	41.98	0.0027	**
KO	695.2	128.3		
D80				
WT	225.7	38.44	0.0095	**
KO	452.1	65.67		
D100				
WT	112.1	26.11	0.0072	**
KO	331.0	67.51		
Tertiary Neurite Length				
D40				
WT	180.2	0	N/A	N/A
KO	58.94	0		
D60				
WT	257.0	93.54	>0.9999	ns
KO	188.1	69.85		
D80				
WT	171.0	44.87	0.6905	ns
KO	151.9	77.53		
D100				
WT	0	0	<0.0001	****
KO	419.4	174.0		

6.2.3. Number of primary branches

As with primary branch length, there was no marked difference in in the number of primary branches at day 40 (WT: 2.700 ±0.3000 vs. KO: 2.619 ±0.2338, p=0.8005). From day 60, *SGCE*ko neurons had a higher number of primary branches than WT, with this being significantly different at day 60 (WT: 2.442 ±0.1210 vs. KO: 3.733 ±0.3488, p=0.0001). Thereafter, the difference in number of primary branches between the two lines declines, with the difference at day 80 (WT: 2.718 ±0.2109 vs. KO: 2.828 ±0.2110, p=0.5303), and day 100 being negligible (WT: 2.636 ±0.1431 vs. KO: 3.219 ±0.0.2830, p=0.2467) **(Figure 6.5, Table 6.4)**.
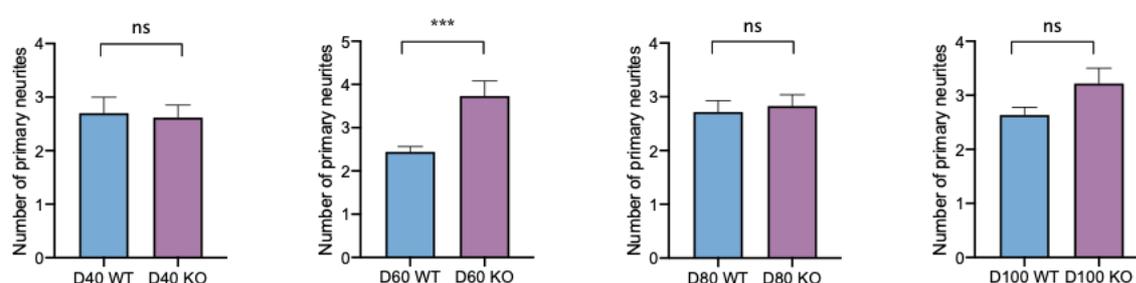
Figure 6.5 Number of primary branches

*SGCE*ko (KO) and iCas9 (WT) were analysed for number of primary branches present. In general, neurons derived from *SGCE*ko hESCs did not show any significant difference in the number of primary branches present other than at day 60, where KO neurons displayed more primary neurites than WT. Data represent three independent rounds of cortical differentiation. Error bars represent mean ±SEM. Statistics show results of Mann-Whitney tests; *=p≤0.05, **=p≤0.01, ***=p≤0.001, ****p≤0.0001.

Table 6.4 Mann-Whitney test to analyse differences in number of primary branches present between WT and *SGCE*ko neurons

Number of Primary Branches	Mean	SEM	p-value	Summary
D40				
WT	2.700	0.3000	0.8005	ns
KO	2.619	0.2338		
D60				
WT	2.442	0.8725	0.0001	***
KO	3.733	0.3488		
D80				
WT	2.718	0.2109	0.5303	ns
KO	2.828	0.2110		
D100				
WT	2.636	0.1431	0.2467	ns
KO	3.219	0.2830		

6.2.4. Number of secondary branches

As with the number of primary branches, there was also no significant difference in the number of secondary branches at day 40 (WT: 3.167 ±0.7923 *vs.* KO: 3.143 ±0.3902, p=0.7318). At day 60, unlike with the number of primary branches, there was no significant difference in number of secondary branches (WT: 2.286 ±0.1983 *vs.* KO: 2.923 ±0.2878, p=0.1147). However, from day 80, *SGCE*ko neurons began to display a more complex dendritic structure, with significant differences in number of secondary branches beginning to emerge (WT: 2.619 ±0.2715 *vs.* KO: 4.125 ±0.4007, p=0.0045) and continuing until D100 (WT: 2.125 ±0.2196 *vs.* KO: 3.440 ±0.4658, p=0.0407) **(Figure 6.6, Table 6.5)**.
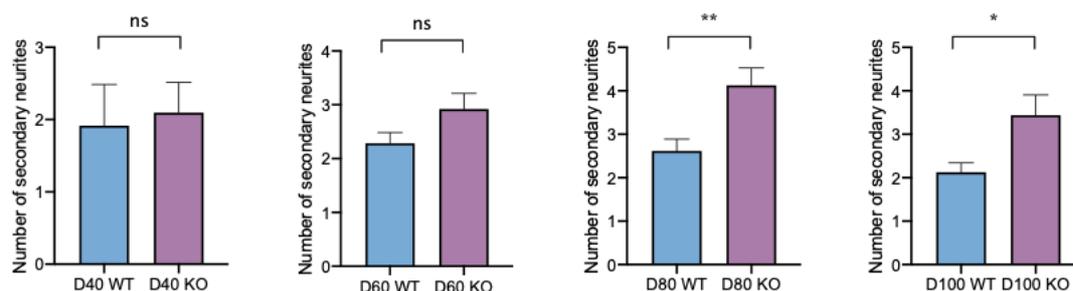
Figure 6.6 Number of secondary branches

*SGCE*ko (KO) and iCas9 (WT) were analysed for number of secondary branches present. Neurons derived from *SGCE*ko hESCs had more secondary branches present from day 60, with this becoming significant from day 80. Data represent three independent rounds of cortical differentiation. Error bars represent mean ±SEM. Statistics show results of Mann-Whitney tests; *=p≤0.05, **=p≤0.01, ***=p≤0.001, ****p≤0.0001.

Table 6.5 Mann-Whitney test to analyse differences in number of secondary branches present between WT and *SGCE*ko neurons

Number of Secondary Branches	Mean	SEM	p-value	Summary
D40				
WT	3.167	0.7923	0.7318	ns
KO	3.143	0.3902		
D60				
WT	2.286	0.1983	0.1147	ns
KO	2.923	0.2878		
D80				
WT	2.619	0.2715	0.0045	**
KO	4.125	0.4007		
D100				
WT	2.125	0.2196	0.0407	*
KO	3.440	0.4658		

6.2.5. Number of tertiary branches

As with tertiary branch length, no statistical comparison could be made at day 40 as only one of the neurons analysed displayed any tertiary branching. No statistical differences were observed in the number of tertiary branches at days 60 or 80 (D60 - WT: 2.250 ±0.1637 *vs.* KO: 2.667 ±0.8028, p=0.7336; D80 - WT: 2.333 ±0.2108 *vs.* KO: 1.800μm ±0.2000, p=0.2727). However, by day 100, *SGCE*ko neurons exhibited a far more complex dendritic structure compared to WT neurons, with a mean number of 3.100 ±0.7667 tertiary branches observed, whilst none of the WT neurons analysed displayed any tertiary branching (**Figure 6.7**, **Table 6.6**).
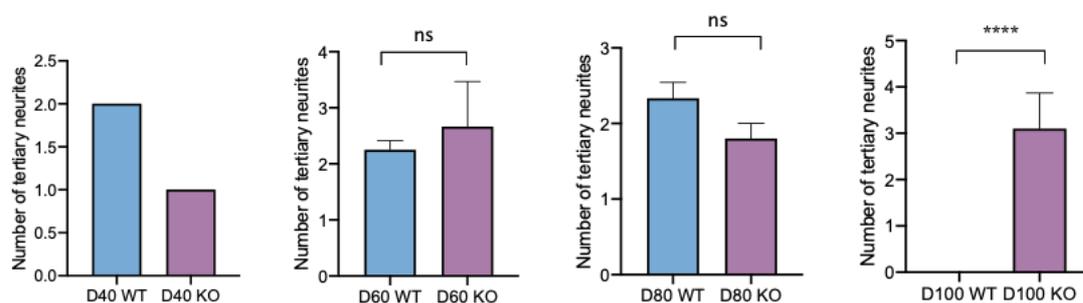
Figure 6.7 Number of tertiary branches

*SGCE*ko (KO) and iCas9 (WT) were analysed for number of tertiary branches present. Significant differences were only observed at day 100, with neurons derived from *SGCE*ko hESCs having more tertiary branches present. Data represent three independent rounds of cortical differentiation. Error bars represent mean ±SEM. Statistics show results of Mann-Whitney tests; *=p≤0.05, **=p≤0.01, ***=p≤0.001, ****p≤0.0001.

Table 6.6 Mann-Whitney test to analyse differences in number of secondary branches present between WT and *SGCE*ko neurons

Number of Tertiary Branches	Mean	SEM	p-value	Summary
D40				
WT	2.000	0	N/A	N/A
KO	1.000	0		
D60				
WT	2.250	0.1637	0.7336	ns
KO	2.667	0.8028		
D80				
WT	2.333	0.2108	0.2727	ns
KO	1.800	0.2000		
D100				
WT	0	0	<0.0001	****
KO	3.100	0.7667		
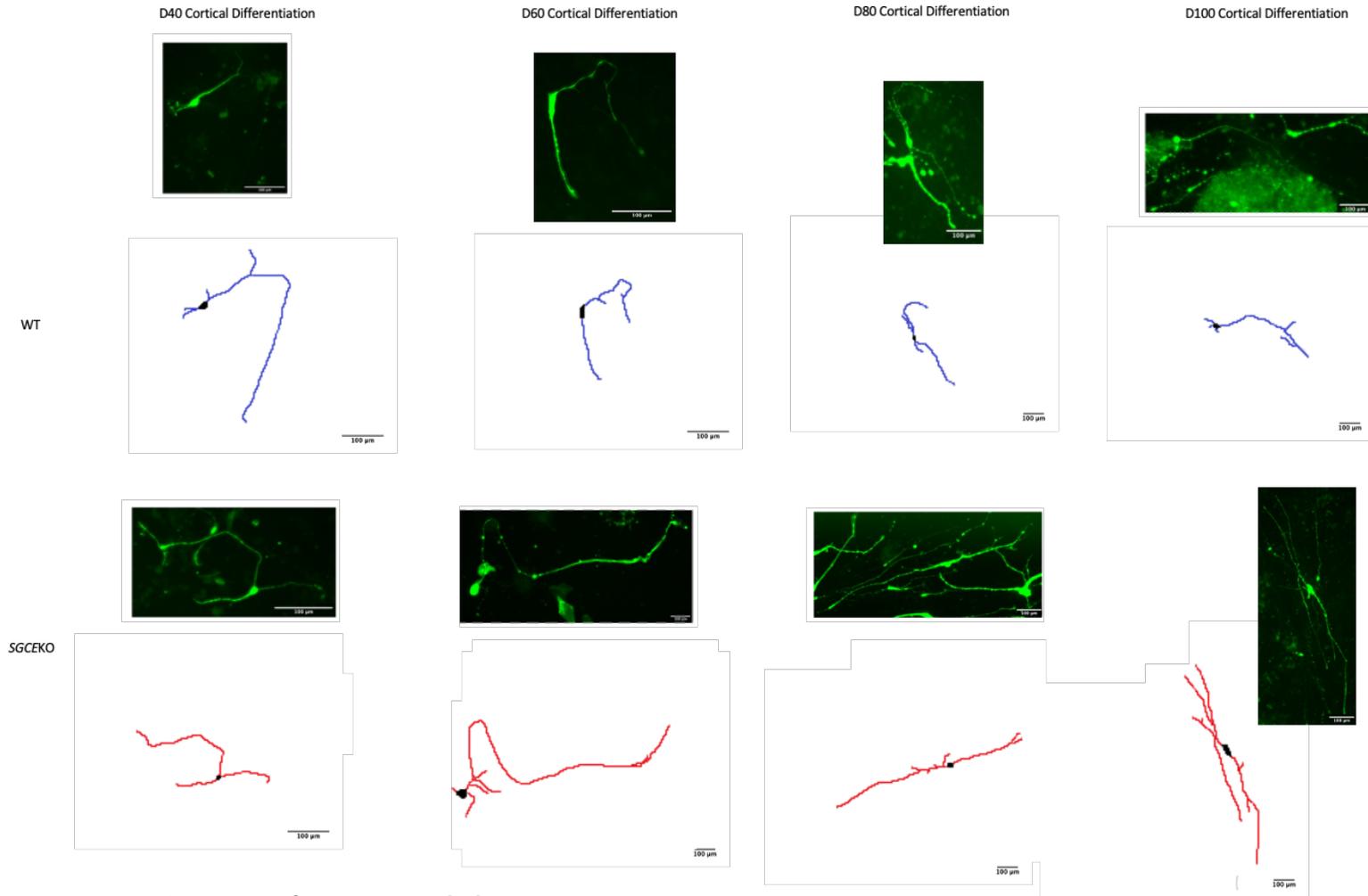
Figure 6.8 Representative traces of neuron morphology

Actual and representative traces showing the morphology of *SGCE*ko and WT neurons at days 40, 60, 80 and 100 of cortical differentiation. Scale bars are 100μm.

6.2.6. Soma area

A gradual increase in soma area was observed in *SGCE*ko neurons over the course of the differentiation from 92.78μm^2 ±7.558 at day 40 to 208.2μm^2 ±12.88 at day 100. WT soma area also increased from day 40 (81.42μm^2 ±13.80) until day 80 (163.4μm^2 ±9.807), after which evidence of the beginnings of cell body retraction appeared at day 100 (133.9μm^2 ±9.230). At all timepoints, the soma area was larger in *SGCE*ko neurons compared to WT, with this being significant from day 60 and most pronounced at day 100 (D60 - WT: 115.8μm^2 ±5.239 vs. KO: 165.8μm^2 ±15.25, p=0.0262; D80 - WT: 163.4μm^2 ±9.807 vs. KO: 199.7μm^2 ±11.66, p=0.0185; D100 - WT: 133.9μm^2 ±9.230 vs. KO: 208.2μm^2 ±12.88, p<0.0001) **(Figure 6.9, Table 6.7)**.
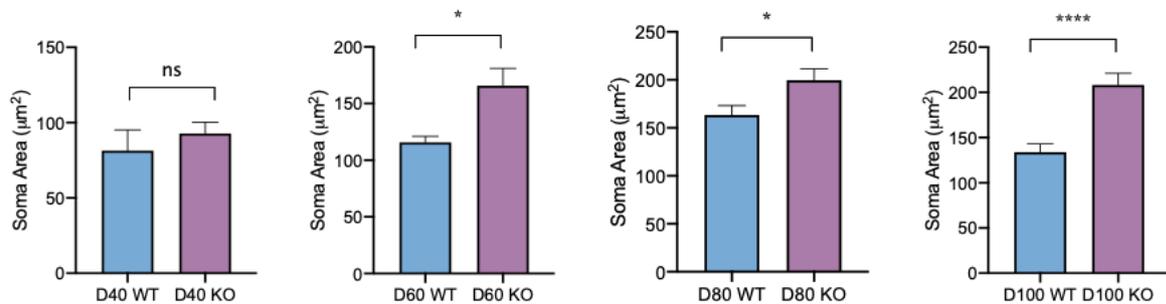
Figure 6.9 Soma area

*SGCE*ko (KO) and iCas9 (WT) were analysed for soma area. Neurons derived from *SGCE*ko hESCs had significantly larger soma areas at days 60 and 100, with no significant difference found at days 40 and 80. Data represent three independent rounds of cortical differentiation. Error bars represent mean ±SEM. Statistics show results of Mann-Whitney tests; *=p≤0.05, **=p≤0.01, ***=p≤0.001, ****p≤0.0001.

Table 6.7 Mann-Whitney test to analyse soma area differences between WT and SGCEko neurons

Soma Area	Mean (μm^2)	SEM	p-value	Summary
D40				
WT	81.42	13.80	0.6240	ns
KO	92.78	7.558		
D60				
WT	115.8	5.239	0.0262	*
KO	165.8	15.25		
D80				
WT	163.4	9.807	0.0185	*
KO	199.7	11.66		
D100				
WT	133.9	9.230	<0.0001	****
KO	208.2	12.88		

In summary, investigation of neuronal morphology suggests that loss of ε-sarcoglycan expression and function impacts excitatory cortical neurons (McAllister, Katz and Lo, 1996; Lüthi *et al.*, 2001), with key areas of distinction including:

- Longer total neurite length in the KO line at all time points.

- Comparable primary branch length between WT and KO lines other than at day 60.

- KO line demonstrates increased numbers of primary and secondary neurite branches from day 60, with these features continuing to day 100.

- Increased amount of tertiary branching at day 100 in KO line.

- Evidence of a larger soma area in KO line at all time points, compared to WT controls, with evidence of soma contraction at d100 in WT line not observed in the KO counterpart.

6.3. Discussion

This chapter provides initial insights into the effect of loss of ε-sarcoglycan expression and function on the morphological features of excitatory cortical projection neurons. Overall, neurons derived from *SGCE*ko hESCs produced longer, more branched neurons from day 60 of differentiation, with this difference being predominantly driven by the development of secondary branches, while the length of primary neurites overall remained consistent between *SGCE*ko and WT neurons. *SGCE*ko neurons displayed larger soma areas throughout the differentiation, with significant differences observed at days 60 and 100.

Cytoskeletal regulators are essential for generating and maintaining correct dendritic architecture. The cytoskeletal regulators Rho, Rac and Cdc42 play an essential role, with constitutively active mutants of these GTPases resulting in a marked increase in the number of basal dendrites in pyramidal neurons (Threadgill, Bobb and Ghosh, 1997). ε-sarcoglycan is a member of the sarcoglycan family, a group of single-pass transmembrane glycoproteins that forms a subcomplex of the dystrophin-glycoprotein complex (DGC). The DGC connects the cell's cytoskeleton to the extracellular matrix through the interaction of extracellular matrix proteins with α-dystroglycan, dystrophin, the cytosolic region of β-dystroglycan and cytoskeletal structures (Prins *et al.*, 2009; Allen, Whitehead and Froehner, 2016). In cases of muscle atrophy linked to defects in the DGC, expression and activity levels of H-Ras, RhoA and Cdc42 were decreased, suggesting a physical linkage between the DGC and GTPases (Chockalingam *et al.*, 2002). Although evidence to date suggests that the DGC complex doesn't exist in the same form in brain tissue, recent immunoaffinity purification studies have demonstrated co-precipitation of ε-sarcoglycan with β-dystroglycan, suggesting a DGC-like complex in the brain (Waite *et al.*, 2016). Given these similarities, it is possible that ε-sarcoglycan mutations could disturb small

GTPase signalling with subsequent impact on dendritic arborisation, with further work needed to investigate this in detail.

Calcium signalling plays an important role in regulating dendritic branching and growth with increases in intracellular calcium levels promoting an increase in dendritic branching. In comparison, pharmacological blockade of synaptic activity, for example with the NMDA receptor antagonist APV, or the AMPA receptor antagonist CNQX, decreases the rate of dendritic growth in developing neurons (Rajan and Cline, 1998). Neuronal calcium influx results in activation of two major signalling targets; calcium/calmodulin-dependent protein kinases (CaMKs), and mitogen-activated kinase (MAPK). CAMKIIα has been shown to stabilise or restrict dendritic growth in mammalian cortical neurons *in vitro* (Redmond, Kashani and Ghosh, 2002), whereas CAMKIIβ has a positive effect on fine dendrite development, mediated by direct interaction with cytoskeletal actin (Fink *et al.*, 2003). MAPK signalling, which can be activated by calcium influx via NMDA receptors and voltage-sensitive calcium channels, has also been implicated in mediating the effects of calcium influx on dendrite growth in cortical neurons. The cAMP-response element binding protein (CREB), CREST, a calcium-regulated transcriptional activator and CREB-binding protein (CBP) are likely involved in the regulation of a transcriptional programme that is involved in activity-induced dendritic development (Aizawa *et al.*, 2004; Konur and Ghosh, 2005). Furthermore, there is evidence that release of calcium from internal stores can influence dendrite dynamics, with blockade of local events resulting in rapid retraction of dendrites (Lohmann, Myhr and Wong, 2002). BDNF is also an important mediator of activity-dependent dendritic growth and is regulated by calcium signalling in cortical neurons, exerting a major influence on cortical dendrite development (Shieh *et al.*, 1998; Tao *et al.*, 1998; Gorski *et al.*, 2003). **Chapter 4** described disruption of spontaneous calcium activity in *SGCE*ko cortical neurons, with an increase in overall percentage activity. Given the importance of calcium activity in dendritic growth and branching, it is possible that this increased calcium activity observed in *SGCE*ko neurons may contribute to the increased length and complexity of the dendritic branching observed in these cultures.

As described in **chapter 5**, single-cell electrophysiology studies revealed that *SGCE*ko neurons displayed a consistently larger capacitance in comparison to WT neurons. Cell capacitance is directly linked to cell surface area, with a larger capacitance suggesting a larger cell. The presence of both a larger soma and lengthier neurites in the *SGCE*ko line suggest that both may be contributing to this increased surface area. However, the difference in neurite length between WT and KO lines was both overall higher, and more consistent, suggesting that it may be this component of neuronal cell morphology that is driving the observed increase in capacitance.

A range of receptors, channels and signalling molecules are present in the dendritic arbor of a neuron, including extra-synaptic NMDA (Petralia *et al.*, 2010; Papouin *et al.*, 2012) and GABA (Kasugai *et al.*, 2010) receptors that control numerous aspects of neuronal function (Ratnayaka *et al.*, 2011). An increase in neuron size (both soma area and neurite length) has the potential to impact the number and

density of ion channels in the cell surface membrane, with effect on the functional characteristics of the cell. There is evidence that increased dendritic complexity may be associated with fast action potential kinetics, with larger dendrites leading to faster action potential onset (Goriounova *et al.*, 2018). Dendrites of pyramidal neurons express an abundance of voltage- and calcium-gated ion channels. The longer secondary neurites observed in *SGCE*ko cultures may allow increased expression of channels, which could account for some of the hyperexcitability observed. Further experiments to investigate the presence and abundance of synaptic proteins could also prove beneficial to unravelling the longer, more branched neuronal morphology phenotype observed in the *SGCE*ko line. To examine this, immunocytochemistry allowing the visualisation of the presynaptic protein synaptophysin and the postsynaptic protein PSD-95 could be performed. This could be performed alongside qPCR experiments.

Dendritic morphology is also an important factor in modulating neuronal firing however, the underlying mechanisms remain largely unknown. Either reducing or enlarging the dendritic tree, or altering the topological structure through modification of total dendritic length, can change a cell's firing pattern and ultimately impact information processing and cognition (van Elburg and van Ooyen, 2010). More and/or longer dendrites can also increase the opportunities for communication, with the number of synaptic connections that a given neuron can form determined by the branching of its dendritic tree. Long-term potentiation can induce an increase in the number and stability of spines, which is associated with increased synaptic strength and increased surface AMPA receptor expression (Berry and Nedivi, 2017). In the cortex, the majority of excitatory synapses are formed on dendritic spines. As there is evidence of exaggerated LTP-like plasticity in patients with dystonia, it is plausible that the longer, more branched neurons observed in the *SGCE*ko neurons in this study may also exhibit a higher number of dendritic spines, however further investigation would be needed in order to determine this in greater detail.

As outlined above, dendritic morphology can impact neuronal excitability however, the converse – neuronal hyperexcitability influencing neurite growth and development – could also represent an important factor in the model described in this thesis. Several studies have shown that increased neuronal activity promotes dendritic growth and branching complexity during cortical and hippocampal development (McAllister, Katz and Lo, 1996; Lüthi *et al.*, 2001). In contrast, studies focusing on epileptiform disorders have shown chronic network hyperexcitability to be accompanied by a marked decreased in dendritic branching of neocortical and hippocampal neurons (Nishimura, Owens and Swann, 2008; Reid *et al.*, 2014). These paradoxical outcomes could, in part, be explained by the scale and extent of changes in activity that are experimentally induced. It has been proposed that dendrite growth can be augmented if activity is amplified within typical physiological ranges and/or over reasonably brief periods of time (minutes to hours). However, compensatory mechanisms that attempt

to re-establish standard levels of neuronal activity may be induced when activity is atypically elevated for extended periods of times (Turrigiano and Nelson, 2004; Nishimura, Owens and Swann, 2008).

In the pmaxGFP plasmid (3.49kb), maxGFP expression is driven by a cytomegalovirus (CMV) promotor. This creates a limitation in that labelling of cells was not purely limited to neurons, rather all cells in the culture had the potential to express GFP, including non-neuronal cells such as glia. All dendritic branching analysis carried out in this thesis was conducted based on morphology, potentially permitting errors, with the possibility that some non-neuronal cells have been characterised. One way to overcome this issue would be to co-stain with a neuronal-specific marker, or another would be the use of a neuronal-specific promotor. Perhaps superior to this would be the addition of a fluorescent dye to the internal solution during electrophysiology experiments. This would allow electrophysiological recordings to be carried out, with post-hoc staining to assess dendritic morphology on those same neurons.

In summary, the findings presented in this chapter suggest that loss of ε-sarcoglycan expression and function impacts neuronal morphology during differentiation towards an excitatory cortical cell lineage which may either cause or be the consequence of the functional characteristics observed in Chapters 4 and 5.

7. General Discussion

7.1. Summary

This thesis has sought to investigate the impact of loss of expression of the epsilon-sarcoglycan protein on the development of excitatory cortical neurons during differentiation. Using this hESC model, work has focused on changes to phenotypic (chapters 3 and 6) and functional (chapters 4 and 5) characteristics of glutamatergic cortical neurons as a result of loss of expression of the *SGCE* gene. The results demonstrated that loss of epsilon sarcoglycan expression did not result in marked changes to the differentiation of hESCs towards a cortical neuronal lineage, with no deficits in the formation of either NPCs or more mature neuronal cells. Investigation of the functional properties of *SGCE*ko cortical neurons revealed differences in spontaneous calcium activity and multiple electrophysiological characteristics compared to the isogenic WT control line, suggesting a hyperexcitable phenotype. More specifically, calcium imaging studies found the *SGCE*ko neuronal cultures to demonstrate a higher overall level of calcium activity, together with lower amplitudes, longer rise times and shorter fall times when evaluating the event shape. Whole cell patch-clamp electrophysiological studies demonstrated a similar pattern of increased excitability, with *SGCE*ko neurons displaying shorter AP half-width, faster rate of rise of the AP upstroke, and a more rapid maximum rate of AP repolarisation. In addition, *SGCE*ko neurons displayed more frequent and longer trains in response to current step injection, indicating a more hyperexcitable phenotype in comparison to their isogenic WT counterparts. Follow-up experiments examining neurite arborisation revealed abnormalities in neuronal architecture, with neurons deficient in ε-sarcoglycan expression displaying a more extensive and more complex dendritic arbor morphology. Collectively, these findings suggest an important role for the epsilon-sarcoglycan protein in excitatory cortical neuronal development, and provide an initial step in delineating the cellular changes that may contribute to the pathophysiological processes underpinning Myoclonus Dystonia.

7.2. Areas of interest

7.2.1. Potassium channels

One of the most interesting findings presented in this thesis was the significantly shorter fall times of calcium transients together with the faster rates of repolarisation and shorter half-widths of the action potentials generated by the *SGCE*ko neurons when compared to the WT controls. A potential explanation for these changes may lie in potassium ion channel dysfunction. Potassium channels are the most diverse of all ion channels and underlie several functions controlling the excitability of neurons including; i) determining the resting membrane potential, ii) frequency of the APs, and iii) AP duration

and shape (Greene and Hoshi, 2017). Many potassium channel subtypes are involved in the repolarisation phase of an action potential, helping to control action potential frequency and duration. Loss of multiple potassium channel subtypes have been demonstrated in conditions characterised by neuronal hyperexcitability, most notably $K_V1.1$, $K_V3.3$, $K_V4.3$ and $K_V4.2$ channels (***Figure 7.1***) (Toledo-Rodriguez *et al.*, 2005).

Figure 7.1 Potassium channels associated with neuronal hyperexcitability
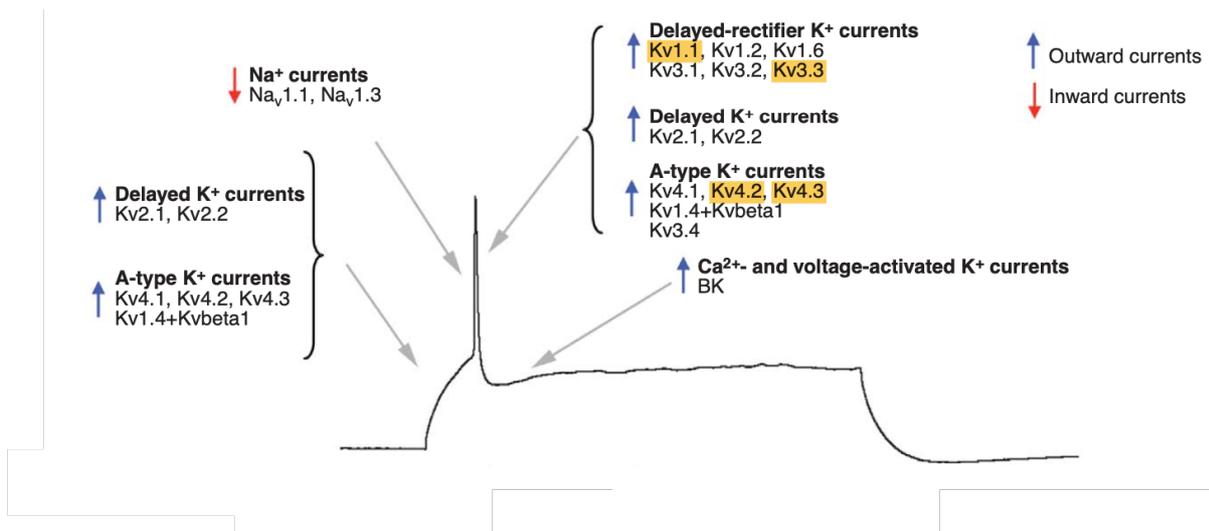
Schematic of inward and outward currents and ion channels underlying each current, with those linked to neuronal excitability highlighted in yellow. Adapted from Toledo-Rodriguez *et al.*, 2005.

7.2.2. Actin cytoskeleton

As described in chapter six, cortical neurons deficient in ε-sarcoglycan protein displayed a more complex and extensive dendritic arbor. Establishment and maintenance of dendritic structure is controlled, in part, by cytoskeletal elements with actin filaments playing a critical role in maintaining neuronal polarity (Tsaneva-Atanasova *et al.*, 2009). ε-sarcoglycan is a component of the dystrophin-glycoprotein complex, which links the actin cytoskeleton to the extracellular matrix. Mutations to *SGCE* impair trafficking of the mutant protein to the plasma membrane (Esapa *et al.*, 2007), which could potentially impact the development of the dendritic arbor. Alterations to dendritic spine dynamics have previously been shown to precede the onset of motor symptoms in a mouse model of Huntington's disease, suggesting that decreased stability of the cortical synaptic circuitry may underlie the early development of symptoms in Huntington's disease (Calabresi *et al.*, 2016).

7.2.3. Potential mechanism of action

One of the major uncertainties to emerge from investigations undertaken in this thesis is whether the differences in neuronal morphology are a cause or consequence of the functional phenotypes observed. For example, could the increased length and complexity of dendritic branching lead to the increased activity observed, both in terms of calcium signalling and electrophysiology studies, or could the vice versa be true? A recent study carried out by Li *et al*., 2021, demonstrated how *Sgce* KO and KI mice showed increased numbers of dendrites and branches in Purkinje cells compared to WT. Furthermore, in hippocampal neurons cultured from *Sgce* KO and KI mice, the number of dendritic spines were dramatically higher than in WT neurons, with the number of excitatory synaptic terminals also being significantly higher. Li *et al*., postulate that *SGCE* may act as a brake on synaptogenesis, with mutations to the *SGCE* gene leading to excessive excitatory synaptic terminals and consequently enhanced excitatory transmission (Li *et al.*, 2021). This data, combined with the evidence presented in section 7.2.2 that reiterates the importance of the link between ε-sarcoglycan, the dystrophin glycoprotein complex and the actin skeleton, potentially imply that architectural changes drive the functional changes observed. The next logical step in this investigation would be to explore the number and density of pre- and post-synaptic terminals using immunocytochemistry and qPCR.

7.3. Implications for Myoclonus Dystonia

Although dystonia is widely recognised as a circuit-based disorder, it is important to investigate neuronal subtype specific phenotypic and functional abnormalities in order to gain a more detailed understanding of how these changes are expressed on a cellular level. There are several plausible explanations for the motor symptoms observed in patients with myoclonus dystonia, one of which being that the dystonic component is largely driven by aberrant cortical signalling to muscles. The next question would be, is the hyperkinetic cortical signalling we observe the result of changes in other neuronal subtypes whose downstream effects are the changes observed in the cortical neurons described in this thesis. Another option, and potentially more plausible, is that the genetic changes impact all neuronal subtypes involved in these circuits, and it is this collective effect that is responsible for the disorder phenotype observed clinically.

A large proportion of patients with dystonia present with additional psychiatric conditions. Myoclonus dystonia due to *SGCE* mutations has been linked obsessive-compulsive disorder, anxiety-related disorder, and alcohol dependence, suggesting that loss of *SGCE* expression may have a pleiotropic clinical effect, although it remains possible that these non-motor symptoms represent the secondary sequelae of a chronic, disabling, motor disorder (Peall *et al.*, 2016). Recently, Mencacci *et al.* explored the potential for genetic overlap between dystonic and psychiatric disorders (N. Mencacci *et al.*, 2020). Dysregulation of synaptic signalling in frontal cortical pyramidal neurons, as well as striatal medium

spiny neurons and adult nigral dopaminergic neurons was found to be a large contributor to pathogenesis associated with multiple dystonia-associated genes. Moreover, their study indicated that psychiatric symptoms associated with dystonia are likely to be intrinsic to its pathophysiology.

Some of the changes that have been identified in this study may have therapeutic potential; modulation of ion channels and receptors using oral medical therapy may be one such option. These could include blockers of calcium channels (e.g. Amlodipine) to reduce high-frequency repetitive firing observed in *SGCE*ko cortical neurons, or modulators of potassium channels (e.g. Retigabine) to increase the action potential decay time. This may help increase the half-width of action potentials and consequently reduce excitability of cortical glutamatergic neurons.

Given that the neurons generated in this thesis are likely to resemble very early-stage human neurons, it is quite plausible that the findings presented are representative of a very early, subtle developmental phenotype, that perhaps develops/worsens later in childhood when M-D patients present with clinical symptoms. This neuronal-cell model could be used to investigate a broad range of therapeutic strategies, not solely pharmacological drug screening. iPSC-derived neuron models of various diseases have been used to test candidate compounds, hormones and growth factors. For example, insulin-growth factor 1 (IGF1) was tested on Rett syndrome iPSC-derived neurons and found to rescue the disease phenotype by increasing glutamatergic synapse number (de Souza *et al.*, 2017). Consequently, after completing phase II trials (Glaze *et al.*, 2017), a phase III trial has been planned to assess the benefit and safety of Trofinetide, a small molecule analogue of IGF1. More recently, gene therapy using neural stem/progenitor cells derived from iPSC cells has been demonstrated to inhibit glioblastoma cell growth (Tamura *et al.*, 2020).

7.3.1. Axon initial segment

The specialised structure known as the axon initial segment (AIS) resides between axonal and somatodendritic domains in neurons and serves as the site of action potential firing as well as helping to maintain neuronal polarity. It contains a high density of voltage-gated ion channels, with the cytoskeletal submembrane networks serving as scaffolds for these membrane-based ion channels. In order to modulate neuronal excitability and maintain steady-state firing rates, components of the AIS, including the cytoskeleton and ion channels undergo activity-dependent structural changes. Aberrant hyperexcitability of neuronal activity is often observed in frontotemporal dementia (FTD) with tau pathology. FTD-patient iPSC-derived cortical neurons show disrupted activity-dependent plasticity of the AIS and impaired homeostasis of neuronal activity by impacting AIS cytoskeleton, causing dysregulation of neuronal network function (Sohn *et al.*, 2019). As hyperexcitability is the fundamental characteristic of *SGCE*ko cortical neurons in this thesis, it would be interesting to investigate whether

impairment of AIS plasticity contributes to the observed phenotype. Here, immunocytochemistry could be used to label ankyrin (AnkG), a cytoskeletal submembrane protein in the hESC-derived cortical neurons in order to determine length of the AIS.

7.4. Study limitations

7.4.1. Neuron maturity

A key limiter in the use of stem-cell derived neurons for functional investigations is their relative lack of maturity when compared to even the early stages of human neuronal development. This is perhaps unsurprising given that the typical human gestation period is approximately three-times longer than the 100-day protocol used in this thesis to generate post-mitotic 'mature' neurons. A study investigating gene expression of hiPSC-derived neurons in comparison to the Allen BrainSpan Atlas found that hiPSC-derived neurons grown as a 2D monolayer resemble human neurons from the late first to early second trimester (Brennand *et al.*, 2015). Although our protocol incorporated both the small molecules DAPT and PD033291 and hypoxic (2% oxygen incubator) culture conditions, to synchronise neuronal development and better reflect *in vivo* conditions respectively, the neuronal cultures analysed nevertheless displayed relatively immature functional properties despite being cultured for up to 100 days.

Several attempts to improve functional maturation have been reported over the past few years. In 2015, Bardy *et al* developed a neuronal medium containing major ion concentrations similar to that of human cerebrospinal fluid (hCSF) (Bardy *et al.*, 2015). More recently, a comparative study assessing the functional and cellular properties of iPSC-derived 3D neural aggregates (NAs) cultured in either BrainPhys-based medium or hCSF found NAs exposed to hCSF displayed increased neurogenesis, gliogenesis, synapse formation, neurite outgrowth and suppression of residing neural stem cell proliferation, leading to the formation of synchronously active neuronal circuits *in vitro* (Izsak *et al.*, 2020). It is difficult to determine exactly which factors are responsible for enhancing neuronal maturation in hCSF however, the increased gliogenesis may cause the secretion of additional pro-maturation factors, promoting further neurite growth and synapse development. Hedegaard *et al.,* have shown how iPSC-derived astrocytes can exert pro-maturational effects on developing networks of iPSC-derived cortical neurons, with synapse-associated extracellular signalling implicated in achieving the pro-maturational effects observed (Hedegaard, Monzó N-Sandoval, *et al.*, 2020). Microglia also promote survival and maturation of neurons, with microglia demonstrated to have an involvement in synaptic organisation and trophic neuronal support during development, as well as having an influence on neuronal excitability (Bachiller *et al.*, 2018). They also play an important role in the formation

(Weinhard *et al.*, 2018), maturation (Miyamoto *et al.*, 2016) and pruning (Kim *et al.*, 2017) of immature synapses.

As discussed in section 3.3, one of the limitations of this study is the lack of characterisation performed on non-neuronal cells. It is likely that the cultures generated using the differentiation protocol described in this thesis contain some glial cells as well as neurons, which may be providing some amount of pro-maturational benefit.

As human cortical development is maximal at weeks 5-20 of gestation, yet at their most mature our hESC-neurons resemble early foetal brain tissue, it is likely that we are capturing only very early functional changes, and as a result this approach may not illustrate key functional and developmental changes that may become apparent later in development.

7.4.2. Compound heterozygous loss of *SGCE*

In order to create a cell line that did not express the ε-sarcoglycan protein, a compound heterozygous line with biallelic loss of *SGCE* expression was generated. However, this does not exactly mirror the genotypic changes observed in MD when the typical clinical phenotype is observed. Here the pathogenic variant is typically paternally inherited, in conjunction with imprinting of the maternal allele, leading to loss of expression of the *SGCE* gene. To overcome these differences in underlying genotype, the work described above could be undertaken in patient-derived iPSC lines in which preservation of the imprinting of the maternal allele was confirmed, this ensuring that the functional effects described above are indeed typical of the changes that may underpin the pathophysiology of MD. As imprinting status is so dynamic and fluid during embryogenesis, it is important to confirm that imprinting is preserved at all stages (i.e., prior to reprogramming, following reprogramming and post-differentiation). One way to potentially preserve maternal imprinting could be directly convert patient fibroblasts or blood into functional neurons, bypassing the need for a pluripotent state.

7.4.3. 2D monolayer culture system

The work presented in this thesis involved characterisation of neuronal cells grown in a 2-dimensional (2D) monolayer culture, not reflective of the *in vivo* brain environment where neurons co-exist with other cell types in three dimensions. To overcome this problem, pluripotent stem cells have been differentiated into 3-dimensional (3D) structures called organoids (Mariani *et al.*, 2012; Lancaster and Knoblich, 2014; Qian *et al.*, 2016) which allow better interaction between different cell types. Single-cell RNA sequencing analysis has revealed significant similarities in gene expression profiles between cerebral organoids and the foetal human cerebral cortex (Camp *et al.*, 2015). Stable cell-cell interaction at physiological proximity and density is encouraged with long-term culture of brain organoids.

However, there are several limitations when working with organoids, not least their relative lack of reproducibility, although significant improvements to protocols have been made over recent years in order to address this variation. Although organoid cultures better mimic the native form of the brain, delivery of small molecular factors, nutrients and oxygen to the inner layers is inevitably difficult. This not only results in irregularities to the efficiency of organoid development, but also often results in high levels of atrophy and expression of stress markers in the surviving cells (Camp *et al.*, 2015; Xiang, Tanaka and Patterson, 2017).

7.5. Future directions

7.5.1. RNA-sequencing

RNA sequencing (RNA-seq) uses next-generation sequencing techniques to reveal the presence and quantity of RNA in a biological sample at a given moment. Over the last decade it has become a crucial tool in transcriptome-wide analysis of differential gene and gene pathway expression, and differential splicing of mRNA. RNA-seq could be used to gain insight into the mechanisms driving the functional changes described in this thesis, and allow for a broad and unbiased view of pathways involved. For example, a potential concept to explain the high levels of calcium activity observed in the experiments in chapter 4 could be the aberrant expression, or excessive activation, of pre- or post-synaptic calcium membrane receptors resulting in excessive network excitability and hyperkinetic movements. Differential gene expression analysis is likely to result in hundreds of highlighted genes therefore, stringent thresholds are needed in order to prevent 'false positives' in the downstream analysis (Koch *et al.*, 2018). Functional enrichment analysis could then be used to assign biological relevance to a set of genes. The resulting gene ontology enrichment terms may, for example., describe biological processes, molecular functions, or cellular components. RNAseq experiments could provide a beneficial way of identifying up- or down-regulation of receptor subtypes. Following this, qPCR and western blot analysis to examine those calcium receptors could be used to assess RNA and protein expression levels respectively.

Furthermore, a technique known as 'patch-seq' has recently been developed that allows the combination of single-cell RNA-seq with patch-clamping electrophysiological recording and morphological analysis of single human neurons *in vitro*. This permits links between functional properties, morphology and gene expression to be explored through multimodal profiling of neurons and could assist in unravelling the cellular mechanism underlying myoclonus dystonia (Cadwell *et al.*, 2016; van den Hurk *et al.*, 2018).

7.5.2. Voltage-clamp patch clamp

The whole-cell patch clamp experiments undertaken as part of this study were conducted in current-clamp mode and recorded the change in voltage throughout the cells. As discussed in Chapter 5, voltage-gated sodium and potassium channels are critical for action potential generation and decay, and their functional expression is key in regulating physiological maturity of neurons. Voltage-clamp experiments showing ionic currents associated with individual neurons could provide further insight into ions channels potentially affected by loss of ε-sarcoglycan.

7.5.3. Multi-electrode array (MEA)

Multi-electrode array (MEA) recordings could provide good supporting evidence to the whole-cell patch-clamp experiments presented in this thesis. Previous studies have used both whole-cell patch clamp and MEA studies to provide complementary functional information from PSC-neurons. For example, iPSC-derived neurons from Amyotrophic Lateral Sclerosis patients displayed a hyperexcitable phenotype characterised by increases in both spontaneous and induced AP firing in patch clamp and MEA studies (Kiskinis *et al.*, 2014). MEA experiments would allow the investigation of a whole network, permitting the detection of extracellular changes in potential caused by firing of neurons from a whole population, rather than a single neuron. As multiple levels of evidence suggest dystonia to be a network-based disorder, an overview of electrical changes on a network level is a key future area of investigation. This approach would also enable measurement of network level response to pharmacological manipulation, as well as potentially enabling a higher throughput system for future drug screening studies.

7.5.4. Other neuronal subtypes

Murine and human clinical studies also suggest that the striatal cholinergic system plays an important role in the pathophysiology of dystonia, with loss of inhibitory function observed at spinal, brainstem and cortical levels (Berardelli *et al.*, 1998). Typically, nervous system activity is balanced by excitatory and inhibitory circuits functioning collectively. However, in addition to the neuronal hyperexcitability described in this thesis, previous work also suggests that disruption to inhibition is also a contributing factor, leading not only to the development of dystonic symptoms, but also the loss of muscle selectivity and overflow of the excess movement.

The striatum, the predominant input region of the basal ganglia, receives considerable convergent glutamatergic input from the entire cortex. Organisation of the basal ganglia is hypothesised to be divided into the direct pathway, which helps facilitate the desired movement, and the indirect pathway, which inhibits unwanted movements (Mink, 1996). In dystonia, there is thought to be an imbalance

between both pathways, leading to the direct pathway being overactive or the indirect pathway underactive (Hallett, 2006). The striatum also receives inhibitory input from fast-spiking interneurons, which are also hypothesised to balance the excitatory cortical and thalamic input to the striatum. Inhibitory GABAergic striatal medium spiny neurons (MSNs) receive converging excitatory glutamatergic input from the cortex and thalamus, as well as inhibitory input from globus pallidus feedback projections and feedforward inhibition from striatal interneurons. Parvalbumin-positive fast-spiking interneurons (FSIs) are the primary source of feedforward inhibition on MSNs, and receive direct inputs from the cortex. Spike timing of MSNs is largely controlled by the powerful feedforward inhibition exerted by FSIs, and this feedforward inhibition is hypothesised to balance cortical and thalamic excitation. A rodent model of paroxysmal dystonia displayed diminished numbers of striatal FSI that was associated with abnormal movements (Gernert *et al.*, 2000). The imbalance between inhibition and excitation is clearly an important phenomenon in dystonia pathophysiology. With a hyperexcitable phenotype displayed by *SGCE*ko cortical neurons in this study, it is important to investigate how these glutamatergic neurons would behave in a network system.

Other neuronal subtypes likely to be of importance in the pathogenesis of Myoclonus Dystonia, as well as dystonic disorders more widely, include both midbrain dopaminergic neurons and cell types within the cerebellum, most notably Purkinje cells. Animal models have also provided evidence of disruption to the midbrain monoaminergic neurotransmission with a paternally inherited *Sgce* heterozygous knockout murine model displaying abnormally high levels of dopamine and its metabolites in the striatum. In addition, reduced dopamine D2 receptor (D2R) availability is observed in neuroimaging studies of DYT11 myoclonus dystonia patients (Beukers *et al.*, 2009; Zhang *et al.*, 2012). Furthermore, the importance of the cerebellum in myoclonus dystonia has become more clear over recent years, with acute cerebellar knockdown of *Sgce* reproducing salient features of MD in mice (Washburn *et al.*, 2019). The evidence provided here affirms the importance of investigating the effect of loss of ε-sarcoglycan in other neuronal subtypes, both individually and in a network-based structure.

7.5.5. Co-Cultures

As dystonia is widely considered to be a network disorder, investigating distinct neuronal subtypes in a co-culture system could prove useful in determining changes in connectivity and synaptic function. A co-culture system involving multiple combinations of the neuronal types described above, efficient differentiation protocols being widely available for all of them, could allow region-specific circuits to be reproduced *in vitro*. In order to restrict each neuronal population to contact only, allowing subtype-specific medium to be replaced in individual chambers, novel microfluidic cell culture platforms have been optimised and established. These involve cell culture plates consisting of two adjacent, but independent chambers that are connected by short grooves which permit neuronal processes to pass

through chambers and form synapses with neurons in the neighbouring chamber (Fantuzzo *et al.*, 2017, 2019; Virlogeux *et al.*, 2018). In these models, defined synaptic connections between neuronal subtypes have been determined by synapsin staining and excitatory neuronal stimulation has been demonstrated to evoke excitatory post-synaptic current responses in neurons in adjacent chambers. Co-cultures would also assist in achieving an *in-vivo*-like morphology with mature dendritic spines.

7.5.6. Organoids

To expand on the work carried out in this thesis, the differentiation of WT and *SGCE*ko hESCs into regional organoids could prove beneficial. Over recent years, work to improve the variability previously observed both within and between organoids has been undertaken with brain organoids now becoming more complex, dynamic and representative of in vivo interactions. The Lancaster lab recently generated iPSC-derived organoids that are able to secrete a cerebrospinal fluid-like fluid (Pellegrini *et al.*, 2020). As organoids contain multiple cell types, they provide a more physiological environment for studying brain development *in vitro*, recapitulating some of the features of the human brain, including cellularity, general tissue structure and developmental trajectory. Cerebral cortex organoids have been the most well characterised and most commonly used regional organoids. Their neuronal layers not only contain deep layer and superficial layer neurons, but also interneurons, astrocytes and oligodendrocyte precursor cells (Quadrato *et al.*, 2017). This interaction between different cell types may be crucial in elucidating more complex phenotypes associated with *SGCE* mutations.

Three dimensional cell culture approaches that allow the derivation of tissue resembling features of the human midbrain have also been developed (Tieng *et al.*, 2014; Jo *et al.*, 2016; Qian *et al.*, 2016; Monzel *et al.*, 2017; Kim *et al.*, 2019; Smits *et al.*, 2019). As well as containing electrophysiologically functional neurons that produce and secrete dopamine, midbrain organoids also contain responsive neuronal subtypes such as GABAergic and glutamatergic neurons (Smits and Schwamborn, 2020). Modelling myoclonus dystonia in such cellular systems could provide new insight into disease pathophysiology and has the potential to be exploited in advanced therapeutic development.

7.5.7. iPSCs

As described above, homozygous gene editing of hESC lines does not directly replicate the genotype observed in patients diagnosed with Myoclonus Dystonia. Therefore patient-derived iPSCs represent an important next step in confirming the findings from this study. iPSCs are generated from somatic cells and are reprogrammed using 'Yamanaka factors', a specific set of transcription factors that allow the conversion of somatic cells back to PSCs. Research using two patient iPSC lines, one containing a missense mutation (c.662G>A,p.Gly441Asp) and the other a nonsense mutation (c.289C>T,p.Arg97X), along with their CRISPR-corrected isogenic controls is currently underway in our lab. We hope to

corroborate the results observed in the hESC studies presented in this thesis, demonstrating direct disease relevance.

7.6. Wider applications

The results presented in this thesis provide some initial insight into the functional abnormalities caused by *SGCE* mutations in hESC-derived excitatory cortical neurons. Further investigation is needed to more precisely delineate the molecular mechanisms underpinning the hyperexcitability observed in this model, however, once deciphered, novel therapeutic targets may become apparent. This would allow the application of genetic and pharmacological approaches in order to attempt to correct pathway disruption, and ultimately aid in treating the clinical phenotype. PSC-derived neuronal models have the potential to enable high-throughput screening of candidate therapeutic treatments, representing a significant opportunity for the dystonia research field. At present there are no disease-modifying or curative treatment available for patients with dystonia, with therapies currently available often variably effective, poorly tolerated or repetitive, and only appropriate for selected patients.

7.7. Conclusions

The findings presented in this study provide an insight into how stem cell-derived neurons can be used to model Myoclonus Dystonia and have begun to provide some initial information relating to the functional phenotypes associated with loss of ε-sarcoglycan expression.

8. References

Abbate, I. *et al.* (2005) 'Cell membrane proteins and quasispecies compartmentalization of CSF and plasma HIV-1 from aids patients with neurological disorders', *Infection, Genetics and Evolution*, 5(3), pp. 247–253. doi: 10.1016/j.meegid.2004.08.006.

Abe, K. *et al.* (2004) 'Stability of dendritic spines and synaptic contacts is controlled by αN-catenin', *Nature Neuroscience*. Nat Neurosci, 7(4), pp. 357–363. doi: 10.1038/nn1212.

Aguilo, F. *et al.* (2017) 'THAP1: Role in Mouse Embryonic Stem Cell Survival and Differentiation', *Stem Cell Reports*, 9(1), pp. 92–107. doi: 10.1016/j.stemcr.2017.04.032.

Aizawa, H. *et al.* (2004) 'Dendrite development regulated by CREST, a calcium-regulated transcriptional activator.', *Science (New York, N.Y.)*. Science, 303(5655), pp. 197–202. doi: 10.1126/science.1089845.

Albanese, A. *et al.* (2013) 'Phenomenology and classification of dystonia: A consensus update', *Movement Disorders*, 28(7), pp. 863–873. doi: 10.1002/mds.25475.

Albright, A. L. and Ferson, S. S. (2009) 'Intraventricular baclofen for dystonia: techniques and outcomes', *Journal of Neurosurgery: Pediatrics*, 3(1), pp. 11–14. doi: 10.3171/2008.10.PEDS0847.

Alcamo, E. A. *et al.* (2008) 'Satb2 Regulates Callosal Projection Neuron Identity in the Developing Cerebral Cortex', *Neuron*. Elsevier, 57(3), pp. 364–377. doi: 10.1016/J.NEURON.2007.12.012.

Allen, D. G., Whitehead, N. P. and Froehner, S. C. (2016) 'Absence of Dystrophin Disrupts Skeletal Muscle Signaling: Roles of Ca $^{2+}$, Reactive Oxygen Species, and Nitric Oxide in the Development of Muscular Dystrophy', *Physiological Reviews*, 96(1), pp. 253–305. doi: 10.1152/physrev.00007.2015.

Allen, N. J. and Eroglu, C. (2017) 'Cell Biology of Astrocyte-Synapse Interactions', *Neuron*. Cell Press, 96(3), pp. 697–708. doi: 10.1016/J.NEURON.2017.09.056.

Arber, C. *et al.* (2015) 'Activin A directs striatal projection neuron differentiation of human pluripotent stem cells', *Development*, 142(7), pp. 1375–1386. doi: 10.1242/dev.117093.

Argyelan, M. *et al.* (2009) 'Cerebellothalamocortical connectivity regulates penetrance in dystonia.', *The Journal of neuroscience : the official journal of the Society for Neuroscience*. J Neurosci, 29(31), pp. 9740–7. doi: 10.1523/JNEUROSCI.2300-09.2009.

Arikkath, J. (2012) 'Molecular mechanisms of dendrite morphogenesis', *Frontiers in Cellular Neuroscience*. Frontiers Media SA. doi: 10.3389/fncel.2012.00061.

Armstrong, D. *et al.* (1995) 'Selective dendritic alterations in the cortex of Rett syndrome.', *Journal of neuropathology and experimental neurology*. J Neuropathol Exp Neurol, 54(2), pp. 195–201. doi: 10.1097/00005072-199503000-00006.

Asanuma, K. *et al.* (2005) 'Decreased striatal D2 receptor binding in non-manifesting carriers of the DYT1 dystonia mutation', *Neurology*, 64(2), pp. 347–349. doi: 10.1212/01.WNL.0000149764.34953.BF.

Asmus, F. *et al.* (2001) 'Inherited myoclonus-dystonia syndrome: Narrowing the 7q21-q31 locus in German families', *Annals of Neurology*, 49(1), pp. 121–124. doi: 10.1002/1531-8249(200101)49:1<121::AID-ANA20>3.0.CO;2-8.

Asmus, F. *et al.* (2009) '"Jerky" dystonia in children: Spectrum of phenotypes and genetic testing', *Movement Disorders*, 24(5), pp. 702–709. doi: 10.1002/mds.22426.

Asmus, F. and Gasser, T. (2010) 'Dystonia-plus syndromes', *European Journal of Neurology*. John Wiley & Sons, Ltd (10.1111), 17, pp. 37–45. doi: 10.1111/j.1468-1331.2010.03049.x.

Bachiller, S. *et al.* (2018) 'Microglia in Neurological Diseases: A Road Map to Brain-Disease Dependent-Inflammatory Response', *Frontiers in Cellular Neuroscience*. Frontiers, 12, p. 488. doi: 10.3389/fncel.2018.00488.

Bagur, R. and Hajnóczky, G. (2017) 'Intracellular Ca2+ Sensing: Its Role in Calcium Homeostasis and Signaling.', *Molecular cell*. Mol Cell, 66(6), pp. 780–788. doi: 10.1016/j.molcel.2017.05.028.

Balint, B. and Bhatia, K. P. (2014) 'Dystonia', *Current Opinion in Neurology*, 27(4), pp. 468–476. doi: 10.1097/WCO.0000000000000114.

Bardy, C. *et al.* (2015) 'Neuronal medium that supports basic synaptic functions and activity of human neurons in vitro.', *Proceedings of the National Academy of Sciences of the United States of America*. National Academy of Sciences, 112(20), pp. E2725-34. doi: 10.1073/pnas.1504393112.

Bardy, C. *et al.* (2016) 'Predicting the functional states of human iPSC-derived neurons with single-cell RNA-seq and electrophysiology.', *Molecular psychiatry*. Mol Psychiatry, 21(11), pp. 1573–1588. doi: 10.1038/mp.2016.158.

Berardelli, A. *et al.* (1998) 'The pathophysiology of primary dystonia', *Brain*. Brain, pp. 1195–1212. doi: 10.1093/brain/121.7.1195.

Bergenheim, A. T. *et al.* (2015) 'Selective peripheral denervation for cervical dystonia: long-term follow-up', *Journal of Neurology, Neurosurgery & Psychiatry*. BMJ Publishing Group Ltd, 86(12), pp. 1307–1313. doi: 10.1136/JNNP-2014-307959.

Berger, H. J. *et al.* (2007) 'Writer's cramp: restoration of striatal D2-binding after successful biofeedback-based sensorimotor training.', *Parkinsonism & related disorders*. Elsevier, 13(3), pp. 170–3. doi: 10.1016/j.parkreldis.2006.09.003.

Berman, B., Seeberger, L. and Kumar, R. (2005) 'Long-term safety, efficacy, dosing, and development of resistance with botulinum toxin type B in cervical dystonia', *Movement Disorders*, 20(2), pp. 233–237. doi: 10.1002/mds.20290.

Berridge, M. *et al.* (2000) 'The versatility and universality of calcium signalling', *nature.com*. Available at: https://www.nature.com/articles/35036035 (Accessed: 12 November 2019).

Berridge, M. J. (1998) 'Neuronal calcium signaling', *Neuron*, pp. 13–26. doi: 10.1016/S0896-6273(00)80510-3.

Berry, K. P. and Nedivi, E. (2017) 'Spine Dynamics: Are They All the Same?', *Neuron*. Neuron, pp. 43–55. doi: 10.1016/j.neuron.2017.08.008.

Betizeau, M. *et al.* (2013) 'Precursor Diversity and Complexity of Lineage Relationships in the Outer Subventricular Zone of the Primate', *Neuron*, 80(2), pp. 442–457. doi: 10.1016/j.neuron.2013.09.032.

Beukers, R. J. *et al.* (2009) 'Reduced striatal D2 receptor binding in myoclonus–dystonia', *European Journal of Nuclear Medicine and Molecular Imaging*. Springer-Verlag, 36(2), pp. 269–274. doi: 10.1007/s00259-008-0924-9.

Bharath, R. D. *et al.* (2015) 'Repetitive transcranial magnetic stimulation induced modulations of resting state motor connectivity in writer's cramp', *European Journal of Neurology*, 22(5), pp. 796-e54. doi: 10.1111/ene.12653.

Bilican, B. *et al.* (2014) 'Physiological Normoxia and Absence of EGF Is Required for the Long-Term Propagation of Anterior Neural Precursors from Human Pluripotent Cells', *PLoS ONE*. Edited by J. Pruszak. Public Library of Science, 9(1), p. e85932. doi: 10.1371/journal.pone.0085932.

Black, K. J. *et al.* (2014) 'Spatial Reorganization of Putaminal Dopamine D2-Like Receptors in Cranial and Hand Dystonia', *PLoS ONE*. Edited by K. Herholz. Public Library of Science, 9(2), p. e88121. doi: 10.1371/journal.pone.0088121.

Blanco-Arias, P. *et al.* (2009) 'A C-terminal mutation of ATP1A3 underscores the crucial role of sodium

affinity in the pathophysiology of rapid-onset dystonia-parkinsonism', *Human Molecular Genetics*, 18(13), pp. 2370–2377. doi: 10.1093/hmg/ddp170.

Blood, A. J. *et al.* (2012) 'Evidence for Altered Basal Ganglia-Brainstem Connections in Cervical Dystonia', *PLoS ONE*. Edited by P. L. Gribble. Public Library of Science, 7(2), p. e31654. doi: 10.1371/journal.pone.0031654.

Boddum, K. *et al.* (2017) 'Kv3.1/Kv3.2 channel positive modulators enable faster activating kinetics and increase firing frequency in fast-spiking GABAergic interneurons.', *Neuropharmacology*. Neuropharmacology, 118, pp. 102–112. doi: 10.1016/j.neuropharm.2017.02.024.

Bode, C. *et al.* (2017) 'Altered postnatal maturation of striatal GABAergic interneurons in a phenotypic animal model of dystonia', *Experimental Neurology*, 287(Pt 1), pp. 44–53. doi: 10.1016/j.expneurol.2016.10.013.

Boergermann, J. H. *et al.* (2010) 'Dorsomorphin and LDN-193189 inhibit BMP-mediated Smad, p38 and Akt signalling in C2C12 cells', *The International Journal of Biochemistry & Cell Biology*, 42(11), pp. 1802–1807. doi: 10.1016/j.biocel.2010.07.018.

Bologna, M. and Berardelli, A. (2017) 'Cerebellum: An explanation for dystonia?', *Cerebellum & ataxias*. BioMed Central, 4, p. 6. doi: 10.1186/s40673-017-0064-8.

Bönnemann, C. G. *et al.* (1995) 'Beta-sarcoglycan (A3b) mutations cause autosomal recessive muscular dystrophy with loss of the sarcoglycan complex.', *Nature genetics*. Nat Genet, 11(3), pp. 266–73. doi: 10.1038/ng1195-266.

Brashear, A. *et al.* (2007) 'The phenotypic spectrum of rapid-onset dystonia-parkinsonism (RDP) and mutations in the ATP1A3 gene', *Brain*, 130(3), pp. 828–835. doi: 10.1093/brain/awl340.

Braun, V. and Richter, H.-P. (2002) 'Selective peripheral denervation for spasmodic torticollis: 13-year experience with 155 patients.', *Journal of neurosurgery*, 97(2 Suppl), pp. 207–12. Available at: http://www.ncbi.nlm.nih.gov/pubmed/12296680 (Accessed: 10 September 2019).

Breakefield, X. O. *et al.* (2008) 'The pathophysiological basis of dystonias', *Nature Reviews Neuroscience*, 9(3), pp. 222–234. doi: 10.1038/nrn2337.

Brennand, K. *et al.* (2015) 'Phenotypic differences in hiPSC NPCs derived from patients with schizophrenia', *Molecular Psychiatry*. Nature Publishing Group, 20(3), pp. 361–368. doi: 10.1038/mp.2014.22.

Bressman, S. B. *et al.* (2000) 'The DYT1 phenotype and guidelines for diagnostic testing.', *Neurology*, 54(9), pp. 1746–52. doi: 10.1212/wnl.54.9.1746.

Bressman, S. B. *et al.* (2009) 'Mutations in THAP1 (DYT6) in early-onset dystonia: a genetic screening study.', *The Lancet. Neurology*. NIH Public Access, 8(5), pp. 441–6. doi: 10.1016/S1474-4422(09)70081-X.

Brewer, G. J. and Cotman, C. W. (1989) 'Survival and growth of hippocampal neurons in defined medium at low density: advantages of a sandwich culture technique or low oxygen', *Brain Research*. Elsevier, 494(1), pp. 65–74. doi: 10.1016/0006-8993(89)90144-3.

Brini, M. *et al.* (2014) 'Neuronal calcium signaling: function and dysfunction.', *Cellular and molecular life sciences : CMLS*. Cell Mol Life Sci, 71(15), pp. 2787–814. doi: 10.1007/s00018-013-1550-7.

Britanova, O. *et al.* (2008) 'Satb2 Is a Postmitotic Determinant for Upper-Layer Neuron Specification in the Neocortex', *Neuron*. Cell Press, 57(3), pp. 378–392. doi: 10.1016/J.NEURON.2007.12.028.

Broadbelt, K., Byne, W. and Jones, L. B. (2002) 'Evidence for a decrease in basilar dendrites of pyramidal cells in schizophrenic medial prefrontal cortex.', *Schizophrenia research*. Schizophr Res, 58(1), pp. 75–81. doi: 10.1016/s0920-9964(02)00201-3.

Brookes, P. S. *et al.* (2004) 'Calcium, ATP, and ROS: a mitochondrial love-hate triangle', *American*

Journal of Physiology-Cell Physiology. American Physiological Society, 287(4), pp. C817–C833. doi: 10.1152/ajpcell.00139.2004.

Burciu, R. G. *et al.* (2017) 'Functional activity of the sensorimotor cortex and cerebellum relates to cervical dystonia symptoms', *Human Brain Mapping*, 38(9), pp. 4563–4573. doi: 10.1002/hbm.23684.

Burke, R. E., Fahn, S. and Marsden, C. D. (1986) 'Torsion dystonia: a double-blind, prospective trial of high-dosage trihexyphenidyl.', *Neurology*, 36(2), pp. 160–4. doi: 10.1212/wnl.36.2.160.

Burr, A. R. and Molkentin, J. D. (2015) 'Genetic evidence in the mouse solidifies the calcium hypothesis of myofiber death in muscular dystrophy', *Cell Death & Differentiation*. Nature Publishing Group, 22(9), pp. 1402–1412. doi: 10.1038/cdd.2015.65.

Bystron, I., Blakemore, C. and Rakic, P. (2008) 'Development of the human cerebral cortex: Boulder Committee revisited', *Nature Reviews Neuroscience*. Nature Publishing Group, 9(2), pp. 110–122. doi: 10.1038/nrn2252.

Cadwell, C. R. *et al.* (2016) 'Electrophysiological, transcriptomic and morphologic profiling of single neurons using Patch-seq', *Nature Biotechnology*. Nature Publishing Group, 34(2), pp. 199–203. doi: 10.1038/nbt.3445.

Calabresi, P. *et al.* (2016) 'Hyperkinetic disorders and loss of synaptic downscaling', *Nature Neuroscience*. Nature Publishing Group, 19(7), pp. 868–875. doi: 10.1038/nn.4306.

Calderon, D. P. *et al.* (2011) 'The neural substrates of rapid-onset Dystonia-Parkinsonism', *Nature Neuroscience*, 14(3), pp. 357–365. doi: 10.1038/nn.2753.

Cambray, S. *et al.* (2012) 'Activin induces cortical interneuron identity and differentiation in embryonic stem cell-derived telencephalic neural precursors', *Nature Communications*, 3(1), p. 841. doi: 10.1038/ncomms1817.

Camp, J. G. *et al.* (2015) 'Human cerebral organoids recapitulate gene expression programs of fetal neocortex development.', *Proceedings of the National Academy of Sciences of the United States of America*. National Academy of Sciences, 112(51), pp. 15672–7. doi: 10.1073/pnas.1520760112.

Campbell, D. B. and Hess, E. J. (1999) 'L-type calcium channels contribute to the tottering mouse dystonic episodes.', *Molecular pharmacology*. Mol Pharmacol, 55(1), pp. 23–31. doi: 10.1124/mol.55.1.23.

Carbon, M. *et al.* (2004) 'Microstructural white matter changes in carriers of the DYT1 gene mutation.', *Annals of neurology*. Ann Neurol, 56(2), pp. 283–6. doi: 10.1002/ana.20177.

Carbon, M. *et al.* (2008) 'Microstructural white matter changes in primary torsion dystonia.', *Movement disorders : official journal of the Movement Disorder Society*. NIH Public Access, 23(2), pp. 234–9. doi: 10.1002/mds.21806.

Carbon, M. *et al.* (2009) 'Abnormal striatal and thalamic dopamine neurotransmission: Genotype-related features of dystonia', *Neurology*, 72(24), pp. 2097–2103. doi: 10.1212/WNL.0b013e3181aa538f.

Carbon, M. *et al.* (2010) 'Increased sensorimotor network activity in DYT1 dystonia: a functional imaging study.', *Brain : a journal of neurology*. Brain, 133(Pt 3), pp. 690–700. doi: 10.1093/brain/awq017.

de Carvalho Aguiar, P. *et al.* (2004) 'Mutations in the Na+/K+-ATPase α3 Gene ATP1A3 Are Associated with Rapid-Onset Dystonia Parkinsonism', *Neuron*, 43(2), pp. 169–175. doi: 10.1016/j.neuron.2004.06.028.

Caverzasi, E. *et al.* (2018) 'Abnormal age-related cortical folding and neurite morphology in children with developmental dyslexia', *NeuroImage: Clinical*. Neuroimage Clin, 18, pp. 814–821. doi: 10.1016/j.nicl.2018.03.012.

Cayrol, C. *et al.* (2007) 'The THAP-zinc finger protein THAP1 regulates endothelial cell proliferation through modulation of pRB/E2F cell-cycle target genes', *Blood*, 109(2), pp. 584–594. doi: 10.1182/blood-2006-03-012013.

Chambers, S. M. *et al.* (2009) 'Highly efficient neural conversion of human ES and iPS cells by dual inhibition of SMAD signaling.', *Nature biotechnology*. NIH Public Access, 27(3), pp. 275–80. doi: 10.1038/nbt.1529.

Chan, P. *et al.* (2005) ?'-Sarcoglycan immunoreactivity and mRNA expression in mouse brain', *The Journal of Comparative Neurology*. Wiley-Blackwell, 482(1), pp. 50–73. doi: 10.1002/cne.20377.

Chang, J. W. *et al.* (2002) 'Unilateral globus pallidus internus stimulation improves delayed onset post-traumatic cervical dystonia with an ipsilateral focal basal ganglia lesion', *J Neurol Neurosurg Psychiatry*, 73, pp. 588–590. doi: 10.1136/jnnp.73.5.588.

Charles, P. D. *et al.* (2014) 'Cervical dystonia and pain: characteristics and treatment patterns from CD PROBE (Cervical Dystonia Patient Registry for Observation of OnabotulinumtoxinA Efficacy).', *Journal of neurology*. J Neurol, 261(7), pp. 1309–19. doi: 10.1007/s00415-014-7343-6.

Charlesworth, G. *et al.* (2012) 'Mutations in ANO3 Cause Dominant Craniocervical Dystonia: Ion Channel Implicated in Pathogenesis', *The American Journal of Human Genetics*. Cell Press, 91(6), pp. 1041–1050. doi: 10.1016/J.AJHG.2012.10.024.

Charlesworth, G. *et al.* (2015) 'Mutations in HPCA cause autosomal-recessive primary isolated dystonia.', *American journal of human genetics*. Am J Hum Genet, 96(4), pp. 657–65. doi: 10.1016/j.ajhg.2015.02.007.

Chen, B. *et al.* (2008) 'The Fezf2-Ctip2 genetic pathway regulates the fate choice of subcortical projection neurons in the developing cerebral cortex.', *Proceedings of the National Academy of Sciences of the United States of America*. National Academy of Sciences, 105(32), pp. 11382–7. doi: 10.1073/pnas.0804918105.

Chen, B., Schaevitz, L. R. and McConnell, S. K. (2005) 'Fezl regulates the differentiation and axon targeting of layer 5 subcortical projection neurons in cerebral cortex.', *Proceedings of the National Academy of Sciences of the United States of America*. National Academy of Sciences, 102(47), pp. 17184–9. doi: 10.1073/pnas.0508732102.

Chen, C. H. *et al.* (2014) 'Short latency cerebellar modulation of the basal ganglia.', *Nature neuroscience*. NIH Public Access, 17(12), pp. 1767–75. doi: 10.1038/nn.3868.

Chen, R. *et al.* (1997) 'Impaired inhibition in writer's cramp during voluntary muscle activation.', *Neurology*, 49(4), pp. 1054–9. Available at: http://www.ncbi.nlm.nih.gov/pubmed/9339689 (Accessed: 22 March 2019).

Chen, T.-W. *et al.* (2013) 'Ultrasensitive fluorescent proteins for imaging neuronal activity.', *Nature*. Howard Hughes Medical Institute, 499(7458), pp. 295–300. doi: 10.1038/nature12354.

Chen, X. *et al.* (2000) 'Selective Denervation and Resection of Cervical Muscles in the Treatment of Spasmodic Torticollis: Long-Term Follow-Up Results in 207 Cases', *Stereotactic and Functional Neurosurgery*, 75(2–3), pp. 96–102. doi: 10.1159/000048389.

Cho, S. W. *et al.* (2013) 'Targeted genome engineering in human cells with the Cas9 RNA-guided endonuclease', *Nature Biotechnology*, 31(3), pp. 230–232. doi: 10.1038/nbt.2507.

Chockalingam, P. S. *et al.* (2002) 'Dystrophin-glycoprotein complex and Ras and Rho GTPase signaling are altered in muscle atrophy', *American Journal of Physiology - Cell Physiology*. Am J Physiol Cell Physiol, 283(2 52-2). doi: 10.1152/ajpcell.00529.2001.

Chuang, C., Fahn, S. and Frucht, S. J. (2002) 'The natural history and treatment of acquired hemidystonia: report of 33 cases and review of the literature.', *Journal of neurology, neurosurgery, and psychiatry*. J Neurol Neurosurg Psychiatry, 72(1), pp. 59–67. doi: 10.1136/jnnp.72.1.59.

Cif, L. *et al.* (2010) 'Long-term follow-up of DYT1 dystonia patients treated by deep brain stimulation: An open-label study', *Movement Disorders*, 25(3), pp. 289–299. doi: 10.1002/mds.22802.

Cline, H. T. (2001) 'Dendritic arbor development and synaptogenesis', *Current Opinion in Neurobiology*. Curr Opin Neurobiol, pp. 118–126. doi: 10.1016/S0959-4388(00)00182-3.

Clouaire, T. *et al.* (2005) 'The THAP domain of THAP1 is a large C2CH module with zinc-dependent sequence-specific DNA-binding activity', *Proceedings of the National Academy of Sciences*, 102(19), pp. 6907–6912. doi: 10.1073/pnas.0406882102.

Cohen-Gadol, A. A. *et al.* (2003) 'Selective peripheral denervation for the treatment of intractable spasmodic torticollis: experience with 168 patients at the Mayo Clinic', *Journal of Neurosurgery*, 98(6), pp. 1247–1254. doi: 10.3171/jns.2003.98.6.1247.

Colleoni, S. *et al.* (2010) 'Long-term culture and differentiation of CNS precursors derived from anterior human neural rosettes following exposure to ventralizing factors', *Experimental Cell Research*. Academic Press Inc., 316(7), pp. 1148–1158. doi: 10.1016/j.yexcr.2010.02.013.

Cong, L. *et al.* (2013) 'Multiplex Genome Engineering Using CRISPR/Cas Systems', *Science*, 339(6121), pp. 819–823. doi: 10.1126/science.1231143.

Contarino, M. F. *et al.* (2017) 'Clinical Practice: Evidence-Based Recommendations for the Treatment of Cervical Dystonia with Botulinum Toxin', *Frontiers in Neurology*, 8, p. 35. doi: 10.3389/fneur.2017.00035.

Cuenca-León, E. *et al.* (2009) 'Late-onset episodic ataxia type 2 associated with a novel loss-of-function mutation in the CACNA1A gene.', *Journal of the neurological sciences*. J Neurol Sci, 280(1–2), pp. 10–4. doi: 10.1016/j.jns.2009.01.005.

Dahlstrand, J., Lardelli, M. and Lendahl, U. (1995) 'Nestin mRNA expression correlates with the central nervous system progenitor cell state in many, but not all, regions of developing central nervous system.', *Brain research. Developmental brain research*. Brain Res Dev Brain Res, 84(1), pp. 109–29. doi: 10.1016/0165-3806(94)00162-s.

Dang, M. T. *et al.* (2005) 'Generation and characterization of Dyt1 ΔGAG knock-in mouse as a model for early-onset dystonia', *Experimental Neurology*, 196(2), pp. 452–463. doi: 10.1016/j.expneurol.2005.08.025.

Dang, M. T. *et al.* (2012) 'An anticholinergic reverses motor control and corticostriatal LTD deficits in Dyt1 ΔGAG knock-in mice', *Behavioural Brain Research*, 226(2), pp. 465–472. doi: 10.1016/j.bbr.2011.10.002.

DeAndrade, M. P. *et al.* (2011) 'Characterization of Atp1a3 mutant mice as a model of rapid-onset dystonia with parkinsonism.', *Behavioural brain research*. NIH Public Access, 216(2), pp. 659–65. doi: 10.1016/j.bbr.2010.09.009.

DeSimone, J. C. *et al.* (2016) 'In vivo imaging reveals impaired connectivity across cortical and subcortical networks in a mouse model of DYT1 dystonia.', *Neurobiology of disease*, 95, pp. 35–45. doi: 10.1016/j.nbd.2016.07.005.

Deutschländer, A. *et al.* (2005) 'Sporadic rapid-onset dystonia-parkinsonism syndrome: Failure of bilateral pallidal stimulation', *Movement Disorders*, 20(2), pp. 254–257. doi: 10.1002/mds.20296.

van den Dool, J. *et al.* (2019) 'Long-Term Specialized Physical Therapy in Cervical Dystonia: Outcomes of a Randomized Controlled Trial', *Archives of Physical Medicine and Rehabilitation*. W.B. Saunders, 100(8), pp. 1417–1425. doi: 10.1016/J.APMR.2019.01.013.

Dove, L. S. *et al.* (2000) 'Altered calcium homeostasis in cerebellar Purkinje cells of leaner mutant mice.', *Journal of neurophysiology*. J Neurophysiol, 84(1), pp. 513–24. doi: 10.1152/jn.2000.84.1.513.

Dragicevic, E. *et al.* (2014) 'Cav1.3 channels control D2-autoreceptor responses via NCS-1 in substantia nigra dopamine neurons.', *Brain : a journal of neurology*. Brain, 137(Pt 8), pp. 2287–302. doi:

10.1093/brain/awu131.

Du, W. *et al.* (2005) 'Calcium-sensitive potassium channelopathy in human epilepsy and paroxysmal movement disorder.', *Nature genetics*. Nat Genet, 37(7), pp. 733–8. doi: 10.1038/ng1585.

Duchen, M. R. (1999) 'Contributions of mitochondria to animal physiology: from homeostatic sensor to calcium signalling and cell death', *The Journal of Physiology*, 516(1), pp. 1–17. doi: 10.1111/j.1469-7793.1999.001aa.x.

Dulhunty, A. (2006) 'EXCITATION–CONTRACTION COUPLING FROM THE 1950s INTO THE NEW MILLENNIUM', *Clinical and Experimental Pharmacology and Physiology*, 33(9), pp. 763–772. doi: 10.1111/j.1440-1681.2006.04441.x.

van Elburg, R. A. J. and van Ooyen, A. (2010) 'Impact of Dendritic Size and Dendritic Topology on Burst Firing in Pyramidal Cells', *PLoS Computational Biology*. Edited by L. J. Graham. Public Library of Science, 6(5), p. e1000781. doi: 10.1371/journal.pcbi.1000781.

Elkabetz, Y. *et al.* (2008) 'Human ES cell-derived neural rosettes reveal a functionally distinct early neural stem cell stage', *Genes and Development*, 22(2), pp. 152–165. doi: 10.1101/gad.1616208.

Emoto, K. (2012) 'Signaling mechanisms that coordinate the development and maintenance of dendritic fields', *Current Opinion in Neurobiology*. Curr Opin Neurobiol, pp. 805–811. doi: 10.1016/j.conb.2012.04.005.

Englund, C. *et al.* (2005) 'Pax6, Tbr2, and Tbr1 are expressed sequentially by radial glia, intermediate progenitor cells, and postmitotic neurons in developing neocortex.', *The Journal of neuroscience : the official journal of the Society for Neuroscience*. Society for Neuroscience, 25(1), pp. 247–51. doi: 10.1523/JNEUROSCI.2899-04.2005.

Epidemiological Study of Dystonia in Europe (ESDE) Collaborative Group (2000) 'A prevalence study of primary dystonia in eight European countries', *Journal of Neurology*. Available at: https://link.springer.com/article/10.1007/s004150070094 (Accessed: 14 May 2019).

Erecińska, M. and Silver, I. A. (2001) 'Tissue oxygen tension and brain sensitivity to hypoxia.', *Respiration physiology*, 128(3), pp. 263–76. doi: 10.1016/s0034-5687(01)00306-1.

Erogullari, A. *et al.* (2014) 'THAP1, the gene mutated in DYT6 dystonia, autoregulates its own expression', *Biochimica et Biophysica Acta (BBA) - Gene Regulatory Mechanisms*, 1839(11), pp. 1196–1204. doi: 10.1016/j.bbagrm.2014.07.019.

Erro, R. *et al.* (2018) 'High frequency somatosensory stimulation in dystonia: Evidence fordefective inhibitory plasticity', *Movement Disorders*, 33(12), pp. 1902–1909. doi: 10.1002/mds.27470.

Erro, R. and Bhatia, K. P. (2019) 'Unravelling of the paroxysmal dyskinesias.', *Journal of neurology, neurosurgery, and psychiatry*. J Neurol Neurosurg Psychiatry, 90(2), pp. 227–234. doi: 10.1136/jnnp-2018-318932.

Esapa, C. T. *et al.* (2007) 'SGCE missense mutations that cause myoclonus-dystonia syndrome impair ε-sarcoglycan trafficking to the plasma membrane: modulation by ubiquitination and torsinA', *Human Molecular Genetics*, 16(3), pp. 327–342. doi: 10.1093/hmg/ddl472.

Espuny-Camacho, I. *et al.* (2013) 'Pyramidal Neurons Derived from Human Pluripotent Stem Cells Integrate Efficiently into Mouse Brain Circuits In Vivo', *Neuron*, 77(3), pp. 440–456. doi: 10.1016/j.neuron.2012.12.011.

Ettinger, A. J., Feng, G. and Sanes, J. R. (1997) 'ε-Sarcoglycan, a Broadly Expressed Homologue of the Gene Mutated in Limb-Girdle Muscular Dystrophy 2D', *Journal of Biological Chemistry*, 272(51), pp. 32534–32538. doi: 10.1074/jbc.272.51.32534.

Fang, A. *et al.* (2019) 'Effects of astrocyte on neuronal outgrowth in a layered 3D structure', *BioMedical Engineering OnLine*. BioMed Central, 18(1), p. 74. doi: 10.1186/s12938-019-0694-6.

Fantuzzo, J. A. *et al.* (2017) 'µNeurocircuitry: Establishing in vitro models of neurocircuits with human neurons.', *Technology*. NIH Public Access, 5(2), pp. 87–97. doi: 10.1142/S2339547817500054.

Fantuzzo, J. A. *et al.* (2019) 'Compartmentalized Devices as Tools for Investigation of Human Brain Network Dynamics', *Developmental Dynamics*. John Wiley & Sons, Ltd, 248(1), pp. 65–77. doi: 10.1002/dvdy.24665.

Filip, P. *et al.* (2017) 'Disruption in cerebellar and basal ganglia networks during a visuospatial task in cervical dystonia', *Movement Disorders*, 32(5), pp. 757–768. doi: 10.1002/mds.26930.

Filipović, S. R. *et al.* (1997) 'Impairment of cortical inhibition in writer's cramp as revealed by changes in electromyographic silent period after transcranial magnetic stimulation.', *Neuroscience letters*, 222(3), pp. 167–70. Available at: http://www.ncbi.nlm.nih.gov/pubmed/9148241 (Accessed: 22 March 2019).

Fink, C. C. *et al.* (2003) 'Selective Regulation of Neurite Extension and Synapse Formation by the β but not the α Isoform of CaMKII', *Neuron*. Cell Press, 39(2), pp. 283–297. doi: 10.1016/S0896-6273(03)00428-8.

FitzGerald, J. J. *et al.* (2014) 'Long-term outcome of deep brain stimulation in generalised dystonia: a series of 60 cases.', *Journal of neurology, neurosurgery, and psychiatry*. BMJ Publishing Group Ltd, 85(12), pp. 1371–6. doi: 10.1136/jnnp-2013-306833.

Foncke, E. M. J. *et al.* (2009) 'Is Psychopathology Part of the Phenotypic Spectrum of Myoclonus-dystonia?', *Cognitive and Behavioral Neurology*, 22(2), pp. 127–133. doi: 10.1097/WNN.0b013e3181a7228f.

Fremont, R. *et al.* (2014a) 'Abnormal High-Frequency Burst Firing of Cerebellar Neurons in Rapid-Onset Dystonia-Parkinsonism', *Journal of Neuroscience*, 34(35), pp. 11723–11732. doi: 10.1523/JNEUROSCI.1409-14.2014.

Fremont, R. *et al.* (2014b) 'Abnormal High-Frequency Burst Firing of Cerebellar Neurons in Rapid-Onset Dystonia-Parkinsonism', *Journal of Neuroscience*, 34(35), pp. 11723–11732. doi: 10.1523/JNEUROSCI.1409-14.2014.

Fremont, R. *et al.* (2017) 'A role for cerebellum in the hereditary dystonia DYT1', *eLife*, 6. doi: 10.7554/eLife.22775.

Furukawa, Y. (2004) 'Update on dopa-responsive dystonia: locus heterogeneity and biochemical features.', *Advances in neurology*, 94, pp. 127–38. Available at: http://www.ncbi.nlm.nih.gov/pubmed/14509665 (Accessed: 9 September 2019).

Ganos, C. *et al.* (2018) 'Cortical inhibitory function in cervical dystonia', *Clinical Neurophysiology*, 129(2), pp. 466–472. doi: 10.1016/j.clinph.2017.11.020.

Gasiunas, G. *et al.* (2012) 'Cas9-crRNA ribonucleoprotein complex mediates specific DNA cleavage for adaptive immunity in bacteria', *Proceedings of the National Academy of Sciences*, 109(39), pp. E2579–E2586. doi: 10.1073/pnas.1208507109.

Gaspard, N. *et al.* (2008) 'An intrinsic mechanism of corticogenesis from embryonic stem cells', *Nature*, 455(7211), pp. 351–357. doi: 10.1038/nature07287.

Gaspard, N. and Vanderhaeghen, P. (2011) 'Laminar fate specification in the cerebral cortex', *F1000 Biology Reports*. doi: 10.3410/B3-6.

Gavarini, S. *et al.* (2010) 'Direct interaction between causative genes of DYT1 and DYT6 primary dystonia', *Annals of Neurology*, 68(4), pp. 549–553. doi: 10.1002/ana.22138.

Gernert, M. *et al.* (2000) 'Deficit of striatal parvalbumin-reactive GABAergic interneurons and decreased basal ganglia output in a genetic rodent model of idiopathic paroxysmal dystonia.', *The Journal of neuroscience : the official journal of the Society for Neuroscience*. J Neurosci, 20(18), pp. 7052–8. doi: 10.1523/JNEUROSCI.20-18-07052.2000.

Gernert, M. *et al.* (2002) 'Altered discharge pattern of basal ganglia output neurons in an animal model of idiopathic dystonia.', *The Journal of neuroscience : the official journal of the Society for Neuroscience*, 22(16), pp. 7244–53. doi: 20026724.

Gerrits, M. C. F. *et al.* (2006) 'Phenotype-genotype correlation in Dutch patients with myoclonus-dystonia', *Neurology*, 66(5), pp. 759–761. doi: 10.1212/01.wnl.0000201192.66467.a3.

Gerschenfeld, H. M. (1973) 'Chemical transmission in invertebrate central nervous systems and neuromuscular junctions.', *Physiological reviews*. Physiol Rev, 53(1), pp. 1–119. doi: 10.1152/physrev.1973.53.1.1.

Geyer, H. L. and Bressman, S. B. (2006) 'The diagnosis of dystonia.', *The Lancet. Neurology*, 5(9), pp. 780–90. doi: 10.1016/S1474-4422(06)70547-6.

Ghatan, S. *et al.* (2016) 'Intraventricular Baclofen for Treatment of Severe Dystonia Associated with Glutaryl-CoA Dehydrogenase Deficiency (GA1): Report of Two Cases', *Movement Disorders Clinical Practice*. John Wiley & Sons, Ltd, 3(3), pp. 296–299. doi: 10.1002/mdc3.12278.

Giffin, N. J., Benton, S. and Goadsby, P. J. (2002) 'Benign paroxysmal torticollis of infancy: four new cases and linkage to CACNA1A mutation.', *Developmental medicine and child neurology*. Dev Med Child Neurol, 44(7), pp. 490–3. doi: 10.1017/s0012162201002407.

Gimeno, H. *et al.* (2019) 'Cognitive approach to rehabilitation in children with hyperkinetic movement disorders post-DBS', *Neurology*, 92(11), p. 10.1212/WNL.0000000000007092. doi: 10.1212/WNL.0000000000007092.

Glantz, L. A. and Lewis, D. A. (2000) 'Decreased dendritic spine density on prefrontal cortical pyramidal neurons in schizophrenia.', *Archives of general psychiatry*. Arch Gen Psychiatry, 57(1), pp. 65–73. doi: 10.1001/archpsyc.57.1.65.

Glasgow, S. D. *et al.* (2019) 'Approaches and Limitations in the Investigation of Synaptic Transmission and Plasticity.', *Frontiers in synaptic neuroscience*. Frontiers Media SA, 11, p. 20. doi: 10.3389/fnsyn.2019.00020.

Glaze, D. G. *et al.* (2017) 'A Double-Blind, Randomized, Placebo-Controlled Clinical Study of Trofinetide in the Treatment of Rett Syndrome.', *Pediatric neurology*. Pediatr Neurol, 76, pp. 37–46. doi: 10.1016/j.pediatrneurol.2017.07.002.

González, F. *et al.* (2014) 'An iCRISPR platform for rapid, multiplexable, and inducible genome editing in human pluripotent stem cells.', *Cell stem cell*. NIH Public Access, 15(2), pp. 215–226. doi: 10.1016/j.stem.2014.05.018.

Goodchild, R. E. and Dauer, W. T. (2004) 'Mislocalization to the nuclear envelope: An effect of the dystonia-causing torsinA mutation', *Proceedings of the National Academy of Sciences*, 101(3), pp. 847–852. doi: 10.1073/pnas.0304375101.

Goodchild, R. E., Kim, C. E. and Dauer, W. T. (2005) 'Loss of the dystonia-associated protein torsinA selectively disrupts the neuronal nuclear envelope', *Neuron*. Neuron, 48(6), pp. 923–932. doi: 10.1016/j.neuron.2005.11.010.

Goriounova, N. A. *et al.* (2018) 'Large and fast human pyramidal neurons associate with intelligence', *eLife*, 7. doi: 10.7554/eLife.41714.

Gorman, K. M. *et al.* (2019) 'Bi-allelic Loss-of-Function CACNA1B Mutations in Progressive Epilepsy-Dyskinesia.', *American journal of human genetics*. Elsevier, 104(5), pp. 948–956. doi: 10.1016/j.ajhg.2019.03.005.

Gorski, J. A. *et al.* (2003) 'Brain-Derived Neurotrophic Factor Is Required for the Maintenance of Cortical Dendrites', *Journal of Neuroscience*. Society for Neuroscience, 23(17), pp. 6856–6865. doi: 10.1523/JNEUROSCI.23-17-06856.2003.

Grabowski, M. *et al.* (2003) 'The epsilon-sarcoglycan gene (SGCE), mutated in myoclonus-dystonia

syndrome, is maternally imprinted', *European Journal of Human Genetics*, 11(2), pp. 138–144. doi: 10.1038/sj.ejhg.5200938.

Granata, A. *et al.* (2008) 'The Dystonia-associated Protein TorsinA Modulates Synaptic Vesicle Recycling', *Journal of Biological Chemistry*, 283(12), pp. 7568–7579. doi: 10.1074/jbc.M704097200.

Greene, D. L. and Hoshi, N. (2017) 'Modulation of Kv7 channels and excitability in the brain.', *Cellular and molecular life sciences : CMLS*. NIH Public Access, 74(3), pp. 495–508. doi: 10.1007/s00018-016-2359-y.

Greig, L. C. *et al.* (2013) 'Molecular logic of neocortical projection neuron specification, development and diversity.', *Nature reviews. Neuroscience*. NIH Public Access, 14(11), pp. 755–69. doi: 10.1038/nrn3586.

Grienberger, C. and Konnerth, A. (2012) 'Imaging Calcium in Neurons', *Neuron*. Cell Press, 73(5), pp. 862–885. doi: 10.1016/J.NEURON.2012.02.011.

Grillet, M. *et al.* (2016) 'Torsins Are Essential Regulators of Cellular Lipid Metabolism', *Developmental Cell*. Cell Press, 38(3), pp. 235–247. doi: 10.1016/J.DEVCEL.2016.06.017.

Grütz, K. *et al.* (2017) 'Faithful SGCE imprinting in iPSC-derived cortical neurons: an endogenous cellular model of myoclonus-dystonia.', *Scientific reports*. Nature Publishing Group, 7, p. 41156. doi: 10.1038/srep41156.

Gunhanlar, N. *et al.* (2018) 'A simplified protocol for differentiation of electrophysiologically mature neuronal networks from human induced pluripotent stem cells.', *Molecular psychiatry*. Nature Publishing Group, 23(5), pp. 1336–1344. doi: 10.1038/mp.2017.56.

Hales, C. M., Rolston, J. D. and Potter, S. M. (2010) 'How to culture, record and stimulate neuronal networks on micro-electrode arrays (MEAs).', *Journal of visualized experiments : JoVE*. MyJoVE Corporation, (39). doi: 10.3791/2056.

Hall, A. and Lalli, G. (2010) 'Rho and Ras GTPases in axon growth, guidance, and branching.', *Cold Spring Harbor perspectives in biology*. Cold Spring Harb Perspect Biol. doi: 10.1101/cshperspect.a001818.

Hallett, M. (2006) *Pathophysiology of dystonia*, *J Neural Transm*. Springer-Verlag. Available at: http://eknygos.lsmuni.lt/springer/340/12.Dystonia/2 Item.pdf (Accessed: 25 August 2020).

Hallett, M. (2011) 'Neurophysiology of dystonia: The role of inhibition', *Neurobiology of Disease*. NIH Public Access, pp. 177–184. doi: 10.1016/j.nbd.2010.08.025.

Hamann, M. *et al.* (2017) 'Alterations of M1 and M4 acetylcholine receptors in the genetically dystonic (dt) hamster and moderate antidystonic efficacy of M1 and M4 anticholinergics', *Neuroscience*, 357, pp. 84–98. doi: 10.1016/j.neuroscience.2017.05.051.

Hamann, M. and Richter, A. (2002) 'Effects of striatal injections of GABA(A) receptor agonists and antagonists in a genetic animal model of paroxysmal dystonia.', *European journal of pharmacology*, 443(1–3), pp. 59–70. doi: 10.1016/s0014-2999(02)01546-7.

Haws, C. M. and Lansman, J. B. (1991) 'Calcium-permeable ion channels in cerebellar neurons from mdx mice.', *Proceedings. Biological sciences*. Proc Biol Sci, 244(1311), pp. 185–9. doi: 10.1098/rspb.1991.0068.

Hedegaard, A., Monzón-Sandoval, J., *et al.* (2020) 'Pro-maturational Effects of Human iPSC-Derived Cortical Astrocytes upon iPSC-Derived Cortical Neurons', *Stem Cell Reports*. Cell Press, 15(1), pp. 38–51. doi: 10.1016/J.STEMCR.2020.05.003.

Hedegaard, A., Monzó N-Sandoval, J., *et al.* (2020) 'Stem Cell Reports Article Pro-maturational Effects of Human iPSC-Derived Cortical Astrocytes upon iPSC-Derived Cortical Neurons', *Stem Cell Reports*, 15, pp. 38–51. doi: 10.1016/j.stemcr.2020.05.003.

Helassa, N. *et al.* (2017) 'Biophysical and functional characterization of hippocalcin mutants responsible for human dystonia.', *Human molecular genetics*. Oxford University Press, 26(13), pp. 2426–2435. doi: 10.1093/hmg/ddx133.

Hess, C. W. and Saunders-Pullman, R. (2006) 'Movement disorders and alcohol misuse', *Addiction Biology*. John Wiley & Sons, Ltd (10.1111), 11(2), pp. 117–125. doi: 10.1111/j.1369-1600.2006.00017.x.

Hewett, J. W. *et al.* (2006) 'Dystonia-causing mutant torsinA inhibits cell adhesion and neurite extension through interference with cytoskeletal dynamics', *Neurobiology of Disease*, 22(1), pp. 98–111. doi: 10.1016/j.nbd.2005.10.012.

Hierholzer, J. *et al.* (1994) 'Dopamine D2 receptor imaging with iodine-123-iodobenzamide SPECT in idiopathic rotational torticollis.', *Journal of nuclear medicine : official publication, Society of Nuclear Medicine*, 35(12), pp. 1921–7. Available at: http://www.ncbi.nlm.nih.gov/pubmed/7989970 (Accessed: 30 October 2017).

Hisatsune, C. *et al.* (2013) 'IP3R1 deficiency in the cerebellum/brainstem causes basal ganglia-independent dystonia by triggering tonic Purkinje cell firings in mice', *Frontiers in Neural Circuits*, 7, p. 156. doi: 10.3389/fncir.2013.00156.

Horisawa, S. *et al.* (2019) 'A single case of MRI-guided focused ultrasound ventro-oral thalamotomy for musician's dystonia', *Journal of Neurosurgery*, 131(2), pp. 384–386. doi: 10.3171/2018.5.JNS173125.

Houeto, J.-L. *et al.* (2007) 'Acute Deep-Brain Stimulation of the Internal and External Globus Pallidus in Primary Dystonia', *Archives of Neurology*. American Medical Association, 64(9), p. 1281. doi: 10.1001/archneur.64.9.1281.

Hrvoj-Mihic, B. *et al.* (2017) 'Basal Dendritic Morphology of Cortical Pyramidal Neurons in Williams Syndrome: Prefrontal Cortex and Beyond', *Frontiers in Neuroscience*. Frontiers, 11, p. 419. doi: 10.3389/fnins.2017.00419.

Huang, Y. and Putney, J. W. (1998) 'Relationship between intracellular calcium store depletion and calcium release-activated calcium current in a mast cell line (RBL-1).', *The Journal of biological chemistry*. American Society for Biochemistry and Molecular Biology, 273(31), pp. 19554–9. doi: 10.1074/jbc.273.31.19554.

Huang, Z., Bassil, C. F. and Murphy, S. K. (2013) 'Methylation-Specific PCR', in *Methods in molecular biology (Clifton, N.J.)*, pp. 75–82. doi: 10.1007/978-1-62703-547-7_7.

Hughes, A. J., Lees, A. J. and Marsden, C. D. (1991) 'Paroxysmal dystonic head tremor', *Movement Disorders*. John Wiley & Sons, Ltd, 6(1), pp. 85–86. doi: 10.1002/mds.870060118.

van den Hurk, M. *et al.* (2018) 'Patch-Seq Protocol to Analyze the Electrophysiology, Morphology and Transcriptome of Whole Single Neurons Derived From Human Pluripotent Stem Cells', *Frontiers in Molecular Neuroscience*. Frontiers, 11, p. 261. doi: 10.3389/fnmol.2018.00261.

Huttenlocher, P. R. and Dabholkar, A. S. (1997) 'Regional differences in synaptogenesis in human cerebral cortex', *The Journal of Comparative Neurology*, 387(2), pp. 167–178. doi: 10.1002/(SICI)1096-9861(19971020)387:2<167::AID-CNE1>3.0.CO;2-Z.

Hwu, W. L. *et al.* (2000) 'Dopa-responsive dystonia is induced by a dominant-negative mechanism.', *Annals of neurology*, 48(4), pp. 609–13. Available at: http://www.ncbi.nlm.nih.gov/pubmed/11026444 (Accessed: 9 September 2019).

Ichinose, H. and Nagatsu, T. (1997) 'Molecular genetics of hereditary dystonia--mutations in the GTP cyclohydrolase I gene.', *Brain research bulletin*, 43(1), pp. 35–8. doi: 10.1016/s0361-9230(96)00353-x.

Ikeda, K. *et al.* (2013) 'Enhanced inhibitory neurotransmission in the cerebellar cortex of *Atp1a3* -

deficient heterozygous mice', *The Journal of Physiology*, 591(13), pp. 3433–3449. doi: 10.1113/jphysiol.2012.247817.

Ito, N. *et al.* (2016) 'Decreased N-TAF1 expression in X-linked dystonia-parkinsonism patient-specific neural stem cells.', *Disease models & mechanisms*. Company of Biologists, 9(4), pp. 451–62. doi: 10.1242/dmm.022590.

Iwabuchi, S. *et al.* (2013) 'Minimal Change in the cytoplasmic calcium dynamics in striatal GABAergic neurons of a DYT1 dystonia knock-in mouse model.', *PloS one*. PLoS One, 8(11), p. e80793. doi: 10.1371/journal.pone.0080793.

Izsak, J. *et al.* (2020) 'Human Cerebrospinal Fluid Promotes Neuronal Circuit Maturation of Human Induced Pluripotent Stem Cell-Derived 3D Neural Aggregates', *Stem Cell Reports*, 14(6), pp. 1044–1059. doi: 10.1016/j.stemcr.2020.05.006.

Jaeger, I. *et al.* (2011) 'Temporally controlled modulation of FGF/ERK signaling directs midbrain dopaminergic neural progenitor fate in mouse and human pluripotent stem cells', *Development*, 138(20), pp. 4363–4374. doi: 10.1242/dev.066746.

Jan, L. Y. and Jan, Y. N. (2012) 'Voltage-gated potassium channels and the diversity of electrical signalling', *Journal of Physiology*. J Physiol, pp. 2591–2599. doi: 10.1113/jphysiol.2011.224212.

Jan, Y. N. and Jan, L. Y. (2010) 'Branching out: Mechanisms of dendritic arborization', *Nature Reviews Neuroscience*. Nat Rev Neurosci, pp. 316–328. doi: 10.1038/nrn2836.

Jang, M. J. and Nam, Y. (2015) 'NeuroCa: integrated framework for systematic analysis of spatiotemporal neuronal activity patterns from large-scale optical recording data', *Neurophotonics*, 2(3), p. 035003. doi: 10.1117/1.NPh.2.3.035003.

Jinek, M. *et al.* (2012) 'A Programmable Dual-RNA-Guided DNA Endonuclease in Adaptive Bacterial Immunity', *Science*, 337(6096), pp. 816–821. doi: 10.1126/science.1225829.

Jinek, M. *et al.* (2013) 'RNA-programmed genome editing in human cells', *eLife*, 2. doi: 10.7554/eLife.00471.

Jinnah, H. A. *et al.* (2000) 'Calcium channel agonists and dystonia in the mouse', *Movement Disorders*. John Wiley & Sons, Ltd, 15(3), pp. 542–551. doi: 10.1002/1531-8257(200005)15:3<542::AID-MDS1019>3.0.CO;2-2.

Jinnah, H. A. and Hess, E. J. (2018) 'Evolving concepts in the pathogenesis of dystonia', *Parkinsonism & Related Disorders*, 46, pp. S62–S65. doi: 10.1016/j.parkreldis.2017.08.001.

Jo, J. *et al.* (2016) 'Midbrain-like Organoids from Human Pluripotent Stem Cells Contain Functional Dopaminergic and Neuromelanin-Producing Neurons.', *Cell stem cell*. Cell Stem Cell, 19(2), pp. 248–257. doi: 10.1016/j.stem.2016.07.005.

Jochim, A. *et al.* (2017) 'Microstructural white matter abnormalities in patients with COL6A3 mutations (DYT27 dystonia)', *Parkinsonism & Related Disorders*. doi: 10.1016/j.parkreldis.2017.10.008.

Jog, M. *et al.* (2011) 'Causes for treatment delays in dystonia and hemifacial spasm: a Canadian survey.', *The Canadian journal of neurological sciences. Le journal canadien des sciences neurologiques*. Can J Neurol Sci, 38(5), pp. 704–11. doi: 10.1017/s0317167100012270.

Johnson, M. A. *et al.* (2007) 'Functional neural development from human embryonic stem cells: Accelerated synaptic activity via astrocyte coculture', *Journal of Neuroscience*. J Neurosci, 27(12), pp. 3069–3077. doi: 10.1523/JNEUROSCI.4562-06.2007.

Jones, E. V, Cook, D. and Murai, K. K. (2012) 'A neuron-astrocyte co-culture system to investigate astrocyte-secreted factors in mouse neuronal development.', *Methods in molecular biology (Clifton, N.J.)*. Methods Mol Biol, 814, pp. 341–52. doi: 10.1007/978-1-61779-452-0_22.

Kaiser, F. J. *et al.* (2010) 'The dystonia gene DYT1 is repressed by the transcription factor THAP1 (DYT6)', *Annals of Neurology*, 68(4), pp. 554–559. doi: 10.1002/ana.22157.

Kaji, R., Bhatia, K. and Graybiel, A. M. (2018) 'Pathogenesis of dystonia: is it of cerebellar or basal ganglia origin?', *Journal of Neurology, Neurosurgery & Psychiatry*, 89(5), pp. 488–492. doi: 10.1136/jnnp-2017-316250.

Kalus, P. *et al.* (2000) 'The dendritic architecture of prefrontal pyramidal neurons in schizophrenic patients.', *Neuroreport*. Neuroreport, 11(16), pp. 3621–5. doi: 10.1097/00001756-200011090-00044.

Kamm, C. *et al.* (2008) 'NOVEL ATP1A3 MUTATION IN A SPORADIC RDP PATIENT WITH MINIMAL BENEFIT FROM DEEP BRAIN STIMULATION', *Neurology*, 70(Issue 16, Part 2), pp. 1501–1503. doi: 10.1212/01.wnl.0000310431.41036.e0.

Kaplan, F. S. *et al.* (1986) 'Enhanced survival of rat neonatal cerebral cortical neurons at subatmospheric oxygen tensions in vitro', *Brain Research*, 384(1), pp. 199–203. doi: 10.1016/0006-8993(86)91240-0.

Karimi, M. *et al.* (2011) 'Decreased striatal dopamine receptor binding in primary focal dystonia: A D2 or D3 defect?', *Movement Disorders*, 26(1), pp. 100–106. doi: 10.1002/mds.23401.

Kasugai, Y. *et al.* (2010) 'Quantitative localisation of synaptic and extrasynaptic GABAA receptor subunits on hippocampal pyramidal cells by freeze-fracture replica immunolabelling', *European Journal of Neuroscience*. Eur J Neurosci, 32(11), pp. 1868–1888. doi: 10.1111/j.1460-9568.2010.07473.x.

Kemp, P. J. *et al.* (2016) 'Improving and accelerating the differentiation and functional maturation of human stem cell-derived neurons: role of extracellular calcium and GABA.', *The Journal of physiology*. Wiley-Blackwell, 594(22), pp. 6583–6594. doi: 10.1113/JP270655.

Khorkova, O. and Golowasch, J. (2007) 'Neuromodulators, not activity, control coordinated expression of ionic currents', *Journal of Neuroscience*. J Neurosci, 27(32), pp. 8709–8718. doi: 10.1523/JNEUROSCI.1274-07.2007.

Kilpinen, H. *et al.* (2017) 'Common genetic variation drives molecular heterogeneity in human iPSCs', *Nature*, 546(7658), pp. 370–375. doi: 10.1038/nature22403.

Kim, H. *et al.* (2019) 'Modeling G2019S-LRRK2 Sporadic Parkinson's Disease in 3D Midbrain Organoids.', *Stem cell reports*. Elsevier, 12(3), pp. 518–531. doi: 10.1016/j.stemcr.2019.01.020.

Kim, H. J. *et al.* (2017) 'Deficient autophagy in microglia impairs synaptic pruning and causes social behavioral defects', *Molecular Psychiatry*. Nature Publishing Group, 22(11), pp. 1576–1584. doi: 10.1038/mp.2016.103.

Kim, J.-E. *et al.* (2011) 'Investigating synapse formation and function using human pluripotent stem cell-derived neurons.', *Proceedings of the National Academy of Sciences of the United States of America*. National Academy of Sciences, 108(7), pp. 3005–10. doi: 10.1073/pnas.1007753108.

Kirkeby, A. *et al.* (2012) 'Generation of Regionally Specified Neural Progenitors and Functional Neurons from Human Embryonic Stem Cells under Defined Conditions', *Cell Reports*, 1(6), pp. 703–714. doi: 10.1016/j.celrep.2012.04.009.

Kiskinis, E. *et al.* (2014) 'Pathways disrupted in human ALS motor neurons identified through genetic correction of mutant SOD1.', *Cell stem cell*. Cell Stem Cell, 14(6), pp. 781–95. doi: 10.1016/j.stem.2014.03.004.

Klein, C. *et al.* (2000) 'A major locus for myoclonus-dystonia maps to chromosome 7q in eight families', *Elsevier*. Available at: https://www.sciencedirect.com/science/article/pii/S0002929707629619 (Accessed: 13 September 2019).

Klein, C. and Fahn, S. (2013) 'Translation of Oppenheim's 1911 paper on dystonia', *Movement Disorders*. John Wiley & Sons, Ltd, 28(7), pp. 851–862. doi: 10.1002/mds.25546.

Koch, C. M. *et al.* (2018) 'A Beginner's Guide to Analysis of RNA Sequencing Data.', *American journal of respiratory cell and molecular biology*. American Thoracic Society, 59(2), pp. 145–157. doi: 10.1165/rcmb.2017-0430TR.

Köhling, R. *et al.* (2004) 'Increased excitability in cortico-striatal synaptic pathway in a model of paroxysmal dystonia', *Neurobiology of Disease*, 16(1), pp. 236–245. doi: 10.1016/j.nbd.2004.01.012.

Kole, M. H. P. and Stuart, G. J. (2012) 'Signal Processing in the Axon Initial Segment', *Neuron*. Neuron, pp. 235–247. doi: 10.1016/j.neuron.2012.01.007.

Konopaske, G. T. *et al.* (2014) 'Prefrontal cortical dendritic spine pathology in schizophrenia and bipolar disorder.', *JAMA psychiatry*. JAMA Psychiatry, 71(12), pp. 1323–31. doi: 10.1001/jamapsychiatry.2014.1582.

Konur, S. and Ghosh, A. (2005) 'Calcium Signaling and the Control of Dendritic Development', *Neuron*. Cell Press, 46(3), pp. 401–405. doi: 10.1016/J.NEURON.2005.04.022.

Kriks, S. *et al.* (2011) 'Dopamine neurons derived from human ES cells efficiently engraft in animal models of Parkinson's disease', *Nature*, 480(7378), pp. 547–551. doi: 10.1038/nature10648.

Kupsch, A. *et al.* (2003) 'Deep brain stimulation in dystonia', *Journal of Neurology*, 250(S1), pp. i47–i52. doi: 10.1007/s00415-003-1110-2.

Kupsch, A. *et al.* (2006) 'Pallidal Deep-Brain Stimulation in Primary Generalized or Segmental Dystonia', *New England Journal of Medicine*, 355(19), pp. 1978–1990. doi: 10.1056/NEJMoa063618.

Lancaster, M. A. *et al.* (2013) 'Cerebral organoids model human brain development and microcephaly', *Nature*, 501(7467), pp. 373–379. doi: 10.1038/nature12517.

Lancaster, M. A. and Knoblich, J. A. (2014) 'Generation of cerebral organoids from human pluripotent stem cells', *Nature Protocols*. Nature Publishing Group, 9(10), pp. 2329–2340. doi: 10.1038/nprot.2014.158.

Lazzari, G. *et al.* (2006) 'Direct Derivation of Neural Rosettes from Cloned Bovine Blastocysts: A Model of Early Neurulation Events and Neural Crest Specification In Vitro', *Stem Cells*. Wiley, 24(11), pp. 2514–2521. doi: 10.1634/stemcells.2006-0149.

van de Leemput, J. *et al.* (2014) 'CORTECON: a temporal transcriptome analysis of in vitro human cerebral cortex development from human embryonic stem cells.', *Neuron*. Neuron, 83(1), pp. 51–68. doi: 10.1016/j.neuron.2014.05.013.

Lendahl, U., Zimmerman, L. B. and McKay, R. D. (1990) 'CNS stem cells express a new class of intermediate filament protein.', *Cell*. Cell, 60(4), pp. 585–95. doi: 10.1016/0092-8674(90)90662-x.

Li, J. *et al.* (2021) 'Mutation in ε-Sarcoglycan Induces a Myoclonus-Dystonia Syndrome-Like Movement Disorder in Mice', *Neuroscience Bulletin*. Springer, 37(3), pp. 311–322. doi: 10.1007/s12264-020-00612-5.

Liu, X. *et al.* (2012) 'Extension of cortical synaptic development distinguishes humans from chimpanzees and macaques.', *Genome research*. Cold Spring Harbor Laboratory Press, 22(4), pp. 611–22. doi: 10.1101/gr.127324.111.

Livak, K. J. and Schmittgen, T. D. (2001) 'Analysis of Relative Gene Expression Data Using Real-Time Quantitative PCR and the 2−ΔΔCT Method', *Methods*, 25(4), pp. 402–408. doi: 10.1006/meth.2001.1262.

Lohmann, C., Myhr, K. L. and Wong, R. O. L. (2002) 'Transmitter-evoked local calcium release stabilizes developing dendrites', *Nature*. Nature Publishing Group, 418(6894), pp. 177–181. doi: 10.1038/nature00850.

Longair, M. H., Baker, D. A. and Armstrong, J. D. (2011) 'Simple Neurite Tracer: open source software for reconstruction, visualization and analysis of neuronal processes.', *Bioinformatics (Oxford,*

England). Bioinformatics, 27(17), pp. 2453–4. doi: 10.1093/bioinformatics/btr390.

Löscher, W. *et al.* (1989) 'The *sz* mutant hamster: A genetic model of epilepsy or of paroxysmal dystonia?', *Movement Disorders*, 4(3), pp. 219–232. doi: 10.1002/mds.870040304.

Lozano, A. M. *et al.* (1997) 'Globus pallidus internus pallidotomy for generalized dystonia', *Movement Disorders*. John Wiley & Sons, Ltd, 12(6), pp. 865–870. doi: 10.1002/mds.870120606.

Lu, K. P. and Means, A. R. (1993) 'Regulation of the cell cycle by calcium and calmodulin', *Endocrine Reviews*, 14(1), pp. 40–58. doi: 10.1210/edrv-14-1-40.

Ludwig, T. E. *et al.* (2006) 'Derivation of human embryonic stem cells in defined conditions', *Nature Biotechnology*, 24(2), pp. 185–187. doi: 10.1038/nbt1177.

Lüthi, A. *et al.* (2001) 'NMDA receptor activation limits the number of synaptic connections during hippocampal development', *Nature Neuroscience*, 4(11), pp. 1102–1107. doi: 10.1038/nn744.

Makino, S. *et al.* (2007) 'Reduced neuron-specific expression of the TAF1 gene is associated with X-linked dystonia-parkinsonism.', *American journal of human genetics*. Elsevier, 80(3), pp. 393–406. doi: 10.1086/512129.

Mali, P. *et al.* (2013) 'RNA-guided human genome engineering via Cas9.', *Science (New York, N.Y.)*. NIH Public Access, 339(6121), pp. 823–6. doi: 10.1126/science.1232033.

Maltese, M. *et al.* (2017) 'Abnormal striatal plasticity in a DYT11/SGCE myoclonus dystonia mouse model is reversed by adenosine A2A receptor inhibition', *Neurobiology of Disease*. Academic Press Inc., 108, pp. 128–139. doi: 10.1016/j.nbd.2017.08.007.

Maltese, M. *et al.* (2018) 'Early structural and functional plasticity alterations in a susceptibility period of DYT1 dystonia mouse striatum', *eLife*. eLife Sciences Publications Limited, 7, p. e33331. doi: 10.7554/eLife.33331.

Manuel, M. N. *et al.* (2015) 'Regulation of cerebral cortical neurogenesis by the Pax6 transcription factor.', *Frontiers in cellular neuroscience*. Front Cell Neurosci, 9, p. 70. doi: 10.3389/fncel.2015.00070.

Mariani, J. *et al.* (2012) 'Modeling human cortical development in vitro using induced pluripotent stem cells.', *Proceedings of the National Academy of Sciences of the United States of America*. National Academy of Sciences, 109(31), pp. 12770–5. doi: 10.1073/pnas.1202944109.

Marín, O. and Mü Ller, U. (2014) 'Lineage origins of GABAergic versus glutamatergic neurons in the neocortex', *Current Opinion in Neurobiology*, 26, pp. 132–141. doi: 10.1016/j.conb.2014.01.015.

Maroof, A. M. *et al.* (2013) 'Directed Differentiation and Functional Maturation of Cortical Interneurons from Human Embryonic Stem Cells', *Cell Stem Cell*, 12(5), pp. 559–572. doi: 10.1016/j.stem.2013.04.008.

Marras, C. *et al.* (2016) 'Nomenclature of genetic movement disorders: Recommendations of the international Parkinson and movement disorder society task force.', *Movement disorders : official journal of the Movement Disorder Society*. Mov Disord, 31(4), pp. 436–57. doi: 10.1002/mds.26527.

Marsh, W. A. *et al.* (2014) 'Systematic review and meta-analysis of the duration of clinical effect of onabotulinumtoxinA in cervical dystonia', *BMC Neurology*, 14(1), p. 91. doi: 10.1186/1471-2377-14-91.

Martella, G. *et al.* (2014) 'Regional specificity of synaptic plasticity deficits in a knock-in mouse model of DYT1 dystonia', *Neurobiology of Disease*, 65, pp. 124–132. doi: 10.1016/j.nbd.2014.01.016.

Martínez-Cerdeño, V. (2017) 'Dendrite and spine modifications in autism and related neurodevelopmental disorders in patients and animal models.', *Developmental neurobiology*. NIH Public Access, 77(4), pp. 393–404. doi: 10.1002/dneu.22417.

McAllister, A. K., Katz, L. C. and Lo, D. C. (1996) 'Neurotrophin Regulation of Cortical Dendritic Growth Requires Activity', *Neuron*. Cell Press, 17(6), pp. 1057–1064. doi: 10.1016/S0896-6273(00)80239-1.

McAllister, A. K., Katz, L. C. and Lo, D. C. (1997) 'Opposing Roles for Endogenous BDNF and NT-3 in Regulating Cortical Dendritic Growth', *Neuron*. Cell Press, 18(5), pp. 767–778. doi: 10.1016/S0896-6273(00)80316-5.

McNally, E. M. (2013) 'The Sarcoglycans'. Landes Bioscience. Available at: https://www.ncbi.nlm.nih.gov/books/NBK6317/ (Accessed: 11 March 2021).

van der Meer, J. N. *et al.* (2012) 'White matter abnormalities in gene-positive myoclonus-dystonia', *Movement Disorders*, 27(13), pp. 1666–1672. doi: 10.1002/mds.25128.

Mencacci, N. *et al.* (2020) 'Transcriptomic analysis of dystonia-associated genes reveals functional convergence within specific cell types and shared neurobiology with psychiatric disorders', *Brain*, 94(15 Supplement). doi: 10.1101/2020.01.31.928978.

Mencacci, N. E. *et al.* (2015) 'A missense mutation in KCTD17 causes autosomal dominant myoclonus-dystonia.', *American journal of human genetics*. Elsevier, 96(6), pp. 938–47. doi: 10.1016/j.ajhg.2015.04.008.

Mencacci, N. E. *et al.* (2020) 'Transcriptomic analysis of dystonia-associated genes reveals functional convergence within specific cell types and shared neurobiology with psychiatric disorders', *bioRxiv*. Cold Spring Harbor Laboratory, p. 2020.01.31.928978. doi: 10.1101/2020.01.31.928978.

Meng, Y. *et al.* (2018) 'Treatment of a Patient With Task-Specific Writing Tremor Using Magnetic Resonance-Guided Focused Ultrasound', *Canadian Journal of Neurological Sciences / Journal Canadien des Sciences Neurologiques*, 45(4), pp. 474–477. doi: 10.1017/cjn.2018.19.

Menozzi, E. *et al.* (2019) 'Twenty years on: Myoclonus-dystonia and ε-sarcoglycan — neurodevelopment, channel, and signaling dysfunction', *Movement Disorders*. John Wiley & Sons, Ltd, p. mds.27822. doi: 10.1002/mds.27822.

Miller, I. *et al.* (2018) 'Ki67 is a Graded Rather than a Binary Marker of Proliferation versus Quiescence.', *Cell reports*. NIH Public Access, 24(5), pp. 1105-1112.e5. doi: 10.1016/j.celrep.2018.06.110.

Mink, J. W. (1996) 'The basal ganglia: focused selection and inhibition of competing motor programs.', *Progress in neurobiology*. Prog Neurobiol, 50(4), pp. 381–425. doi: 10.1016/s0301-0082(96)00042-1.

Miyamoto, A. *et al.* (2016) 'Microglia contact induces synapse formation in developing somatosensory cortex.', *Nature communications*. Nat Commun, 7, p. 12540. doi: 10.1038/ncomms12540.

Molyneaux, B. J. *et al.* (2007) 'Neuronal subtype specification in the cerebral cortex', *Nature Reviews Neuroscience*, pp. 427–437. doi: 10.1038/nrn2151.

Monzel, A. S. *et al.* (2017) 'Derivation of Human Midbrain-Specific Organoids from Neuroepithelial Stem Cells.', *Stem cell reports*. Stem Cell Reports, 8(5), pp. 1144–1154. doi: 10.1016/j.stemcr.2017.03.010.

Motta, F., Stignani, C. and Antonello, C. E. (2008) 'Effect of Intrathecal Baclofen on Dystonia in Children With Cerebral Palsy and the Use of Functional Scales', *Journal of Pediatric Orthopaedics*, 28(2), pp. 213–217. doi: 10.1097/BPO.0b013e3181653b2a.

Müller, J. *et al.* (2002) 'The prevalence of primary dystonia in the general community', *Neurology*. Wolters Kluwer Health, Inc. on behalf of the American Academy of Neurology, 56(11), pp. 1579–1581. doi: 10.1212/01.wnl.0000026474.12594.0d.

Munchau, A. *et al.* (2001) 'Prospective study of selective peripheral denervation for botulinum-toxin resistant patients with cervical dystonia', *Brain*, 124(4), pp. 769–783. doi: 10.1093/brain/124.4.769.

Murakami, N. *et al.* (2017) 'Establishment of DYT5 patient-specific induced pluripotent stem cells with a GCH1 mutation.', *Stem cell research*, 24, pp. 36–39. doi: 10.1016/j.scr.2017.07.029.

Murphy, T. H. *et al.* (1992) 'Spontaneous synchronous synaptic calcium transients in cultured cortical

neurons.', *The Journal of neuroscience : the official journal of the Society for Neuroscience*. J Neurosci, 12(12), pp. 4834–45. doi: 10.1523/JNEUROSCI.12-12-04834.1992.

Nagy, J. *et al.* (2017) 'Altered neurite morphology and cholinergic function of induced pluripotent stem cell-derived neurons from a patient with Kleefstra syndrome and autism', *Translational Psychiatry*. Nature Publishing Group, 7(7), p. e1179. doi: 10.1038/TP.2017.144.

Nair, P., Whalen, W. J. and Buerk, D. (1975) 'Po2 of cat cerebral cortex: Response to breathing N2 and 100% O2', *Microvascular Research*, 9(2), pp. 158–165. doi: 10.1016/0026-2862(75)90077-1.

Naismith, T. V *et al.* (2004) 'TorsinA in the nuclear envelope.', *Proceedings of the National Academy of Sciences of the United States of America*. National Academy of Sciences, 101(20), pp. 7612–7. doi: 10.1073/pnas.0308760101.

Nardocci, N. *et al.* (2008) 'Myoclonus–dystonia syndrome: Clinical presentation, disease course, and genetic features in 11 families', *Movement Disorders*, 23(1), pp. 28–34. doi: 10.1002/mds.21715.

Negri, J., Menon, V. and Young-Pearse, T. L. (2020) 'Assessment of Spontaneous Neuronal Activity In Vitro Using Multi-Well Multi-Electrode Arrays: Implications for Assay Development.', *eNeuro*. Society for Neuroscience, 7(1). doi: 10.1523/ENEURO.0080-19.2019.

Neher, E. (1998) 'Vesicle pools and Ca2+ microdomains: New tools for understanding their roles in neurotransmitter release', *Neuron*, pp. 389–399. doi: 10.1016/S0896-6273(00)80983-6.

Neher, E. and Sakaba, T. (2008) 'Multiple Roles of Calcium Ions in the Regulation of Neurotransmitter Release', *Neuron*, 59(6), pp. 861–872. doi: 10.1016/j.neuron.2008.08.019.

Nelson, S. B., Sugino, K. and Hempel, C. M. (2006) 'The problem of neuronal cell types: a physiological genomics approach', *Trends in Neurosciences*. Elsevier Current Trends, 29(6), pp. 339–345. doi: 10.1016/J.TINS.2006.05.004.

Neychev, V. K. *et al.* (2008) 'The basal ganglia and cerebellum interact in the expression of dystonic movement', *Brain*, 131(9), pp. 2499–2509. doi: 10.1093/brain/awn168.

Niday, Z. and Tzingounis, A. V. (2018) 'Potassium Channel Gain of Function in Epilepsy: An Unresolved Paradox', *Neuroscientist*. NIH Public Access, pp. 368–380. doi: 10.1177/1073858418763752.

Nieto, M. *et al.* (2004) 'Expression of Cux-1 and Cux-2 in the subventricular zone and upper layers II-IV of the cerebral cortex', *The Journal of Comparative Neurology*, 479(2), pp. 168–180. doi: 10.1002/cne.20322.

Nigro, V. *et al.* (1996) 'Autosomal recessive limb-girdle muscular dystrophy, LGMD2F, is caused by a mutation in the delta-sarcoglycan gene.', *Nature genetics*. Nat Genet, 14(2), pp. 195–8. doi: 10.1038/ng1096-195.

Nishimura, M., Owens, J. and Swann, J. W. (2008) 'Effects of Chronic Network Hyperexcitability on the Growth of Hippocampal Dendrites', *Neurobiology of disease*. NIH Public Access, 29(2), p. 267. doi: 10.1016/J.NBD.2007.08.018.

Niswender, C. M. and Conn, P. J. (2010) 'Metabotropic Glutamate Receptors: Physiology, Pharmacology, and Disease', *Annual Review of Pharmacology and Toxicology*, 50(1), pp. 295–322. doi: 10.1146/annurev.pharmtox.011008.145533.

Noguchi, S. *et al.* (1995) 'Mutations in the dystrophin-associated protein gamma-sarcoglycan in chromosome 13 muscular dystrophy.', *Science (New York, N.Y.)*. Science, 270(5237), pp. 819–22. doi: 10.1126/science.270.5237.819.

Nowycky, M. C. and Thomas, A. P. (2002) 'Intracellular calcium signaling.', *Journal of cell science*. The Company of Biologists Ltd, 115(Pt 19), pp. 3715–6. doi: 10.1242/jcs.00078.

Nygaard, T. G. *et al.* (1990) 'Dopa-responsive dystonia: the spectrum of clinical manifestations in a large North American family.', *Neurology*, 40(1), pp. 66–9. doi: 10.1212/wnl.40.1.66.

Nygaard, T. G. *et al.* (1999) 'Localization of a gene for myoclonus-dystonia to chromosome 7q21-q31', *Annals of Neurology*, 46(5), pp. 794–798. doi: 10.1002/1531-8249(199911)46:5<794::AID-ANA19>3.0.CO;2-2.

O'Farrell, C. A. *et al.* (2009) 'Mutant torsinA interacts with tyrosine hydroxylase in cultured cells', *Neuroscience*, 164(3), pp. 1127–1137. doi: 10.1016/j.neuroscience.2009.09.017.

Obeso, J. A. *et al.* (1983) 'Myoclonic dystonia.', *Neurology*. Wolters Kluwer Health, Inc. on behalf of the American Academy of Neurology, 33(7), pp. 825–30. doi: 10.1212/WNL.33.7.825.

Oblak, A. L. *et al.* (2014) 'Rapid-onset dystonia-parkinsonism associated with the I758S mutation of the ATP1A3 gene: a neuropathologic and neuroanatomical study of four siblings', *Acta Neuropathologica*. Springer, 128(1), p. 81. doi: 10.1007/S00401-014-1279-X.

Ogawa, M. *et al.* (1995) 'The reeler gene-associated antigen on cajal-retzius neurons is a crucial molecule for laminar organization of cortical neurons', *Neuron*, 14(5), pp. 899–912. doi: 10.1016/0896-6273(95)90329-1.

Oppenheim and H. (1911) 'Uber eineeigenartige Krampfkrankheit des kind-lichen und jugendlichen Alters (Dysbasia lordotica lordotica progressive, Dystonia musculorum deformans)', *Neurol Cbl*, 30, pp. 1090–1107. Available at: https://ci.nii.ac.jp/naid/10024845792/ (Accessed: 14 May 2019).

Ozawa, E. *et al.* (2005) 'Molecular and cell biology of the sarcoglycan complex.', *Muscle & nerve*. Muscle Nerve, 32(5), pp. 563–76. doi: 10.1002/mus.20349.

Ozelius, L. J. *et al.* (1997) 'The early-onset torsion dystonia gene (DYT1) encodes an ATP-binding protein', *Nature Genetics*. Nature Publishing Group, 17(1), pp. 40–48. doi: 10.1038/ng0997-40.

Ozelius, L. J. and Bressman, S. B. (2011) 'Genetic and clinical features of primary torsion dystonia', *Neurobiology of Disease*. Academic Press, 42(2), pp. 127–135. doi: 10.1016/J.NBD.2010.12.012.

Papouin, T. *et al.* (2012) 'Synaptic and extrasynaptic NMDA receptors are gated by different endogenous coagonists', *Cell*. Cell, 150(3), pp. 633–646. doi: 10.1016/j.cell.2012.06.029.

Park, H. R. *et al.* (2016) 'Long-Term Clinical Outcome of Internal Globus Pallidus Deep Brain Stimulation for Dystonia', *PLOS ONE*. Edited by P. Gonzalez-Alegre. Public Library of Science, 11(1), p. e0146644. doi: 10.1371/journal.pone.0146644.

Patel, T. P. *et al.* (2015) 'Automated quantification of neuronal networks and single-cell calcium dynamics using calcium imaging.', *Journal of neuroscience methods*. NIH Public Access, 243, pp. 26–38. doi: 10.1016/j.jneumeth.2015.01.020.

Peall, K. J. *et al.* (2013) 'SGCE mutations cause psychiatric disorders: clinical and genetic characterization', *Brain*, 136, pp. 294–303. doi: 10.1093/brain/aws308.

Peall, K. J. *et al.* (2014) 'SGCE and myoclonus dystonia: motor characteristics, diagnostic criteria and clinical predictors of genotype', *Journal of Neurology*, 261(12), pp. 2296–2304. doi: 10.1007/s00415-014-7488-3.

Peall, K. J. *et al.* (2016) 'Psychiatric disorders, myoclonus dystonia and *SGCE* : an international study', *Annals of Clinical and Translational Neurology*, 3(1), pp. 4–11. doi: 10.1002/acn3.263.

Pellegrini, L. *et al.* (2020) 'Human CNS barrier-forming organoids with cerebrospinal fluid production.', *Science (New York, N.Y.)*. Science, 369(6500). doi: 10.1126/science.aaz5626.

Penzes, P. *et al.* (2011) 'Dendritic spine pathology in neuropsychiatric disorders', *Nature Neuroscience*. Nature Publishing Group, 14(3), pp. 285–293. doi: 10.1038/nn.2741.

Perea, G. and Araque, A. (2010) 'GLIA modulates synaptic transmission', *Brain Research Reviews*. Elsevier, 63(1–2), pp. 93–102. doi: 10.1016/J.BRAINRESREV.2009.10.005.

Perlmutter, J. S. *et al.* (1997) 'Decreased [18F]spiperone binding in putamen in idiopathic focal dystonia.', *The Journal of neuroscience : the official journal of the Society for Neuroscience*, 17(2), pp.

843–50. Available at: http://www.ncbi.nlm.nih.gov/pubmed/8987805 (Accessed: 31 October 2017).

Perrier, A. L. *et al.* (2004) 'Derivation of midbrain dopamine neurons from human embryonic stem cells', *Proceedings of the National Academy of Sciences*, 101(34), pp. 12543–12548. doi: 10.1073/pnas.0404700101.

Perruchoud, D. *et al.* (2014) 'Focal dystonia and the Sensory-Motor Integrative Loop for Enacting (SMILE)', *Frontiers in Human Neuroscience*. Frontiers, 8, p. 458. doi: 10.3389/fnhum.2014.00458.

Petanjek, Z. *et al.* (2011) 'Extraordinary neoteny of synaptic spines in the human prefrontal cortex.', *Proceedings of the National Academy of Sciences of the United States of America*. National Academy of Sciences, 108(32), pp. 13281–6. doi: 10.1073/pnas.1105108108.

Petralia, R. S. *et al.* (2010) 'Organization of NMDA receptors at extrasynaptic locations', *Neuroscience*. Neuroscience, 167(1), pp. 68–87. doi: 10.1016/j.neuroscience.2010.01.022.

Pfaffl, M. W. (2001) 'A new mathematical model for relative quantification in real-time RT-PCR.', *Nucleic acids research*, 29(9), p. e45. Available at: http://www.ncbi.nlm.nih.gov/pubmed/11328886 (Accessed: 2 January 2019).

Phukan, J. *et al.* (2011) 'Primary dystonia and dystonia-plus syndromes: clinical characteristics, diagnosis, and pathogenesis', *The Lancet Neurology*. Elsevier, 10(12), pp. 1074–1085. doi: 10.1016/S1474-4422(11)70232-0.

Piccinin, C. C. *et al.* (2015) 'Diffuse Decreased Gray Matter in Patients with Idiopathic Craniocervical Dystonia: A Voxel-Based Morphometry Study', *Frontiers in Neurology*. Frontiers, 5, p. 283. doi: 10.3389/fneur.2014.00283.

Pineda, R. H. *et al.* (2008) 'Kv1 potassium channel complexes in vivo require Kvbeta2 subunits in dorsal spinal neurons.', *Journal of neurophysiology*. J Neurophysiol, 100(4), pp. 2125–36. doi: 10.1152/jn.90667.2008.

Platel, J.-C., Dave, K. A. and Bordey, A. (2008) 'Control of neuroblast production and migration by converging GABA and glutamate signals in the postnatal forebrain.', *The Journal of physiology*. J Physiol, 586(16), pp. 3739–43. doi: 10.1113/jphysiol.2008.155325.

Polleux, F., Morrow, T. and Ghosh, A. (2000) 'Semaphorin 3A is a chemoattractant for cortical apical dendrites', *Nature*. Nature Publishing Group, 404(6778), pp. 567–573. doi: 10.1038/35007001.

Pozzi, D. *et al.* (2017) 'An improved method for growing neurons: Comparison with standard protocols.', *Journal of neuroscience methods*. J Neurosci Methods, 280, pp. 1–10. doi: 10.1016/j.jneumeth.2017.01.013.

Prè, D. *et al.* (2014) 'A Time Course Analysis of the Electrophysiological Properties of Neurons Differentiated from Human Induced Pluripotent Stem Cells (iPSCs)', *PLoS ONE*. Edited by K. Aalto-Setala. Public Library of Science, 9(7), p. e103418. doi: 10.1371/journal.pone.0103418.

Premi, E. *et al.* (2016) 'Functional Connectivity Networks in Asymptomatic and Symptomatic *DYT1* Carriers', *Movement Disorders*, 31(11), pp. 1739–1743. doi: 10.1002/mds.26725.

Prins, K. W. *et al.* (2009) 'Dystrophin is a microtubule-associated protein.', *The Journal of cell biology*. Rockefeller University Press, 186(3), pp. 363–9. doi: 10.1083/jcb.200905048.

Qian, X. *et al.* (2016) 'Brain-Region-Specific Organoids Using Mini-bioreactors for Modeling ZIKV Exposure.', *Cell*. Elsevier, 165(5), pp. 1238–1254. doi: 10.1016/j.cell.2016.04.032.

Quadrato, G. *et al.* (2017) 'Cell diversity and network dynamics in photosensitive human brain organoids', *Nature*. Nature Publishing Group, 545(7652), pp. 48–53. doi: 10.1038/nature22047.

Quartarone, A. *et al.* (2008) 'Abnormal plasticity of sensorimotor circuits extends beyond the affected body part in focal dystonia', *Journal of Neurology, Neurosurgery & Psychiatry*, 79(9), pp. 985–990. doi: 10.1136/jnnp.2007.121632.

Queiroz, M. A. R. *et al.* (2012) 'Physical therapy program for cervical dystonia: A study of 20 cases', *Functional Neurology*, 27(3), pp. 187–192. Available at: http://www.ncbi.nlm.nih.gov/pubmed/23402680 (Accessed: 10 October 2019).

Quinn, N. P. (1996) 'Essential myoclonus and myoclonus dystonia', *Movement Disorders*. Wiley-Blackwell, 11(2), pp. 119–124. doi: 10.1002/mds.870110202.

Rajan, I. and Cline, H. T. (1998) 'Glutamate receptor activity is required for normal development of tectal cell dendrites in vivo', *Journal of Neuroscience*. J Neurosci, 18(19), pp. 7836–7846. doi: 10.1523/JNEUROSCI.18-19-07836.1998.

Ramdhani, R. A. *et al.* (2014) 'What's special about task in dystonia? A voxel-based morphometry and diffusion weighted imaging study', *Movement Disorders*, 29(9), pp. 1141–1150. doi: 10.1002/mds.25934.

Ramirez, J. M. *et al.* (2018) 'Advances in cellular and integrative control of oxygen homeostasis within the central nervous system.', *The Journal of physiology*. Wiley-Blackwell, 596(15), pp. 3043–3065. doi: 10.1113/JP275890.

Ratnayaka, A. *et al.* (2011) 'Extrasynaptic vesicle recycling in mature hippocampal neurons.', *Nature communications*. Nat Commun, 2, p. 531. doi: 10.1038/ncomms1534.

Rauschenberger, L. *et al.* (2020) 'Striatal dopaminergic dysregulation and dystonia-like movements induced by sensorimotor stress in a pharmacological mouse model of rapid-onset dystonia-parkinsonism', *Experimental Neurology*. Academic Press, 323, p. 113109. doi: 10.1016/J.EXPNEUROL.2019.113109.

Redmond, L. *et al.* (2000) 'Nuclear Notch1 signaling and the regulation of dendritic development.', *Nature neuroscience*. Nat Neurosci, 3(1), pp. 30–40. doi: 10.1038/71104.

Redmond, L. and Ghosh, A. (2001) 'The role of Notch and Rho GTPase signaling in the control of dendritic development', *Current Opinion in Neurobiology*. Elsevier Current Trends, 11(1), pp. 111–117. doi: 10.1016/S0959-4388(00)00181-1.

Redmond, L., Kashani, A. H. and Ghosh, A. (2002) 'Calcium Regulation of Dendritic Growth via CaM Kinase IV and CREB-Mediated Transcription', *Neuron*. Cell Press, 34(6), pp. 999–1010. doi: 10.1016/S0896-6273(02)00737-7.

Reid, C. A. *et al.* (2014) 'Reduced dendritic arborization and hyperexcitability of pyramidal neurons in a Scn1b-based model of Dravet syndrome', *Brain*, 137(6), pp. 1701–1715. doi: 10.1093/brain/awu077.

Richter, A. and Löscher, W. (1996) 'Antidystonic effects of L-type Ca^{2+} channel antagonists in a hamster model of idiopathic dystonia.', *European journal of pharmacology*. Eur J Pharmacol, 300(3), pp. 197–202. doi: 10.1016/0014-2999(95)00878-0.

Rittiner, J. E. *et al.* (2016) 'Functional Genomic Analyses of Mendelian and Sporadic Disease Identify Impaired eIF2α Signaling as a Generalizable Mechanism for Dystonia', *Neuron*, 92(6), pp. 1238–1251. doi: 10.1016/j.neuron.2016.11.012.

Ritz, K. *et al.* (2011) 'SGCE isoform characterization and expression in human brain: implications for myoclonus–dystonia pathogenesis?', *European Journal of Human Genetics*, 19(4), pp. 438–444. doi: 10.1038/ejhg.2010.206.

Rodacker, V., Toustrup-Jensen, M. and Vilsen, B. (2006) 'Mutations Phe785Leu and Thr618Met in Na^+,K^+-ATPase, Associated with Familial Rapid-onset Dystonia Parkinsonism, Interfere with Na^+ Interaction by Distinct Mechanisms', *Journal of Biological Chemistry*, 281(27), pp. 18539–18548. doi: 10.1074/jbc.M601780200.

Rosa, F. *et al.* (2020) 'In Vitro Differentiated Human Stem Cell-Derived Neurons Reproduce Synaptic Synchronicity Arising during Neurodevelopment', *Stem Cell Reports*. Cell Press, 15(1), pp. 22–37. doi: 10.1016/J.STEMCR.2020.05.015.

Roubertie, A. *et al.* (2008) 'Benign paroxysmal tonic upgaze, benign paroxysmal torticollis, episodic ataxia and CACNA1A mutation in a family.', *Journal of neurology*. J Neurol, 255(10), pp. 1600–2. doi: 10.1007/s00415-008-0982-8.

Royeck, M. *et al.* (2008) 'Role of axonal NaV1.6 sodium channels in action potential initiation of CA1 pyramidal neurons.', *Journal of neurophysiology*. J Neurophysiol, 100(4), pp. 2361–80. doi: 10.1152/jn.90332.2008.

Rozanski, V. E. *et al.* (2017) 'The role of the pallidothalamic fibre tracts in deep brain stimulation for dystonia: A diffusion MRI tractography study', *Human Brain Mapping*, 38(3), pp. 1224–1232. doi: 10.1002/hbm.23450.

Ruge, D. *et al.* (2011) 'Shaping reversibility? Long-term deep brain stimulation in dystonia: the relationship between effects on electrophysiology and clinical symptoms', *Brain*, 134(7), pp. 2106–2115. doi: 10.1093/brain/awr122.

Rushton, D. J. *et al.* (2013) 'Stimulation of GABA-induced Ca2+ influx enhances maturation of human induced pluripotent stem cell-derived neurons.', *PloS one*. PLoS One, 8(11), p. e81031. doi: 10.1371/journal.pone.0081031.

Sander, S. E. and Richter, A. (2007) 'Effects of intrastriatal injections of glutamate receptor antagonists on the severity of paroxysmal dystonia in the dtsz mutant', *European Journal of Pharmacology*, 563(1–3), pp. 102–108. doi: 10.1016/j.ejphar.2007.01.067.

Sandonà, D. and Betto, R. (2009) 'Sarcoglycanopathies: molecular pathogenesis and therapeutic prospects.', *Expert reviews in molecular medicine*. Cambridge University Press, 11, p. e28. doi: 10.1017/S1462399409001203.

Schwaller, B. (2010) 'Cytosolic Ca2+ buffers.', *Cold Spring Harbor perspectives in biology*. doi: 10.1101/cshperspect.a004051.

Schwingenschuh, P. *et al.* (2010) 'Distinguishing SWEDDs patients with asymmetric resting tremor from Parkinson's disease: a clinical and electrophysiological study.', *Movement disorders : official journal of the Movement Disorder Society*. Europe PMC Funders, 25(5), pp. 560–9. doi: 10.1002/mds.23019.

Sciamanna, G. *et al.* (2012) 'Cholinergic dysfunction alters synaptic integration between thalamostriatal and corticostriatal inputs in DYT1 dystonia.', *The Journal of neuroscience : the official journal of the Society for Neuroscience*. NIH Public Access, 32(35), pp. 11991–2004. doi: 10.1523/JNEUROSCI.0041-12.2012.

Sciamanna, G. *et al.* (2020) 'Optogenetic Activation of Striatopallidal Neurons Reveals Altered HCN Gating in DYT1 Dystonia', *Cell Reports*, 31(7). doi: 10.1016/j.celrep.2020.107644.

Segawa, M., Nomura, Y. and Nishiyama, N. (2003) 'Autosomal dominant guanosine triphosphate cyclohydrolase I deficiency (Segawa disease)', *Annals of Neurology*, 54(S6), pp. S32–S45. doi: 10.1002/ana.10630.

Šestan, N., Artavanis-Tsakonas, S. and Rakic, P. (1999) 'Contact-Dependent Inhibition of Cortical Neurite Growth Mediated by Notch Signaling', *Science*. American Association for the Advancement of Science, 286(5440), pp. 741–746. doi: 10.1126/SCIENCE.286.5440.741.

Sethi, K. D., Rodriguez, R. and Olayinka, B. (2012) 'Satisfaction with botulinum toxin treatment: a cross-sectional survey of patients with cervical dystonia', *Journal of Medical Economics*. Taylor & Francis, 15(3), pp. 419–423. doi: 10.3111/13696998.2011.653726.

Sharma, N. (2019) 'Neuropathology of Dystonia.', *Tremor and other hyperkinetic movements (New York, N.Y.)*. Ubiquity Press, 9, p. 569. doi: 10.7916/d8-j6sx-b156.

Shi, M. *et al.* (2013) 'Glia co-culture with neurons in microfluidic platforms promotes the formation and stabilization of synaptic contacts.', *Lab on a chip*. NIH Public Access, 13(15), pp. 3008–21. doi:

10.1039/c3lc50249j.

Shi, Y., Kirwan, P. and Livesey, F. J. (2012) 'Directed differentiation of human pluripotent stem cells to cerebral cortex neurons and neural networks', *Nature Protocols*, 7(10), pp. 1836–1846. doi: 10.1038/nprot.2012.116.

Shieh, P. B. *et al.* (1998) 'Identification of a Signaling Pathway Involved in Calcium Regulation of BDNF Expression', *Neuron*. Cell Press, 20(4), pp. 727–740. doi: 10.1016/S0896-6273(00)81011-9.

Shirley, T. L. *et al.* (2008) 'Paroxysmal dyskinesias in mice.', *Movement disorders : official journal of the Movement Disorder Society*. Mov Disord, 23(2), pp. 259–64. doi: 10.1002/mds.21829.

Smith, R. H., Guilbeau, E. J. and Reneau, D. D. (1977) 'The oxygen tension field within a discrete volume of cerebral cortex', *Microvascular Research*, 13(2), pp. 233–240. doi: 10.1016/0026-2862(77)90088-7.

Smits, L. M. *et al.* (2019) 'Modeling Parkinson's disease in midbrain-like organoids', *npj Parkinson's Disease*. Nature Publishing Group, 5(1), p. 5. doi: 10.1038/s41531-019-0078-4.

Smits, L. M. and Schwamborn, J. C. (2020) 'Midbrain Organoids: A New Tool to Investigate Parkinson's Disease', *Frontiers in Cell and Developmental Biology*. Frontiers, 8, p. 359. doi: 10.3389/fcell.2020.00359.

Sohn, P. D. *et al.* (2019) 'Pathogenic Tau Impairs Axon Initial Segment Plasticity and Excitability Homeostasis', *Neuron*. Cell Press, 104(3), pp. 458-470.e5. doi: 10.1016/J.NEURON.2019.08.008.

Song, C.-H. *et al.* (2014) 'Subtle microstructural changes of the cerebellum in a knock-in mouse model of DYT1 dystonia.', *Neurobiology of disease*. NIH Public Access, 62, pp. 372–80. doi: 10.1016/j.nbd.2013.10.003.

Song, C. H. *et al.* (2012) 'Functional analysis of dopaminergic systems in a DYT1 knock-in mouse model of dystonia', *Neurobiology of Disease*, 48(1), pp. 66–78. doi: 10.1016/j.nbd.2012.05.009.

Song, C. H. *et al.* (2013) 'Subtle microstructural changes of the striatum in a DYT1 knock-in mouse model of dystonia', *Neurobiology of Disease*. Neurobiol Dis, 54, pp. 362–371. doi: 10.1016/j.nbd.2013.01.008.

de Souza, J. S. *et al.* (2017) 'IGF1 neuronal response in the absence of MECP2 is dependent on TRalpha 3.', *Human molecular genetics*. Hum Mol Genet, 26(2), pp. 270–281. doi: 10.1093/hmg/ddw384.

Spacey, S. D. *et al.* (2005) 'Two novel CACNA1A gene mutations associated with episodic ataxia type 2 and interictal dystonia.', *Archives of neurology*. Arch Neurol, 62(2), pp. 314–6. doi: 10.1001/archneur.62.2.314.

Spitzer, N. C. (2006) 'Electrical activity in early neuronal development', *Nature*. Nature, 444(7120). doi: 10.1038/NATURE05300.

Stancik, E. K. *et al.* (2010) 'Heterogeneity in Ventricular Zone Neural Precursors Contributes to Neuronal Fate Diversity in the Postnatal Neocortex', *Journal of Neuroscience*, 30(20), pp. 7028–7036. doi: 10.1523/JNEUROSCI.6131-09.2010.

Storm, J. F. (1990) 'Chapter 12 Potassium currents in hippocampal pyramidal cells', *Progress in Brain Research*. Prog Brain Res, 83(C), pp. 161–187. doi: 10.1016/S0079-6123(08)61248-0.

Studer, L. *et al.* (2000) 'Enhanced proliferation, survival, and dopaminergic differentiation of CNS precursors in lowered oxygen.', *The Journal of neuroscience : the official journal of the Society for Neuroscience*. Society for Neuroscience, 20(19), pp. 7377–83. doi: 10.1523/JNEUROSCI.20-19-07377.2000.

Stutzmann, G. E. and Mattson, M. P. (2011) 'Endoplasmic reticulum Ca(2+) handling in excitable cells in health and disease.', *Pharmacological reviews*. American Society for Pharmacology and Experimental Therapeutics, 63(3), pp. 700–27. doi: 10.1124/pr.110.003814.

Sweney, M. T., Newcomb, T. M. and Swoboda, K. J. (2015) 'The Expanding Spectrum of Neurological

Phenotypes in Children With ATP1A3 Mutations, Alternating Hemiplegia of Childhood, Rapid-onset Dystonia-Parkinsonism, CAPOS and Beyond', *Pediatric neurology*. NIH Public Access, 52(1), p. 56. doi: 10.1016/J.PEDIATRNEUROL.2014.09.015.

Tagliati, M. *et al.* (2004) 'Deep brain stimulation for dystonia', *Expert Review of Medical Devices*, 1(1), pp. 33–41. doi: 10.1586/17434440.1.1.33.

Takahashi, K. *et al.* (2007) 'Induction of Pluripotent Stem Cells from Adult Human Fibroblasts by Defined Factors', *Cell*, 131(5), pp. 861–872. doi: 10.1016/j.cell.2007.11.019.

Takahashi, K. and Yamanaka, S. (2006) 'Induction of Pluripotent Stem Cells from Mouse Embryonic and Adult Fibroblast Cultures by Defined Factors', *Cell*, 126(4), pp. 663–676. doi: 10.1016/j.cell.2006.07.024.

Tamura, R. *et al.* (2020) 'Gene Therapy Using Neural Stem/Progenitor Cells Derived from Human Induced Pluripotent Stem Cells: Visualization of Migration and Bystander Killing Effect', *Human Gene Therapy*. Mary Ann Liebert, Inc., publishers 140 Huguenot Street, 3rd Floor New Rochelle, NY 10801 USA , 31(5–6), pp. 352–366. doi: 10.1089/hum.2019.326.

Tanabe, L. M. *et al.* (2009) 'Primary dystonia: molecules and mechanisms.', *Nature reviews. Neurology*. NIH Public Access, 5(11), pp. 598–609. doi: 10.1038/nrneurol.2009.160.

Tang, X. *et al.* (2013) 'Astroglial cells regulate the developmental timeline of human neurons differentiated from induced pluripotent stem cells.', *Stem cell research*. NIH Public Access, 11(2), pp. 743–57. doi: 10.1016/j.scr.2013.05.002.

Tao, X. *et al.* (1998) 'Ca2+ Influx Regulates BDNF Transcription by a CREB Family Transcription Factor-Dependent Mechanism', *Neuron*. Cell Press, 20(4), pp. 709–726. doi: 10.1016/S0896-6273(00)81010-7.

Tarabykin, V. *et al.* (2001) 'Cortical upper layer neurons derive from the subventricular zone as indicated by Svet1 gene expression.', *Development (Cambridge, England)*, 128(11), pp. 1983–93. Available at: http://www.ncbi.nlm.nih.gov/pubmed/11493521 (Accessed: 1 October 2019).

Tassorelli, C. *et al.* (2006) 'Botulinum toxin and neuromotor rehabilitation: An integrated approach to idiopathic cervical dystonia', *Movement Disorders*, 21(12), pp. 2240–2243. doi: 10.1002/mds.21145.

Telezhkin, V. *et al.* (2016) 'Forced cell cycle exit and modulation of GABA $_A$, CREB, and GSK3β signaling promote functional maturation of induced pluripotent stem cell-derived neurons', *American Journal of Physiology-Cell Physiology*. American Physiological Society Bethesda, MD, 310(7), pp. C520–C541. doi: 10.1152/ajpcell.00166.2015.

Telezhkin, V. *et al.* (2018) 'Kv7 channels are upregulated during striatal neuron development and promote maturation of human iPSC-derived neurons.', *Pflugers Archiv : European journal of physiology*. Springer, 470(9), pp. 1359–1376. doi: 10.1007/s00424-018-2155-7.

Termsarasab, P. *et al.* (2016) 'Neural correlates of abnormal sensory discrimination in laryngeal dystonia.', *NeuroImage. Clinical*. Elsevier, 10, pp. 18–26. doi: 10.1016/j.nicl.2015.10.016.

Tezenas du Montcel, S. *et al.* (2005) 'Epsilon sarcoglycan mutations and phenotype in French patients with myoclonic syndromes', *Journal of Medical Genetics*, 43(5), pp. 394–400. doi: 10.1136/jmg.2005.036780.

Thomson, J. A. (1998) 'Embryonic Stem Cell Lines Derived from Human Blastocysts', *Science*, 282(5391), pp. 1145–1147. doi: 10.1126/science.282.5391.1145.

Threadgill, R., Bobb, K. and Ghosh, A. (1997) 'Regulation of dendritic growth and remodeling by Rho, Rac, and Cdc42.', *Neuron*. Neuron, 19(3), pp. 625–34. doi: 10.1016/s0896-6273(00)80376-1.

Tian, Y., Schreiber, R. and Kunzelmann, K. (2012) 'Anoctamins are a family of Ca2+-activated Cl-channels.', *Journal of cell science*. The Company of Biologists Ltd, 125(Pt 21), pp. 4991–8. doi: 10.1242/jcs.109553.

Tiberi, L., Vanderhaeghen, P. and van den Ameele, J. (2012) 'Cortical neurogenesis and morphogens: diversity of cues, sources and functions', *Current Opinion in Cell Biology*. Elsevier Current Trends, 24(2), pp. 269–276. doi: 10.1016/J.CEB.2012.01.010.

Tiderington, E. *et al.* (2013) 'How long does it take to diagnose cervical dystonia?', *Journal of the neurological sciences*. NIH Public Access, 335(1–2), pp. 72–4. doi: 10.1016/j.jns.2013.08.028.

Tieng, V. *et al.* (2014) 'Engineering of midbrain organoids containing long-lived dopaminergic neurons.', *Stem cells and development*. Stem Cells Dev, 23(13), pp. 1535–47. doi: 10.1089/scd.2013.0442.

Togashi, H. *et al.* (2002) 'Cadherin Regulates Dendritic Spine Morphogenesis', *Neuron*. Cell Press, 35(1), pp. 77–89. doi: 10.1016/S0896-6273(02)00748-1.

Toledo-Rodriguez, M. *et al.* (2005) 'Cellular signalling properties in microcircuits.', *Trends in neurosciences*. Elsevier, 28(10), pp. 534–40. doi: 10.1016/j.tins.2005.08.001.

van Tricht, M. J. *et al.* (2012) 'Cognition and psychopathology in myoclonus-dystonia', *Journal of Neurology, Neurosurgery & Psychiatry*, 83(8), pp. 814–820. doi: 10.1136/jnnp-2011-301386.

Tsaneva-Atanasova, K. *et al.* (2009) 'Quantifying neurite growth mediated by interactions among secretory vesicles, microtubules, and actin networks.', *Biophysical journal*. Biophys J, 96(3), pp. 840–57. doi: 10.1016/j.bpj.2008.10.036.

Turrigiano, G. G. and Nelson, S. B. (2004) 'Homeostatic plasticity in the developing nervous system', *Nature Reviews Neuroscience*, 5(2), pp. 97–107. doi: 10.1038/nrn1327.

Udupa, K. and Chen, R. (2019) 'Motor cortical circuits in Parkinson disease and dystonia', in *Handbook of clinical neurology*, pp. 167–186. doi: 10.1016/B978-0-444-64142-7.00047-3.

Vaine, C. A. *et al.* (2017) 'X-linked Dystonia-Parkinsonism patient cells exhibit altered signaling via nuclear factor-kappa B', *Neurobiology of Disease*, 100, pp. 108–118. doi: 10.1016/j.nbd.2016.12.016.

Valente, E. M. *et al.* (2005) 'The epsilon-sarcoglycan gene in myoclonic syndromes', *Neurology*, 64(4), pp. 737–739. doi: 10.1212/01.WNL.0000151979.68010.9B.

Van Essen, D. C., Donahue, C. J. and Glasser, M. F. (2018) 'Development and Evolution of Cerebral and Cerebellar Cortex', *Brain, Behavior and Evolution*. Karger Publishers, 91(3), pp. 158–169. doi: 10.1159/000489943.

Verkhratsky, A. and Nedergaard, M. (2014) 'Astroglial cradle in the life of the synapse', *Philosophical Transactions of the Royal Society B: Biological Sciences*. The Royal Society, 369(1654), p. 20130595. doi: 10.1098/rstb.2013.0595.

Vidailhet, M. *et al.* (2001) 'A major locus for several phenotypes of myoclonus-dystonia on chromosome 7q', *Neurology*, 56(9), pp. 1213–1216. doi: 10.1212/WNL.56.9.1213.

Vidailhet, M. *et al.* (2005) 'Bilateral Deep-Brain Stimulation of the Globus Pallidus in Primary Generalized Dystonia', *New England Journal of Medicine*. Massachusetts Medical Society, 352(5), pp. 459–467. doi: 10.1056/NEJMoa042187.

Virlogeux, A. *et al.* (2018) 'Reconstituting Corticostriatal Network on-a-Chip Reveals the Contribution of the Presynaptic Compartment to Huntington's Disease.', *Cell reports*. Cell Rep, 22(1), pp. 110–122. doi: 10.1016/j.celrep.2017.12.013.

Volkmann, J. *et al.* (2014) 'Pallidal neurostimulation in patients with medication-refractory cervical dystonia: a randomised, sham-controlled trial', *The Lancet Neurology*, 13(9), pp. 875–884. doi: 10.1016/S1474-4422(14)70143-7.

Wahnschaffe, U. *et al.* (1990) 'Neuropathological studies in a mutant hamster model of paroxysmal dystonia', *Movement Disorders*. Mov Disord, 5(4), pp. 286–293. doi: 10.1002/mds.870050405.

Waite, A. J. *et al.* (2016) 'Myoclonus dystonia and muscular dystrophy: ε-sarcoglycan is part of the

dystrophin-associated protein complex in brain.', *Movement disorders : official journal of the Movement Disorder Society*. Mov Disord, 31(11), pp. 1694–1703. doi: 10.1002/mds.26738.

Wakamori, M. *et al.* (1998) 'Single tottering mutations responsible for the neuropathic phenotype of the P-type calcium channel.', *The Journal of biological chemistry*. American Society for Biochemistry and Molecular Biology, 273(52), pp. 34857–67. doi: 10.1074/jbc.273.52.34857.

Washburn, S. *et al.* (2019) 'Acute cerebellar knockdown of Sgce reproduces salient features of myoclonus-dystonia (DYT11) in mice', *eLife*, 8. doi: 10.7554/eLife.52101.

Weinhard, L. *et al.* (2018) 'Microglia remodel synapses by presynaptic trogocytosis and spine head filopodia induction.', *Nature communications*. Nat Commun, 9(1), p. 1228. doi: 10.1038/s41467-018-03566-5.

Weise, D. *et al.* (2006) 'The two sides of associative plasticity in writer's cramp', *Brain*, 129(10), pp. 2709–2721. doi: 10.1093/brain/awl221.

Wendell, B. and Lake, M. D. (2018) 'Intrathecal Baclofen Infusion', *Contemporary Neurosurgery*, 40(14), p. 6. doi: 10.1097/01.CNE.0000546557.80258.6b.

Whitford, K. L. *et al.* (2002) 'Regulation of Cortical Dendrite Development by Slit-Robo Interactions', *Neuron*. Cell Press, 33(1), pp. 47–61. doi: 10.1016/S0896-6273(01)00566-9.

Wider, C. *et al.* (2008) 'Study of a Swiss dopa-responsive dystonia family with a deletion in GCH1: redefining DYT14 as DYT5.', *Neurology*. Neurology, 70(16 Pt 2), pp. 1377–83. doi: 10.1212/01.wnl.0000275527.35752.c5.

Wijemanne, S. and Jankovic, J. (2015) 'Dopa-responsive dystonia--clinical and genetic heterogeneity.', *Nature reviews. Neurology*. Nat Rev Neurol, 11(7), pp. 414–24. doi: 10.1038/nrneurol.2015.86.

Williams, D. W. and Truman, J. W. (2004) 'Mechanisms of dendritic elaboration of sensory neurons in Drosophila: insights from in vivo time lapse.', *The Journal of neuroscience : the official journal of the Society for Neuroscience*. J Neurosci, 24(7), pp. 1541–50. doi: 10.1523/JNEUROSCI.4521-03.2004.

Wilson, D. F. *et al.* (1991) 'Effect of hyperventilation on oxygenation of the brain cortex of newborn piglets', *Journal of Applied Physiology*, 70(6), pp. 2691–2696. doi: 10.1152/jappl.1991.70.6.2691.

Wong, R. O. L. and Ghosh, A. (2002) 'ACTIVITY-DEPENDENT REGULATION OF DENDRITIC GROWTH AND PATTERNING'. doi: 10.1038/nrn941.

Xiang, Y., Tanaka, Y. and Patterson, B. (2017) 'Fusion of Regionally Specified hPSC-Derived Organoids Models Human Brain Development and Interneuron Migration', *Cell Stem Cell*, 21, pp. 383–398. doi: 10.1016/j.stem.2017.07.007.

Xiao, J. (2003) 'Cloning, developmental regulation and neural localization of rat ε-sarcoglycan', *Molecular Brain Research*, 119(2), pp. 132–143. doi: 10.1016/j.molbrainres.2003.09.004.

Xiao, J., Gong, S. and LeDoux, M. S. (2007) 'Caytaxin deficiency disrupts signaling pathways in cerebellar cortex', *Neuroscience*. Pergamon, 144(2), pp. 439–461. doi: 10.1016/J.NEUROSCIENCE.2006.09.042.

Xu, J. *et al.* (2010) '[3H]4-(dimethylamino)-N-(4-(4-(2-methoxyphenyl)piperazin-1-yl) butyl)benzamide: a selective radioligand for dopamine D(3) receptors. II. Quantitative analysis of dopamine D(3) and D(2) receptor density ratio in the caudate-putamen.', *Synapse (New York, N.Y.)*. NIH Public Access, 64(6), pp. 449–59. doi: 10.1002/syn.20748.

Yalcin-Cakmakli, G. *et al.* (2018) 'Striatal Cholinergic Interneurons in a Knock-in Mouse Model of L-DOPA-Responsive Dystonia.', *Frontiers in systems neuroscience*. Frontiers Media SA, 12, p. 28. doi: 10.3389/fnsys.2018.00028.

Yang, J. *et al.* (2014) 'Diffusion tensor imaging in blepharospasm and blepharospasm-oromandibular dystonia', *Journal of Neurology*. Springer, 261(7), pp. 1413–1424. doi: 10.1007/s00415-014-7359-y.

Yellajoshyula, D. *et al.* (2017) 'The DYT6 Dystonia Protein THAP1 Regulates Myelination within the Oligodendrocyte Lineage', *Developmental Cell*, 42(1), pp. 52-67.e4. doi: 10.1016/j.devcel.2017.06.009.

Yokoi, F. *et al.* (2006) 'Myoclonus, Motor Deficits, Alterations in Emotional Responses and Monoamine Metabolism in e-Sarcoglycan Deficient Mice', *J. Biochem*, 140, pp. 141–146. doi: 10.1093/jb/mvj138.

Yu, X. and Malenka, R. C. (2003) 'β-catenin is critical for dendritic morphogenesis', *Nature Neuroscience*. Nat Neurosci, 6(11), pp. 1169–1177. doi: 10.1038/nn1132.

Zakirova, Z. *et al.* (2018) 'Mutations in THAP1/DYT6 reveal that diverse dystonia genes disrupt similar neuronal pathways and functions.', *PLoS genetics*. Public Library of Science, 14(1), p. e1007169. doi: 10.1371/journal.pgen.1007169.

Zeuner, K. E. *et al.* (2015) 'Increased volume and impaired function: the role of the basal ganglia in writer's cramp.', *Brain and behavior*. Wiley-Blackwell, 5(2), p. e00301. doi: 10.1002/brb3.301.

Zhang, L. *et al.* (2011) 'Altered Dendritic Morphology of Purkinje cells in Dyt1 ΔGAG Knock-In and Purkinje Cell-Specific Dyt1 Conditional Knockout Mice', *PLoS ONE*. Edited by T. Yoshikawa. Public Library of Science, 6(3), p. e18357. doi: 10.1371/journal.pone.0018357.

Zhang, L. *et al.* (2012) 'Alteration of striatal dopaminergic neurotransmission in a mouse model of DYT11 myoclonus-dystonia.', *PloS one*. Public Library of Science, 7(3), p. e33669. doi: 10.1371/journal.pone.0033669.

Zhang, S.-C. *et al.* (2001) 'In vitro differentiation of transplantable neural precursors from human embryonic stem cells', *Nature Biotechnology*, 19(12), pp. 1129–1133. doi: 10.1038/nbt1201-1129.

Zimprich, A. *et al.* (2001) 'Mutations in the gene encoding ε-sarcoglycan cause myoclonus–dystonia syndrome', *Nature Genetics*, 29(1), pp. 66–69. doi: 10.1038/ng709.

Zoons, E. *et al.* (2011) 'Structural, functional and molecular imaging of the brain in primary focal dystonia—A review', *NeuroImage*, 56(3), pp. 1011–1020. doi: 10.1016/j.neuroimage.2011.02.045.

Zoons, E. *et al.* (2017) 'Lower serotonin transporter binding in patients with cervical dystonia is associated with psychiatric symptoms', *EJNMMI Research*. Springer Berlin Heidelberg, 7(1), p. 87. doi: 10.1186/s13550-017-0338-4.

Zucker, R. S. (1999) 'Calcium- and activity-dependent synaptic plasticity.', *Current opinion in neurobiology*, 9(3), pp. 305–13. Available at: http://www.ncbi.nlm.nih.gov/pubmed/10395573 (Accessed: 8 June 2018).